

NONLINEAR DYNAMIC TRANSFER FUNCTIONS FOR
CERTAIN RETINAL NEURONAL SYSTEMS

Thesis by

Panagiotis Zissis Marmarelis

In Partial Fulfillment of the Requirements
For the Degree of
Doctor of Philosophy

California Institute of Technology
Pasadena, California
1972

(Submitted December 9, 1971)

ACKNOWLEDGMENTS

I am grateful to Professor Gilbert D. McCann, my advisor, whose insight and enthusiasm continuously stimulated me, and for his guidance and perspicacious criticisms throughout my graduate work.

I am grateful to Dr. Ken-Ichi Naka without whose encouragement, experimental expertise and aid this work would not have been possible.

I thank Professors D.H. Fender, G. Ingargiola, G.R. Gavalas and Dr. J.F. Korsh for enlightening discussions. Thanks are also due to Drs. D. Arnett, G. Balanis, M. Raheb and A. Varvatsis for helpful discussions and suggestions.

I thank D. Knutsen and B. Elgin for help with programming and D. Aranovich, B. Ellert, A. Broers, and C. Lu for technical assistance. The numerous secretaries, and especially Mrs. Karen Current, who helped with the preparation of this manuscript have my deep appreciation.

I thank the California Institute of Technology for providing me with financial support through various assistantships and for its superb research environment and facilities.

ABSTRACT

The applicability of the white-noise method to the identification of a nonlinear system is investigated. Subsequently, the method is applied to certain vertebrate retinal neuronal systems and nonlinear, dynamic transfer functions are derived which describe quantitatively the information transformations starting with the light-pattern stimulus and culminating in the ganglion response which constitutes the visually-derived input to the brain. The retina of the catfish, Ictalurus punctatus, is used for the experiments.

The Wiener formulation of the white-noise theory is shown to be impractical and difficult to apply to a physical system. A different formulation based on crosscorrelation techniques is shown to be applicable to a wide range of physical systems provided certain considerations are taken into account. These considerations include the time-invariancy of the system, an optimum choice of the white-noise input bandwidth, nonlinearities that allow a representation in terms of a small number of characterizing kernels, the memory of the system and the temporal length of the characterizing experiment. Error analysis of the kernel estimates is made taking into account various sources of error such as noise at the input and output, bandwidth of white-noise input and the truncation of the gaussian by the apparatus.

Nonlinear transfer functions are obtained, as sets of kernels, for several neuronal systems: Light \rightarrow Receptors, Light \rightarrow Horizontal, Horizontal \rightarrow Ganglion, Light \rightarrow Ganglion and Light \rightarrow ERG. The derived models can predict, with reasonable accuracy, the system response to

any input. Comparison of model and physical system performance showed close agreement for a great number of tests, the most stringent of which is comparison of their responses to a white-noise input. Other tests include step and sine responses and power spectra.

Many functional traits are revealed by these models. Some are: (a) the receptor and horizontal cell systems are nearly linear (small signal) with certain "small" nonlinearities, and become faster (latency-wise and frequency-response-wise) at higher intensity levels, (b) all ganglion systems are nonlinear (half-wave rectification), (c) the receptive field center to ganglion system is slower (latency-wise and frequency-response-wise) than the periphery to ganglion system, (d) the lateral (eccentric) ganglion systems are just as fast (latency and frequency response) as the concentric ones, (e) (bipolar response) = (input from receptors) - (input from horizontal cell), (f) receptive field center and periphery exert an antagonistic influence on the ganglion response, (g) implications about the origin of ERG, and many others.

An analytical solution is obtained for the spatial distribution of potential in the S-space, which fits very well experimental data. Different synaptic mechanisms of excitation for the external and internal horizontal cells are implied.

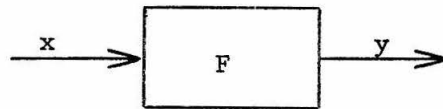
TABLE OF CONTENTS

<u>Chapter</u>	<u>Title</u>	<u>Page</u>
I.	Introduction	1
II.	The Wiener theory of nonlinear system identification	6
III.	Considerations for the application of the white-noise method	27
IV.	Materials and methods	50
V.	Transfer functions of Light \rightarrow Receptor systems	65
VI.	The Light \rightarrow Horizontal cell system	93
VII.	Spatial distribution of horizontal cell potential	142
VIII.	Ganglion Transfer functions	174
IX.	Transfer functions of Light \rightarrow ERG system	229
X.	Summary and discussion of results	251
	References	262

CHAPTER I

INTRODUCTION

The problem of identification of systems (also known as "system characterization," "system measurement" and "system evaluation") is one of the first problems that confronts scientists in a great variety of fields. It is the task of determining the input-output relationship of the system under study, in the form of a mathematical representation (or model), that is, the determination of the system functional F ($y=F(x)$) where x is the system input and y is the system output.



We may distinguish two different goals of the identification process; one, we could call "functional identification" and corresponds to finding what F is and the other, we could call "structural identification" and corresponds to finding how F is computed by the physical system. The second goal presupposes some a priori information about the system's internal structure and it usually takes the form of estimating the system parameters. The first goal treats the system as a black box and is, therefore, a more primitive process in the whole modeling procedure. For this purpose, we give the following definition of the identification problem: Given a system $y = F(x)$ choose a set of inputs $\{x\}$ such that the input-output pairs $\{x_i, y_i\}$ will allow you to determine F .

The identification problem was first formulated in connection with basic questions in the fields of adaptive control,

filtering, prediction and estimation theory [1b,16,32b,33b,42a,54a,54b, 100]. The basic theories that deal with system identification were first developed in these fields and have since been applied in virtually all fields of science. This generality of the applicability of the system identification theory is due to our being used to study systems in terms of "cause-effect," "input-output," "stimulus-response," "y is related to x," etc.

The object of the theory is the derivation of a mathematical or (or otherwise concise) model/concept that allows the prediction of the output (or effect or response) for a given input (or cause or stimulus). Such a model is desirable because, (a) it summarizes the functional properties of the system under study, (b) it allows conceptualization of the relevant information processing done by the system and its role in a complex environment, (c) can be used as a guide in posing new meaningful questions about the system's structure and (d) makes the presence of the physical system unnecessary as far as performing stimulus-response experiments. Point (d) is especially important for the study of biological systems since experiments, in this case, are very cumbersome and difficult. Many questions, then, could be answered by use of the derived model (assuming it is a good model) instead of performing a "real" experiment.

In the case of linear systems (i.e. the class of systems that obey the principle of superposition) the identification procedure is well established and straightforward since a linear system can be identified by its response to any aperiodic input signal such as an impulse or step function. In practice, however, a series of sine

waves of different frequencies is used as the test input and Bode plots of the system gain and phase are obtained.

Techniques of linear system theory have been used extensively in the study of nonlinear systems. There are basically two reasons for this: first is the simplicity and completeness of linear theory and second is the near absence of powerful and general nonlinear system theories. Often a nonlinear system has been studied through linear techniques using "small signals" or by making certain "linearizing" assumptions about its behavior. Biological systems, however, seldom behave linearly even under "small signal" conditions (see, for example, [42b,78], papers on the pupillary-reflex system, neural threshold systems and the many "unidirectional rate sensitivity" biological systems in [12] among many others). In fact, for optimal functioning of a biological system, nonlinearities are often essential. Examples are the logarithmic transformation of the sensory input in order to accommodate large ranges, the threshold mechanism of neuron to increase reliability of the information processing, the unidirectional rate sensitivity mechanism to distinguish direction and many others.

Linear and linearizing techniques have often been used yielding useful results [12,22,23,78,79]. Certain specialized methods for nonlinear system analysis exist such as the phase-plane and describing function techniques and others [13,28,29,87,95,98]. However, all these methods have serious limitations and are applicable to rather narrow classes of nonlinear systems.

Starting with Wiener's original work in 1942 [92] a general theory of nonlinear system analysis and synthesis has been in

development [2,6,7,25,41,93,99]. The theory is applicable to all systems that are time-invariant and have a finite memory and therefore it covers a very wide range of physical systems. Wiener proposed that a nonlinear system can be identified by its response to gaussian white-noise, since with such an input, there is a non-zero probability that any given function over a finite interval of time will be closely represented by some sample of this noise, and therefore, the system will effectively be tested with all possible inputs.

In spite of Wiener's theory generality and power very few attempts have been made to apply it to the analytical study of nonlinear systems and the results obtained from such attempts have not been quite satisfactory [31,37,81]. The difficulties in applying the method to biological systems are: (a) conditions for convergence of the Wiener series are not known, (b) computation time increases almost exponentially with the order of the computed kernel and (c) the low signal to noise ratio and high internal noise usually encountered in biological systems. These difficulties can be minimized for biological systems for which the input and output variables can be measured with accuracy (high signal to noise ratio), with low system internal noise and whose nature of nonlinearity allows a fairly accurate representation by taking the first few terms of the Wiener series. An attempt has been made to apply the Wiener theory on the pupillary-reflex system by Stark [81]. Katzenelson and Gould adapted a variant of the Wiener theory [36] which they applied to the pupillary-reflex system [37]. The results of these attempts to characterize the pupillary system using the Wiener theory were not satisfactory mainly

because of the large internal noise (present in the pupil system) which is independent of the input and therefore cannot be reduced by filtering [37,80].

Harris has applied another variant of the Wiener theory due to Bose [6] in which he characterized a continuous stirred-tank reactor system which has a two-level input [31]. The system was first simulated on a digital computer and then characterized. The identification procedure was simplified by the fact that the input switched only between two states and could therefore be treated as a binary variable.

In this work we apply a variant of the Wiener theory due to Lee and Schetzen [41] and characterize several neuronal systems of the vertebrate (catfish) retina. These systems describe the information transformations performed by the retina starting with light patterns and ending with the ganglion cell outputs which constitute the retina-transformed light pattern information that becomes the neural input to the brain.

CHAPTER II

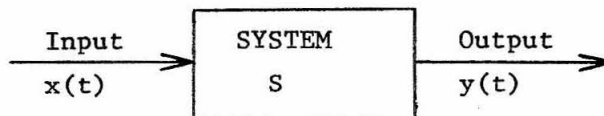
THE WIENER THEORY OF NONLINEAR SYSTEM IDENTIFICATION

1. White-noise approach in nonlinear system characterization

One of the main concerns in the analysis-synthesis problem of a nonlinear system is that of finding a proper mathematical representation of the system. This representation must be such that it is convenient to handle algebraically and computationally and it must reveal certain basic functional characteristics of the system under study. Without going further into the representation problem for nonlinear systems we note that, for these purposes, the concept of a functional representation has been well established by a series of investigators [2, 17, 25, 89, 92, 93, 97, 99, others].

Volterra [89] is credited with originally applying the concept of a functional to expand the input-output relationship of a nonlinear system in a power series with functionals as terms. A functional is a function whose argument is a function and whose value is a number. For example, definite integration is a functional whose argument is the integrand and whose value is the value of the definite integral.

Consider a system S with input $x(t)$ and output $y(t)$.



At any time t , the system can be considered to be a functional whose value is $y(t)$ - the value of the output at this time - and whose argument is $[x(\tau), \tau \leq t]$, a function that describes the whole past input to the system. Therefore the system can be written mathematically as,

$$(1) \quad y(t) = S[t; x(\tau), \tau \leq t]$$

The well-known convolution integral for linear systems,

$$y(t) = \int_0^t h(t-\tau)x(\tau)d\tau$$

is an example of a functional. In fact Volterra's functional series as well as Wiener's representation for nonlinear systems [15, 92, 93] are simply generalizations of the convolution integral representation of a linear system. The Volterra series is,

$$(2) \quad y(t) = h_0 + \int_{-\infty}^{\infty} h_1(\tau)x(t-\tau)d\tau + \int_{-\infty}^{\infty} \int_{-\infty}^{\infty} h_2(\tau_1, \tau_2)x(t-\tau_1)x(t-\tau_2)d\tau_1 d\tau_2 \\ + \int_{-\infty}^{\infty} \int_{-\infty}^{\infty} \int_{-\infty}^{\infty} h_3(\tau_1, \tau_2, \tau_3)x(t-\tau_1)x(t-\tau_2)x(t-\tau_3)d\tau_1 d\tau_2 d\tau_3 + \dots$$

where the integral kernels $h_1(\tau)$, $h_2(\tau_1, \tau_2)$, \dots , are zero for any of their arguments being less than zero since a physical system must satisfy the causality principle. From (2) it is easily seen that the second term describes the linear behavior and that the higher order terms are generalizations of the linear convolution integral.

Wiener constructed a hierarchy of functionals of increasing order which are orthogonal to each other with respect to a gaussian white noise input and whose sum characterizes the system [93].

Wiener's approach is approximately as follows: The functional of zero order is h_0 . The functional of first order is

$$\int h_1(\tau)x(t-\tau)d\tau + K_1$$

where $x(t)$ is a gaussian white process. Then, he uses a method very similar to the Gram-Schmidt orthogonalization procedure to make the functional of the second order orthogonal to the functionals of zero

order and first order. Then he makes the functional of third order orthogonal to the functionals of second, first and zero orders and so on. At each step he normalizes the resulting functional.

Finally, Wiener showed that the relationship between the input $x(t)$ and the output $y(t)$ of system S can be written as

$$(3) \quad y(t) = \sum_{n=0}^{\infty} G_n [h_n, x(t)]$$

where $\{G_i\}$ is the set of orthogonal functionals derived by the process described and $\{h_i\}$ is the set of Wiener kernels. Each h_k is a symmetrical function with respect to its arguments. The first four Wiener functionals are:

$$G_0 [h_0, x(t)] = h_0$$

$$G_1 [h_1, x(t)] = \int_0^{\infty} h_1(\tau) x(t-\tau) d\tau$$

$$G_2 [h_2, x(t)] = \iint_0^{\infty} h_2(\tau_1, \tau_2) x(t-\tau_1) x(t-\tau_2) d\tau_1 d\tau_2 - \\ - P \int_0^{\infty} h_2(\tau_1, \tau_1) d\tau_1$$

$$G_3 [h_3, x(t)] = \iiint_0^{\infty} h_3(\tau_1, \tau_2, \tau_3) x(t-\tau_1) x(t-\tau_2) x(t-\tau_3) d\tau_1 d\tau_2 d\tau_3 - \\ - 3P \iint h_3(\tau_1, \tau_2, \tau_3) x(t-\tau_1) d\tau_1, d\tau_2$$

where the power density spectrum of white noise $x(t)$ is $\Phi_{xx}(f) = P$.

Thus, system S is described by a set of kernels $\{h_i\}$ which can be considered to be generalized "impulse responses" of the system. To see this and also to get an insight as to the meaning of the kernels let us consider the following example [81]. Consider a system S

which is completely described by the linear and quadratic terms of the series, that is

$$y(t) = \int_0^{\infty} h_1(\tau) x(t-\tau) d\tau + \iint_0^{\infty} h_2(\tau_1, \tau_2) x(t-\tau_1) x(t-\tau_2) d\tau_1 d\tau_2$$

The response of S to an impulse at $t = 0$, i. e. $x(t) = \delta(t)$, is

$$y(t) = \int_0^{\infty} h_1(\tau) \delta(t-\tau) d\tau + \iint_0^{\infty} h_2(\tau_1, \tau_2) \delta(t-\tau_1) \delta(t-\tau_2) d\tau_1 d\tau_2$$

or

$$y(t) = h_1(t) + h_2(t, t)$$

The response of S to an impulse at $t = t_0$, i. e. $x(t) = \delta(t-t_0)$, is

$$y(t) = h_1(t-t_0) + h_2(t-t_0, t-t_0)$$

The response of S to a stimulus consisting of an impulse at $t = 0$ and an impulse at $t = t_0$, i. e. $x(t) = \delta(t) + \delta(t-t_0)$, is

$$y(t) = \int_0^{\infty} h_1(\tau) [\delta(t-\tau) + \delta(t-\tau-t_0)] d\tau + \iint_0^{\infty} h_2(\tau_1, \tau_2) [\delta(t-\tau_1) + \delta(t-\tau_1-t_0)] [\delta(t-\tau_2) + \delta(t-\tau_2-t_0)] d\tau_1 d\tau_2$$

or

$$y(t) = h_1(t) + h_1(t-t_0) + h_2(t, t) + h_2(t, t-t_0) + h_2(t-t_0, t) + h_2(t-t_0, t-t_0)$$

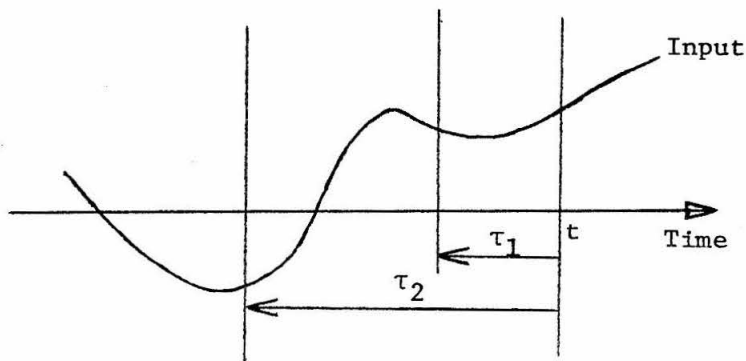
If we subtract algebraically from the response to the two impulses the contributions (responses) of each impulse when each alone acted upon the system, we have left

$$h_2(t, t-t_0) + h_2(t-t_0, t)$$

which, since $h_2(\tau_1, \tau_2)$ is a symmetric function, reduces to

$$2 h_2(t, t-t_0)$$

Therefore it is seen that the second-order kernel $h_2(\tau_1, \tau_2)$ gives a quantitative measure of the nonlinear "cross-talk" between the two impulses as a function of time t for each separation, t_0 , between the impulses. It is this term, $2 h_2(t, t-t_0)$ which represents the deviation from "time superposition." That is the deviation of the system response to the two-pulse stimulus from the sum of the responses to each stimulus impulse separately. Note that this example does not clearly interpret the meaning of $h_2(\tau_1, \tau_2)$ along the diagonal $[\tau_1 = \tau_2]$, even though we can get an idea of it by letting the two pulses come very close together until they almost coincide. The value of $h_2(\tau_1, \tau_2)$ for $\tau_1 \neq \tau_2$ gives the nonlinear deviation due to interaction between portions of the input signal τ_1 and τ_2 seconds in the past.



It can easily be shown that if the system consists of a no-memory nonlinearity followed by a linear system then $h_2(\tau_1, \tau_2) = 0$ for $\tau_1 \neq \tau_2$ and the system obeys "time superposition"; that is, in this

case, the response of the system to the sum of two or more impulses is equal to the sum of the responses of the system to each impulse separately and the values of $h_2(\tau_1, \tau_2)$ for $\tau_1 = \tau_2$ are a continuous series of impulses of varying strength. In conclusion, we see that the magnitude of the kernels gives an indication of the nonlinear cross-talk between different (in past time) portions of the input.

A system is completely characterized once its set of kernels $\{h_i\}$ is determined. This method is applicable to a very large class of systems. This is the class of systems that are time-invariant, have a finite memory and whose inputs and outputs are bounded. Excluded are systems whose characteristics change with time and systems with infinite memory such as oscillators. Therefore, compared with other methods of nonlinear system analysis such as the phase plane technique or the describing function technique [13, 28, 87] the Wiener method has a much greater range of applicability and it can describe nearly all physical systems.

The use of white noise, which is a random function of time, as input in order to characterize a system is based on the following idea: Given a long enough record of the system response to a white-noise ensemble member there is a finite probability that any given function of time will be represented arbitrarily closely over a finite interval of time by some sample of this white-noise input function. In this way the system is tested with every possible input time function and all frequencies over which the noise has a flat spectrum. Thus, two systems are equivalent if and only if they respond identically to white noise because then they will respond identically to any other input.

This is the justification for deriving nonlinear transfer functions by performing white noise experiments. The objective, then, becomes to find a mathematical model that responds to white noise the same way the physical system responds to white noise.

2. The Wiener formulation of the white-noise theory

Given a time-invariant, physical system S with input $x(t)$ and output $y(t)$, the output at time t is a function of the present value and past values of the input [6, 93],

$$(1) \quad y(t) = S[x(\tau), \tau \leq t] \quad .$$

The function $[x(\tau), \tau \leq t]$ can be expanded into a series of orthonormal functions like the family of Laguerre functions, $\{\varphi_i(\tau)\}$,

$$(2) \quad x(-\tau) = \sum_{n=0}^{\infty} c_n \varphi_n(\tau), \quad \tau \geq 0 \quad .$$

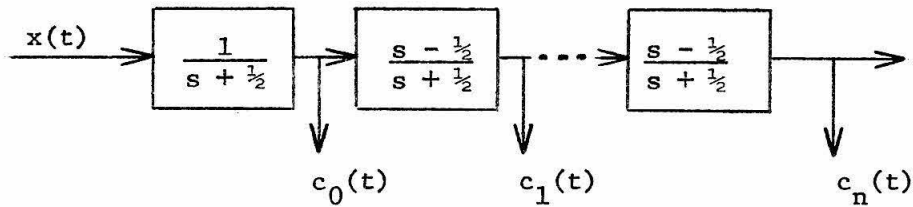
The set of coefficients $\{c_i\}$ completely describes $[x(\tau), \tau \leq t]$ and the present is considered as $t = 0$ and time going backwards. The Laguerre functions form a complete orthonormal system in the interval $(0, \infty)$ and are defined by

$$(3) \quad \varphi_n(t) = \frac{e^{-t/2}}{n!} \frac{d^n}{dt^n} (t^n e^{-t}), \quad t \geq 0, \quad n = 0, 1, 2, \dots \quad .$$

We easily obtain the coefficients $\{c_i\}$, by

$$(4) \quad c_n = \int_0^{\infty} x(-\tau) \varphi_n(\tau) d\tau \quad .$$

Wiener chose the Laguerre family of functions to expand the past of the system input because these functions have certain desirable mathematical properties (we will describe later) and they can be easily generated by analog equipment. The Laguerre coefficients can be generated by the network shown below,



where s is the Laplace transform variable. Or, equivalently, the Laguerre coefficients are given as solutions of the following set of linear differential equations:

$$\frac{dr_m}{dt} + \frac{1}{2} r_m = x(t) - \sum_{i=0}^{m-1} r_i(t) \quad , \quad i = 0, 1, \dots, n$$

$$r_i(0) = 0 \quad , \quad i = 0, 1, \dots, n$$

At each time t , the outputs of this network give the values of the coefficients $\{c_i\}$ which completely describe the input $x(t)$ up to this time t . This can be shown very easily from equations (3) and (4).

For $x(t)$ being a gaussian white process it can be shown that

- (a) Each c_i has a gaussian distribution,
- (b) c_K and c_m are statistically independent random variables.
- (c) All c_i have the same mean and variance.

Given these properties of the coefficients $\{c_i\}$ and after standardizing them so that they have zero mean and unit variance, it is easily seen that the joint probability distribution is

$$(5) \quad p(c_0, c_1, \dots, c_n) = (2\pi)^{-\frac{n}{2}} \exp\left[-\frac{1}{2}(c_0^2 + c_1^2 + \dots + c_n^2)\right]$$

In practice we would use a finite number, $n+1$, of coefficients c_i to describe the past of the input. Then (1) becomes

$$(6) \quad y(t) = S[c_0(t), c_1(t), \dots, c_n(t)]$$

S is now a function of $n+1$ variables and it can be expanded in terms of the class of Hermite functions which constitute an orthonormal family over the interval $(-\infty, \infty)$ [11]. The n th normalized Hermite polynomial is defined as

$$\eta_n(z) = (-1)^n (2^n n! \pi^{\frac{1}{2}})^{-\frac{1}{2}} e^{z^2} \frac{d^n}{dz^n} e^{-z^2}$$

and the corresponding Hermite function is

$$\psi_n(z) = e^{-\frac{z^2}{2}} \eta_n(z)$$

Expanding (6) we get

$$(7) \quad y(t) = \sum_{i=0}^{\infty} \sum_{j=0}^{\infty} \dots \sum_{k=0}^{\infty} a_{ij\dots k} \psi_i(c_0) \psi_j(c_1) \dots \psi_k(c_n)$$

$$= \sum_{i=0}^{\infty} \sum_{j=0}^{\infty} \dots \sum_{k=0}^{\infty} a_{ij\dots k} \eta_i(c_0) \eta_j(c_1) \dots \eta_k(c_n) \cdot \exp\left[-\frac{1}{2}(c_0^2 + \dots + c_n^2)\right]$$

The coefficients $\{a_{ij\dots k}\}$ characterize system S completely and the identification problem reduces to the problem of determining these coefficients. That is, knowing the set of these coefficients for a particular system we can compute the response of this system to any input by use of equation (7). It can be shown [6] that the coefficients are given by

$$(8) \quad a_{ij\dots k} = (2\pi)^{\frac{n}{2}} E \{y(t)\eta_i(c_0)\eta_j(c_1)\dots\eta_k(c_n)\}$$

where $y(t)$ is the response of the system to a white noise input $x(t)$ and $\{c_0, c_1, \dots, c_n\}$ the set of coefficients that characterize $x(t)$ at each time. Equation (8) is obtained by performing a minimum mean-square-error fit between the actual response of the system, $y(t)$, and the response as given by (7) over the entire range of the input-output record (where input $x(t)$ is gaussian white noise).

After the system has been tested with white noise for a sufficiently long time and both the input $x(t)$ and the output $y(t)$ have been recorded we proceed as shown diagrammatically in Fig. 2.1A in order to determine the set of characterizing coefficients $\{a_{ij\dots k}\}$. In this analysis procedure the coefficients are evaluated serially and each time the whole length of the records has to be used. Once these coefficients have been determined they can be used to synthesize the nonlinear model of the system in terms of equation (7). The synthesis procedure is shown diagrammatically in Fig. 2.1B.

The application of the white-noise theory under this Wiener-formulation is very impractical and very difficult for the following reasons:

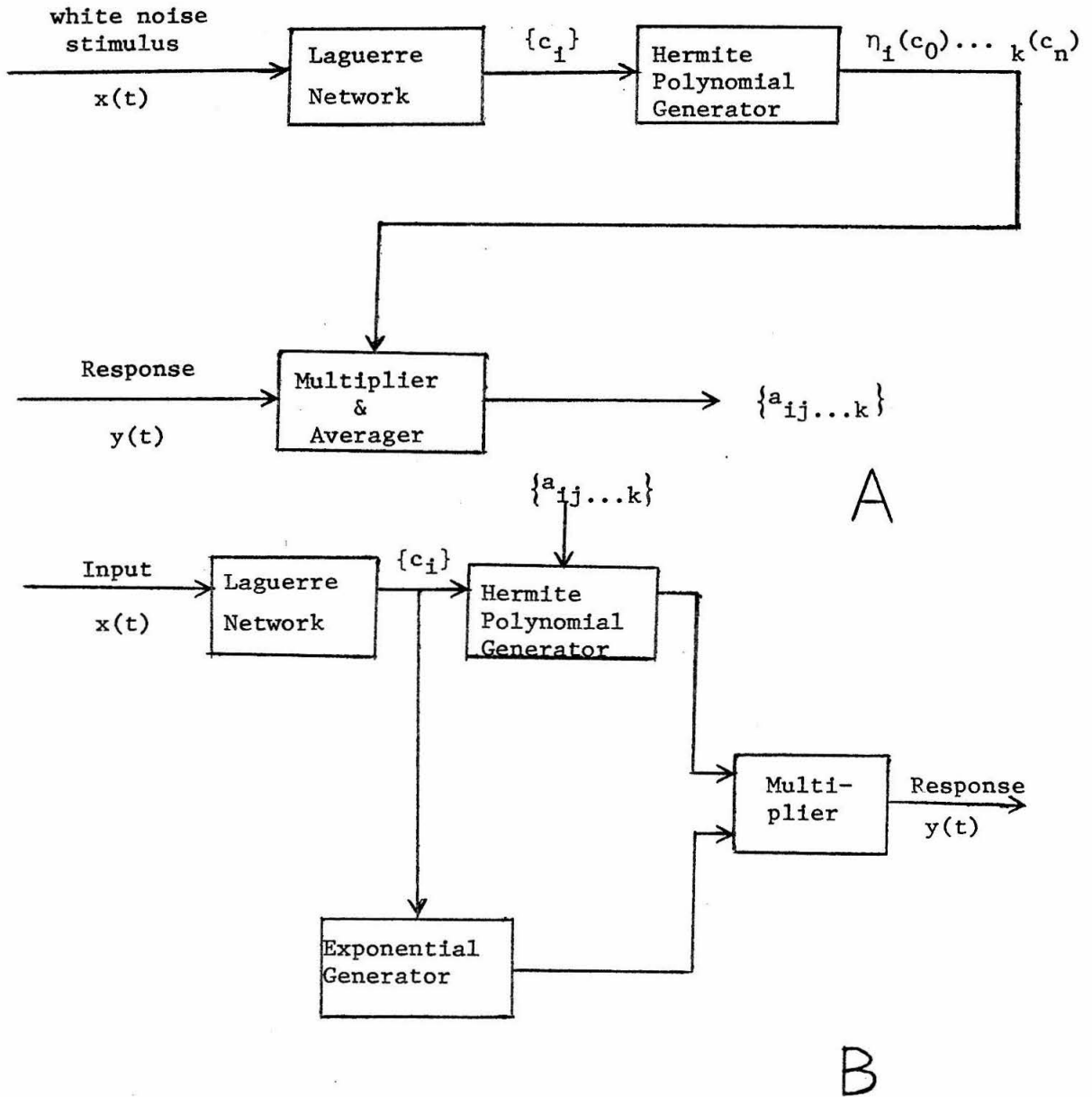


Fig. 2.1

Flow diagrams for the analysis (A) and synthesis (B) phases of the Wiener formulation of the white-noise method of nonlinear system identification.

(a) The number of coefficients needed to characterize almost any system, linear or nonlinear, is extremely large. If n coefficients are used in the Laguerre expansion to describe the past of the input at any time and p coefficients are used to expand the system functional in terms of Hermite functions, then the number of coefficients needed to characterize the system is p^n . Exploratory calculations showed that even for a simple nonlinear system such as a non-memory squarer p has to be approximately 10 to 20 and for a nonzero memory system n has to be also 10 to 20 giving the huge numbers of coefficients of 10^{10} to 20^{20} to be evaluated

(b) The computation required for the evaluation of the characterizing coefficients is extremely long especially since the computation has to be performed serially (Fig. 2.1A). In the synthesis phase, when the response to a particular input is desired the computation is again very long because of the multitude of the coefficients and the repeated Laguerre and Hermite expansions, as shown in Fig. 2.1B.

(c) It is desirable to be able to assign some meaning to the characterizing coefficients $\{a_{ij\dots k}\}$ that would reveal some features of the structure of the system. This is impossible under this form of the theory. The coefficients $\{a_{ij\dots k}\}$ are purely formal mathematical quantities and it appears futile to attempt to draw an analogy between them and properties of the system which they characterize.

(d) The method is basically a curve fitting procedure and not a descriptive algebra of systems that is desired in order to be able to manipulate systems as building blocks for more and more complicated structures. This point is very crucial for the study of biological

systems and especially for the ambitious undertaking of the study of the very complicated structure of the brain.

(e) A linear system which is characterized very simply by the classical linear theory is characterized very clumsily by this method. A vast number of coefficients $\{a_{ij} \dots k\}$ are needed to identify a linear system. This is due to the fact that a very large number of Hermite polynomials is needed so that their sum would cancel out the effect of the highly nonlinear exponential transformation.

(f) It is very difficult to incorporate into Wiener's method any a priori information about the system so as to plan the computation for shorter length and to reduce the number of the characterizing coefficients. Point (e) is an example of this serious shortcoming of this very general method: The method in being so very general fails to recognize a simple situation and treat it accordingly.

(g) The derived nonlinear model is too cumbersome to use for prediction or comparison with experimental results even if a digital computer is available.

All these difficulties encountered in the practical application of the theory point out that other formulations of the white-noise theory must be sought if it is to be made a working tool for identifying nonlinear systems.

3. The Lee-Schetzen formulation

The Lee-Schetzen approach of the nonlinear identification problem starts with the Wiener functional series and it shows how the set of Wiener kernels $\{h_i\}$ can be evaluated by use of cross-correlation techniques [41, 72].

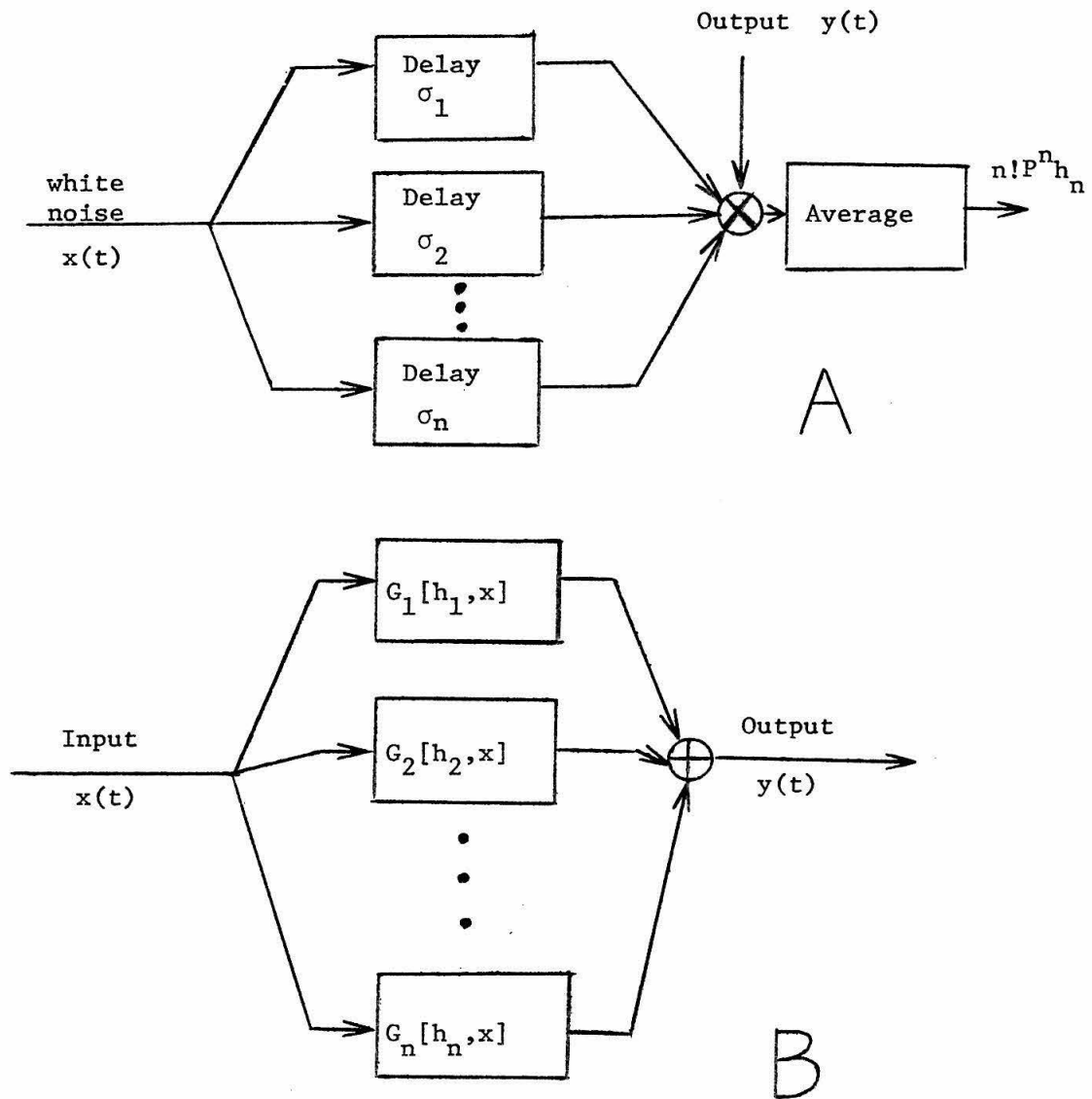


Fig. 2

Kernel estimation (A) and final model (B).

Specifically, given a system S that has been subjected to a white-noise input $x(t)$ and whose response to this input is $y(t)$, Lee and Schetzen have shown that the Wiener kernels are given by

$$(1) \quad h_n(\sigma_1, \dots, \sigma_n) = \frac{1}{n! P^n} \mathbb{E} \{y(t) x(t-\sigma_1) \dots x(t-\sigma_n)\}, \sigma_1 \neq \sigma_j$$

where P is the power level of the white-noise signal. Fig. 2.2A shows diagrammatically the evaluation of the kernels by this method. Fig. 2.2B shows how the derived model is constructed and used to predict the response of the system to any desired input.

Equation (1) can be altered slightly to permit evaluation of the kernels along any diagonal $\sigma_i = \sigma_j$ [41],

$$h_n(\sigma_1, \sigma_2, \dots, \sigma_n) = \frac{1}{n! P^n} \mathbb{E} \left\{ \left[y(t) - \sum_{k=0}^{n-1} G_k [h_k, x(t)] \right] x(t-\sigma_1) \dots x(t-\sigma_n) \right\}$$

a formula which is valid for all $(\sigma_1, \sigma_2, \dots, \sigma_n)$.

This formulation of the white-noise theory has several advantages over the Wiener formulation and it makes it feasible (with some restrictions) to identify a physical nonlinear system by subjecting it to a white-noise stimulus.

First, it directly estimates the kernels which, as we saw early in this chapter, have a definite physical meaning; they can reveal interesting properties and provide an insight to the structure of the system under study.

Second, the cross correlation method is much simpler computationally because it does not involve the cumbersome Laguerre and Hermite transformations.

Third, a linear system is easily recognized by the cross correlation method, the derived model takes a simple form and therefore the computational burden is reduced while the insight into the nature of the system is increased.

Fourth, the synthesis problem is very simple. Estimating the response to a particular input involves only a few integrations.

Fifth, it is very easy to construct alternative structural models once the kernels are known, such as structures consisting of linear filters (for which powerful theories exist) and multipliers.

Sixth, in the Wiener formulation it can be considered that the kernels are expanded in terms of the orthogonal family of Laguerre functions, and since this expansion, for any practical application, has to be truncated there is an inherent approximation error in the Wiener formulation. This truncation error does not occur in the cross correlation method.

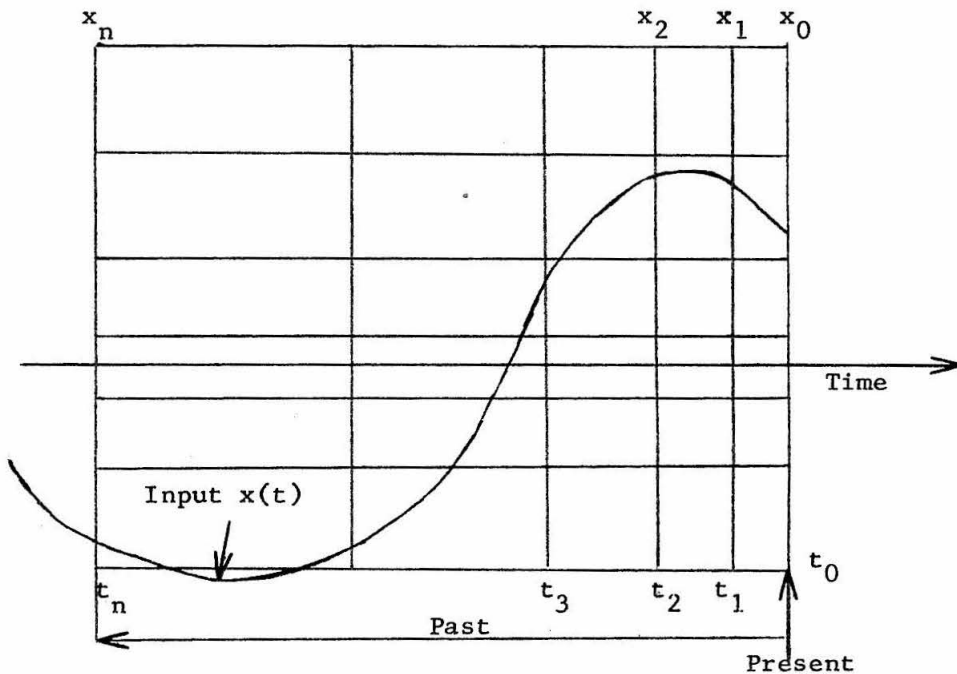
Seventh, a priori information about the system can be utilized to reduce the identification effort by reducing the computational burden.

4. Other formulations of the white-noise theory

There are other formulations of the white-noise theory [6, 36, 52, 76, 95, 97], each one of which may prove suitable for a particular type of nonlinear system. Bose [6] uses ^{an} orthogonal class of functions, which he calls gate-functions, and which are simply square unit pulses in time, in order to partition the function space of the past of the input into nonoverlapping (orthogonality of the gate

functions) cells. This formulation of the theory would be most suitable for systems with strong saturating elements. Katzenelson and Gould [36] use the Volterra series to develop a systematic approach that leads to a set of simultaneous integral equations. An iteration procedure is given for their solution. This approach seems best for the synthesis of optimal nonlinear filters. In [52, 76, 97] combinations of one or more impulses are used to calculate characterizing coefficients or functions.

Starting with the basic notion of the functional as the mathematical description of a system and utilizing the white-noise approach one can devise several schemata for system identification. A very simple one would be the following. A grid is superposed over the past of the input in such a way that it covers the whole memory of the system and the total range of amplitudes of the input.



At any time t , the present input and its past are described by a vector of real numbers that give the ordinates of the grid-squares at the fixed times $(t_0, t_1, t_2, \dots, t_n)$. This vector is put in correspondence with the value of the system output at this time, y_0 , thus forming the input-output vector $(t_0, t_1, \dots, t_n, y_0)$. As the system is being tested with white-noise, new input-output vectors are formed. Eventually, the system will have been exhaustively tested for all combinations of values of the input sensors x_0, x_1, \dots, x_n . All these vectors could be easily stored in some form of auxiliary storage (disc, magnetic tape) of a digital computer and used as the "model" of the system. As an abstraction from this data base one could fit a function $F(x_0, x_1, \dots, x_n)$ over the whole set of vectors which would then be the transfer function of the system. This function could be used to predict the response of the system to any input.

There are several noteworthy features of this formulation of the white-noise theory. First, it does not require a white-noise input from the statistical point of view since the method simply enumerates input-output correspondences. Instead, a more expedient way would be to put the input under computer control and enumerate all the possible combinations of sensor values (x_0, x_1, \dots, x_n) . This would drastically cut down the testing time required for identifying the system. This is very important in view of the nature of the experiments on the nervous system (short experiment-life, drift). Second, the grid square size can be varied depending on its position, thus more heavily weighing the more important regions of the signal. For example, it would usually be desired to have the sensors more

densely placed near t_0 than t_n since the immediate past usually affects the present output more than the remote past. Also, the horizontal grid lines could be more densely spaced near the non-linearity of the system, e. g. where saturation might occur. Third, this formulation is conceptually very simple and it can readily be amended to fit any system peculiarities. Fourth, it can answer many questions about properties of the system under study provided a suitable computer system exists to manipulate and abstract information from the resulting data base of input-output vectors. Such a system partially exists in our laboratory (Phase II) [18, 24, 44, 48, 50] and it is now being greatly extended. It appears that the new version would be very appropriate for this kind of manipulation and abstraction, thus making this formulation of the white-noise theory an attractive tool for studying neuronal systems.

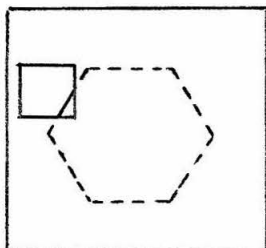
In this work the cross-correlation formulation of the white-noise theory is used to obtain nonlinear dynamic transfer functions for several neuronal chains that play an important role in the organization of the receptive field of the vertebrate retina and whose outputs constitute the retina-transformed information contained in the stimulating light patterns that becomes the input to the brain.

5. Discussion of the white-noise theory

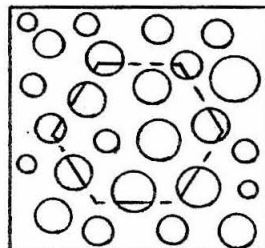
There are several considerations to be made and techniques to be used for the successful practical application of the white-noise method of identifying a nonlinear system. All of these are examined in the next chapter.

The idea of using white-noise to derive a transfer function for a nonlinear system is a very ingenuous one because it tests a system exhaustively with a very large variety of inputs and it forms a transfer characteristic which takes into account the response of the system to all these inputs. In a sense, the "average" transfer characteristic is formed. Especially, if it is considered that there has been a habit (left over because of the beauty of linear theory) among bio-scientists to use steps, pulses and sine waves to derive transfer functions of obviously nonlinear systems, the white-noise approach offers a tremendous improvement. It should also be stressed that a biological system seldom behaves linearly. In fact, from the functional point of view, nonlinearities in biological systems appear to be a necessity as is, for example, the logarithmic transformation of the sensory input in order to accommodate large ranges of input.

At this point a simplified analogy may be helpful to understand the difference between the two kinds of approach. The analogy is a game in which one is presented with a picture completely covered with sand and he is given the task of finding what the picture under the sand looks like. The traditional bioscientist removes a little square



Case A



Case B

(Case A) of the sand and from what he sees in that square he tries to guess the content of the whole picture. This corresponds very aptly to testing a nonlinear system with steps or sines and from the response to such inputs deriving transfer functions for any other kind of input. In the white-noise approach holes are poked randomly over the entire area of the picture (Case B) and the content of the picture is guessed from what is found in all these holes. This is so because the system is tested with a very large variety of inputs randomly (or nonrandomly) selected from the input function space.

This kind of approach is preferable to the classical approach and should prove very usefull for research in the living nervous system. It is a realization of the concepts suggested for new research strategies by McCann [51], who points out the need toward ". . . . the development of more complex experiments that will simultaneously gather more information both within one of the traditional areas of experimentation and across these areas" in order to study successfully the informational relationships in living neuronal systems.

CHAPTER III

CONSIDERATIONS FOR THE APPLICATION
OF THE WHITE-NOISE METHOD

1. Introduction

The application of the white-noise method for the characterization of a physical system is difficult and involved. The amount of difficulty depends on the nature of the nonlinearities of the system and the degree of accuracy which we require from the derived model. In certain cases the application of the theory will produce poor results after long experimental procedures and digital computations. Therefore, it is desirable to develop certain preliminary criteria and simple experiments which would give an indication of how complex the problem is and how successful the white-noise method can be expected to be in a particular case.

In developing these criteria and tests we should take into account the characteristics of the system and the limitations imposed by the tools available to us for its study.

First, we should decide the conditions under which the experiment should be conducted, such as the amplitude range and frequency bandwidth of the stimulating noise, the temporal length of the experiment and several others.

Second, we should estimate the computational length and complexity which is required to derive the desired nonlinear model within a certain degree of accuracy.

Third, we should estimate the errors resulting from various sources and how they affect the results.

Fourth, we should be able to interpret the derived model and draw some conclusions about the system characteristics.

2. Preliminary conditions of the white-noise experiment

Once a particular system has been chosen for study by the white-noise method several preliminary decisions have to be made. The input and output of the system have to be clearly defined. It must be shown that the system receives no other time-varying inputs during the experiment.

The time-invariancy of the system must be proved. A system is time-invariant if the form of the system response is independent of the particular time at which the input is applied. This can be easily checked by performing several simple experiments repeatedly at different intervals of time and comparing the system responses.

The amplitude range of the stimulus must be chosen such that it covers the most "interesting" region of operation. This could depend on the location of amplitude-dependent nonlinearities and the range of inputs encountered during the natural operation of the system. This choice determines the validity range of the model.

Biological (neuronal) systems are usually sensitive over large ranges of the stimulus amplitude (4 log units of sensitivity are very common). The dynamic range of the instruments that produce the stimulus and record the response rarely exceeds two orders of magnitude. Therefore the choice of the stimulus range must be made very carefully to reveal the "interesting" properties of the system. Sometimes it will be necessary to perform more than a single white-noise experiment in order to cover the whole operational range of

the system.

The white-noise theory has been formulated for an input that is ideal white-noise. In practice, of course, white-noise sources exhibit a flat power spectrum only over a certain range of frequencies with cutoffs at high frequencies. It was found that if the bandwidth of the white-noise extends too much beyond the system bandwidth (at the high frequency end) then undesirable effects take place in the computation of the kernels (see section 4). However, the input noise bandwidth should cover the system bandwidth completely so that the system becomes tested with all frequencies of interest.

Let $g(\tau)$ be the impulse response of the low-pass filter that transforms ideal white-noise $x_i(t)$ to the real white-noise $x_r(t)$ used in the experiment for the system identification. Then

$$(1) \quad x_r(t) = \int_{-\infty}^{\infty} g(\tau) x_i(t-\tau) d\tau \quad .$$

Let us consider for purposes of illustration, the calculation of the second degree kernel. The arguments can be readily generalized to the n th degree kernel.

To compute $h_2(\tau_1, \tau_2)$, we compute the cross correlation $\varphi_{y x_r x_r}(\tau_1, \tau_2)$ between the system output and the real white-noise which gives an estimate $\hat{h}_2(\tau_1, \tau_2)$. We have

$$\varphi_{y x_r x_r}(\tau_1, \tau_2) = E \{ y(t) x_r(t-\tau_1) x_r(t-\tau_2) \} \quad .$$

Using (1) we obtain

$$\varphi_{y x_r x_r}(\tau_1, \tau_2) = E \left[y(t) \int g(v_1) x_i(t-\tau_1-v_1) dv_1 \cdot \int g(v_2) x_i(t-\tau_2-v_2) dv_2 \right]$$

which finally becomes

$$(2) \quad \varphi_{y_{\mathbf{r}} x_{\mathbf{r}}}(\tau_1, \tau_2) = \iint g(v_1)g(v_2) \varphi_{y_{\mathbf{i}} x_{\mathbf{i}}}(\tau_1+v_1, \tau_2+v_2)dv_1 dv_2$$

Taking Fourier transforms and recalling the relation between $\varphi_{y_{\mathbf{r}} x_{\mathbf{r}}}$ and h_2 we get

$$(3) \quad H_2(\omega_1, \omega_2) = \frac{\hat{H}_2(\omega_1, \omega_2)}{G(\omega_1) \cdot G(\omega_2)}$$

where $G(\omega)$ is the Fourier transform of $g(\tau)$ and $H_2(\omega_1, \omega_2)$, $\hat{H}_2(\omega_1, \omega_2)$ are the two-dimensional Fourier transforms of $h_2(\tau_1, \tau_2)$, $\hat{h}_2(\tau_1, \tau_2)$ respectively. From (3) we note that if $g(\tau)$ is assumed to be a low-pass filter and if the noise bandwidth completely covers the system bandwidth then $\hat{h}_2(\tau_1, \tau_2)$ and $h_2(\tau_1, \tau_2)$ are very close and no additional computation is necessary to correct for the non-ideality of the white-noise. Nevertheless, it is possible from (3) or (2) (by numerically solving the integral equation) to correct the error introduced by using finite-bandwidth white noise.

We note that the error will be large for the high frequencies for which the gain of low-pass filter $G(\omega)$ is substantially different than 1. Therefore, the input noise bandwidth should be large enough to cover the whole frequency range in which the system responds.

Given a system S , we need to decide how many kernels to compute to get a satisfactory model. We can get an idea of this number by performing a few simple preliminary experiments where the system is tested by sine inputs and the resulting response is analyzed as to its harmonic content. It is simple to show that a model

that includes up to the n th order term of the Wiener series can produce at most an n th order harmonic.

For almost all the systems studied in this work the harmonic content beyond the second harmonic is small and the series was truncated after the second order term. We will investigate and justify this approximation as we discuss each system under study.

The extent to which the kernels must be computed, that is how big should (τ_1, \dots, τ_n) be for $h_n(\tau_1, \dots, \tau_n)$ to be zero, depends solely on the memory of the system. The memory M of a system S can be loosely defined as that length of time that is required for the effect of the input on the output at time $t-M$ to become zero at time t . A simple preliminary two-pulse experiment can be performed to measure M . The system is stimulated by an impulse at time t and an impulse at time $t + \alpha$. Delay α is increased until the response of the system to the second impulse is identical to the response to the first impulse. Then α is equal to M . Admittedly, such a determination of memory length does not account for the nonlinear interaction of many pulses that could, conceivably, shorten or lengthen the system memory but it is assumed that such an effect is small (especially, since for most systems under consideration here the effect of past input on present output attenuates exponentially). In any case a safety factor can be employed in determining the extent to which the kernels are computed. The length of memory of the system is also needed to determine the white-noise bandwidth and the length of the experiment (for reliable estimates of the kernels).

The bandwidth of the system should be estimated in order to determine the white-noise bandwidth and consequently the sampling rate of the input-output records. This can be done approximately from preliminary testing with sine inputs.

Finally, the temporal length of the white-noise experiment should be decided. This depends on the variance we are willing to tolerate in the estimates of the statistical averages that the cross-correlations indicate. Since the finite record length introduces an error in the kernel estimates it is treated in detail in another section and a formula is derived for the determination of the record length.

3. Computational Considerations

In the analysis phase, the main difficulty in the computational process is the calculation of the high order correlation functions. The amount of computation increases with the order of the computed correlation, the length of the record and the extent to which each kernel is computed.

Using a simple rectangular rule of integration we have

$$\varphi_{yx \dots x}(\tau_1, \dots, \tau_n) = \frac{\sum_{i=1}^N y(t_i) x(t_i + \tau_1) \dots x(t_i + \tau_n)}{N}$$

where N is the number of points in the record. We could use more accurate numerical integration schemes but that would merely complicate the discussion without increasing the generality in the basic results.

The number of points m for which each kernel is computed depends on the memory M of the system and is given by

$$(1) \quad m = \frac{M}{\Delta t}$$

where Δt is the sampling interval of the records. Considering that the kernels are symmetric functions of their arguments the number of points we have to calculate for the n th order kernel (for $n < m$) is given by

$$(2) \quad \binom{m+n-1}{n} = \frac{(m+n-1)(m+n-2) \dots (m)}{n!}$$

Of more interest is the number of multiplications required for the computation of each kernel. This is so because multiplication is a time consuming operation for a digital computer. The number of multiplications for the calculation of the n th order kernel is given by

$$\text{Number of multiplications} = n \cdot N \cdot \left\{ \frac{(m+n-1)(m+n-2) \dots (m)}{n!} \right\} .$$

There is, of course, the usual tradeoff between computation time and storage space. Computing time (i. e. number of multiplications) can be reduced by storing in core intermediate results. As the storage requirements increase with the order of the computed kernel there will be a sharp increase in computing when we are forced to use auxiliary storage (disc, tapes) to hold the intermediate results or even to store the final result.

Let α_n be a constant (dependent on the order n) which accounts for time spent in addressing, storing, etc. Then the total computation time is approximately

$$(3) \quad T_n = \alpha_n \cdot N \cdot n \cdot \left[\frac{(m+n-1)(m+n-2) \dots (m)}{n!} \right]$$

where N is the total number of sample points in the record and m is given by (1).

From (3) we have for the first four kernels,

$$T_1 = \alpha_1 \cdot N \cdot m$$

$$T_2 = \alpha_2 N(m^2 + m)$$

$$T_3 = \alpha_3 N \cdot \frac{m^3 + 3m^2 + 2m}{2}$$

$$T_4 = \alpha_4 N \cdot \frac{m^4 + 6m^3 + 11m^2 + 6m}{6}$$

Therefore, computing time (for $n < m$) increases almost exponentially with the order of the kernel. This is a severe limitation on the order of the kernel that can be computed by conventional means. A digital computer, even though the best available tool for the job today, is not ideally suited for the computation of high order analog correlations. Analog electronic equipment would be more suitable for this purpose. In the synthesis phase the computation is straightforward. It involves the estimation of multidimensional integrals for which there are standard techniques.

The computation of the power spectra involves several subtleties (see Chapter IV).

4. Error Analysis

As shown in Chapter II the kernels are given by

$$h_n(\tau_1, \dots, \tau_n) = \frac{1}{n!P^n} \left[\left[h(t) - \sum_{m=0}^{n-1} G_m [h_m, x(t)] \right] x(t-\tau_1) \dots x(t-\tau_n) \right]$$

where $\{G_1\}$ are the Wiener orthogonal functionals.

In the calculation of the kernels by cross correlation methods, there are several sources of error which coexist. We will examine the effect of each one separately, assuming at each stage that the other error sources do not exist.

There is a statistical error (kernel values are statistical averages) in the kernel (crosscorrelation) evaluation associated with the finiteness of the record length (finite sample). The standard deviation of the computed average from the true average gives an estimate of the statistical error.

Assume we are trying to measure $h_1(\tau)$ which is the average of the random variable $[y(t)x(t-\tau)]$. Let us call the computed estimate $\hat{h}_1(\tau)$. Then, if we use M independent samples of this random variable

$$(1) \quad \text{var}(\hat{h}(\tau)) = \frac{1}{M} \text{var}(y(t)x(t-\tau))$$

where $\text{var}(\hat{h}(\tau))$ is the variance of the computed average and $\text{var}(y(t)x(t-\tau))$ is the standard deviation of the random variable whose average we want to estimate.

As before, the record has N samples but only M of them ($M < N$) are independent. As we will see shortly, M depends on the noise bandwidth and the system memory. We get an estimate of $\text{var}(y(t)x(t-\tau))$ from the record itself by computing

$$\hat{\text{var}}(y(t)x(t-\tau)) = \frac{1}{N} \sum_{i=1}^N \left[y(t_i)x(t_i-\tau) - \sum_{i=1}^N (y(t_i)x(t_i-\tau)/N) \right]^2$$

which finally becomes

$$(2) \quad \hat{\text{var}}(y(t)x(t-\tau)) = \frac{1}{N} \sum_{i=1}^N [y(t_i)x(t_i-\tau)]^2 - \left[\frac{1}{N} \sum_{i=1}^N y(t_i)x(t_i-\tau) \right]^2$$

Thus, from the record and using (2), we can obtain an estimate of $\text{var}(y(t)x(t-\tau))$.

Then, to calculate the $\text{var}(\hat{h}(\tau))$ we need to know the number M of independent samples of $(y(t)x(t-\tau))$ because the estimation of a statistical average for a certain accuracy requires a certain number of independent samples. In turn, this requires a knowledge of time interval (t_2-t_1) for which $(y(t_2)x(t_2-\tau))$ and $(y(t_1)x(t_1-\tau))$ are independent. The quantity (t_2-t_1) depends on the bandwidth f_w of the noise and the system memory, μ . The time interval for which successive input noise samples are independent is $1/f_w$. Then, if

$$\alpha = \max\left(\frac{1}{f_w}, \mu\right)$$

the quantity (t_2-t_1) is equal to 2α , and the length, R , of the required input-output record is

$$(3) \quad R = 2 \cdot \alpha \cdot M$$

where M is chosen large enough (about 100) to produce a small variance of estimate $\hat{h}_1(\tau)$ (see equation (1)). Usually μ is much larger than $1/f_w$ and therefore is the determining factor (except for a no-memory system).

The number of samples, N , of the record, on the other hand, is determined by the $\min\left(\frac{1}{f_w}, \mu\right)$ (because of aliasing) and therefore is given by

$$(4) \quad N = 2.M. \max \left\{ \frac{1}{f_w}, \mu \right\} / \min \left\{ \frac{1}{f_w}, \mu \right\} .$$

Let us consider now the question of statistical accuracy as related to the input noise bandwidth. First, there is an error due to aliasing since we use sampled records instead of continuous ones for the calculations. If the sampling rate is kept constant the aliasing error increases with increasing bandwidth [5,69].

Second, for a given number N of samples the variance of the correlation estimate will increase by increasing the noise bandwidth if we also increase the sampling rate to account for (no aliasing) the expanded bandwidth. This is due to the fact that for a given N the $\min \left\{ \frac{1}{f_w}, \mu \right\}$ is usually smaller for the larger bandwidth and therefore M is smaller (since N is constant).

Third, we will show that the variance of the correlation estimates increases with increasing the noise bandwidth. Again, we will consider $h_1(\tau)$ and the generalization to $h_n(\tau_1, \dots, \tau_n)$ can be made easily. The variance of $h_1(\tau)$ is given by

$$\sigma_h^2 = \text{var}[y(t)x(t-\tau)] = \text{var}\left[x(t-\tau) \int h(\nu)x(t-\nu)d\nu \right]$$

assuming that the system is linear with impulse function $h(\nu)$.

(If higher order kernels existed in the system they would be treated in the same way). We have

$$(5) \quad \sigma_h^2 = E \left\{ \left[x(t-\tau) \int h(\nu)x(t-\nu)d\nu \right]^2 \right\} - \left\{ E \left[x(t-\tau) \int h(\nu)x(t-\nu)d\nu \right] \right\}^2$$

or

$$(6) \quad \sigma_h^2 = \iint h(\nu)h(\mu) \cdot E\{x(t-\tau)x(t-\tau)x(t-\nu)x(t-\mu)\} d\nu d\mu - \\ \{ \int h(\nu) E[x(t-\tau)x(t-\nu)] d\nu \}^2 .$$

The average of the product of four gaussian variables can be written as

$$E\{x(t-\tau)x(t-\tau)x(t-\nu)x(t-\mu)\} = E\{x(t-\tau)x(t-\tau)\} \cdot E\{x(t-\nu)x(t-\mu)\} + \\ + E\{x(t-\tau)x(t-\nu)\} \cdot E\{x(t-\tau)x(t-\mu)\} + E\{x(t-\tau)x(t-\mu)\} \cdot E\{x(t-\tau)x(t-\nu)\}$$

and the second term of (6) can be written as

$$\int \int h(\nu)h(\mu) \cdot E\{x(t-\tau)x(t-\nu)\} \cdot E\{x(t-\tau)x(t-\mu)\} \cdot d\nu .$$

Then, finally we can get

$$(7) \quad \sigma_h^2 = \text{var}(x) \iint h(\mu)h(\nu)\phi(\mu-\nu)d\mu d\nu + \left[\int_0^\infty h(\nu)\phi(\tau-\nu)d\nu \right]^2$$

where

$$\phi(u) = \frac{\omega_0}{\pi} \cdot \frac{\sin(\omega_0 u)}{(\omega_0 u)}$$

is the autocorrelation of input noise $x(t)$ and ω_0 is the bandwidth of this noise.

We propose that σ_h^2 increases as the noise bandwidth ω_0 increases. Let us consider some typical systems. Assume $h(\nu) = e^{-\alpha\nu}$ (i. e., the first-order linear system with Laplace transform $1/(s+\alpha)$). Then, from equation (7), we find that (after some approximations) the variance σ_h^2 increases at least as fast as $\text{arctg}(\omega_0/\alpha)$ with the noise bandwidth ω_0 (see [27], p. 489).

A revealing case is the identity system for which $h(\nu) = \delta(\nu)$.

Then, from (7),

$$\sigma_h^2 = \text{var}(x) \cdot \frac{\omega_0}{\pi} + \left(\frac{\omega_0}{\pi} \right)^2 ;$$

that is, the variance increases with the square of the noise bandwidth ω_0 .

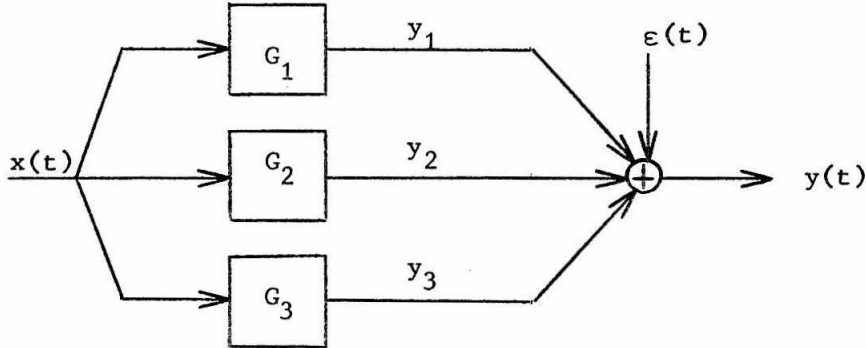
Therefore, it is very plausible that the statistical error will increase if the input noise bandwidth increases. On the other hand, as shown in the previous section, the input noise bandwidth should cover completely the whole frequency range of the system response. We conclude that the input noise bandwidth should be larger than the system bandwidth but should not extend much (about one octave) beyond it.

The power level of the flat portion of the input spectrum should be set equal to 1 (0 db). This normalization is necessary for the following reason. Kernel $h_n(\tau_1, \dots, \tau_n)$ and cross-correlation $\phi_{yxx \dots x}(\tau_1, \dots, \tau_n)$ are related through factor $1/P^n$ where P is the power level of the input noise. Let us examine the dependence of the per unit change of this factor on P . We have

$$\frac{\frac{d}{dP} (1/P^n)}{1/P^n} = -\frac{n}{P}.$$

For $n = 1$ we note that $P = 1$ will result in a per unit change equal to -1 . Therefore, positive and negative errors in the value of P will get 'amplified' the same amount and will tend to cancel out. For $n = 2$ we would have the same effect if $P = 2$. Therefore, a value of P between 1 and 2 will tend to minimize the error resulting from choosing a single value for P in evaluating the kernels. In all of this work we chose P to be 1 because the first-order kernel was deemed the most important and therefore we desired good accuracy for it.

Noise present at the input or at the output or internally in the system could be a serious source of error. We investigate the effect of such noise on the cross-correlation estimates, starting with the case of noise at the output.



Assume $x(t)$ is gaussian white noise and $\phi_{xx}(\tau) = P\delta(\tau)$. Let us make $P = 1$.

To estimate $h_1(\tau)$ we need to estimate $\phi_{yx}(\tau)$:

$$\begin{aligned} \phi_{yx}(\tau) &= E\{x(t-\tau)y(t)\tau\} \\ &= E\{x(t-\tau)[y_1(t)+y_2(t)+y_3(t)+\epsilon(t)]\} \\ &= E\{x(t-\tau)y_1(t)\}+E\{x(t-\tau)y_2(t)\}+E\{x(t-\tau)y_3(t)\}+E\{x(t-\tau)\epsilon(t)\} \\ &= h_1(\tau) + \phi_{x\epsilon}(\tau) \end{aligned}$$

Thus, in general, the error in $h_1(\tau)$ for any τ is

$$(8) \quad \text{error} = \phi_{x\epsilon}(\tau) .$$

Even if the system had higher order nonlinearities (h_4, h_5, h_6, \dots) their contribution to $\phi_{yx}(\tau)$ would be zero because their corresponding functionals would be orthogonal to a gaussian white $x(t)$.

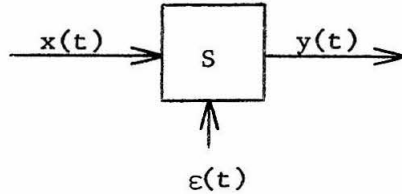
If $x(t)$ and $\epsilon(t)$ are independent, then

$$\phi_{x\epsilon}(\tau) = E\{x(t)\} \cdot E\{\epsilon(t)\} = 0 ,$$

and then

$$\phi_{yx}(\tau) = h_1(\tau) .$$

Let us now consider a case of internal noise which can be considered to be "noise at the output." Input $\epsilon(t)$ is added to the output after it passes through a filter with impulse response $g(\tau)$.



Then,

$$y(t) = \int h_1(\tau)x(t-\tau)d\tau + \int g(\tau)\epsilon(t-\tau)d\tau ,$$

which means that possibly the noise $\epsilon(t)$ follows a different path through the system than the input, in contaminating the output $y(t)$.

We assume this to be a linear path. We have:

$$\begin{aligned} \phi_{yx}(\tau) &= E\{x(t-\tau) [\int h_1(v)x(t-v)dv + \int g(v)\epsilon(t-v)dv]\} \\ &= \int h_1(v)\phi_{xx}(\tau-v)dv + \int g(v)\phi_{x\epsilon}(\tau-v)dv \\ &= h_1(\tau) + \int g(v)\phi_{x\epsilon}(\tau-v)dv . \end{aligned}$$

If $x(t)$ and $\epsilon(t)$ are independent, then $\phi_{x\epsilon}(\tau) = E\{x(t)\} \cdot E\{\epsilon(t)\} = 0$.

Thus, we see that even in this case the error is zero if the input and the noise are independent. Otherwise, the error for any τ is given by

$$(9) \quad \text{error} = \int_0^{\infty} g(v)\phi_{x\epsilon}(\tau-v)dv .$$

If the system under study is linear (only $h_1(\tau)$ is nonzero), then it is seen that the determination of the impulse response by the white-noise method has a serious advantage over the conventional methods. Provided that the contaminating noise is independent of the input white noise, the determination of the impulse response is unaffected by the presence of such internal or external noise.

Let us now compute $h_2(\tau_1, \tau_2)$. First, we need to compute the linear response of the system due to $h_1(\tau)$ and subtract it from the total response. Assume that, as shown before, we computed

$$h_1^*(\tau) = h_1(\tau) + \delta_1(\tau)$$

where $h_1(\tau)$ is the true h_1 and $\delta_1(\tau)$ is the error for any τ . Then,

$$y_{\text{linear}} = \int [h_1(\tau) + \delta_1(\tau)] x(t-\tau) d\tau = y_1(t) + y_\delta(t) .$$

To find $h_2(\tau_1, \tau_2)$ we compute the second-order cross-correlation

$$\begin{aligned} \phi_{y_{\text{xxx}}}(\tau_1, \tau_2) &= E\{[y(t) - y_{\text{linear}}(t)]x(t-\tau_1)x(t-\tau_2)\} \\ &= E\{[\epsilon(t) + y_2(t) + y_3(t) - y_\delta(t)]x(t-\tau_1)x(t-\tau_2)\} . \end{aligned}$$

Consider each term separately:

$$I_1 = \int \epsilon(t)x(t-\tau_1)x(t-\tau_2)dt = \phi_{\text{xxx}\epsilon}(\tau_1, \tau_2)$$

$$\begin{aligned} I_2 &= -E\{y_\delta(t)x(t-\tau_1)x(t-\tau_2)\} \\ &= -E\left\{\int \delta_1(v)x(t-v)dv x(t-\tau_1)x(t-\tau_2)\right\} \\ &= -\int \delta_1(v) \cdot E\{x(t-v)x(t-\tau_1)x(t-\tau_2)\}dv . \end{aligned}$$

The expected value of the product of an odd number of gaussian variables is zero. Therefore,

$$I_2 = 0$$

$$\begin{aligned}
 I_3 &= E\left\{\iint h_2(v_1, v_2)x(t-v_1)x(t-v_2)dv_1 dv_2 \cdot x(t-\tau_1)x(t-\tau_2)\right\} \\
 &= \iint h_2(v_1, v_2)[\delta(v_1-v_2)\delta(\tau_1-\tau_2)+\delta(v_1-\tau_1)\delta(v_2-\tau_2)+ \\
 &\quad +\delta(v_1-\tau_2)\delta(v_2-\tau_1)]dv_1 dv_2 \\
 &= \delta(\tau_1-\tau_2)\int h_2(v_1, v_1)dv_1+h_2(\tau_1, \tau_2)+h_2(\tau_1, \tau_2) \ .
 \end{aligned}$$

But $\int h_2(v_1, v_1)dv_1 = 0$ because we made the constant $h_0 = 0$.

Similarly, the term $E\{y_3(t)x(t-\tau_1)x(t-\tau_2)\}$ is zero because of the orthogonality of the Wiener G-functionals. In fact, even if the system had higher order nonlinearities, their contribution to $\phi_{yxx}(\tau_1, \tau_2)$ would be zero.

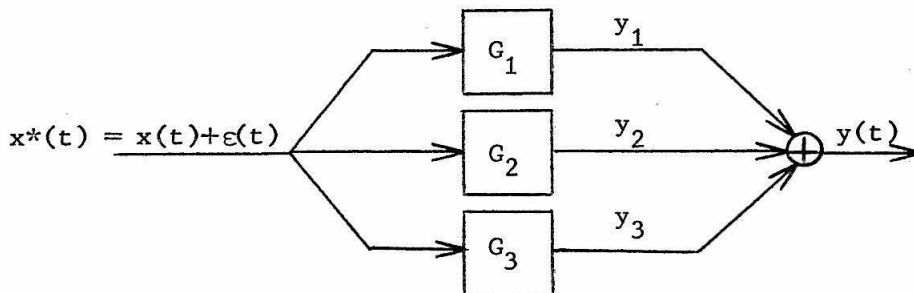
So, clearly, the error term for $\phi_{yxx}(\tau_1, \tau_2)$ is $\phi_{xx\epsilon}(\tau_1, \tau_2)$ for any (τ_1, τ_2) independent of the order of nonlinearity of the system. In general, the error for the n^{th} order cross-correlation

$\phi_{yx\dots x}(\tau_1, \tau_2, \dots, \tau_n)$ is

$$(10) \quad \text{error} = \phi_{xx\dots x\epsilon}(\tau_1, \tau_2, \dots, \tau_n) \ .$$

If $x(t)$ and $\epsilon(t)$ are independent, then we can decompose $\phi_{xx\dots x\epsilon} = E\{xx\dots x\} \cdot E\{\epsilon\}$, and the error becomes zero for odd-order kernels.

Let us now consider the error introduced by the contamination of the input by noise.



To estimate $h_1(\tau)$ we need to calculate $\phi_{yx}(\tau)$:

$$\phi_{yx}(\tau) = E\{x^*(t-\tau)y(t)\} = E\{x^*(t-\tau)[y_1(t)+y_2(t)+y_3(t)]\} .$$

Let us consider each term separately.

$$\begin{aligned} I_1 &= \int x^*(t-\tau)y_1(t)dt \\ &= \int [x(t-\tau)+\epsilon(t-\tau)] \int h_1(v)[x(t-\tau)+\epsilon(t-v)]dv dt \\ &= \int h_1(v)dv [\phi_{xx}(\tau-v)+\phi_{x\epsilon}(\tau-v)+\phi_{\epsilon x}(\tau-v)+\phi_{\epsilon\epsilon}(\tau-v)] . \end{aligned}$$

In the case that $x(t)$ deviates considerably from white noise, and/or the noise $\epsilon(t)$ is significantly large, $h_1(\tau)$ can be found more accurately by solving this integral equation using Fourier transforms or numerical methods. Considering that the right hand side is a sum of convolution integrals, the use of Fourier transforms gives a simple solution.

If $x(t)$ does not deviate from whiteness, then

$$(11) \quad I_1 = h_1(\tau) + \int h_1(v) [\phi_{x\epsilon}(\tau-v) + \phi_{\epsilon x}(\tau-v) + \phi_{\epsilon\epsilon}(\tau-v)] dv$$

$$\begin{aligned} I_2 &= E\{x^*(t-\tau)y_2(t)\} \\ &= E\{[x(t-\tau)+\epsilon(t-\tau)] \iint h_2(v_1, v_2) x^*(t-v_1) x^*(t-v_2) dv_1 dv_2\} \end{aligned}$$

which, after some manipulation, becomes

$$\begin{aligned} I_2 &= \iint h_2(v_1, v_2) [\phi_{xxx}(\tau-v_1, \tau-v_2) + \phi_{xx\epsilon}(\tau-v_1, \tau-v_2) + \phi_{x\epsilon x}(\tau-v_1, \tau-v_2) + \\ &\quad + \phi_{x\epsilon\epsilon}(\tau-v_1, \tau-v_2) + \phi_{\epsilon xx}(\tau-v_1, \tau-v_2) + \phi_{\epsilon x\epsilon}(\tau-v_1, \tau-v_2) \\ &\quad + \phi_{\epsilon\epsilon x}(\tau-v_1, \tau-v_2) + \phi_{\epsilon\epsilon\epsilon}(\tau-v_1, \tau-v_2)] \cdot dv_1 dv_2 . \end{aligned}$$

Note that it can be shown easily that

$$\phi_{x\epsilon\epsilon}(\tau_1, \tau_2) = \phi_{\epsilon x\epsilon}(-\tau_1, \tau_2 - \tau_1) .$$

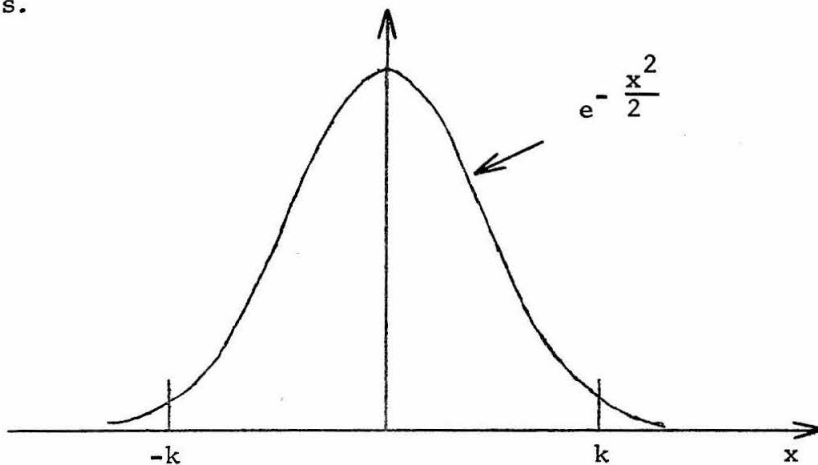
Therefore, we only need to measure one of these ϕ 's for any permutation of (x, ϵ, ϵ) .

I_3 has a similar expression. Skipping the calculus steps,

$$I_3 = \int \int \int h_3(v_1, v_2, v_3) [\phi_{xxxx}(\tau - v_1, \tau - v_2, \tau - v_3) + \phi_{xx\epsilon x} + \phi_{x\epsilon xx} + \phi_{x\epsilon\epsilon x} + \phi_{xxx\epsilon} + \phi_{xx\epsilon\epsilon} + \phi_{x\epsilon\epsilon\epsilon} + \phi_{\epsilon xxx} + \phi_{\epsilon x\epsilon x} + \phi_{\epsilon\epsilon xx} + \phi_{\epsilon\epsilon\epsilon x} + \phi_{\epsilon xx\epsilon} + \phi_{\epsilon x\epsilon\epsilon} + \phi_{\epsilon\epsilon\epsilon\epsilon}] \cdot dv_1 dv_2 dv_3 .$$

We conclude that the error terms increase with the order of nonlinearity of the system, and they are given as convolutions of signal - error correlations with the Wiener kernels. This suggests that errors at the input are much more serious than errors at the output.

Let us examine one such error that occurs naturally during a white-noise experiment. This is the error introduced by the truncation at the gaussian distribution at very low and very high input signal levels.



That is, the input signal is not an ideal gaussian, but is defined by

$$P_r(x) = \begin{cases} \frac{1}{\sqrt{2\pi}} e^{-\frac{x^2}{2}} & \text{if } |x| \leq K \\ 0 & \text{if } |x| > K \end{cases}$$

Then, we define the experimental input $x^*(t)$ by $x^*(t) = x(t) + \epsilon(t)$ where $x(t)$ is ideally gaussian and

$$\epsilon(t) = \begin{cases} 0 & \text{if } |x(t)| < K \\ K - x(t) & \text{if } x(t) > K \\ -K - x(t) & \text{if } x(t) < -K \end{cases}$$

Then, from the formulas just derived, we see that the error depends on terms such as $\phi_{x\epsilon}(\tau)$, $\phi_{\epsilon\epsilon}(\tau)$. We have

$$\phi_{x\epsilon}(\tau) = E[x(t) \cdot \epsilon(t+\tau)] ,$$

and assuming $x(t)$ to be ideal white noise (infinite bandwidth), we get

$$\phi_{x\epsilon}(\tau) = C_K \cdot \delta(\tau)$$

where

$$C_K = \frac{2}{\sqrt{2\pi}} \int_0^{\infty} (Kx - x^2) e^{-\frac{x^2}{2}} dx$$

and

$$\phi_{\epsilon\epsilon}(\tau) = D_K \cdot \delta(\tau)$$

where

$$D_K = \frac{2}{\sqrt{2\pi}} \int_K^{\infty} (K-x)^2 e^{-\frac{x^2}{2}} dx .$$

Therefore (neglecting higher order kernels), the error in the estimate of $h_1(\tau)$ is of the order of

$$\text{error} = C_K + D_K = \frac{2}{\sqrt{2\pi}} \int_K^{\infty} (K^2 - Kx) e^{-\frac{x^2}{2}} dx .$$

The experimental apparatus produces a gaussian that is truncated at about three standard deviations (i. e., $K = 3$). Then the above integral gives

$$\text{error} \simeq 0.02 ,$$

which is, indeed, small compared to 1.

We conclude that the error introduced by the truncation of the gaussian signal is very small for truncations at about three deviations or above.

In any case, we compute $h_1^*(\tau) = h_1(\tau) + \delta_1(\tau)$, where $h_1(\tau)$ is the true first-order kernel and $\delta_1(\tau)$ the error for any τ .

The response of the system due to the linear kernel is

$$y_{\text{linear}} = \int h_1^*(\tau) x^*(t-\tau) d\tau = \int [h_1(\tau) + \delta_1(\tau)] x^*(t-\tau) d\tau = y_1(t) + y_\delta(t) .$$

Subtracting the linear response from the total response, we obtain for the second order cross-correlation,

$$\phi_{y_{\text{xxx}}}(\tau_1, \tau_2) = E\{[y_2(t) + y_3(t) - y_\delta(t)] x^*(t-\tau_1) x^*(t-\tau_2)\} .$$

Again, let us consider each term separately:

$$\begin{aligned} I_1 &= -E\{y_\delta(t)[x(t-\tau_1) + \epsilon(t-\tau_1)][x(t-\tau_2) + \epsilon(t-\tau_2)]\} \\ &= -E\left\{\int \delta_1(v)[x(t-v) + \epsilon(t-v)][x(t-\tau_1) + \epsilon(t-\tau_1)][x(t-\tau_2) + \epsilon(t-\tau_2)] dv\right\} \\ &= -\int \delta_1(v) [\phi_{\text{xxx}}(v-\tau_1, v-\tau_2) + \phi_{\text{x}\epsilon\text{x}} + \phi_{\text{\epsilon}\text{x}\text{x}} + \phi_{\text{\epsilon}\epsilon\text{x}} + \phi_{\text{x}\text{x}\epsilon} + \phi_{\text{x}\epsilon\epsilon} + \phi_{\text{\epsilon}\text{x}\epsilon} + \phi_{\text{\epsilon}\epsilon\epsilon}] dv . \end{aligned}$$

The expressions for I_2 , I_3 are similar.

We notice that the number of error terms increases with the order of the computed kernel. The exact determination of the error depends solely on the correlations of $x(t)$ with $\epsilon(t)$ which can be de-

terminated by investigating $\epsilon(t)$ at the start of the experiment.

In conclusion, errors occurring at the input are more serious than errors occurring at the output or internally and adding to the output. Errors at the input, in general, will produce error terms which tend to increase with the order of the computed kernel and with the order of the nonlinearity of the system. Errors at the output, in general, will produce error terms which do not increase with increasing of either of the above-mentioned orders.

There are additional errors due to the numerical approximation of the integrals and errors resulting from the un-Gaussianness and un-whiteness of the input. If the deviations from Gaussianness and whiteness are severe, then the kernel must be found as solutions of integral equations.

5. Conclusions

The experimental characterization of a system by the white-noise method is possible, but some preliminary calculations and experiments should be made in order to plan the computation intelligently and to reduce the effort required.

The main difficulty is the fact that computation time increases almost exponentially with the order of the computed kernel. Given that we are willing to spend a certain amount of computing time, we can only treat systems whose nonlinearities allow a Wiener representation using only the first few terms. This excludes systems with "sharp" nonlinearities such as thresholds, sharp limiters, etc., even though we can still treat these systems approximately, and in

many cases profitably.

Since the terms of the Wiener series are orthogonal to each other, the model representation improves (in the mean error square sense) with the addition of each term. Moreover, as each new kernel is calculated and the corresponding term added to the series, it is not necessary to re-evaluate the previously determined kernels in order to improve the characterization because of the orthogonality of the model. In fact, it can be shown easily that if the series is truncated after the n^{th} term, the resulting approximation is the best n^{th} order characterization in the mean square error sense.

Examination of the nonlinear kernels can reveal nonlinear characteristics of the system such as facilitation and refractoriness of neuron chains, saturation, rectification, and others. If there is structural evidence (which is sometimes the case in neuronal systems) as to the composition of the system in terms of a cascade combination of two subsystems (linear and nonlinear), examination of the linear and nonlinear kernels can reveal the order of this sequence, that is, whether it is linear - nonlinear or nonlinear - linear [81].

The derived model is in the form of a truncated Wiener series. It can be put in several other forms according to one's inclinations or in order to serve a specific purpose. One such form is in terms of linear filters and multipliers [73]. In any case, the use of the model to predict the response to a certain input is simple, straightforward, and numerically quick and stable.

CHAPTER IV
MATERIALS AND METHODS

1. Structure of the Retina

The vertebrate retina has five building elements: the receptors, bipolar cells, horizontal cells, amacrine cells and ganglion cells. Although there are many sub-classifications, all neurons in the retina fall into one of these five classes. The vertebrate retina has a layered structure and these neurons form specific layers: the receptor nuclei form the external nuclear layer; the bipolar cell, horizontal cell and amacrine cells form the inner nuclear layer and the ganglion cells occupy the most proximal layer of the retina [85].

In the inner nuclear layer, the distal layers are occupied by the horizontal cells while the proximal layer is occupied by the somata of the amacrine cells. The neurons in these three nuclear layers form an extensive connecting network. The layers where complex contacts are made between the neurons in adjacent nuclear layers are called plexiform layers; the external plexiform layer is the site of connection of the receptors with the bipolar and horizontal cells, whereas the inner plexiform layer is the site of contact of the ganglion cells with the three classes of neurons in the inner nuclear layer [85].

During the last few years we have seen two breakthroughs which greatly facilitated the study of the retina; first, the advance made in the dye injection technique and second, the intra-retinal stimulation [4,34,35,62,63,83,91]. The use of these two techniques has clarified many issues which have been subjects of controversy.

We describe briefly the morphology and function of these five classes of neurons.

2. The Receptors:

These are neurons which convert the energy carried by light into electro-chemical energy. The receptors contain photosensitive pigments which absorb the incident photons [32a,71]. Structurally, a receptor consists of three main parts: the outer segment where photons are caught, the cell body, and the receptor base where the signal produced by the receptor is relayed to the second order neurons.

The most ubiquitous visual pigment is the rhodopsin or Vitamin A aldehyde coupled to the opsin. The retinal is in a form of 11-cis and the only action of light is to convert this form into a 11-transform [71].

The rhodopsin which has absorbed a photon splits into two elements, retinal and opsin, following a series of discrete steps. Somewhere in these series of transformations, it is coupled to a process which increases the impedance of the receptor membrane. This increase in the impedance gives rise to a hyperpolarization of the receptor cell membrane (it is accepted now that the receptor cell hyperpolarizes by photic stimulus [88]).

3. Bipolar Cells:

The bipolar cells are the classical second order neurons which connect the receptors with the ganglion cells. The bipolar cells have a dendritic expansion which spreads laterally in the external plexiform layer. The axonal processes extend down to the inner plexiform layer

where arborizations are seen at several discrete levels. Rods are thought to be associated with the large field bipolar cell whereas cones are thought to be associated with the small field bipolar cells [85].

Recent studies with dye injecting electrodes have revealed that the bipolar cells give rise to a slow potential change in response to a stimulus. The polarity of the potential change is a function of the spatial distribution of light over the retina [34,64,91].

4. The Horizontal Cells

There are one to four layers of horizontal cells in the vertebrate retina and they form the distal layer of the inner nuclear layer. In an animal such as the frog or the cat the horizontal cells form a single layer while in some teleosts at least four layers can be seen. In this case, the horizontal cells occupy more than 2/3 of the entire inner nuclear layer.

In the teleost, cones are connected to the cone horizontal cell while rods are connected to the rod horizontal cell [84]. In the mammal both rods and cones are connected to a single horizontal cell [39,82]. The horizontal cells are referred to as the external, intermediate and internal horizontal cells according to their locations in the inner nuclear layer. In the teleost retina there is one more class of horizontal cells called 'snaky' or 'crazy' cells as no description of their nucleus or dendritic extension has yet been obtained [64,84,94].

The horizontal cells give rise to a slow potential change in response to stimulus [86]. In the case where light of any wavelength hyperpolarizes the cell, it is called L-type (or luminosity type)

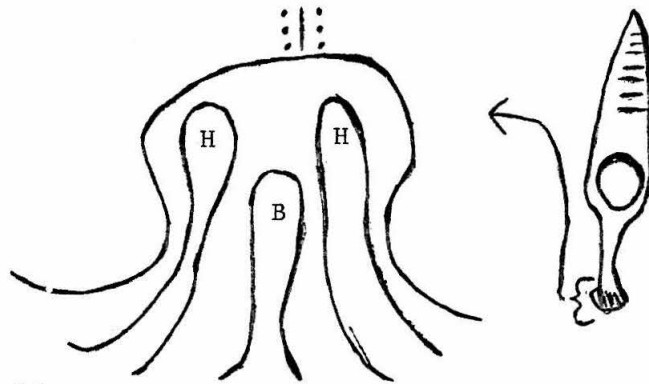
horizontal cell. In the case where light of some wavelength depolarizes the cell while light of other wavelength hyperpolarizes the cell, it is called a C-type (or color type) horizontal cell [45]. The most outstanding functional feature of the horizontal cell is that its potential can spread across many cells over a large retinal area [26, 58,68,83]. It was established that this spread was not due to spread of light. There are two schools of thought on the mechanism of the lateral spread of the horizontal cell potential; one school suggests that a chemical reaction is responsible for the lateral spread [65,66], while the other stipulates that the layer of horizontal cells can be approximated by a laminar structure of low resistivity in the intralaminar space through which the potential can propagate with little attenuation [58,64]. As in the receptors, an increase in the impedance of the horizontal cell membrane seems to be responsible for a hyperpolarizing response.

5. Amacrine Cells

Amacrine cells are literally axon-less neurons located at the innermost layers of the inner nuclear layer. They send dendritic expansions of various shapes into the inner plexiform layer. According to the shape of the extension the amacrine cell can be classified into groups such as the basket type, brush type or diffuse type. Polyah first suggested that the amacrine cells might be involved in the lateral transmission of signals in the retina. By dye injection it was revealed that the amacrine cells give rise to spike potentials superposed on a slow potential change. Not much is known about the amacrine cells [34,91].

6. Ganglion Cells

The ganglion cells form the last stage in the vertebrate retina. Their axons reach the lateral geniculate body wherefrom the signal is fed into the central nervous system. The ganglion axons carry spike discharges. The ganglion cells send their dendritic trees into the inner plexiform layer where they make complex contacts with the bipolar and amacrine processes. The ganglion cells are classified into several types according to the shape of their dendritic trees. The synaptic connections of the outer plexiform layer (among receptor, horizontal and bipolar cells) have the following configuration. Each rod and cone forms a proximal terminal called a spherule and a pedicle respectively. Inside a spherule or a pedicle is a complex structure composed of the bipolar dendrites and horizontal cell dendrites. The simplest schematic model of this structure is as shown below [84,85],



7. Receptive Field

In 1940 Hartline [30] showed that a retinal ganglion cell receives signals from a very large retinal area. A spot of light placed 1-2mm away from the spike recording site (presumably the location of the electrode) could still excite the ganglion cell. This sensitive area is called the receptive field of a ganglion cell and is roughly circular

in shape.

In 1952 Kuffler [40] made another important observation. He showed (in the cat) that the receptive field is not a uniform area but is organized in two concentric discs, one called the receptive field center and the other the surround of the receptive field. In one type of unit a response is observed to the onset of a light stimulus at the center, while the same stimulus causes a response at the offset of light if the stimulus is delivered to the surround. This is an 'ON-center' (OFF-surround) unit. There is a complementary unit called an 'OFF-center' (ON-surround) unit. The center and surround do interact to give rise to a complex response pattern. Obviously a stimulus which give rise to an 'OFF' discharge acts as a depressor. Later, various receptive field types such as a color coded or double opponent fields have been described [33a,90]. However, the concentric field is the most basic unit in the visual pathways. It is easy to imagine that there are two concentric and overlapping areas, one excitatory and one inhibitory which give rise to a concentric field. This is the model proposed by Rodieck and Stone [70a].

During the past few years it has become possible to record responses from the bipolar cells. In all bipolar cells so far examined (except in the mudpuppy) it has been shown that they also possess a concentric receptive field, i.e. a central spot of light gives rise to a polarization of one polarity and a surround gives rise to a response of the opposite polarity [34]. If a spot gives rise to a depolarization it is called an 'ON-center' bipolar cell. If a spot gives rise to a hyperpolarization it is called an 'OFF-center' bipolar cell.

There is evidence to show that the amacrine cells form a complex receptive field. But the field is more complex and subtly organized.

8. Catfish Retina

The catfish is a teleost of older origin. They bear no scales and have a pair of whiskers. The catfish is a bottom feeder. The channel catfish inhabits clearer water and is known as the chick of the channel.

Detwiler [14b] lists the dimensions of the layer of the vertebrate retina. The catfish retina had the least developed inner plexiform layer suggesting a rather simple retinal transformation of the optical information. Morphologically the catfish retina does not differ drastically from the retinas so far examined.

The catfish retina has cones and rods. There are three layers of horizontal cells in the retina [K. Naka, personal communication]. The external horizontal cells form the outermost layer. It has been shown functionally that the external horizontal cells receive signals from 625 ^{nm} ~~nm~~ cones [60,61]. The intermediate horizontal cells are very thin and inconspicuous. No electrical activity has been recorded from this class of horizontal cells. The third class - the 'snaky' horizontal cells - is not a true horizontal cell according to the morphological definition [84,85]. This horizontal cell runs between the layer of the true horizontal cells and the layer of amacrine cells. They do not take a straight course but often bend into the horizontal layers. Although its nucleus has been located no dendrite has been observed. The electrical responses have been recorded for the snaky horizontal cell [N. Matsumoto, personal communication].

The catfish external plexiform layer is the thinnest one so far reported [14b]. No other structural details have yet been examined.

9. Experimental Methods

All experiments described in this thesis utilized the retina of the catfish (Ictalurus punctatus) and were performed by Dr. Ken Naka. The preparation of the retina and the recording techniques have been described by Naka and his associates [55,61,63]. In this work the following stimulus-response experiment were performed:

<u>Stimulus</u>	<u>Response</u>
Light	(extracellular) receptors (mass response)
Light	(intracellular) horizontal cell
(Current injected into horizontal cell)	(extracellular) ganglion cell
Light	(extracellular) ganglion cell
Light	ERG

Fig. 4.1 shows a schematic diagram of the catfish retinal neurons and indicates the stimulating and recording sites for the systems under study in this work.

The stimulus and response data were recorded on magnetic tape (to be later transmitted to a digital computer) and also by a pen writer for preliminary screening of results. The optical system has been described by Naka and Nye [61]. The light source was a Sylvania glow modulator 1B59/R-1130B.

White-noise of limited bandwidth was obtained by the following process. A type 1390-B Random-Noise Generator (General Radio Company, West Concord, Mass.) was used which produces a gaussian random signal that has a flat power spectrum from 5Hz to 500 KHz (five decades of frequency). This electrical signal was recorded on magnetic tape (AMPEX FR-1300) and subsequently copied on another tape at a much slower speed. This process of copying at a slower speed was repeated until the bandwidth of the resulting signal was in the desired range for our systems (essentially d.c. up to 25 Hz or 50 Hz flat power spectrum).

10. Data Processing

The data processing system is shown in schematic form in Fig. 4.2. This system has been developed at the California Institute of Technology and has been extensively used for processing biological data [1,18,24,48,49]. A detailed description can be found in [18,44,50].

LORI is basically a special-purpose computer and multi-channel A/D converter preprocessing the experimental data for on-line transmission to the control computer (IBM 360/44). Continuous signals such as the white-noise inputs and slow potentials were sampled at a rate of 250Hz and transmitted to the central processor where they were stored in auxiliary memory (2314 disc units). Neural spike data such as the ganglion response were transmitted and stored in the TOE (Time of Event) mode which catalogs the time of occurrence of a neuron firing. TOE data were transmitted at a clock rate of 50KHz corresponding to an accuracy of 20 microseconds.

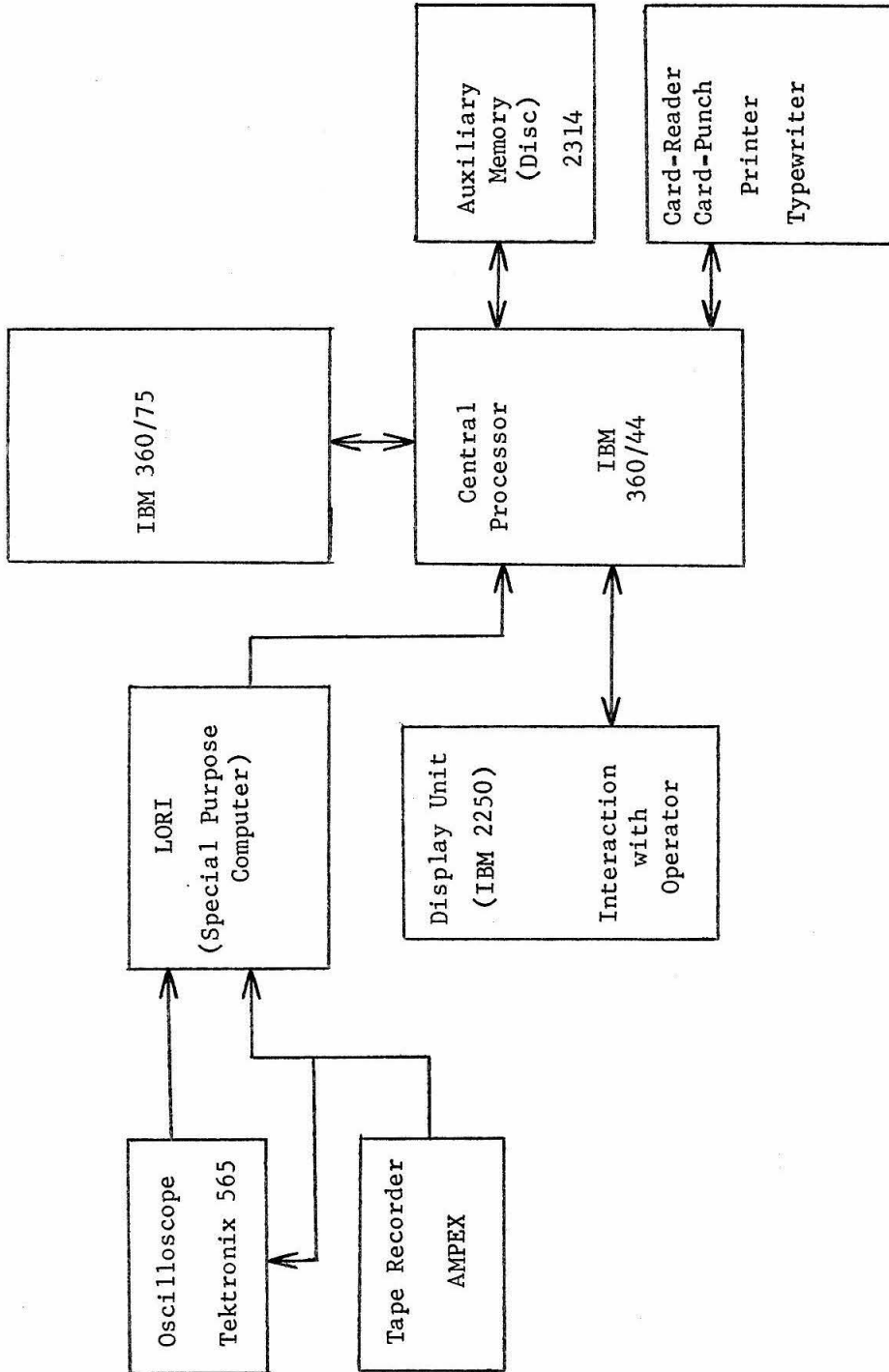


Fig. 4.2. Schematic diagram of the data processing system.

The next step in the data processing procedure involved interaction with the central computer (IBM 360/44) through the IBM 2250 display terminal. This interaction included "eyeballing" of the data and qualitative determination of some features of the input and output records (drift of the average value, nonlinearities, etc.). Preliminary analysis such as auto and cross-correlations and histogramming were also performed at this stage. In general, the interactive nature of the system proved a valuable system feature at this stage.

In the case of the TOE data obtained from the ganglion response the following procedure was followed in order to convert these records into continuous functions of time. The white-noise stimulus record was formed by concatenating ten identical white-noise records. The ganglion responses to the ten runs of identical white-noise were superimposed and histogrammed in time to produce a PST (post-stimulus time) histogram of the ganglion discharge in response to this white-noise input. Thus the ganglion response was converted to a continuous function of time and the difficulty of dealing with the discrete spike events was overcome. Such a procedure resulted in a waveform with some artificially introduced high frequencies which were subsequently filtered out (smoothing) through the use of an appropriate Hanning window [5]. Specifically,

$$y(t_i) = 0.5 y(t_i) + 0.25[y(t_{i-1}) + y(t_{i+1})] \quad .$$

The input and output data were then treated for reduction of long-term drifts. This was accomplished first through 'eyeballing' which indicated the type of drift and second through subtracting the

appropriate mean square curve. Such curves, variably used, included linear trends ($a + bt$), parabolas ($a + bt + ct^2$) and exponentials ($e^{-a(t + b)}$).

Power spectra for the input and output records were subsequently computed. Based on the results of these computations the input data were multiplied by a constant in order to normalize the power level of the flat portion of the input spectrum equal to one (0 db) (see Chapter III). Similarly, the response data were multiplied by a constant to produce an output power spectrum whose power level at intermediate frequencies (3Hz to 7Hz) was equal to one (0 db). This normalization was necessary in order to be able to make meaningful comparisons of the response power spectra for the different systems under study.

Following these normalizations of the input and output records the system kernels $\{h_1\}$ were computed. Starting with the zeroth order kernel (h_0) the system response (described by that kernel) to the white-noise input was calculated and subtracted from the total response before the next higher order kernel was computed [41]. The responses of the derived model to the same white-noise input (as used in the experiment) were calculated for both the linear and nonlinear models as well as their corresponding power spectra. Often, model responses to specialized inputs such as steps and sine waves were also computed. All this processing was done utilizing both computers shown in Fig. 4.2 (IMB 360/44, IBM 360/75) and peripheral devices.

The kernels were computed from cross-correlation between input $x(t)$ and the system response $z(t)$ that remained at each stage (after subtracting), by use of a simple rectangular rule,

$$\phi_{z_x \dots x}(K, \Delta t, \dots, K_n \Delta t) = \frac{1}{u! p^n} \sum_{i=\lambda}^N z(i\Delta t) x(i\Delta t - K_1 \Delta t) \dots x(i\Delta t - K_n \Delta t)$$

where N is the number of samples in the record, $\lambda = \max\{K_1, \dots, K_n\}$ and $\{K_1, \dots, K_n\}$ are between 0 and m ($m\Delta t$ is the extent to which the kernels are computed).

The convolution integrals involved in the computation of the model response were calculated using Simpson's rule.

The computation of the power spectra was done taking into account many of the subtleties and difficulties of this procedure [5,69]. The computational procedure used is outlined below:

The data are in terms of array $\{x_i, i=1, \dots, N\}$ of the signal samples given every Δt . To reduce the variance of the statistical estimates [5,69], the record is broken into three segments, each of duration $(N\Delta t)/3$, the power spectrum of each segment is calculated and the three power spectra are averaged to produce the final estimate. For each segment the power spectrum is calculated as follows. The mean and autocovariance estimates are,

$$\bar{x} = \frac{1}{N} \sum_{i=1}^N x_i$$

$$C_m = \frac{1}{(N-m)} \sum_{i=1}^{N-m} x_i x_{i+m} - \bar{x}^2$$

where $m = 0, 1, 2, \dots, M$ and $M \approx 100$. The initial spectral estimates are given by

$$A_m = C_0 + 2 \sum_{i=1}^{M-1} C_i \cos \frac{im\pi}{M} + C_M \cos(m\pi) - (\Delta t)$$

where $m = 0, 1, 2, \dots, M$. These spectral estimates are, in turn, smoothed by a Hanning window, to produce the final estimates

$$S_m = 0.5 A_m + 0.25 (A_{m+1} + A_{m-1})$$

or, in db, $10 \log_{10} S_m$.

CHAPTER V

TRANSFER FUNCTIONS OF LIGHT → RECEPTOR SYSTEMS

1. Introduction

The receptors (rods and cones) are transducers which convert the energy carried by photons into an electrical signal [71, 88], specifically, a hyperpolarization of the receptor cell membrane. This scheme is supported by a large amount of data obtained during the last few years [3, 4, 91].

Although no direct evidence has been presented to indicate that the hyperpolarization of the receptor membrane is the only instrument in the information transmission to the next neuronal layer, all circumferential evidence indicates that this potential controls the liberation of the transmitter substance at the receptor terminals [9, 10].

Intracellular recording for the receptors has been reported by several authors [3, 4, 91]. The stability of recording which is essential to detailed analysis has not been satisfactory except, possibly, in the case of the turtle eye [3, 4]. Therefore, in this work, we avoid the torturous path of intracellular recording from the receptors and base our analysis on the mass receptor response obtained through stable extracellular recordings. Sillman et. al. [74, 75] have presented convincing evidence that the mass response (or ERG) obtained after treating the retina with sodium aspartate is indeed the late receptor potential which reflects the receptor membrane hyperpolarization.

Presently, there is enough additional evidence obtained from the carp retina (Witkovsky & Ripps, personal communication) and the skate retina [20] to show that this extracellularly recorded potential is due to the receptor potential. We noticed that within a limited intensity range, the response of the receptor to a step input appears to be a linear transformation of the input [74, 75]. This conjecture is also supported by results of (linear) analysis in the cat retina [70b].

A recent report by Baylor, Fuortes and O'Bryan [4] suggests that there is (in turtle) a receptor-to-receptor interaction possibly through the teledendrone. In our Golgi study of the catfish retina we failed to impregnate such a process [unpublished results]. Although we have no evidence supporting or not supporting a receptor-to-receptor interaction, we feel that the catfish receptors are simpler in their organization than the ones in the turtle.

In this chapter we obtain nonlinear dynamic transfer functions of the receptor response due to light patterns which we shall extensively use to study the receptive field behavior of the ganglion cells. These light stimuli are spots (0.3 mm diameter), annuli (0.5 mm inner diameter, 5 mm outer diameter) and uniform light intensity over the whole retina. The transfer functions are obtained by modulating the stimulating light intensity, in each case, in a white-noise fashion and following procedures described in previous chapters to obtain the nonlinear, dynamic characterization of the system in terms of a series of Wiener kernels.

The receptor field is of the order of 5 microns in diameter and therefore several thousand receptors are being stimulated in each stimulus case considered here. The recordings are extracellular and they indicate the mass behavior of the surrounding receptor cells. The contributions of other cells besides the receptors are being suppressed with the addition of sodium aspartate to the preparation.

2. The White-Noise-Derived Models

The procedure to be followed in obtaining the system non-linear models through white-noise stimulation has already been described in previous chapters.

Preliminary harmonic analysis of the system response to white-noise of 50 Hz bandwidth revealed a cutoff of about 10 Hz (with some variation of this value for the different cases of stimulus and intensity levels). In view of these findings, the white-noise bandwidth chosen to perform the characterizing experiments was 25 Hz. The system memory is of the order of 200 msec and the record length, therefore, necessary for a statistical error of 5% (standard deviation) is approximately 40 sec. This was calculated following the formulas derived in Chapter III.

Consequently, the white-noise experiments were performed for all stimulus cases; spot, annulus and uniform light. The average intensity level was fixed for each experiment. Two such average light levels were used; one was a high level of average intensity of 1.5×10^{11} photons/mm².sec and the other a low level of 2.5×10^{10} photons/mm².sec. This average intensity level was modulated in a white-noise fashion, over a dynamic range of approximately 1.8 logarithmic units. Thus, considering that the system has an operating range of about 3-4 log units, we tested the system over its entire range (for two widely different "bias points" by performing two characterizing white-noise tests, one in the low operating range (near cut-off) and the other in the high operating range (near saturation).

The data obtained from these experiments were then treated for slow drift removal (as described in Chapter IV). The input-output records were sampled every 8 msec, a high enough rate to produce a Nyquist folding frequency of 62.5 Hz which is sufficient to describe white-noise of 25 Hz bandwidth. Consequently the first order (linear) and second order (nonlinear) kernels were computed.

Figure 5.1 shows the first order kernels for each case and for both low and high average intensity levels (the latter for spot and uniform light only). The latency is about 15 msec in the case of uniform light of low average intensity and decreases to about 10 msec for high average intensity. In the case of spot stimulation the latency is about 15 msec for high levels and 12 msec for low intensity levels. For annulus stimulation (low level) the latency is about 14 msec.

From these first order kernels we note that all systems under study are underdamped and that the final recovery is larger (longer memory) for system annulus→receptor than it is for systems spot→receptor or uniform→receptor. The characteristics of the latter two systems are, as expected, very similar.

Tables 5.1, 5.2, 5.3, 5.4, 5.5 describe the second order (nonlinear) kernels for all systems under consideration. We will see later that the response contribution of these kernels is small and that the system, within the tested range of 1.8 log-units, is nearly linear. The interpretation of these kernels has been presented in Chapter II in terms of how past portions of the input signal interact

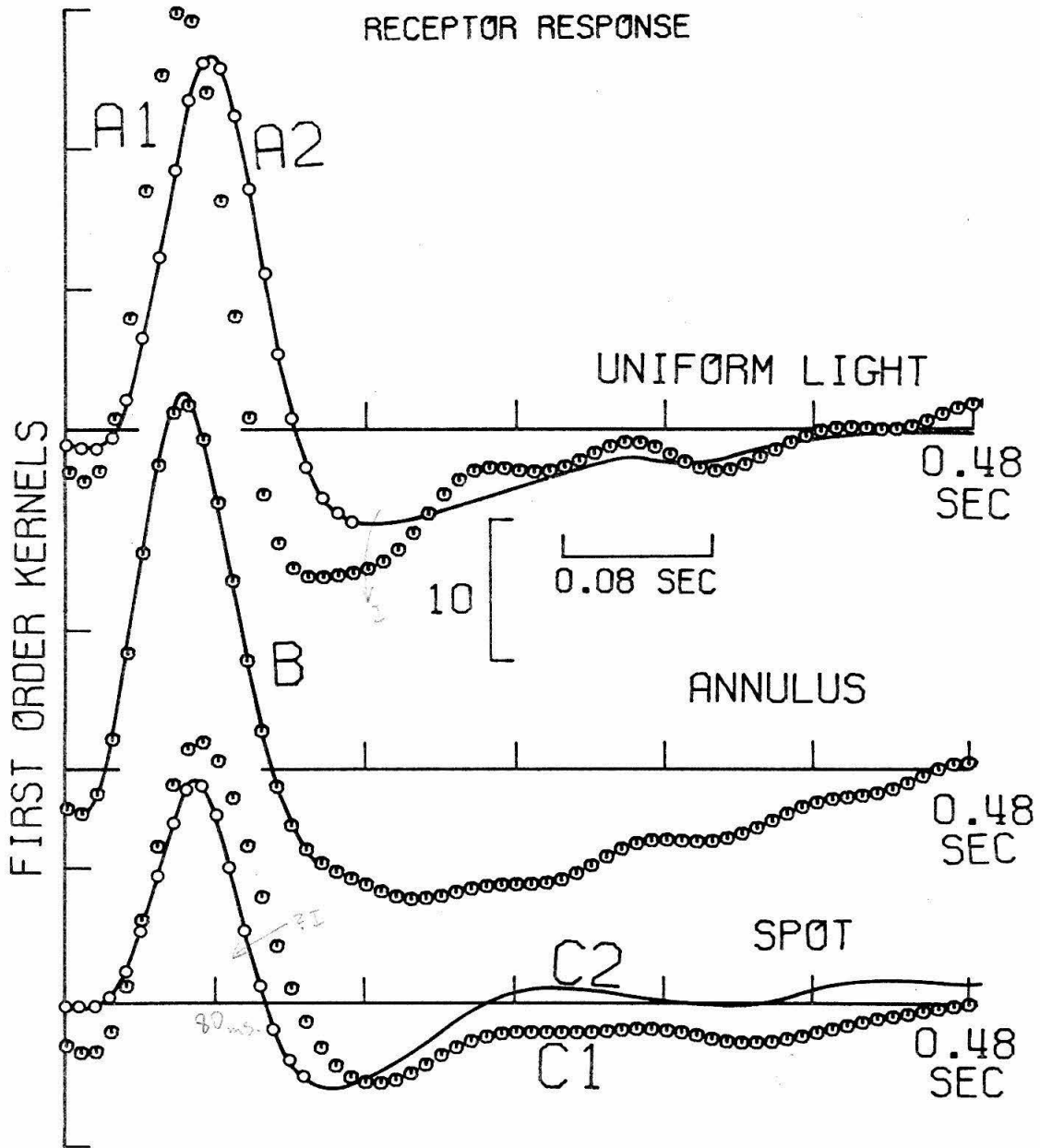


Fig. 5.1. First order kernels for several Light \rightarrow Receptors systems. A1: high mean intensity, A2: low mean intensity, B: low mean intensity, C1: low mean intensity, C2: high mean intensity. Low mean intensity is 2.5×10^{10} photons/mm²·sec and high mean intensity is 1.5×10^{11} photons/mm²·sec.

SECCND ORDER KERNEL

0	0	8	16	24	32	40	48	56	64	72	80	88	96	104	112	120	128	136	144	152	160	
0	4	3	2	1	0	-1	-1	-2	-3	-4	-6	-9	-10	-13	-13	-10	-8	-4	2	6	9	10
8	2	2	2	1	0	-1	-1	-2	-3	-4	-6	-9	-10	-13	-13	-10	-8	-4	2	6	9	10
16	0	2	2	1	0	-1	-1	-2	-3	-4	-6	-9	-10	-13	-13	-10	-8	-4	2	6	9	10
24	-1	0	1	0	1	-1	-1	-2	-3	-4	-6	-9	-10	-13	-13	-10	-8	-4	2	6	9	10
32	-1	-1	0	0	1	-1	-1	-2	-3	-4	-6	-9	-10	-13	-13	-10	-8	-4	2	6	9	10
40	0	0	0	0	-1	-1	-2	-3	-4	-6	-9	-10	-13	-13	-10	-8	-4	2	6	9	10	11
48	-1	1	1	0	-2	-4	-6	-9	-10	-13	-13	-10	-8	-4	2	6	9	10	11	11	11	11
56	-1	1	2	1	-3	-6	-9	-10	-13	-13	-10	-8	-4	2	6	9	10	11	11	11	11	11
64	-1	0	2	2	-2	-8	-12	-13	-13	-10	-8	-4	2	6	9	10	11	11	11	11	11	11
72	0	0	1	2	0	-6	-12	-14	-13	-10	-8	-4	2	6	9	10	11	11	11	11	11	11
80	2	0	0	2	1	-2	-8	-12	-12	-8	-4	2	6	9	10	11	11	11	11	11	11	11
88	2	1	-1	0	1	1	-2	-6	-9	-7	-2	2	6	9	10	11	11	11	11	11	11	11
96	1	1	0	-1	0	1	1	-1	-3	-4	-1	3	6	9	10	11	11	11	11	11	11	11
104	-2	0	0	-1	-1	0	2	2	1	-1	0	2	6	9	10	11	11	11	11	11	11	11
112	-4	0	0	-1	-1	-1	0	1	2	1	1	1	3	6	9	10	11	11	11	11	11	11
120	-3	-4	-2	0	0	-1	-1	-1	0	1	1	1	3	6	9	10	11	11	11	11	11	11
128	-1	-3	-3	-2	0	0	0	-1	-2	-2	-1	0	1	3	6	9	10	11	11	11	11	11
136	1	-1	-3	-3	-1	1	1	0	-2	-3	-3	-3	-2	0	3	6	10	11	11	11	11	11
144	1	1	0	-2	-2	0	2	2	1	-2	-4	-5	-4	-3	0	3	6	10	11	11	11	11
152	1	1	1	0	-1	-1	1	2	2	0	-3	-5	-6	-5	-3	0	3	6	10	11	11	11
160	0	0	0	1	1	0	0	2	2	1	-1	-3	-6	-6	-3	0	3	6	10	11	11	11

Table 5.1

Values of $h_2(\tau_1, \tau_2)$. Spot \rightarrow Receptors. Mean intensity, 2.5×10^{10} photons/mm²·sec. Axes in msec.

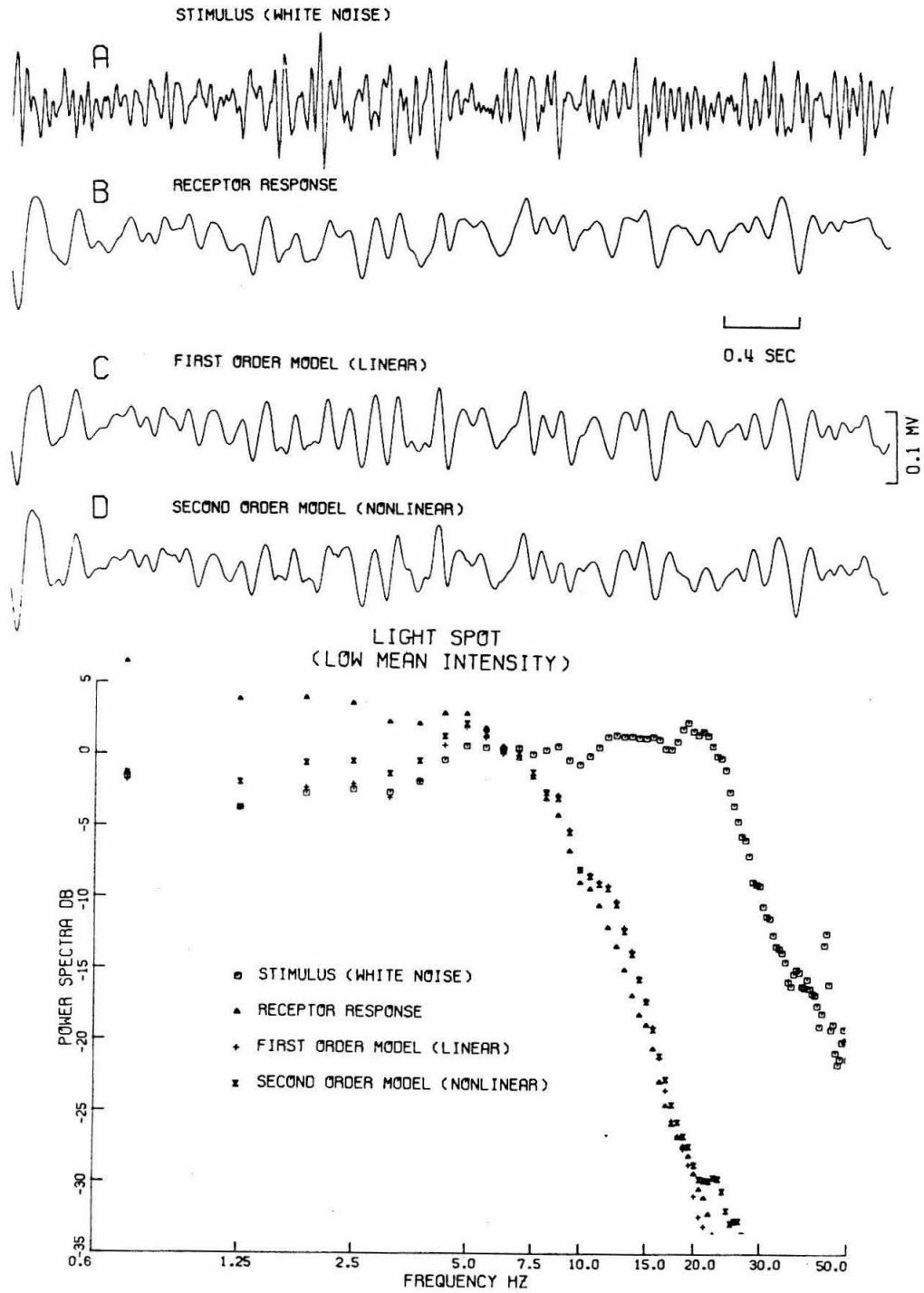


Fig. 5.2. Experimental and model responses to white-noise and corresponding power spectra. System Spot \rightarrow Receptors. Mean intensity 2.5×10^{10} photons/mm²·sec.

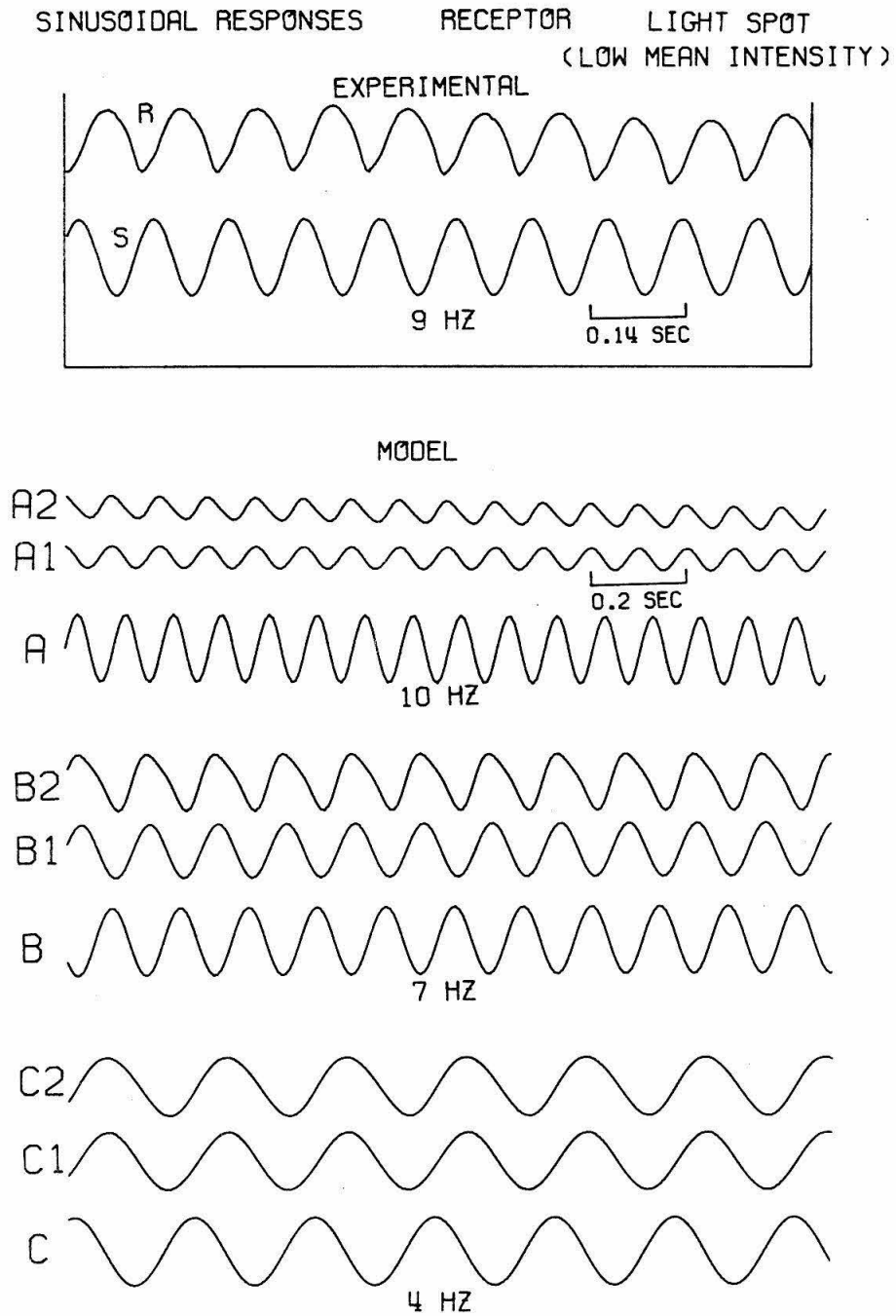


Fig. 5.3. Experimental and model sinusoidal responses. System Spot → REceptors. Mean intensity 2.5×10^{10} photons/mm²·sec. For model, A: stimulus, A1: linear-model response, A2: nonlinear-model response, etc.

SECCND ORDER KERNEL

0	8	16	24	32	40	48	56	64	72	80	88	96	104	112	120	128	136	144	152	160
0	0	2	0	0	0	0	0	0	0	0	0	0	0	0	0	0	0	0	0	0
8	1	2	0	0	0	0	0	0	0	0	0	0	0	0	0	0	0	0	0	0
16	0	2	3	0	0	0	0	0	0	0	0	0	0	0	0	0	0	0	0	0
24	-2	0	2	3	0	0	0	0	0	0	0	0	0	0	0	0	0	0	0	0
32	-5	-2	0	2	3	0	0	0	0	0	0	0	0	0	0	0	0	0	0	0
40	-5	-4	-2	0	2	3	0	0	0	0	0	0	0	0	0	0	0	0	0	0
48	-2	-4	-5	-3	1	3	0	0	0	0	0	0	0	0	0	0	0	0	0	0
56	2	-1	-4	-5	-2	1	4	0	0	0	0	0	0	0	0	0	0	0	0	0
64	2	2	0	-4	-7	-3	2	5	0	0	0	0	0	0	0	0	0	0	0	0
72	1	3	3	0	-8	-8	-4	2	6	0	0	0	0	0	0	0	0	0	0	0
80	0	1	3	3	0	-10	-9	-4	3	7	0	0	0	0	0	0	0	0	0	0
88	0	-1	0	3	-1	-7	-11	-10	-3	4	8	0	0	0	0	0	0	0	0	0
96	2	0	-1	0	2	-2	-8	-11	-9	-2	5	8	0	0	0	0	0	0	0	0
104	1	2	0	-2	-1	1	-3	-8	-10	-7	-1	6	8	0	0	0	0	0	0	0
112	0	2	0	-2	-2	-1	-1	-4	-7	-8	-5	1	5	7	0	0	0	0	0	0
120	-2	0	2	0	-3	-3	-2	-2	-4	-6	-6	-3	1	5	6	0	0	0	0	0
128	-1	-2	0	2	-1	-4	-4	-3	-2	-3	-5	-4	-1	2	4	4	0	0	0	0
136	1	-2	0	2	1	-2	-5	-5	-3	-2	-3	-3	-2	0	3	3	3	0	0	0
144	3	1	-2	-1	1	0	-2	-5	-5	-3	-2	-2	-2	-1	1	3	3	3	0	0
152	2	2	0	-2	-1	0	0	-3	-5	-5	-3	-2	-1	-1	1	2	3	3	2	0
160	0	2	0	-2	-3	-2	0	-1	-3	-5	-5	-3	-2	-1	0	2	3	3	2	1

Table 5.2

Values of $h_2(\tau_1, \tau_2)$. Spot \rightarrow Receptors. Mean intensity 1.5×10^{11} photons/mm²·sec. Axes in msec.

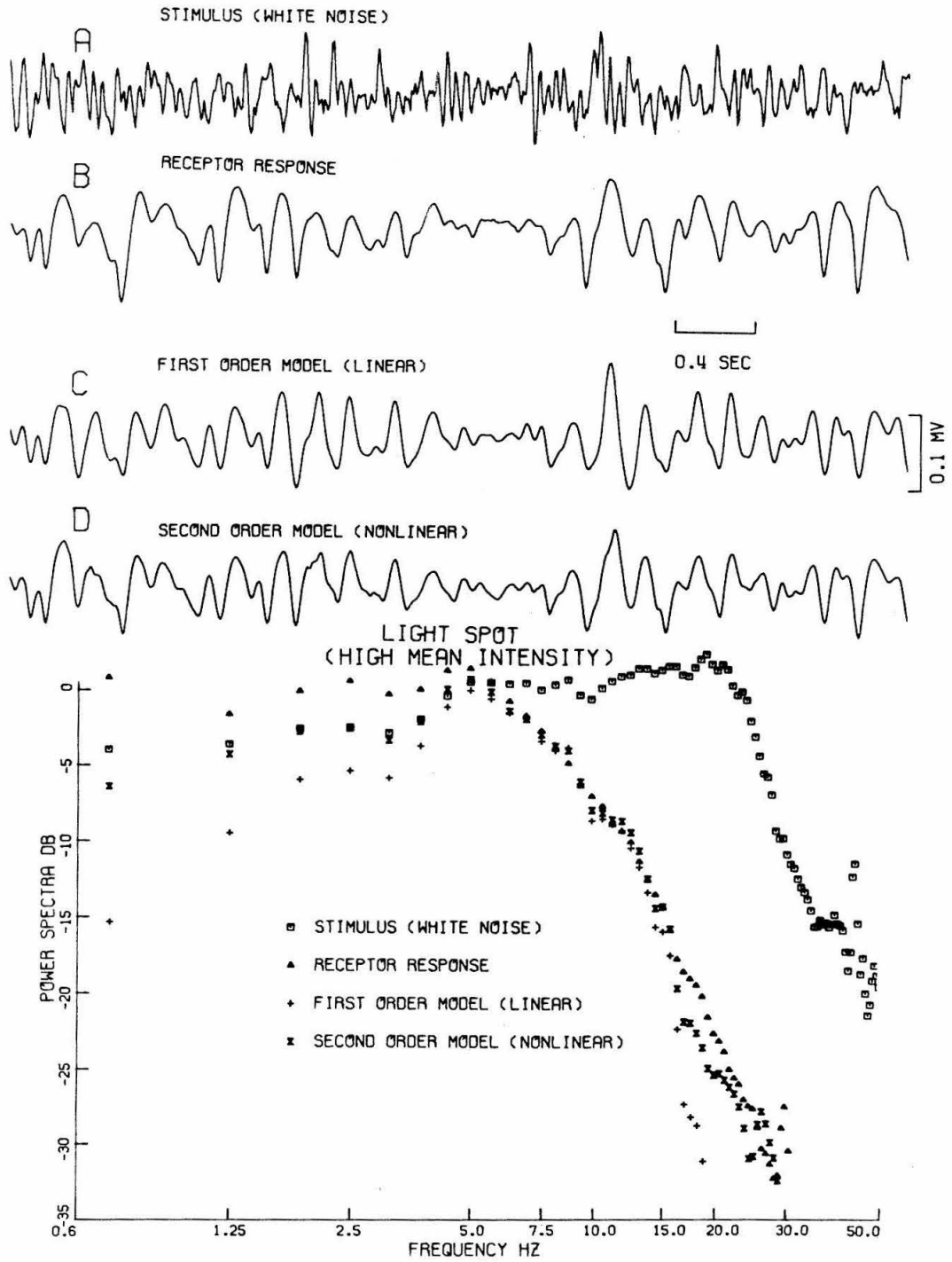


Fig. 5.4. Experimental and model responses to white-noise and corresponding power spectra. System Spot \rightarrow Receptors. Mean intensity 1.5×10^{11} photons/mm²·sec.

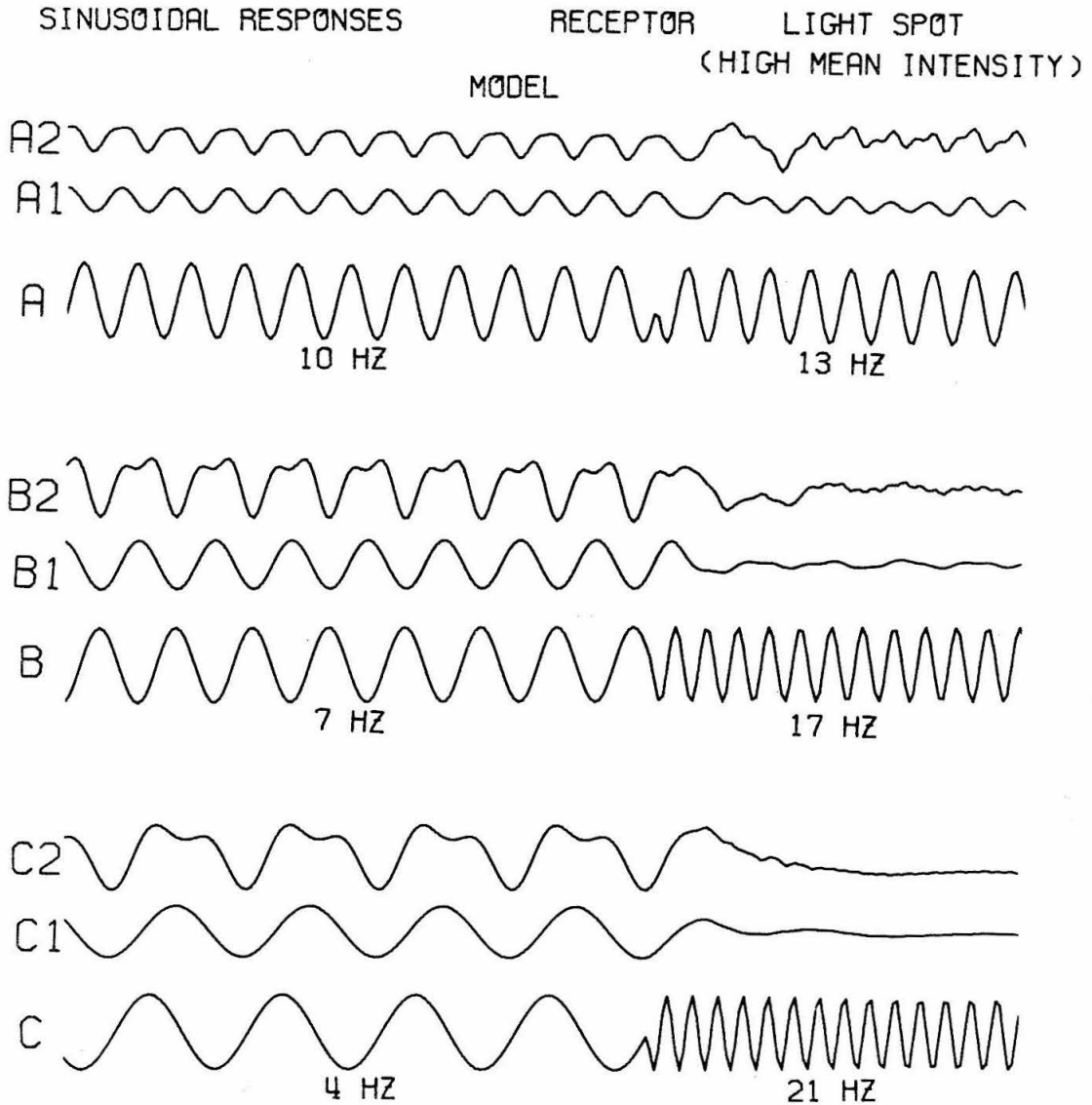


Fig. 5.5. Model sinusoidal responses. System Spot \rightarrow Receptors. Mean intensity, 1.5×10^{11} photons/mm²·sec. A: stimulus, A1: linear-model response, A2: nonlinear model response, etc.

SECOND ORDER KERNEL

0	8	16	24	32	40	48	56	64	72	80	88	96	104	112	120	128	136	144	152	160	
0	14	10	16	10	16	10	16	10	16	10	16	10	16	10	16	10	16	10	16	10	16
8	10	10	10	11	16	10	16	10	16	10	16	10	16	10	16	10	16	10	16	10	16
16	-1	10	0	11	16	10	16	10	16	10	16	10	16	10	16	10	16	10	16	10	16
24	-8	0	11	16	10	16	10	16	10	16	10	16	10	16	10	16	10	16	10	16	10
32	-7	-8	0	11	16	10	16	10	16	10	16	10	16	10	16	10	16	10	16	10	16
40	-1	-6	-8	0	10	16	10	16	10	16	10	16	10	16	10	16	10	16	10	16	10
48	3	-1	-6	-8	0	15	9	15	9	15	9	15	9	15	9	15	9	15	9	15	9
56	4	4	0	-6	-9	-2	9	15	9	15	9	15	9	15	9	15	9	15	9	15	9
64	4	5	0	-6	-9	-2	9	15	9	15	9	15	9	15	9	15	9	15	9	15	9
72	2	4	6	0	-8	-10	-3	9	14	8	13	8	13	8	13	8	13	8	13	8	13
80	1	2	4	6	6	-1	-9	-11	-3	8	13	8	13	8	13	8	13	8	13	8	13
88	1	1	2	4	6	5	-3	-10	-12	-4	7	11	5	9	4	8	4	8	4	8	4
96	1	1	1	2	4	6	3	-4	-11	-12	-4	7	11	5	9	4	8	4	8	4	8
104	0	1	1	0	1	4	5	2	-5	-10	-10	-3	4	6	2	6	2	6	2	6	2
112	-2	0	1	0	1	3	3	3	-1	-4	-8	-7	-1	3	4	3	4	3	4	3	4
120	-2	-2	0	1	0	-1	1	3	2	0	-3	-4	-3	1	2	1	2	1	2	1	2
128	-1	-2	-2	-1	0	-1	0	2	1	0	-1	-1	-1	0	2	1	0	2	1	0	2
136	0	-2	-3	-2	-1	0	-1	-1	0	0	0	1	2	3	2	0	0	2	3	2	0
144	1	0	-2	-3	-2	-1	-1	-2	-1	-1	-1	1	3	5	5	3	3	5	3	3	5
152	0	1	0	-2	-3	-2	-1	-2	-2	-2	-1	-1	1	4	6	6	3	6	3	6	3
160	0	1	1	0	-2	-4	-3	-2	-1	-2	-2	-2	-2	0	4	7	6	3	6	3	7

Table 5.3

Values of $h_2(\tau_1, \tau_2)$. Annulus + Receptors. Mean intensity, 2.5×10^{10} photons/mm²·sec. Axes in msec.

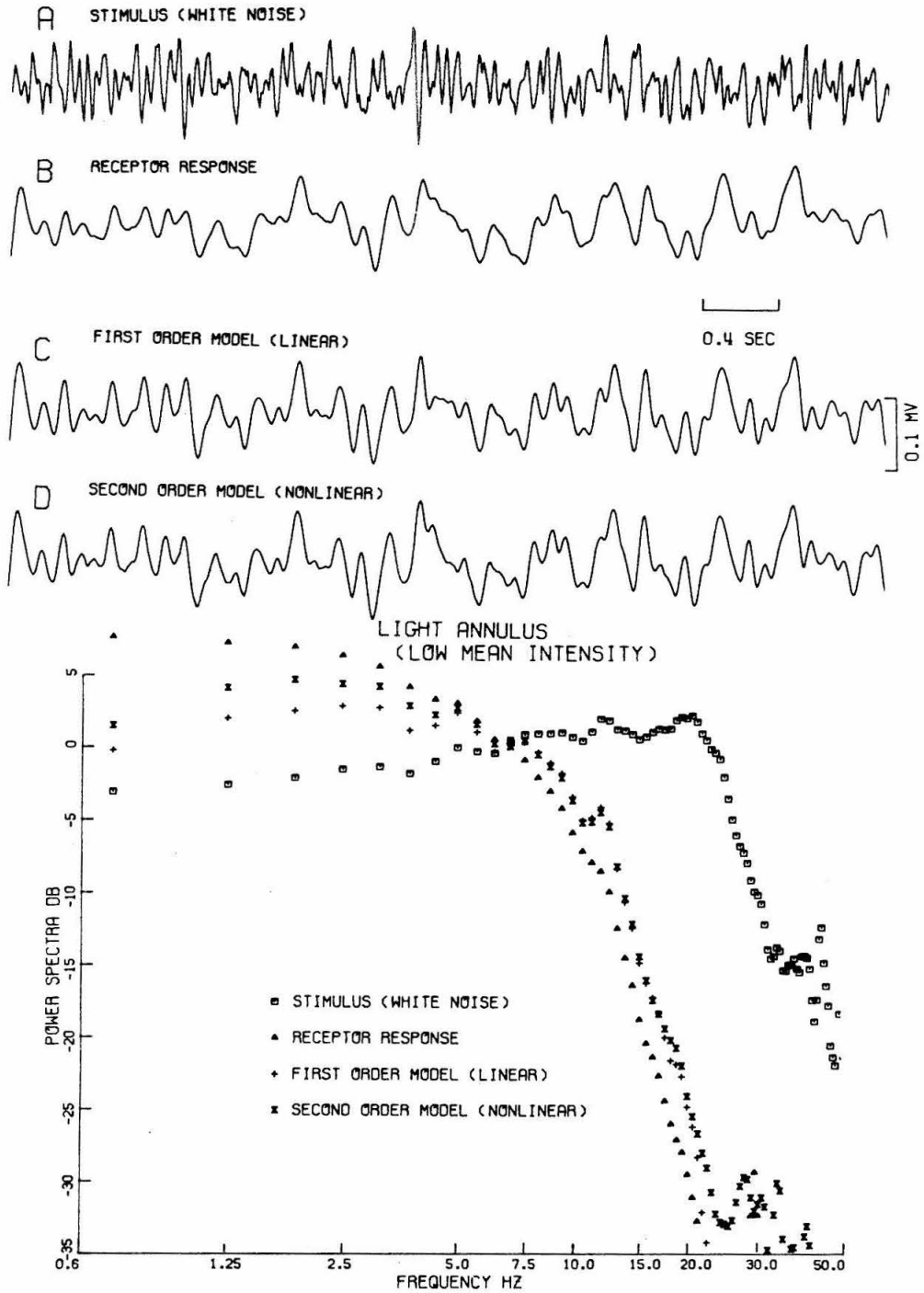


Fig. 5.6. Experimental and model responses to white-noise and corresponding power spectra. System Annulus \rightarrow Receptors. Mean intensity, 2.5×10^{10} photons/mm²·sec.

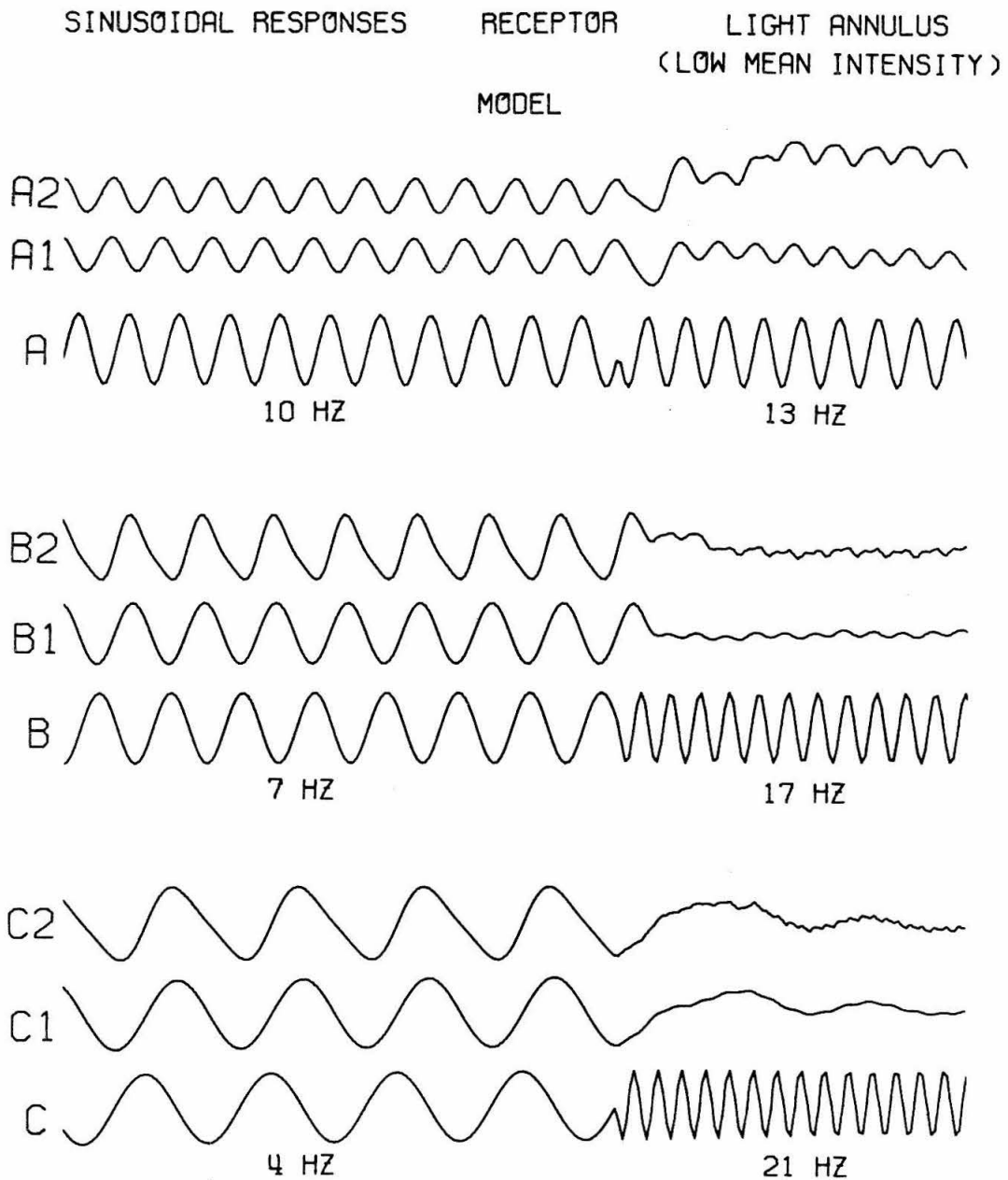


Fig. 5.7. Model sinusoidal responses. System Annulus → Receptors. Mean intensity 2.5×10^{10} photons/mm²·sec. A: stimulus, A1: linear-model response, A2: nonlinear model response, etc.

SECOND ORDER KERNEL

	0	8	16	24	32	40	48	56	64	72	80	88	96	104	112	120	128	136	144	152	160	
0	1																					
8	1	2																				
16	0	1	2																			
24	-1	0	2	3																		
32	-2	-2	0	2	3																	
40	-2	-2	-2	0	1	1																
48	-1	-1	-2	-2	-2	-1	-2															
56	1	0	0	-2	-3	-4	-4	-5														
64	2	2	1	0	-3	-5	-7	-6	-7													
72	3	2	2	2	0	-4	-7	-8	-8	-7												
80	2	3	3	3	2	-1	-5	-6	-9	-7	-6											
88	1	2	2	3	3	2	0	-4	-7	-7	-5	-4										
96	-2	0	1	2	3	4	3	1	-3	-5	-5	-3	-2									
104	-3	-2	0	1	2	3	4	4	2	-1	-3	-3	-2	-1								
112	-3	-3	-1	0	2	3	4	4	4	2	0	-2	-2	-1	0							
120	-1	-3	-3	-1	1	2	3	4	4	4	2	0	-2	-2	0	1						
128	1	-1	-3	-2	0	2	3	3	3	3	2	1	-1	-2	-1	1	2					
136	1	0	-2	-3	-2	0	2	3	3	2	1	0	-1	-2	-2	-1	2	4				
144	0	1	0	-2	-3	-1	1	2	3	2	0	-1	-2	-2	-2	0	3	5				
152	0	0	1	0	-2	-1	-1	1	2	2	0	-2	-3	-3	-2	-2	-1	1	4	6		
160	1	0	1	1	0	-1	-2	-1	1	2	1	-1	-4	-4	-3	-2	-1	-1	2	5	6	

Table 5.4

Values of $h_2(\tau_1, \tau_2)$. Uniform \rightarrow Receptors. Mean intensity, 2.5×10^{10} photons/mm²·sec. Axes in msec.

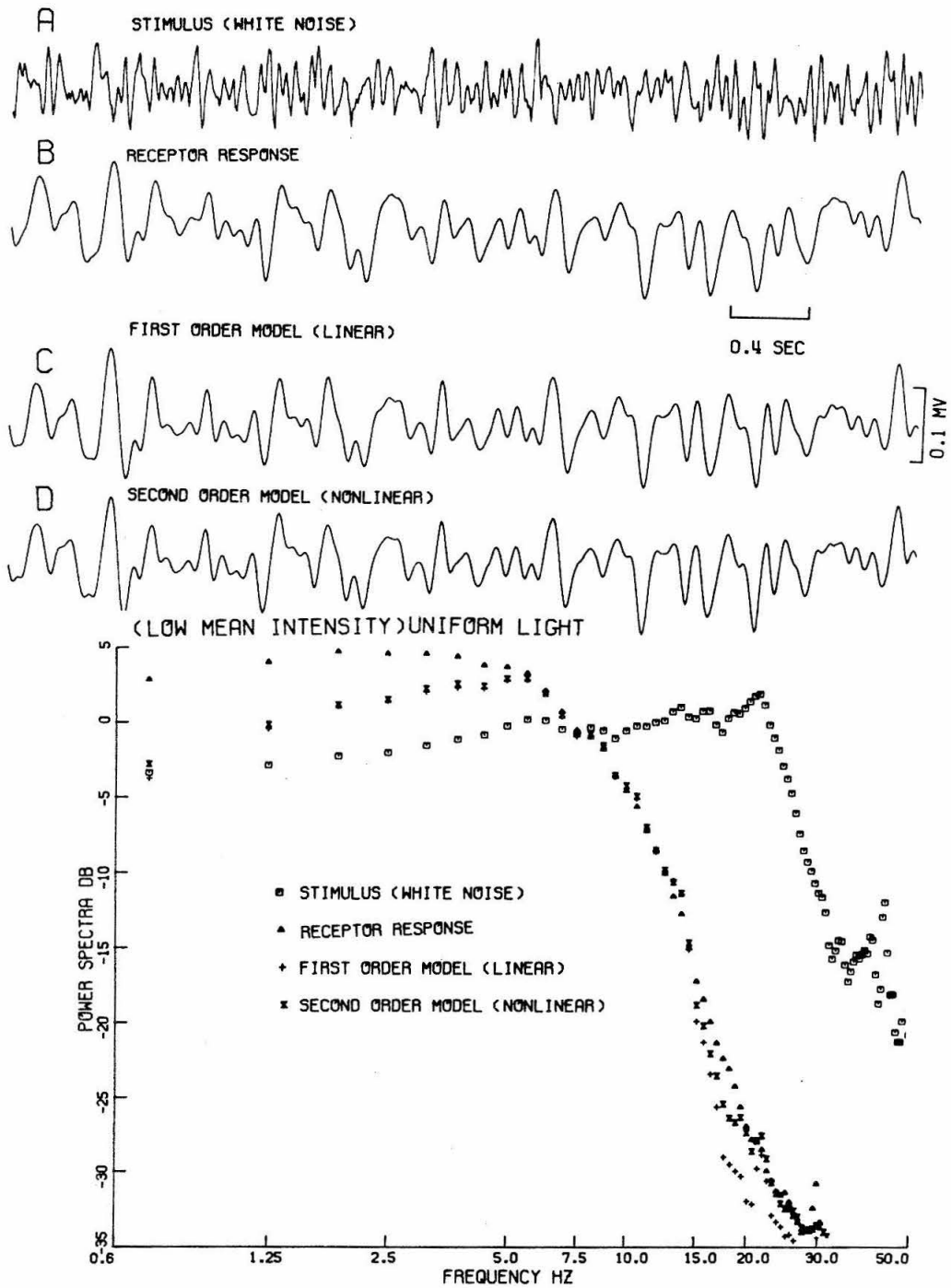


Fig. 5.8. Experimental and model responses to white-noise and corresponding power spectra. System Uniform \rightarrow Receptors. Mean intensity, 2.5×10^{10} photons/mm²·sec.

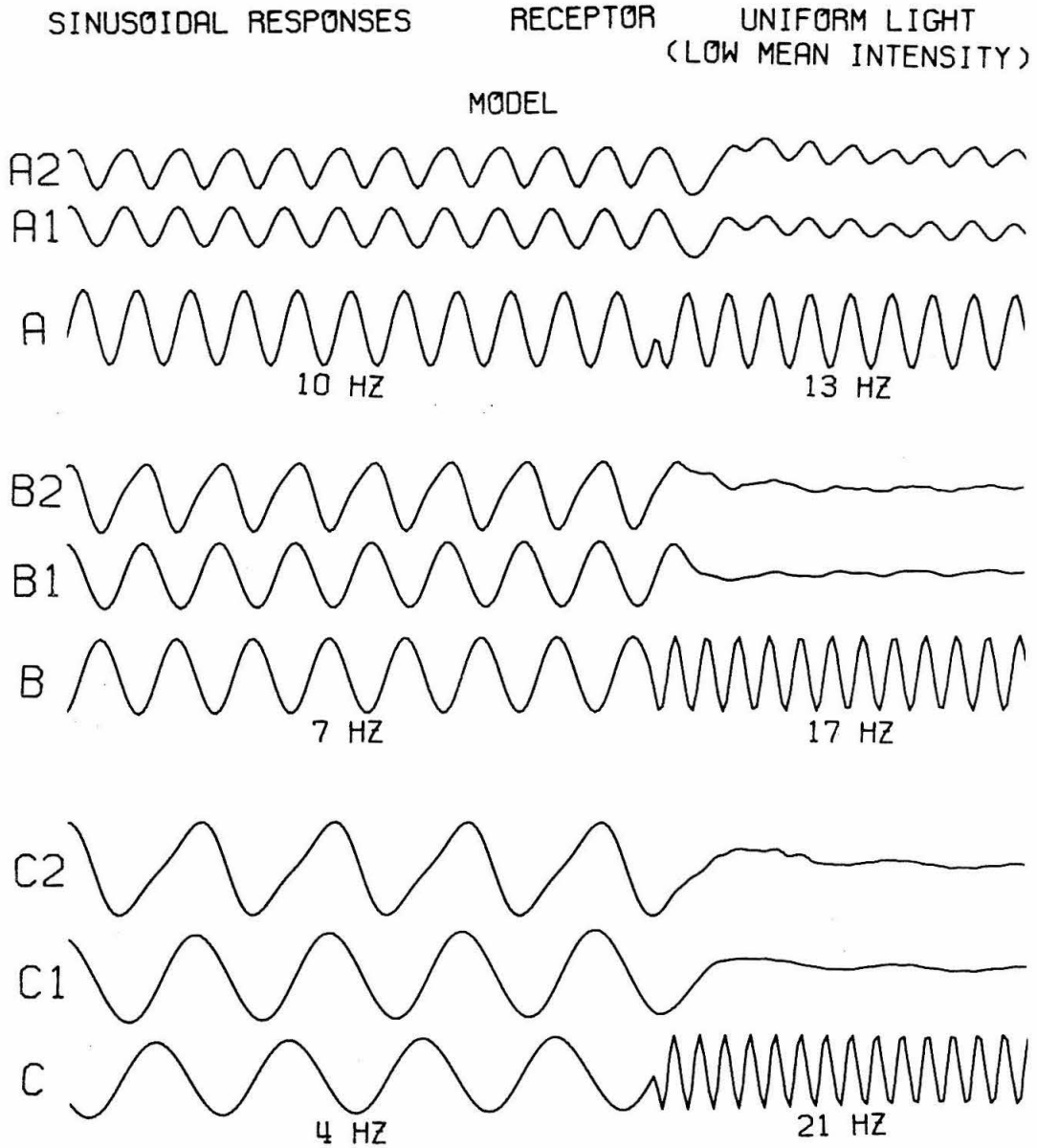


Fig. 5.9. Model sinusoidal responses, System Uniform \rightarrow Receptors. Mean intensity, 2.5×10^{10} photons/mm².sec. A: stimulus, A1: linear-model response, A2: nonlinear-model response, etc.

SECOND ORDER KERNEL

C	0	8	16	24	32	40	48	56	64	72	80	88	96	104	112	120	128	136	144	152	160	
0	5																					
8	4	6																				
16	1	4	5																			
24	0	3	4	3																		
32	-1	2	3	1	-1																	
40	0	2	3	1	-3	-7																
48	1	2	3	1	-3	-9	-12															
56	2	3	3	2	-2	-8	-13	-15														
64	2	3	4	3	-1	-7	-12	-14	-14													
72	3	3	4	3	0	-4	-9	-12	-12	-9												
80	2	2	3	3	2	-2	-7	-10	-9	-6	-2											
88	0	1	2	3	3	0	-4	-7	-7	-4	0	3										
96	-2	-1	0	2	3	2	-1	-4	-5	-3	1	5	6									
104	-3	-3	-1	0	2	2	1	-2	-3	-2	2	5	7	7								
112	-2	-4	-3	-1	0	1	1	-1	-2	-2	1	5	8	7	5							
120	-1	-3	-4	-3	-1	0	1	0	-2	-3	0	4	7	8	5	3						
128	0	-1	-3	-4	-3	-1	0	0	-2	-3	-3	1	5	8	6	3	1					
136	-1	0	-1	-3	-3	-3	-1	0	-1	-3	-4	-3	2	6	7	5	2	0				
144	-2	-1	0	-1	-3	-3	-2	-1	0	-1	-3	-5	-3	2	6	6	4	1	-1			
152	-2	-2	-1	0	-1	-2	-2	-1	0	-1	-3	-5	-3	-3	2	5	6	4	1	0		
160	0	-2	-2	-1	0	0	-1	-2	-2	-1	0	-1	-3	-5	-3	1	5	6	4	1	0	

Table 5.5

Values of $h_2(\tau_1, \tau_2)$. Uniform + Receptors. Mean intensity, 1.5×10^{11} photons/mm²·sec. Axes in msec.

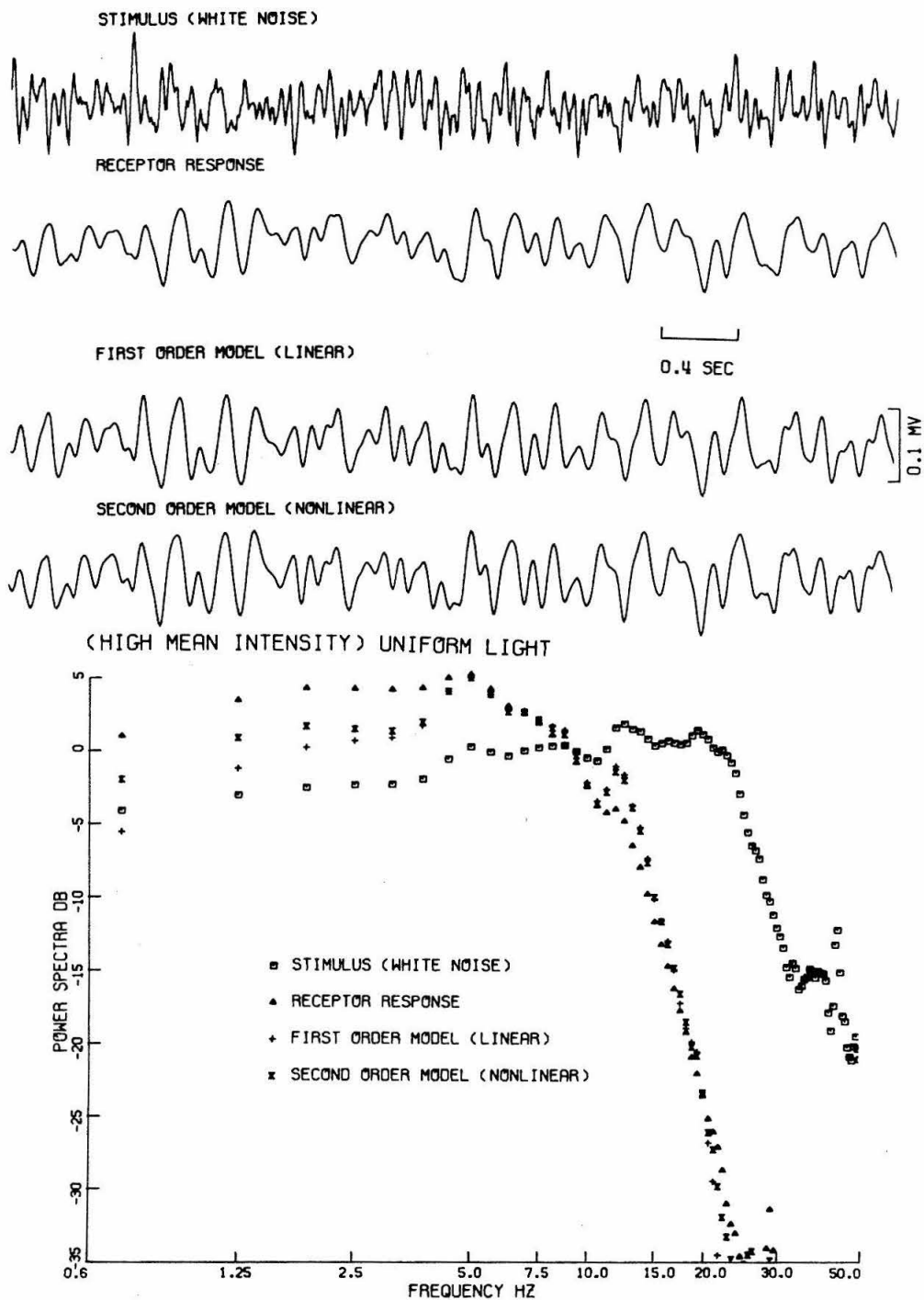


Fig. 5.10. Experimental and model responses to white-noise and corresponding power spectra. System Uniform \rightarrow Receptors. Mean intensity, 1.5×10^{11} photons/mm²·sec.

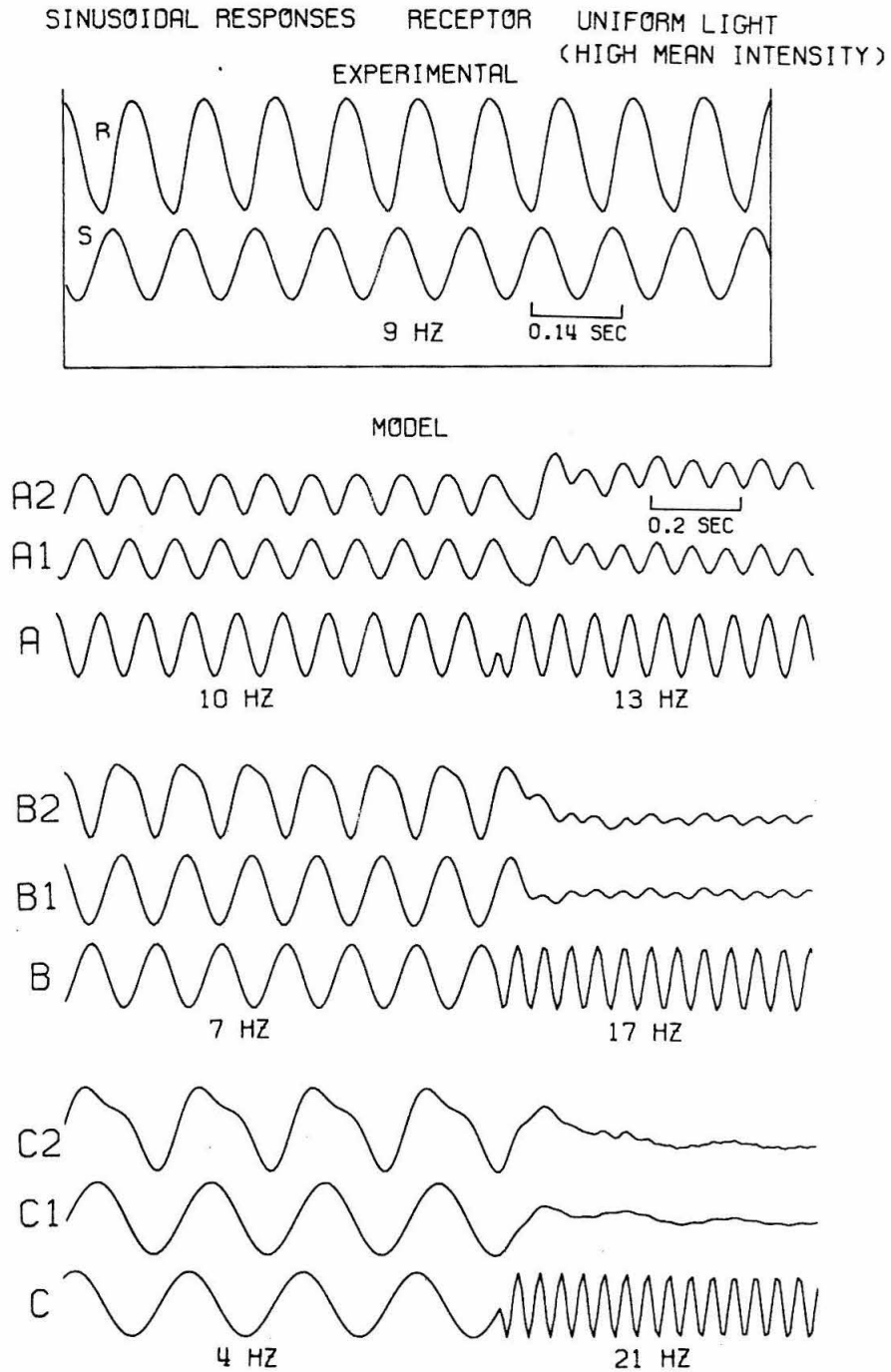


Fig. 5.11. Experimental and model sinusoidal responses. System Uniform \rightarrow Receptors. Mean intensity, 1.5×10^{11} photons/mm²·sec. For model responses, A: stimulus, A1: linear-model response, A2: nonlinear-model response, etc.

to produce a nonlinear "correction" at the output of the system at present time.

The rest of the figures show white-noise responses of all systems, both experimentally obtained and model-predicted (for both linear and nonlinear models) for a portion of the white-noise used in the characterizing experiment. Also, these figures show power spectra for both experimental and model responses as well as some sinusoidal responses predicted by the model and a few obtained experimentally.

From the experimental and model white-noise responses we note that these systems are almost linear since it appears that the addition of the nonlinear terms changes very little the linear model response. Actually, the nonlinear model response does improve the model performance if one carefully considers peak-to-valley ratios and other inconspicuous details. A measure of the goodness of each model is obtained in terms of the mean square error over the entire white-noise record length for each model. These are given below, where h_0 (a constant) is just the average value of the system response (i. e., the zeroth order Wiener kernel).

<u>SYSTEM</u>	<u>Model</u>		
	$\{h_0\}$	linear, $\{h_0, h_1\}$	nonlinear $\{h_0, h_1, h_2\}$
Spot → Receptor			
Low level	100	25	14
High level	100	22	12
Annulus → Receptor			
Low level	100	19	16
Uniform → Receptor			
Low level	100	21	15
High level	100	17	13

The error for model $\{h_0\}$ is normalized to 100 (arbitrary units) and then the errors for the linear and nonlinear models are measured with respect to it. We observe that the systems are, indeed, almost linear with some small nonlinearities as evidenced by the small decrease in error with the addition to the model of the nonlinear "correction" terms.

The power spectra of the white-noise responses of both experimental and model signals show the frequency response for each system and the fact that the model frequency response agrees extremely well with the experimental one.

The model (and some experimental) sinusoidal responses reveal certain interesting characteristics. For system uniform light → receptor a saturation phenomenon is exhibited (as expected) at the high intensity level; also unsymmetrical on-off characteristic (for positive and negative response slopes) and a shift of response

average value with a shift in frequency (for certain high frequencies). These nonlinear phenomena will also be observed for the horizontal cell response and will be discussed in the next chapter. The sinusoidal responses for the spot light→receptor system (high intensity level) show a strong saturation characteristic (Fig. 5.5), while for low intensity level they are fairly linear. This behavior is fairly typical of retinal systems.

Figure 5.12 shows the power spectra of the white-noise responses of all systems. The spot light→receptor and annulus light→receptor systems become much faster responding (rise time etc.) at high intensity levels. The cutoff frequencies for each system are (approximately):

Spot → receptor

low level	:	6 Hz
high level	:	11 Hz

Uniform→receptor

low level	:	7 Hz
high level	:	11 Hz

Annulus→receptor

low level	:	6 Hz
-----------	---	------

We have no high intensity level data for system annulus light→receptor from this same unit (and preparation). However, data from other units indicate that for this system, also, the frequency response cutoff increases with increasing the average level of intensity. We conclude that, for all systems considered

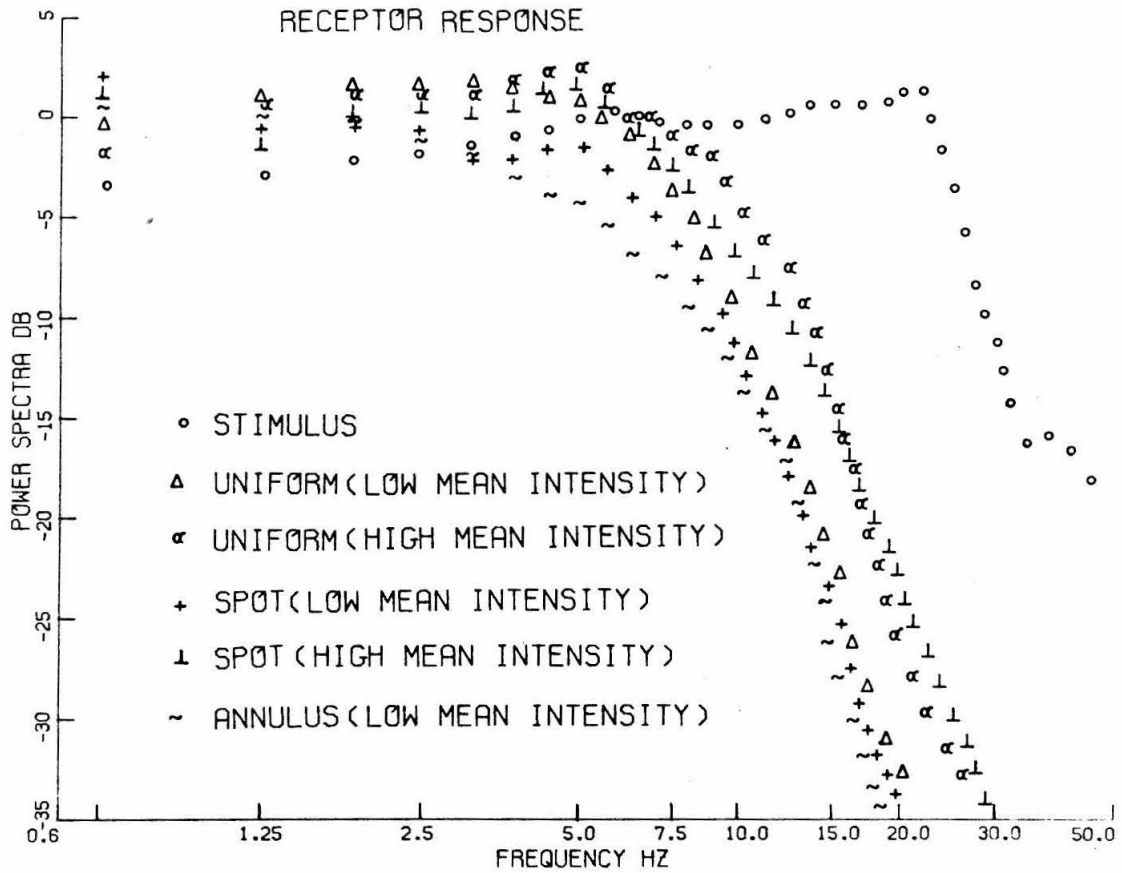


Fig. 5.12. Power spectra of experimental responses to white-noise for several Light \rightarrow Receptors systems. Low mean intensity is 2.5×10^{10} photons/mm²·sec and high mean intensity is 1.5×10^{11} photons/mm²·sec.

here, increasing the mean light intensity makes the system faster-responding dynamically (i. e., shorter rise time, etc.). The high frequency asymptote has a slope of about 12 db/octave indicating that the light→receptor system is of second order (to the extent that the system is considered linear).

3. Conclusions

In this chapter we obtained nonlinear transfer functions for systems, light spot→receptor response, light annulus→receptor response and uniform light→receptor response, and for two widely differing average intensity levels. The transfer functions obtained are very satisfactory in that they predict the system behavior accurately for a number of crucial tests. These tests are comparison of experimental and model white-noise responses, power spectra and sinusoidal tests.

Some system characteristics revealed by these models are the following:

- 1) The receptor responses evoked by the light stimuli used (spot, annulus and uniform) are nearly linear within the tested dynamic range.
- 2) Small nonlinearities exist such as saturation at high intensity levels, unsymmetric positive and negative response slopes to sinewave stimuli and a shift of average response level with a shift in stimulus frequency for the high frequency range (about 13 Hz).
- 3) For all systems considered the latency decreases as the average light level is increased from a maximum of about 15 msec to a minimum of about 10 msec.
- 4) All light→receptor systems studied here become considerably faster at high intensity levels. The cutoff frequency varies from about 6 Hz at low levels to about 11 Hz at high mean intensity levels.

5) The high frequency asymptote for all light-receptor systems considered here is approximately 12 db/octave, indicating a second order system.

CHAPTER VI

THE LIGHT \rightarrow HORIZONTAL CELL SYSTEM

1. Introduction

In this chapter we examine the dynamic aspects of the S-potential generating mechanism and we derive a model of the system that transforms uniform light intensity (varying in time) into the H-cell potential. This model satisfactorily predicts quantitatively the dynamic, nonlinear features of the physical system. The system transfer function is derived by two different methods; one is the white-noise method and the other is the traditional approach of guessing a set of (nonlinear) differential equations and shaping them so that they fit a certain set of data.

In the first approach the system is subjected to a white-noise stimulating light, presented uniformly over a large retinal area (disc of 5mm diameter), and the resulting potential of the H-cell is recorded. The appropriate mathematical model is derived which can describe the dynamic behavior of the system over a range of two log-units of input light intensity. The derived model is the dynamic input-output relationship and it does not describe the underlying physicochemical processes that give rise to the S-potential. However, some insight on the system structure and internal mechanisms can be suggested by interpreting the derived Wiener kernels in conjunction with physiological and histological information available on the system (see Chapter III).

In the second approach we use the usual approach of guessing the transfer function and trying to fit a limited set of data such as

step responses and sinusoidal responses. This alternative model is derived in terms of a set of nonlinear differential equations. These equations describe separately the behavior of each component system such as photoreceptors, synapses, adaptive and inhibitory mechanisms, etc. The form of the equations is determined from partial previous knowledge of the characteristics of these sub-systems and supplemented appropriately so as to correctly fit a set of experimental step and sine wave responses. Emphasis is placed on the nonlinearities of the system. The derived model, in this case, is valid for the total operating range of input light intensity (about four log-units).

Finally, the performance of each model is evaluated and the two approaches (the white-noise and the conventional one) are compared.

It should be mentioned that Spekrijse and Norton [79] have applied a linear analysis technique (sinusoidal excitation) to obtain a linear transfer function for the carp light \rightarrow S-potential system.

2. Horizontal Cell Responses to Pulse and Sine Inputs

All S-potentials recorded from the catfish retina were hyperpolarizing excursions of the H-cell membrane voltage. In the figures they are plotted upwards for the hyperpolarizing direction.

Figure 6.1 shows three sets of pulse responses of the H-cell. In each of the three sets, the initial light level, on which the light pulses are superimposed, is different (being highest for C and lowest for A). In all three cases, after proper normalization, the experimental data follow the tanhlog curve for the maximum value of the H-potential as a function of the light intensity, as described by Naka and Rushton

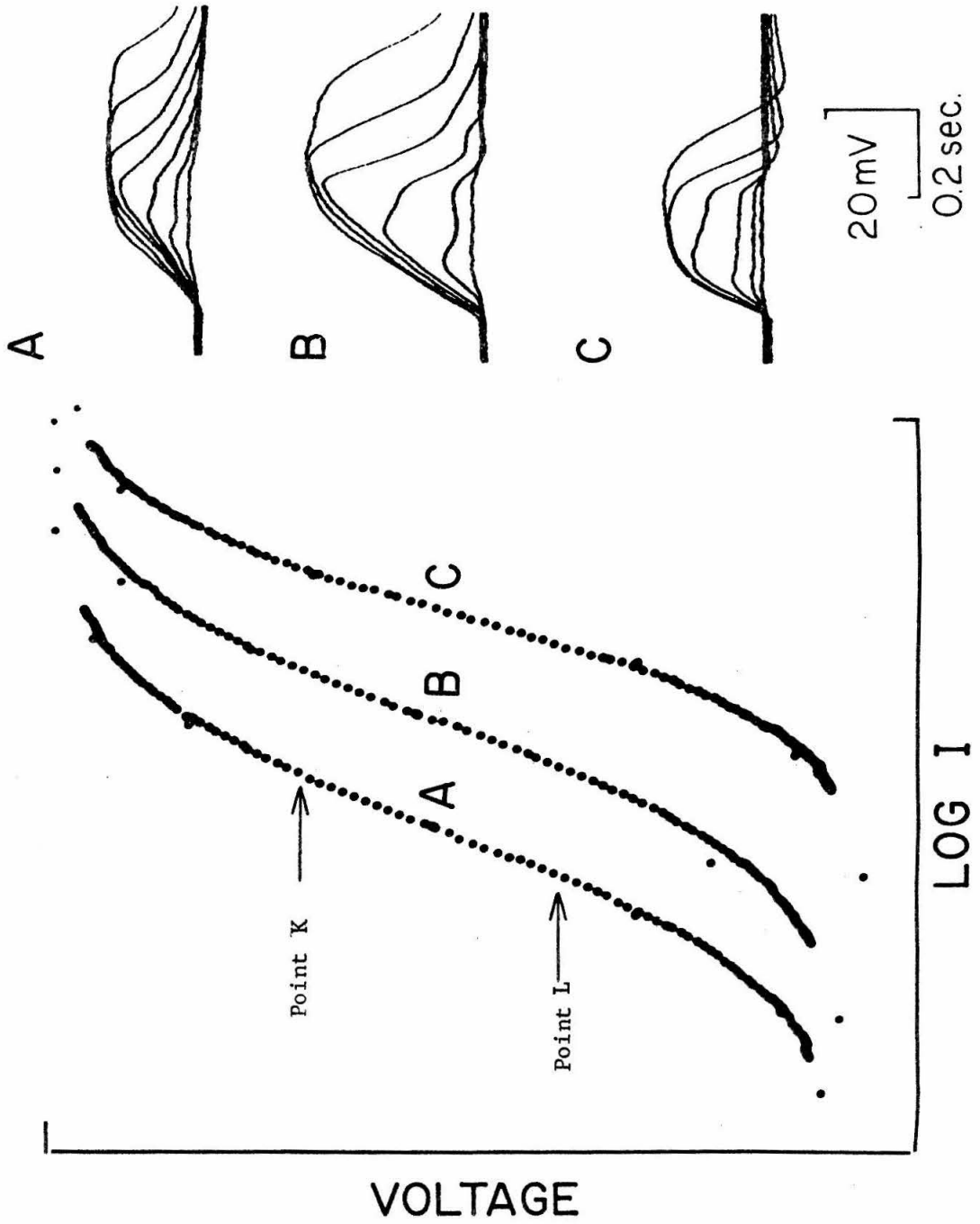


Fig. 6.1 Experimental H-cell step responses. The levels of stimulus steps are 0.4 log-units apart.

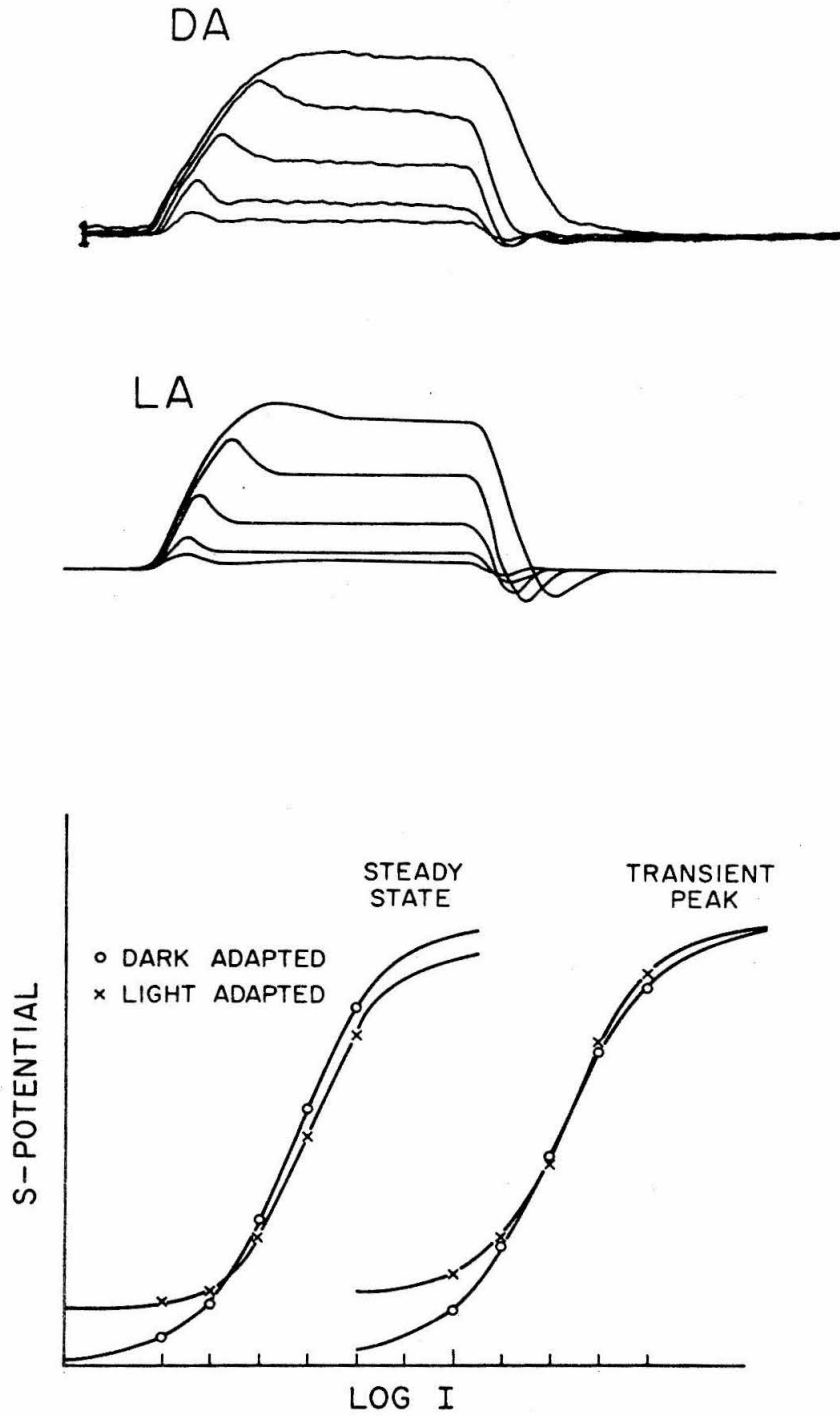


Fig. 6.2

Experimental H-cell responses for dark-adapted (DA) and light-adapted (LA) cases. (Input steps are 0.4 log-units apart).

[55,56,57] and by Naka [60]. Details of this transfer function have been discussed by Lipetz [43].

Figure 6.2 shows additional data recorded from a single unit both in the dark (DA) and light (LA) adapted cases.

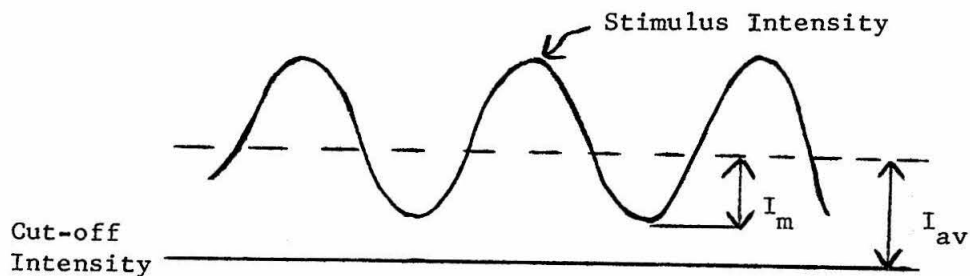
Examining the dynamic characteristics of these pulse responses we note the following:

- a) The on-slope of the H-potential is less steep than the off-slope.
- b) There is an overshoot in the on-phase which is greatest for intermediate values of the voltage.
- c) There is an undershoot in the off-phase in the light adapted case.
- d) There is a saturation effect for high light levels.
- e) The on-slope tends to be constant and independent of the levels of stimulus and response.
- f) For high stimulus levels there is an "overhung" effect in the off-phase. That is, the potential starts to turn off much later than the stimulus turns off.
- g) In the dark-adapted case there is an inflexion point in the off-slope which seems to depend on the voltage level.
- h) There is a higher response gain for the dark adapted system than the light adapted one.
- i) The response-intensity relation is the tanhlog function.

These characteristics of response waveform can be seen in the H-cell responses recorded from other animals including cats and tench and they are not exclusive features of the catfish H-cell responses.

Figures 6.3 through 6.7 show H-cell responses to sinusoidally varying light intensities (and for various average light levels) for the range of frequencies to which the system responds. This covers the range from d.c. to about 20Hz. It shares a common feature of biological systems in that it acts as a low-pass filter with certain nonlinear characteristics.

Figure 6.1 shows the different average light intensities with respect to the S-curve, which were sinusoidally modulated. Modulation depth, m , is defined as the ratio I_m/I_{av} .



The records in Fig. 6.3 were obtained by sine-wave light whose average intensity is at point K (Fig. 6.1) and with a modulation of about 0.6. There are several prominent nonlinear dynamic features in these sinusoidal responses.

a) At frequencies higher than about 3Hz there is a pronounced slow-on, fast-off effect. This effect is much less pronounced at frequencies lower than 3Hz. The effect persists even for "small signals" without diminution.

b) A saturation effect at low frequencies (Fig. 6.3A) for high response levels.

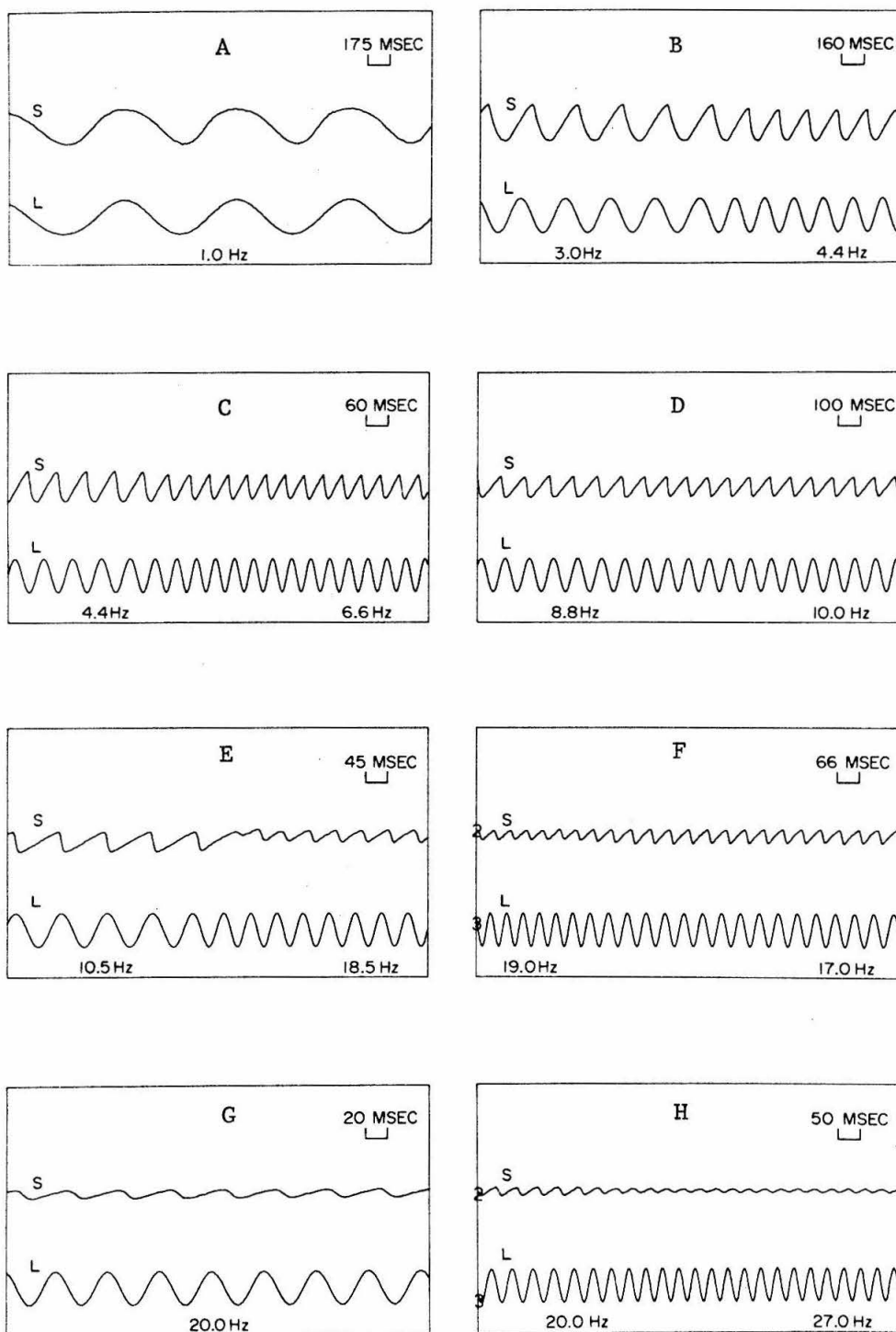


Fig. 6.3. Experimental H-cell sinusoidal responses. L: light stimulus, S: S-potential response. Average light level is at K (Fig. 6.1), modulation depth is 0.6.

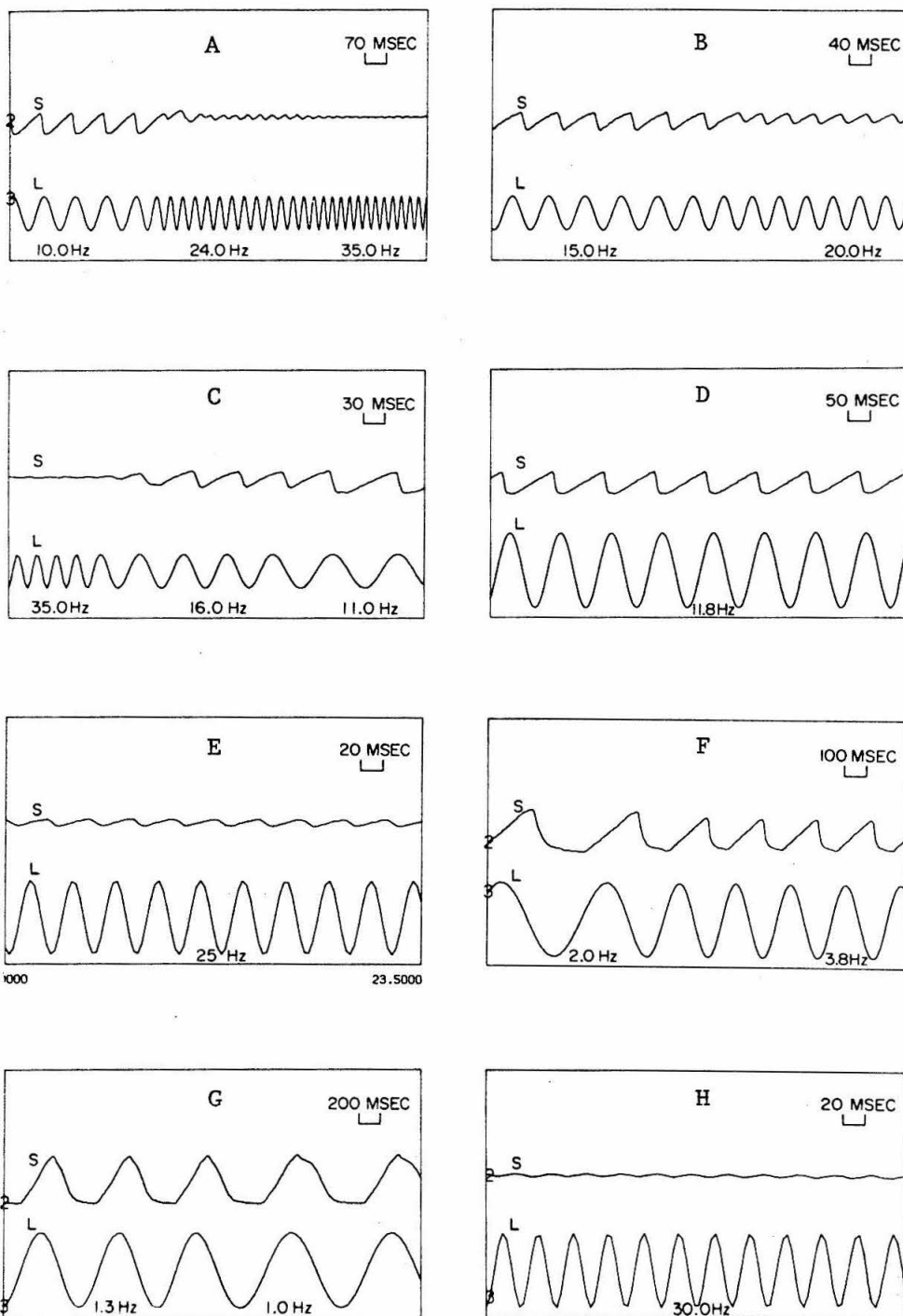


Fig. 6.4

Experimental H-cell sinusoidal responses. L: light stimulus, S: S-potential response. Average light level is at K (Fig. 6.1), modulation depth is 1.0.

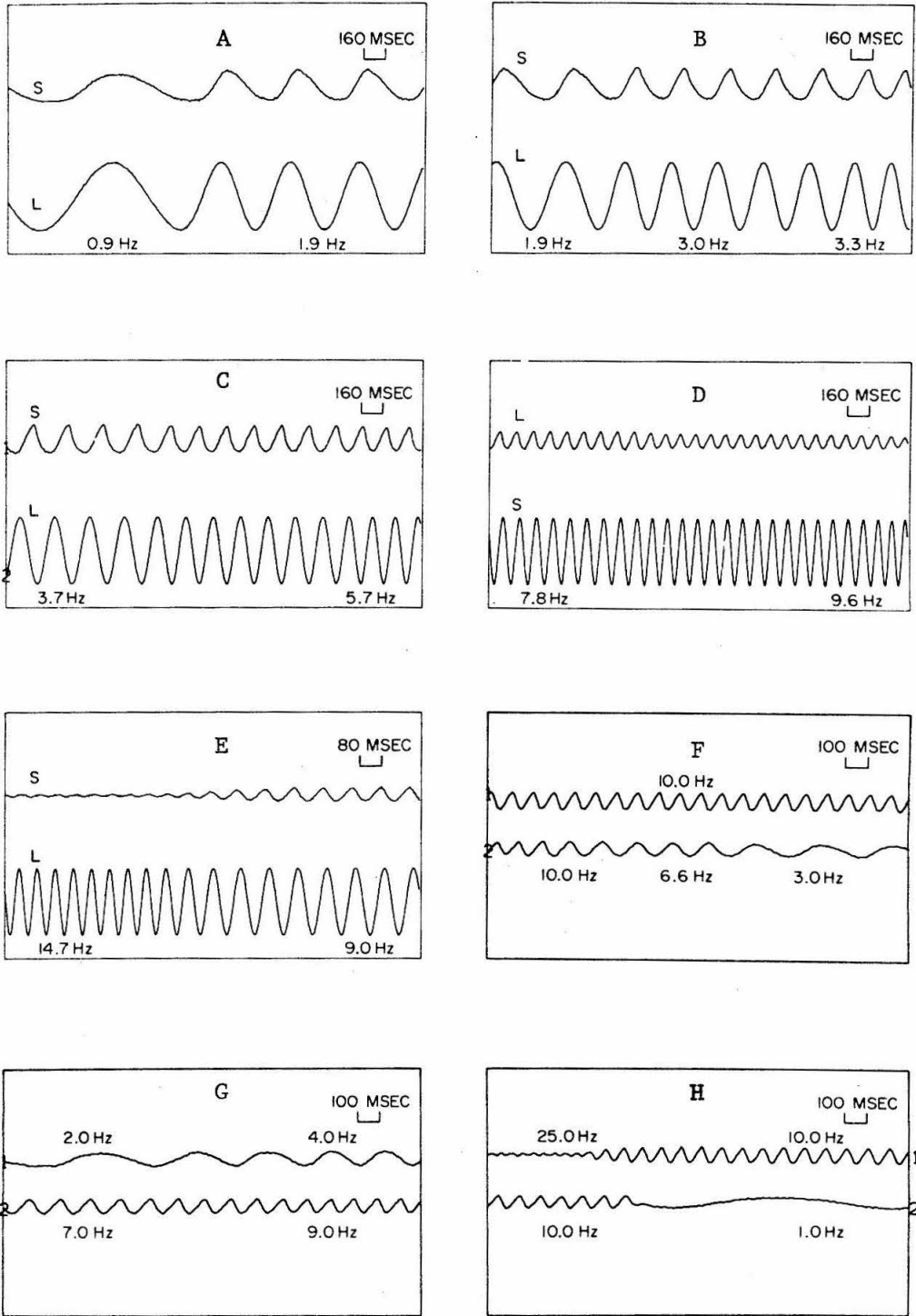


Fig. 6.5. Experimental H-cell sinusoidal responses. L: light stimulus, S: S-potential response. Average light level is at L (Fig. 6.1), modulation depth is 0.8.

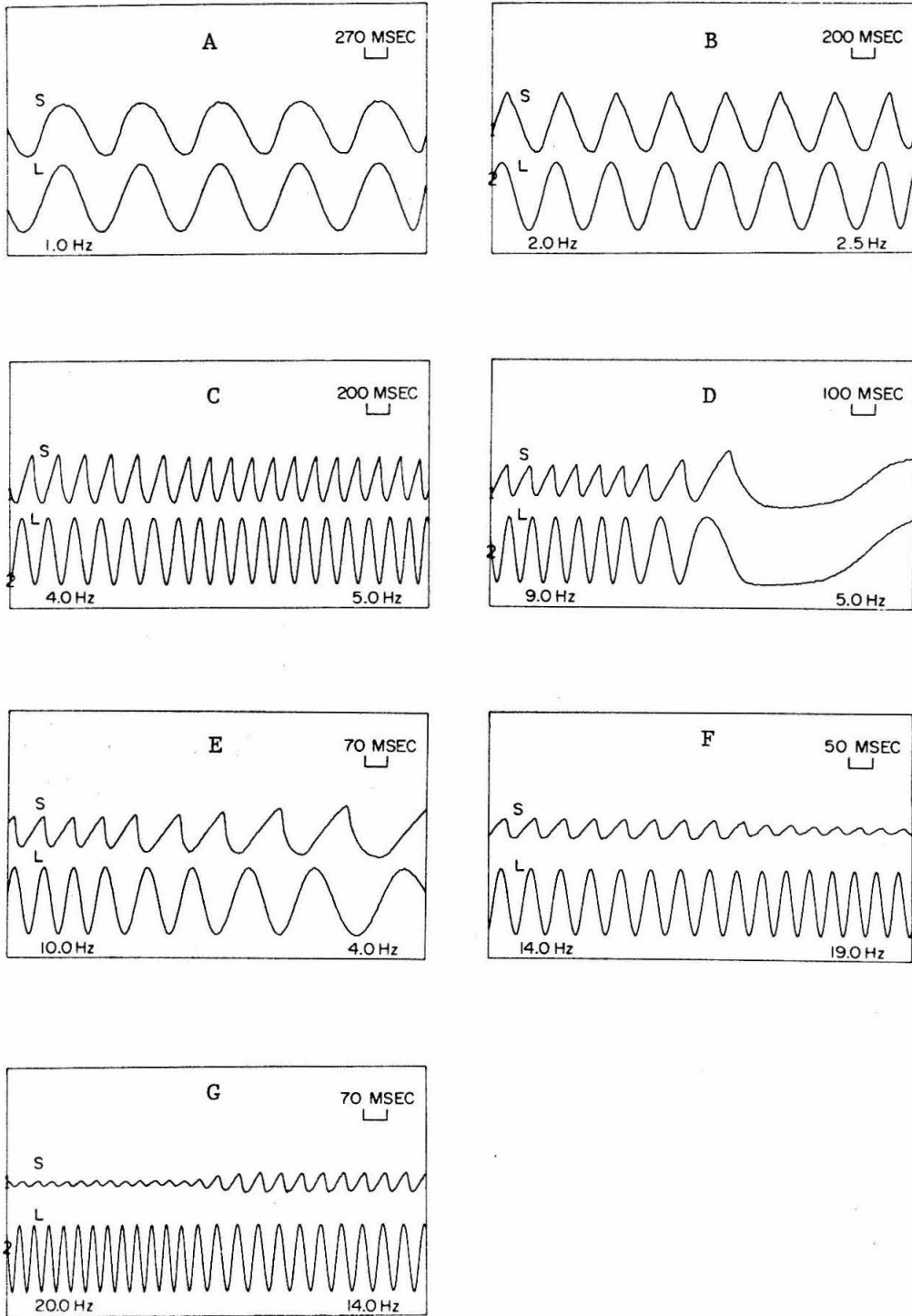


Fig. 6.6. Experimental H-cell sinusoidal responses. L: light stimulus, S: S-potential response. Average light level is at L (Fig. 6.1), modulation depth is 1.0.

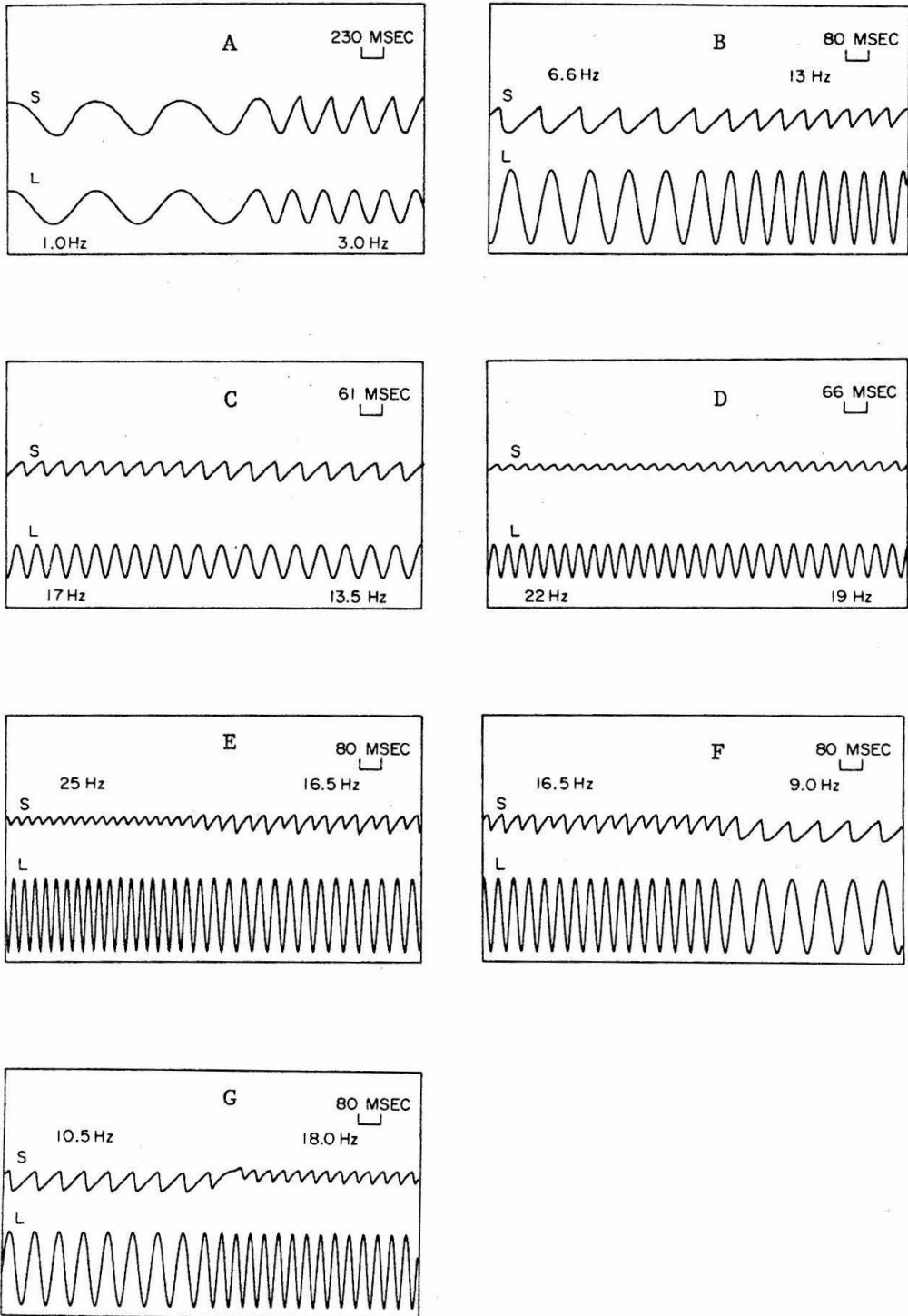


Fig. 6.7. Experimental H-cell sinusoidal responses. L: light stimulus, S: S-potential response. Average light level is at K (Fig. 6.1), modulation depth is 0.8.

c) As the stimulus frequency shifts from a low frequency to a high frequency there is, consistently, an upward shift in the average (d.c.) value of the response. (Fig. 6.3, E,F,H)

In Figure 6.4 the bias point is at K, as in Fig. 6.3, but the modulation depth is nearly 1.0. Again, we observe clearly the d.c. shift resulting from a change in frequency (Fig. 6.4, A,B,C) the slow-on, fast-off effect and a cutoff phenomenon at low frequencies (Fig. 6.4, F,G).

In Fig. 6.5 the bias point is at L (Fig. 6.1) and the modulation depth is 0.8. We note that the slow-on, fast-off effect is less pronounced. The response d.c. shift with a stimulus frequency shift is also diminished greatly. Thus, it appears that both these phenomena occur mainly at higher average light levels (level of point K (Fig. 6.1)). Figure 6.5, F,G,H show only the H-cell responses to sinusoidal stimuli (the stimulus signal is not shown).

In Fig. 6.6 the responses were recorded by sinusoidal light with the bias level at L (Fig. 6.1) and modulation depth nearly 1.0. Again, we note that the slow-on, fast-off effect is less pronounced than that at higher light levels. Also, the d.c. shift of the response with frequency is greatly reduced. At low frequencies, where the gain is high, there is a saturation effect for the high swing and a cutoff effect for the low swing.

In Fig. 6.7 the bias level is at K (Fig. 6.1) and the modulation depth is 0.8. We note the phenomena of slow-on, fast-off and d.c. shift with frequency. In addition, in the frequency range of 15-18 Hz there is another nonlinear phenomenon of alternately big and small

negative swings. This shows the presence of a strong second subharmonic component in the response. This phenomenon was observed only in the frequency range of 15 to 18 Hz and disappeared for the rest of the frequencies. This effect was noticed several times during the course of the experiments but not always. The exact conditions for the existence of this phenomenon are not known but it was noticed that it occurred at high average light levels. Naka has reported this effect [59]. It was not reported by Spekrijse and Norton [79].

All these dynamic features have been observed consistently throughout the course of the experiments. They are nonlinearities which we will incorporate in the differential equation model. These nonlinearities can suggest very useful insights to the underlying structure of the system, as will be seen.

3. Model Derived from White-Noise Test

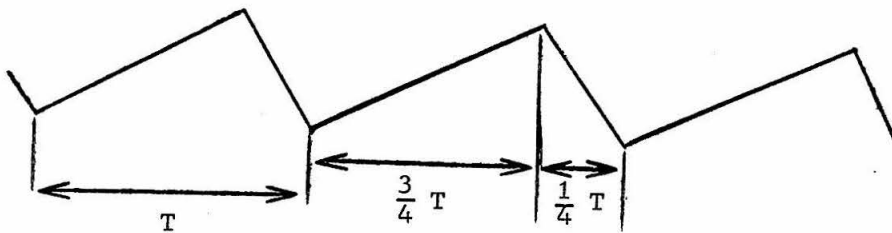
A nonlinear dynamic model of the light \rightarrow S-potential system was derived by performing a white-noise experiment. It was found that this model, inside its range of validity, predicted quite well all the dynamic features we discussed in the previous section.

The stimulus was a uniform light given uniformly upon the retina and modulated in time in a gaussian-white-noise fashion. The average intensity was at point K (Fig. 6.1). The bandwidth of the white-noise was 50Hz. The dynamic range of the light stimulus was about 1.8 log units. This means that

$$\log_{10} \frac{I_{av} + 3\sigma}{I_{av} - 3\sigma} = 1.8$$

where I_{av} is the average light intensity and σ is the standard deviation of the gaussianly distributed amplitude of the input signal. Clearly this dynamic range of the input covers only part of the total operating range of this system. Therefore, we expect the derived model to be valid only within this limited range.

Preliminary harmonic analysis of the catfish H-cell response showed that the system has a cutoff frequency at around 9Hz. Therefore, a white-noise bandwidth of 50Hz was chosen in order to cover completely the system bandwidth. From the H-cell sine responses, by performing Fourier analysis, the number of terms in the Wiener series was decided. These responses with their slow-on, fast-off characteristic,



have the following harmonic content

$$A_n = \frac{1}{n} \sin\left(n\pi \cdot \frac{3}{4}\right)$$

where A_n is the normalized coefficient of the nth harmonic. The following table gives the amplitude values for the first five harmonics with the fundamental normalized to one.

Table

<u>n</u>	<u> A_n </u>
1	1.0
2	.35
3	.11
4	0
5	.04

It is suggested from this preliminary analysis that we only need to compute up to the third order kernel in order to get a satisfactory model.

Applying the results of Chapter III we estimated the memory of the system at about 150 msec and the length of the needed record to about 1 minute. This record length would give a statistical error of less than 5% in the estimation of the kernel values.

Figure 6.8 shows the computed first order kernel $h_1(\tau)$. This kernel represents the impulse response of the linear system which is the best fit (in the mean square sense) for the white noise input-output record. From $h_1(\tau)$ we deduce that the system has a delay of about 15 msec and it is slightly underdamped. $h_1(\tau)$ also gives an estimate of the response rise time, and therefore an estimate of the frequency response.

Table 6.1 lists the values of the second order kernel $h_2(\tau_1, \tau_2)$. This is interpreted, as in Chapter III, to signify the deviations from linearity due to interaction between different (in past time) portions

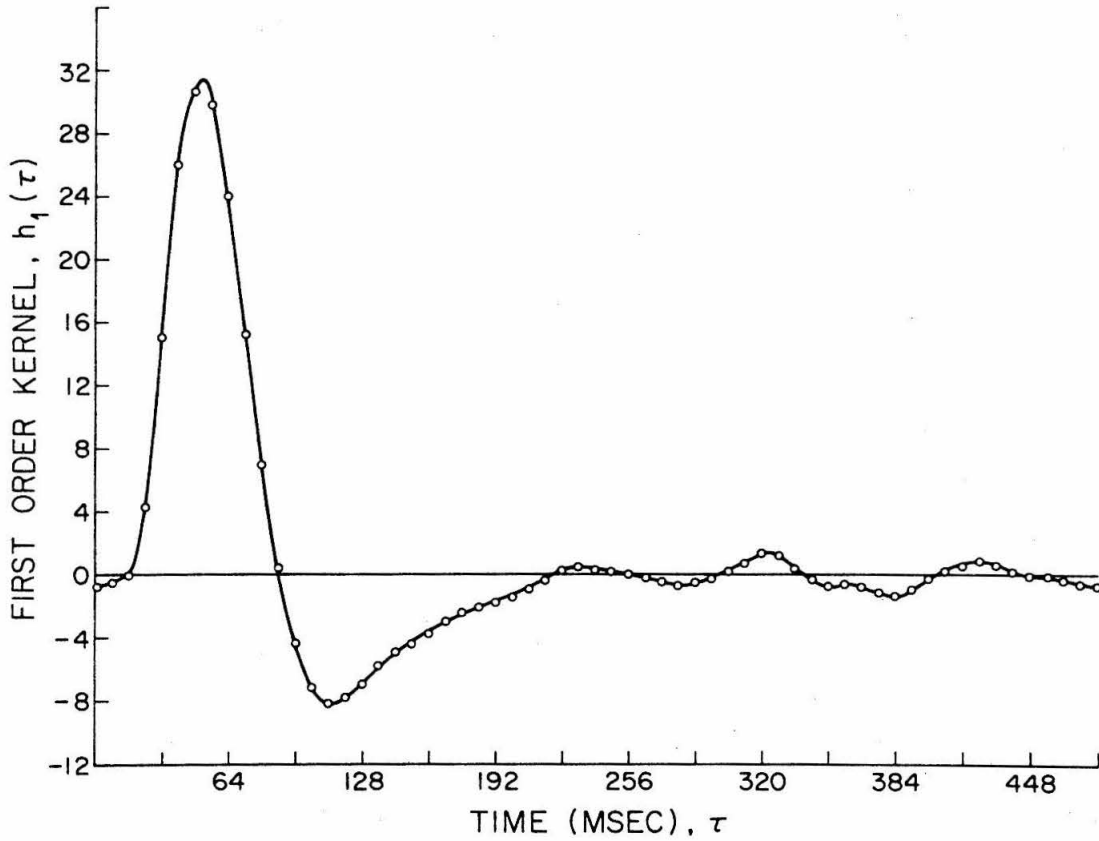


Fig. 6.8

Plot of first order kernel $h_1(\tau)$ for Light \rightarrow Horizontal system. The ordinate units are (normalized) mv/(photons/mm² sec) sec). The average light level is at K (Fig. 6.1) and corresponds to about 1.5×10^{11} photons/mm² sec.

SECOND ORDER KERNEL

0	8	16	24	32	40	48	56	64	72	80	88	96	104	112	120	128	136	144	152
0	3																		
8	0																		
16	-1	1	0																
24	-1	1	1	-2															
32	-1	-2	0	-7	-18														
40	0	-2	-2	-9	-20	-23													
48	1	-2	-2	-6	-18	-22	-16												
56	2	-1	-3	-3	-10	-20	-16	-9											
64	3	1	-2	-4	-2	-8	-14	-8	-4										
72	2	3	1	3	4	4	-2	-5	-4	-4									
80	0	2	3	6	10	7	3	0	-1	-2	-2								
88	-1	0	2	5	12	12	5	1	1	1	1	0							
96	1	1	1	4	10	14	7	0	-1	-2	1	2	0						
104	2	2	1	3	7	10	8	1	-2	-3	-1	3	4	3					
112	0	1	2	1	4	6	5	2	-1	-3	-3	-1	3	5	5				
120	0	0	0	1	3	3	1	1	-1	-3	-3	-2	0	4	6	6			
128	-1	-1	0	2	2	2	0	0	-1	-2	-3	-1	0	1	5	5	6		
136	0	-2	-1	-2	0	0	0	0	0	-1	-1	0	0	1	2	4	3	4	
144	2	1	-1	0	-3	-3	0	0	-1	-1	0	0	1	2	3	2	2	3	3
152	1	2	-1	0	2	-2	-1	0	0	-1	1	1	1	3	2	2	1	0	1

Table 6.1

Values of $h_2(\tau_1, \tau_2)$. Light \rightarrow Horizontal system. Mean intensity, 1.5×10^{11} photons/mm²·sec. Axes in msec.

of the input. The values of the third order kernel $h_3(\tau_1, \tau_2, \tau_3)$ are not easily tabulated but they were computed.

These three kernels completely specify the Wiener functional series up to the third order term. In effect, the set $\{h_1, h_2, h_3\}$ is the nonlinear dynamic model of the system under study.

At this point the following questions arise: How good is this model? How does one measure "goodness" of a nonlinear model for which the principle of superposition does not apply?

According to the Wiener theory and the white-noise philosophy, which we have discussed in Chapter III, the criterion of goodness of a nonlinear model is how well it performs when tested with a white-noise input. Such an input tests a system with a great variety of input functions and is therefore a general and stringent test of "goodness" of a given model. In fact, Wiener showed that two systems are equivalent if and only if they respond identically to a white-noise input. Therefore, "goodness" of model is measured by obtaining the white-noise response of the model and comparing it to the response of the system under study when it is excited by the same random noise. Such a comparison can be partially made in terms of measuring the power spectra of the responses of the two systems (model and physical) to white noise as well as measuring the agreement of the waveshape of these responses in terms of the mean square deviation.

Other criteria of "goodness" of the model consist in comparing the model responses to such specialized inputs as pulses and sine waves to the response of the actual system to the same inputs.

Figure 6.9 shows samples of white-noise responses of the H-cell

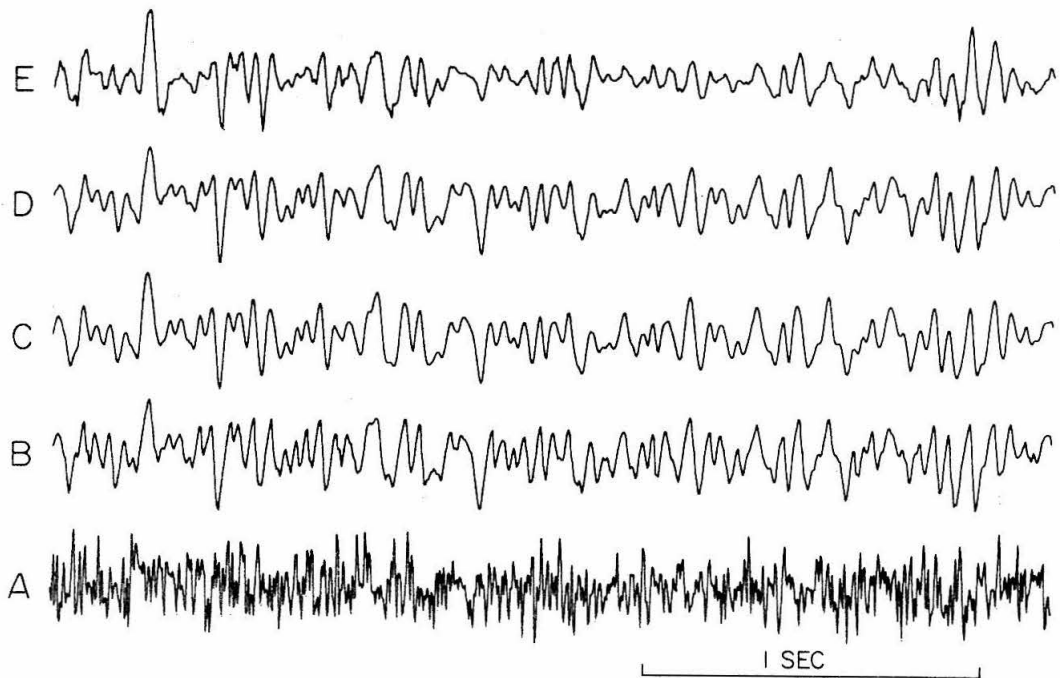
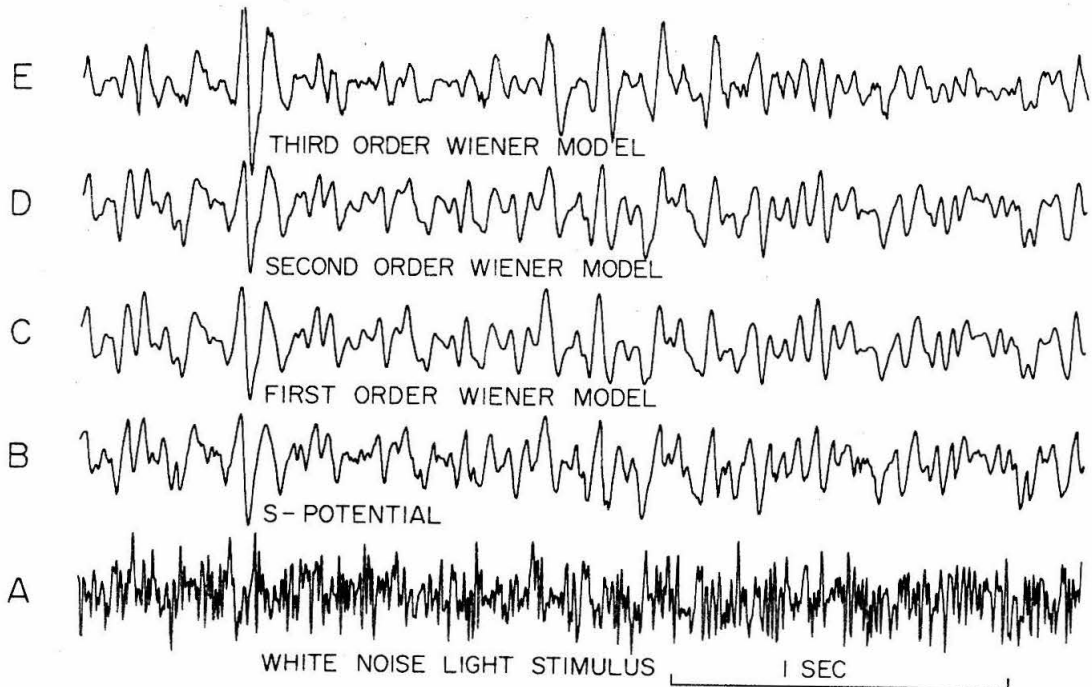


Fig. 6.9. Experimental and model white-noise responses. A: light stimulus, B: experimental H-cell response, C: first order model response, D: second order model response, E: third order model response. Average light level is at K (Fig. 6.1).

and a sequence of model responses to the same input for the first, second and third order Wiener models. We note that the first order model, which is the linear model is quite good in duplicating the H-cell response. This indicates that for this limited dynamic range of the input the system is almost linear. This suggestion is not quite correct if one carefully examines rise and fall slopes and peak to valley relationships.

The second order model appears to be almost the same as the first order one with slight differences. Let us examine the mean square error for the different model cases. The zeroth order model $\{h_0\}$ is just a constant equal to the average value of the response. The mean square error for this model is normalized to be 100 (arbitrary) units. The error is measured over the entire length of the white-noise record. The mean square error for the first order model is 26 units and the error for the second order model is 18 units. There is, therefore, substantial improvement by adding the second order nonlinear term. The improvement is mainly due to correcting rise and fall times of the response and peak to valley relationships. This will become clear when we examine the sine and step responses for this sequence of models.

We should have expected that the third order model would provide even better agreement with the experimental response. In fact, the mean square error, in this case, is 68 units. The reason for this worsening of the model is the following: The system is almost linear and therefore when the linear and quadratic responses are subtracted from the total response the remainder has a very high content of noise.

This very low signal to noise ratio introduces a large error in the computation of the third order crosscorrelation.

The second order model is sufficiently good as far as the white-noise test is concerned. Moreover, the computation of a third order kernel and its subsequent use in the Wiener model series takes inconveniently long computational times. Therefore, in all the following work, we computed the Wiener series up to the second order term. This, in almost all cases, has produced a satisfactory nonlinear model.

Figure 6.10 shows the power spectra of the white noise stimulus, the H-cell response, and the first, second and third order kernels. It is seen that the system has a cutoff frequency around 9Hz. The second order model improves the performance of the linear model significantly in the high frequency region. The third order model deviates considerably in the low frequencies but seems to improve the performance for the high frequencies. This can also be noticed from the white noise response records (Fig. 6.9).

Figure 6.11 shows the (light adapted) linear and nonlinear model responses to pulse inputs of different strengths. The intensity of the strongest pulse is outside the range of validity of the model and it is expected to deviate considerably from experimental results. The general characteristics of the experimental pulse responses are present in these model responses such as the overshoot, undershoot, rise time and fall time. Moreover, the nonlinear model responses (Fig. 6.11,A2) follow the tanhlog curve as shown (Fig. 6.11,C,B), have sharper overshoots and exhibit the slow-on, fast-off effect at the higher response levels. Even though in these general features the

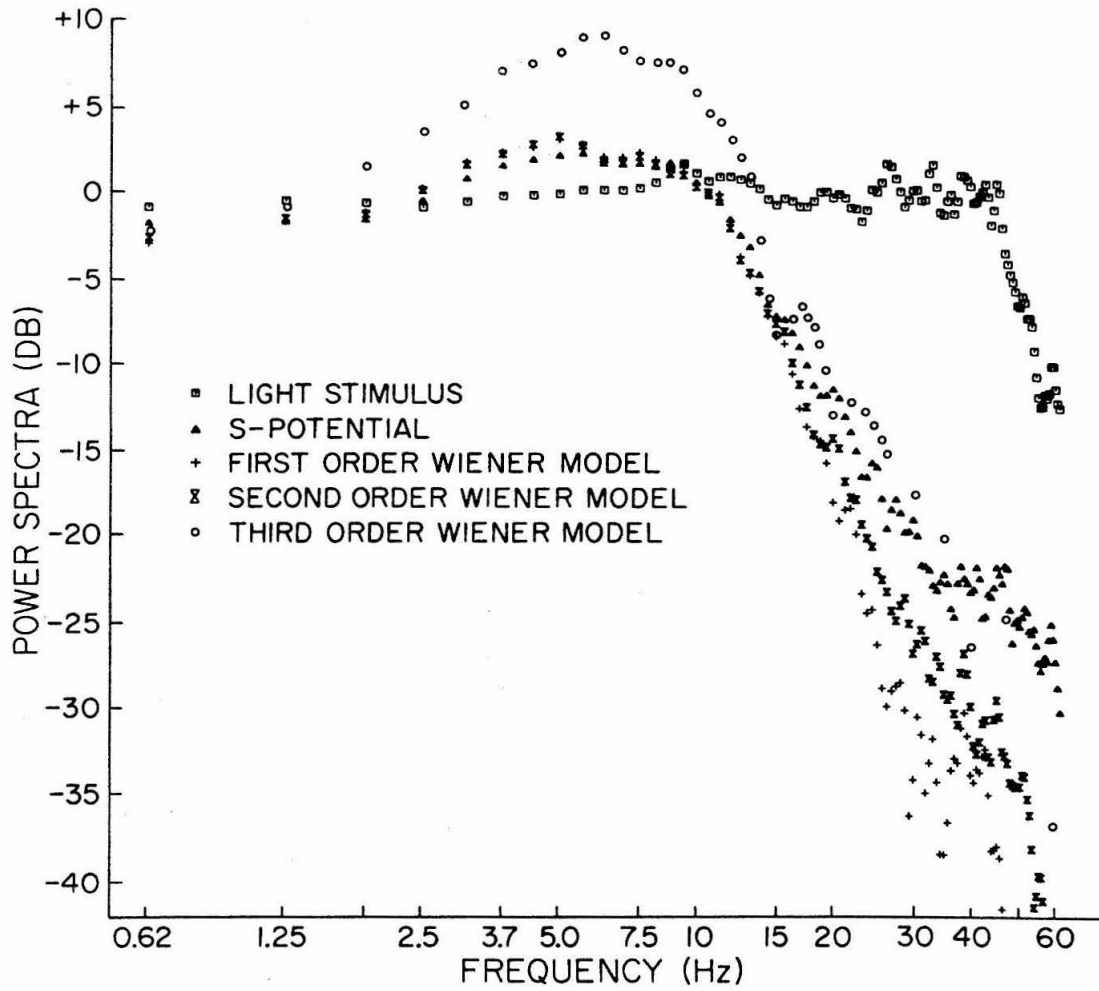


Fig. 6.10

Power spectra for experimental and model white-noise responses for Light → Horizontal system. Average light level at K (Fig. 6.1).

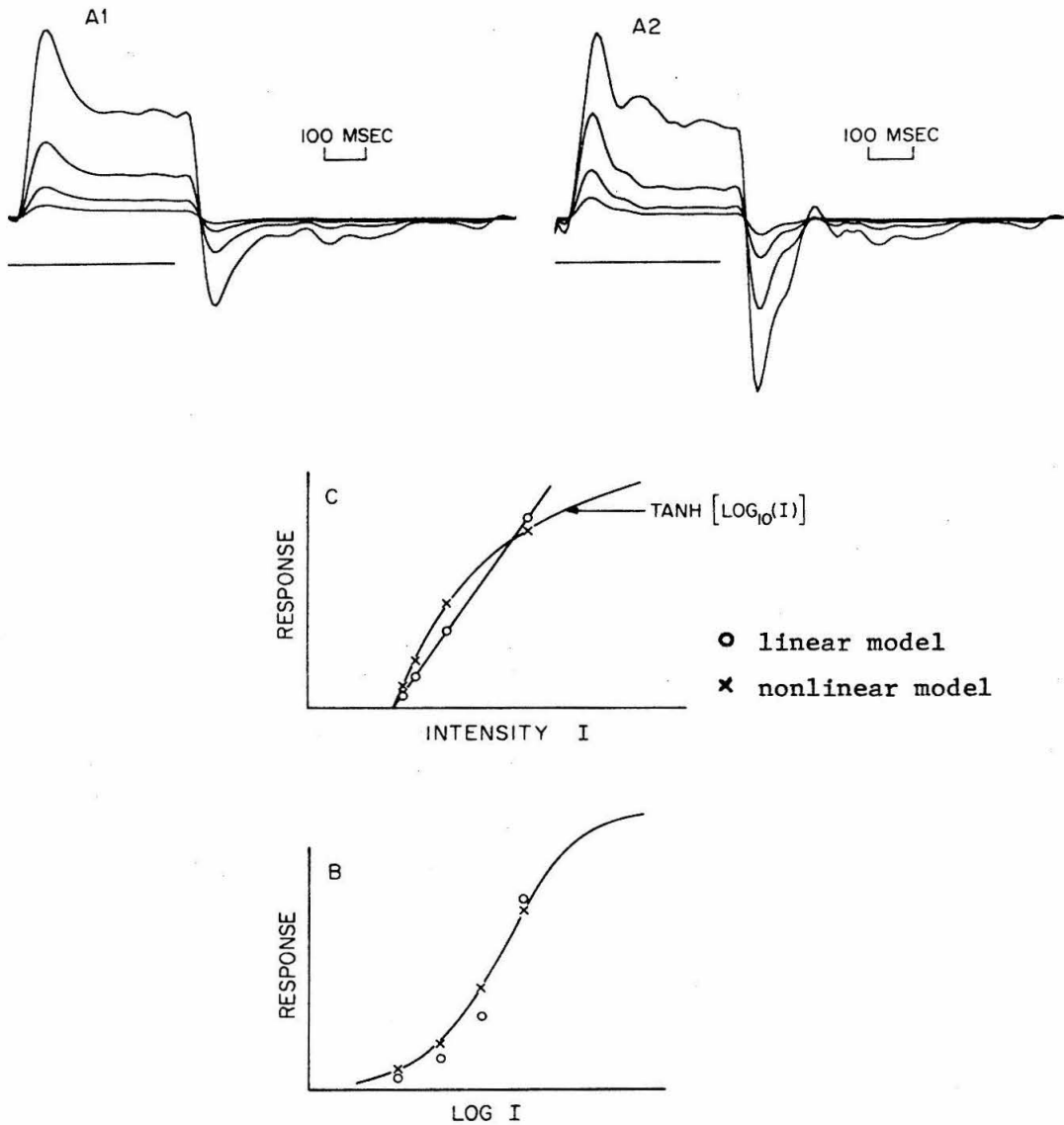
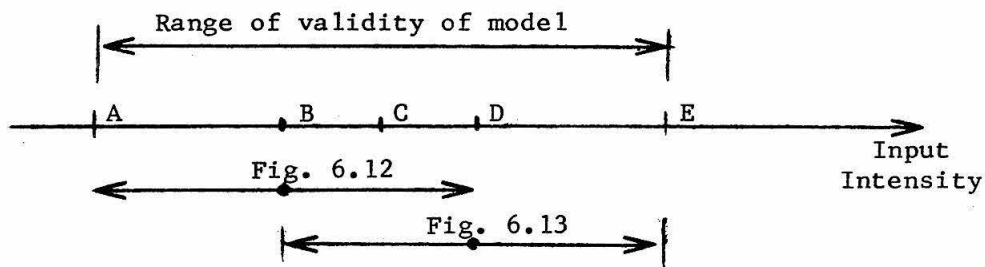


Fig. 6.11. Model step responses for (light-adapted) Light \rightarrow Horizontal system. Stimulus pulse levels are 0.4 log-units apart (highest pulse is outside the range of validity of the model). A1: linear model responses, A2: nonlinear model responses, B: H-cell (peak) response vs. log (intensity), C: H-cell (peak) response vs. intensity.

model characteristics agree well with the experimental ones, if considered in more detail the model responses to step inputs are not quite satisfactory. This is due to the fact that the higher harmonics, which are essential for sharp input changes such as steps, are not present in the second order model.

Figures 6.12 and 6.13 show sinusoidal model responses for a range of frequencies that covers the system bandwidth. The average stimulus level is higher in Fig. 6.12 and lower in Fig. 6.13 than the average stimulus level of the white noise test but the modulation ranges of both are within the range of validity of the model.



The average input level of the white noise is at C and the validity range extends from A to E. The sinusoidal responses of Fig. 6.12 are produced by a stimulus whose average ^{which} is at B and is modulated between A and D. The responses of Fig. 6.13 are due to a stimulus whose average is at point D and whose range of modulation extends from B to E.

Figure 6.12 shows clearly the improvement of the model response that the addition of the nonlinear term produces (trace W2) over the linear model (trace W1). All the nonlinear features we observed in the experimental sinusoidal responses (previous section) are present in the nonlinear model responses. These include,

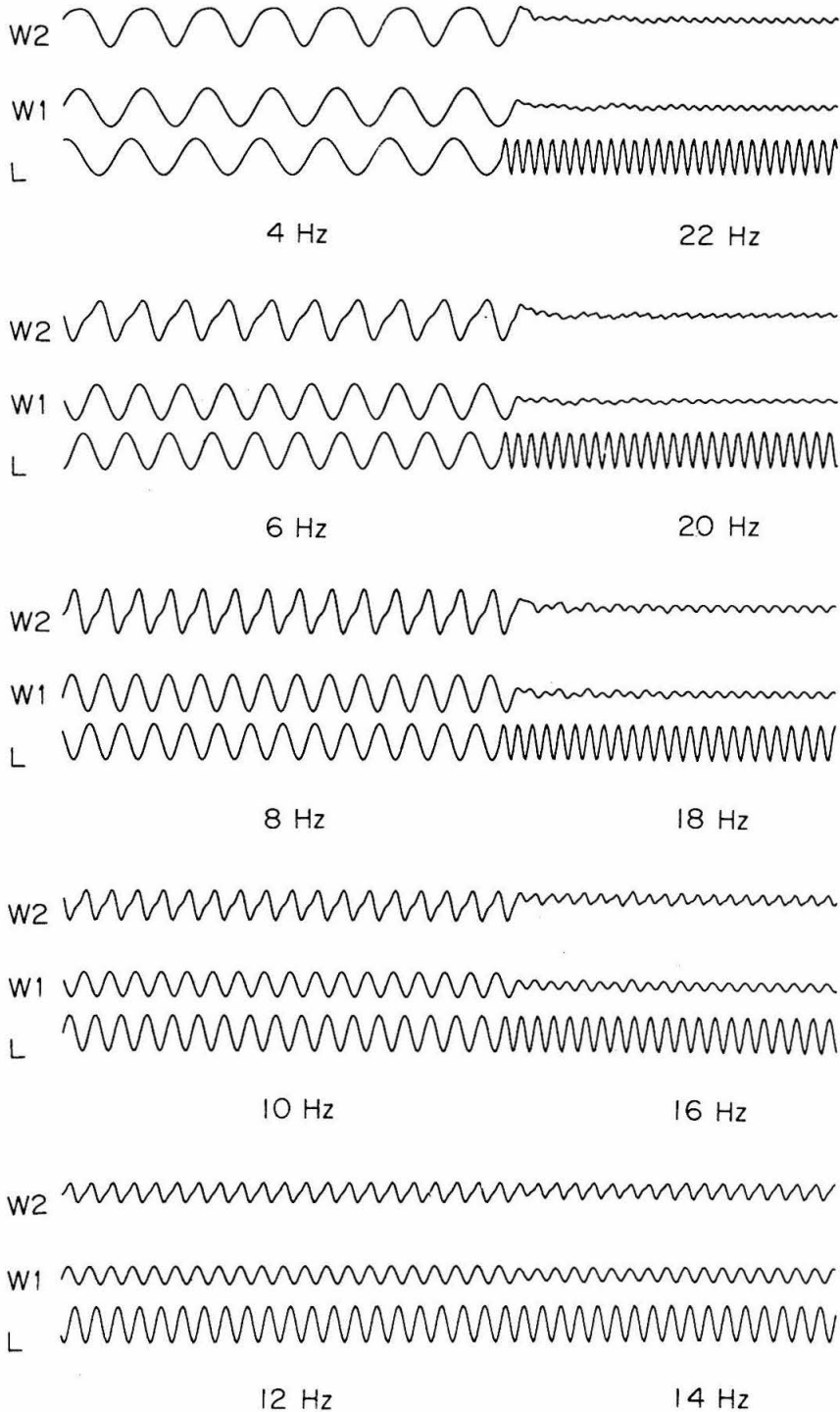


Fig. 6.12. Model sinusoidal responses for Light \rightarrow Horizontal system. L: stimulus, W1: linear model response, W2: nonlinear model response. Average stimulus level is higher than K (Fig. 6.1).

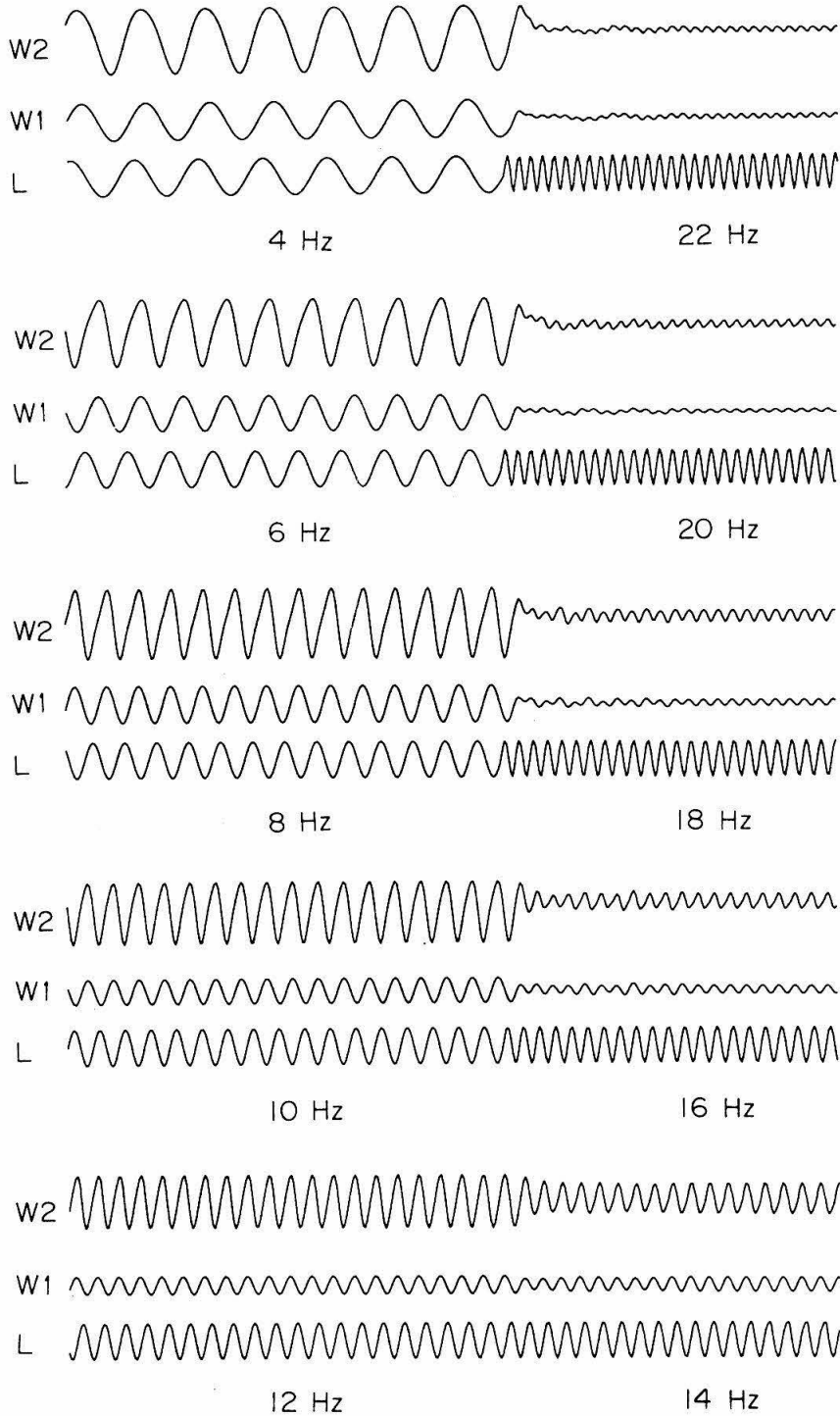


Fig. 6.13. Model sinusoidal responses for Light \rightarrow Horizontal system. L: stimulus, W1: linear model response, W2: nonlinear model response. Average stimulus level is lower than K (Fig. 6.1).

- a) A saturation phenomenon at low frequencies.
- b) A slow-on, fast-off effect (for frequencies higher than 4Hz) persistent even for "small signals."
- c) A shift upwards of the response d.c. level as the frequency is increased.
- d) The correct gain and phase characteristics.

In Fig. 6.13 where the average level is lower but the modulation range the same, the gain is higher due to the logarithmic transformation of the input. Moreover, the nonlinear effects of slow-on, fast-off and response d.c. shift with frequency are less pronounced at this lower level. This is in good agreement with the experimental results discussed in the previous section of this chapter.

In conclusion, the white-noise derived nonlinear model can predict quantitatively within its range of validity, all the nonlinear dynamic effects of the light-to-horizontal cell system satisfactorily. Therefore, the set of kernels (h_1, h_2) is taken to be a reasonably good model of this system.

Figure 6.14 shows power spectra of H-cell responses obtained by stimulating the system with white-noise light of 25Hz bandwidth. The two cases correspond to two widely different average intensity levels, 1 log-unit apart, the low one being near the lower flat portion of the S-curve and the high one being near the higher flat portion of the S-curve. We note that, by increasing the mean light level, the system becomes faster-responding (cutoff frequency changes from about 8Hz to about 12Hz) and also it becomes more underdamped.

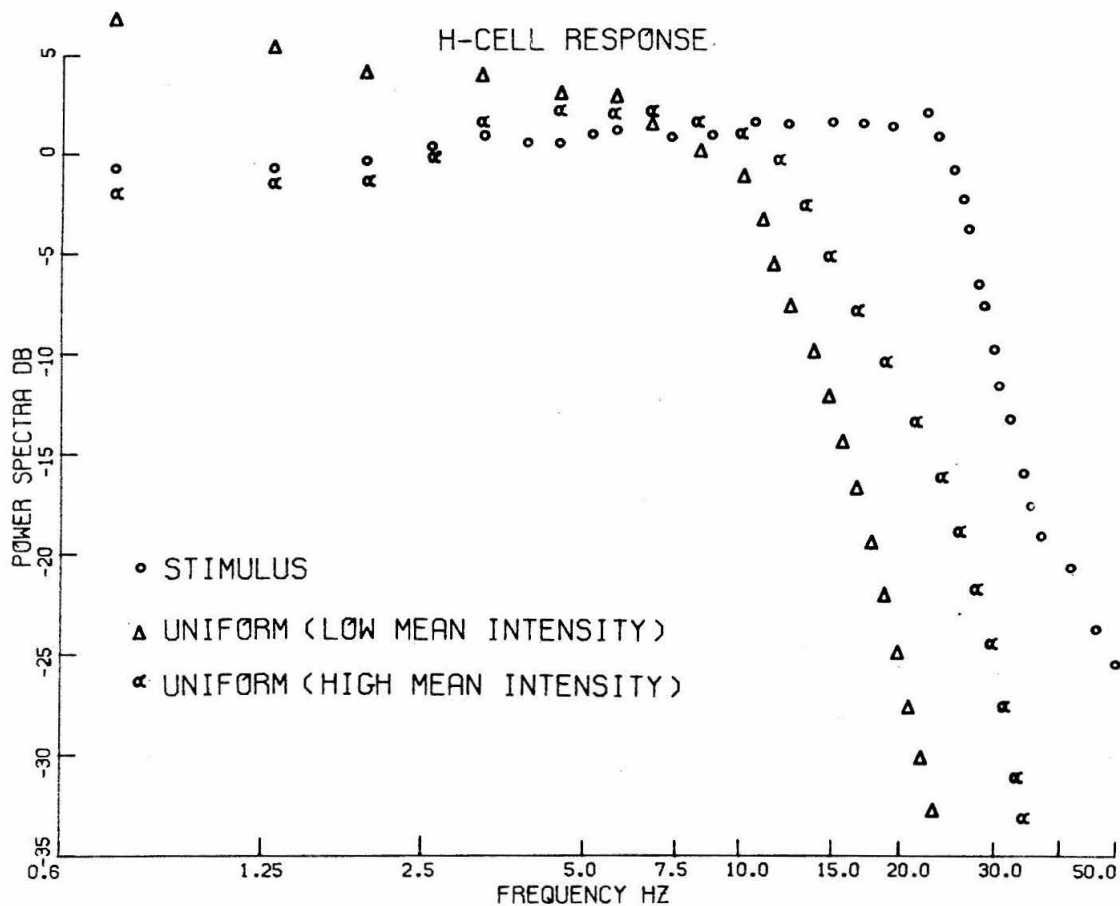


Fig. 6.14. Power spectra of experimental responses to white-noise for system Uniform light \rightarrow Horizontal cell potential. Low mean intensity is 2.5×10^{10} photons/mm²·sec and high mean intensity is 1.5×10^{11} photons/mm²·sec.

4. Structural Model of the Light \rightarrow S-potential System

The model derived by the white-noise method is valid within a limited operational range. Moreover, it reveals little about the system cellular structure. It is mainly a mathematical description of the dynamic input-output transfer characteristic. Nevertheless, the white-noise method is a systematic approach to characterizing a nonlinear system; it can provide some information about the system internal mechanisms; it is uncomplicated to apply once certain preliminary decisions (Chapter III) are made; and it gives good results.

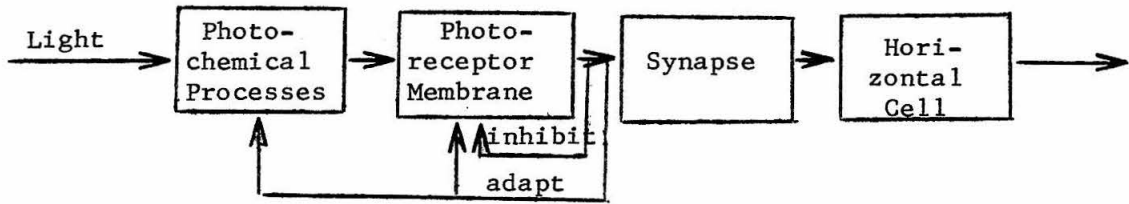
On the other hand, the classical approach to nonlinear model building consists of the following: A set of differential equations is chosen which is assumed to describe the different processes taking place within the system; this set is picked on the basis of limited information about these subsystems and in order to provide for some of the system features; a set of experimental system responses is chosen, usually step and/or sinusoidal responses; the differential equation model responses to these same inputs (step and/or sines) are then compared with the experimental ones; based on this comparison the parameters and/or the form of the equations or the equations themselves are changed trying to obtain a better fit to the data; the process terminates when the modeler decides that a satisfactory fit has been obtained. This approach has been very popular among modelers of biological systems [cf. DeVoe, 14c].

The whole procedure (and its outcome) depends solely on the skill and imagination of the modeler and it is not systematic beyond what is described above. In general, it tends to be time-consuming. The

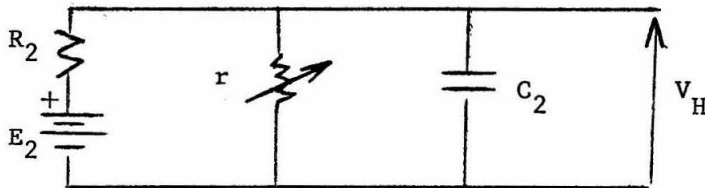
resulting model is usually good only for the chosen set of responses (steps/sines) and not satisfactory for other types of input. Often, as new information about the system is found by the experimenter, it is necessary to change radically all the equations and start the modeling process from the beginning.

In this section we follow the classical approach and obtain a model for the Light \rightarrow Horizontal cell system. The set of equations is fitted to the step and sine responses of this system and they cover the total operating range of the system (about 4 log units of input range).

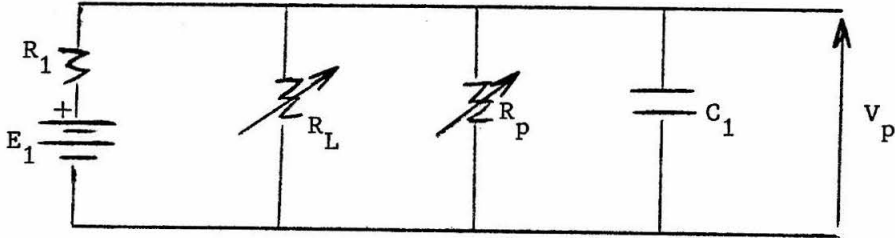
The main subsystems are shown below in their functional order along with inhibitory and adaptive paths



There is evidence (N. Matsumoto, personal communication) that the horizontal cell membrane can be modeled by



where resistance r increases during excitation, and the photoreceptor membrane can also be modeled by



where resistance R_p increases during excitation [4]. Resistive path R_L was added in order to take account of possible inter-receptor interaction, receptor-horizontal cell interaction and negative feedback mechanism within the photoreceptor [cf. 4 and Joe Brown, personal communication]. R_L is controlled by the photoreceptor voltage V_p and R_p is controlled by the photochemical processes.

These membrane models give the tanhlog characteristic for both the photoreceptor [3] and horizontal cell steady state responses [58], since,

$$(1) \quad \frac{V_H}{E_2} = \frac{r/R}{r/R + 1} = \frac{10^J}{10^J + 1} = \frac{e^{J \cdot \ln 10}}{e^{J \cdot \ln 10} + 1} = \frac{1}{2} \left(1 + \tanh \frac{\ln 10}{2} \cdot J \right)$$

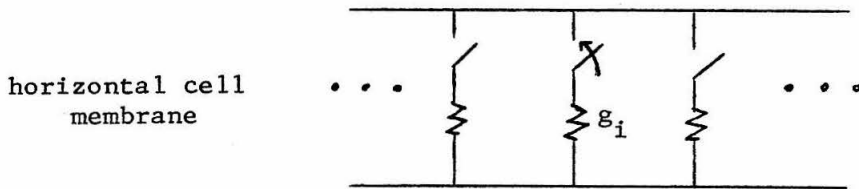
where $J = \log_{10} \frac{r}{R}$ and it is assumed that the excitation is related linearly to the change in r .

It has been assumed in the literature [71] that the light intensity undergoes a logarithmic transformation almost instantaneously in order to accommodate a large range of input. We note, however, that if the existence of a low pass filter (with an appropriately small cutoff frequency) is stipulated preceding this log device (or tanhlog device, to account for cutoff and saturation which are present in all

physical systems) then the experimentally observed d.c. shift of response with frequency is conveniently explained. In fact, by noting the magnitude of shift as a function of frequency the characteristics of this low pass filter can be estimated. On the other hand, if the input is log-transformed instantaneously we would need to stipulate additional nonlinear mechanisms to account for the d.c. shift of the response (see Fig. 6.15).

Figure 6.15 shows how the cascade combination of a low pass filter and a logarithmic device produces a d.c. shift of the output as the frequency changes. This is due to the fact that the slope of the logarithmic function changes rapidly and monotonically and therefore the negative-going swing of the larger-amplitude low frequency gets amplified more than the smaller-amplitude high frequency. Figure 6.15 shows graphically how this effect occurs. In the model the filter transfer function is chosen such that the experimentally observed shifts as a function of frequency are obtained.

Let us consider how the resistance of the horizontal cell membrane changes when excited by the photoreceptor. Naka and Rushton [58] have modeled this resistance as a parallel combination of conductances, g_i ,



which are switched on the network as excitation is received (thus increasing the membrane conductance). For our modeling purposes we can

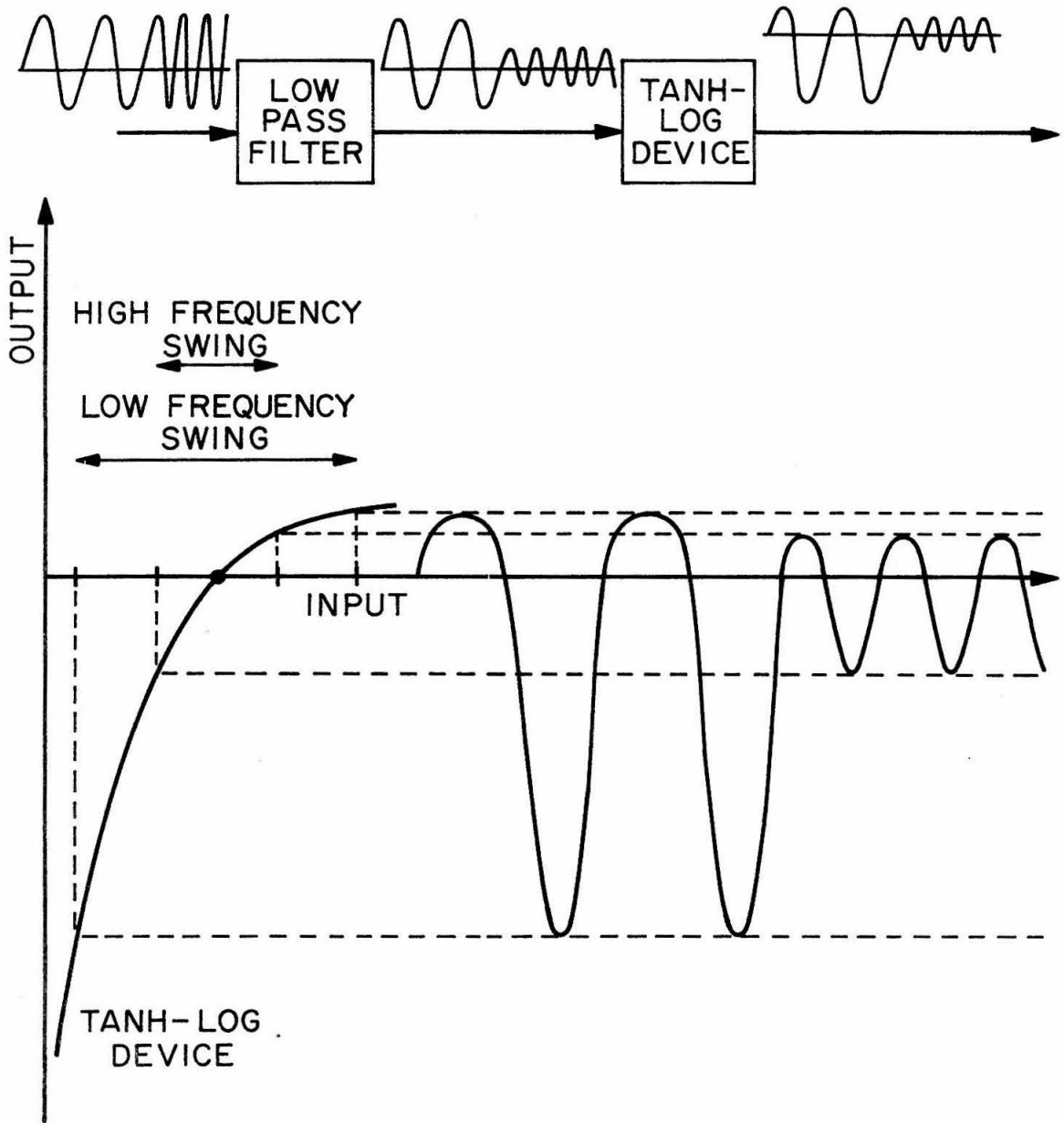


Fig. 6.15. Subsystem configuration that explains the response d.c. shift with a change of frequency (Light \rightarrow Horizontal system). The tanh-log characteristic is plotted and it is shown how the d.c. shift results for two different input frequencies (one low and one high).

stipulate either an increase or a decrease of the membrane conductance and obtain the same effect (tanhlog relationship). Here we assume that conductance decreases with excitation as is the case for the receptor membrane. We will stipulate a dynamic equation for this process which is physiological and explains very naturally the slow-on, fast-off phenomenon which we observe in the experimental records.

Conductance g_i can be thought of as being a transmembrane channel which in the open state has conductance g_i and in the closed state has zero conductance. Let the total number of channels of the membrane be N and the number of closed channels be n . In the case of no excitation the total membrane resistance is

$$r_0 = \frac{1}{g_0} = \frac{1}{Ng_i} = \frac{r_i}{N} \quad (\text{darkness membrane resistance})$$

while in the case of some excitation the membrane resistance becomes

$$(2) \quad r = \frac{1}{g} = \frac{1}{(N-n)g_i} = \frac{r_i}{N} \cdot \frac{1}{1 - \frac{n}{N}}$$

Letting

$$p = \frac{n}{N}$$

where by our definitions, follows that $0 < p < 1$, and

$$(3) \quad r = \frac{r_0}{1-p} \quad .$$

We note that p is the proportion of closed channels. Letting Q be the forcing agent that acts upon the channels to close them and which is proportional to the photoreceptor action on the horizontal cell

membrane, we stipulate the following dynamic equation for the closing of the channels:

$$(4) \quad \underbrace{\frac{dp}{dt}} = \underbrace{(Q - p)} \cdot \underbrace{(1 - p)}$$

Rate of channel closing	Unused agent	Proportion of open channels
-------------------------------	-----------------	-----------------------------------

This equation has a definite physical meaning. It says that the rate at which channels are closing is proportional to the amount of unused agent that is present and to the proportion of open channels. It is an expression similar to the well known formula of conditional probabilities for the occurrence of a composite event.

Equation (4) successfully produces for the model the slow-on, fast-off characteristic. This is, effectively, done by changing the time constant of the system appropriately (term $(1-p)$ in the equation).

We list the differential equations that describe the photochemical processes, the photoreceptor, the synapse and the horizontal cell. Input intensity is R , output horizontal cell voltage is V_H , and photoreceptor voltage is V_p .

ELECTROCHEMICAL PROCESSES

$$(5) \quad \dot{u} = w_e^2 (R-S) - 2J_e w_e S$$

$$(6) \quad \dot{S} = H \tanh (u/H) \quad \text{where} \quad J_e = \frac{J_{eo}}{(1-V_p)V_p}$$

PHOTORECEPTOR

$$(7) \quad \tau_7 \dot{R}_{p0} = P_0 + F_{p0}(V_p - V_{pr}) - R_{p0}$$

R_p is equal to S unless $S < R_{p0}$, in which case $R_p = R_{p0}$

$$(8) \quad \tau_{11} \dot{V}_L = V_p - V_L$$

$$\frac{1}{R_L} = G_L = G_A \frac{V_L}{V_L + G_B} \quad \text{and} \quad X_R = \frac{R_L R_p}{R_L + R_p}$$

$$(9) \quad \tau_p \dot{V}_p = 1 - \left(1 - \frac{R_1}{X_R}\right) \cdot V_p$$

SYNAPSE

$$(10) \quad Q_{12} = V_p + \tau_{12} \dot{V}_p$$

$$(11) \quad \tau_b \dot{p} = (Q_{12} - p)(1 - p)$$

$$(12) \quad Q_{24} = p + \tau_{24} \dot{p}$$

HORIZONTAL CELL

$$(13) \quad \ddot{r} + 2 J_H \omega_H \dot{r} = \omega_H^2 [R_0 - r(1 - Q_{24})]$$

$$\text{where } J_H = \frac{J_{HO}}{(1 - V_H) V_H}$$

$$(14) \quad \tau_H \dot{V}_H = [1 - (1 + R_2/r) \cdot V_H]$$

Equations (5) and (6) describe the dynamics of the photochemical reactions caused by incident light R . The output of these reactions, S , acts upon the photoreceptor membrane to change (increase) resistance R_p . This initial stage is described by a second order system whose

damping ratio J_e , is a function of the photoreceptor output voltage, V_p . The function for J_e is chosen such that J_e is lowest for the intermediate range of V_p . Output S can be thought of as a substance whose production is caused by the incident light R and which acts upon the photoreceptor membrane to change its resistance. The rate of production, \dot{S} , of this substance has saturation and cutoff levels as expected of any physical process. This is depicted by equation (6).

The dynamics of the photoreceptor membrane model, which was proposed earlier, are given by equation (9). Resistance R_p at the absence of excitation, that is the "darkness resistance" of R_p , is R_{p0} . We assume that this resistance changes as a function of the membrane voltage V_p (equation (7)) but, at any time, R_p cannot be less than R_{p0} . Such a control of the "darkness resistance" was found necessary in order to produce the experimentally observed inflexion point of the off-response to pulses (dark adapted system). This formulation also accounts for photoreceptor adaptation. V_{pr} is the resting voltage of the photoreceptor membrane and P_0 is the dark-adapted "darkness resistance" of R_p . Equation (8) describes the inhibitory feedback on the photoreceptor as a change of resistance R_L controlled by the membrane voltage.

The dynamic characteristics of the synapse have been modeled simply by equation (11) which has been explained earlier as describing the rate of channel-closing of the horizontal cell membrane. The input to this process is Q_{12} which is proportional to the photoreceptor voltage V_p and its rate of change (equation (10)). Similarly the output of the synaptic process is proportional to p and its rate (equation (12)).

This dependence of the input and output of the synaptic mechanism was introduced in order to obtain the correct frequency response for the overall system.

Equation (13) describes the dynamics of the resistance change of the H-cell membrane. A second order system is used whose damping is controlled by the membrane voltage V_H . The damping as a function of V_H is chosen such that the damping is lowest for the intermediate range, in accordance with the experimental observations. Resistance r is changed by agent Q_{24} and at steady state is given by

$$r = \frac{R_o}{1 - Q_{24}}$$

where R_o is the no-excitation resistance (in accordance with the conductance-channel model described above).

Equation (14) describes the dynamics of the H-cell membrane that has been proposed earlier. The horizontal cell voltage, V_H is the final output of the system.

The parameter values are:

$$\begin{aligned} \omega_e &= 2\pi(15) \text{ sec}^{-1} , & J_{eo} &= 0.06 , & H &= 5000. \\ \tau_7 &= \frac{1}{2\pi(3)} \text{ sec} , & P_o &= 0.5 , & F_{po} &= 10.0 \\ \tau_{11} &= 0.04 , & G_A &= 0.16 , & G_B &= 0.7 \\ R_1 &= 12.0 , & \tau_p &= \frac{1}{2\pi(30)} \text{ sec} . \\ \tau_{12} &= \frac{1}{2\pi(14)} \text{ sec} , & \tau_b &= \frac{1}{2\pi(30)} \text{ sec} , & \tau_{24} &= \frac{1}{2\pi(14)} \text{ sec} \\ \omega_H &= 2\pi(15) \text{ sec}^{-1} , & J_{HO} &= 0.05 , & \tau_H &= \frac{1}{2\pi(13)} \\ R_2 &= 5.0 , & R_o &= 1.0 \end{aligned}$$

The photoreceptor potential V_p and the horizontal cell potential V_H are normalized from zero to one.

We call the model described by these equations a 'structural model' because it depicts an organization of interacting subsystems. The parameter values of the equations were adjusted so that we would obtain a good fit of the experimental responses to pulse and sine stimuli.

Figures 6.1 and 6.2 show experimental responses of the H-cell potential to pulses of light whose strength increases successively by 0.4 log-units. Both the dark adapted (DA) and light adapted (LA) cases are shown. Plots of the steady state response and transient peak as a function of the logarithm of the intensity are shown.

Figure 6.16 shows the responses of the structural model to pulses whose strength increases by 0.4 log units. Both the model photoreceptor (A',B') and horizontal cell (A,B) responses are shown for the dark adapted (A,A') and light adapted (B,B') cases. It is noted that the agreement between model and experiment is extremely good. All the dynamic features discussed earlier are present in the model responses. These include:

- a) The response-intensity relation being the tanhlog function (graph at bottom of Fig. 6.16).
- b) Overshoot for the on response which is maximum for the intermediate response range.
- c) Slow-on, fast-off phenomenon.
- d) Overhang effect for high intensity levels.
- e) Slope inflexion of the off-response in the dark adapted case.

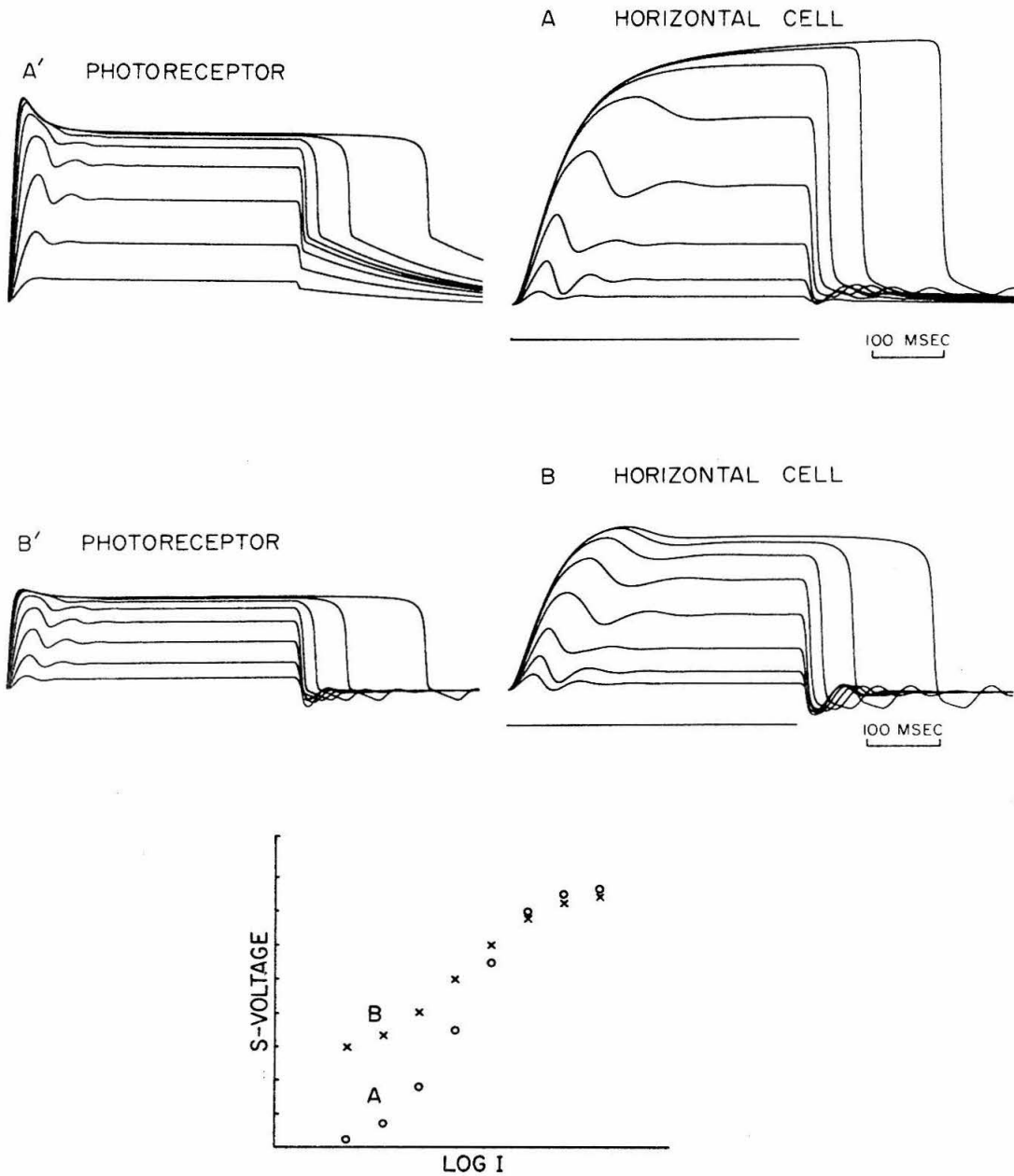


Fig. 6.16. Structural model step responses (photoreceptor and H-cell). Stimulus steps are 0.4 log-units apart in magnitude. Plots A',A are for the dark-adapted and B,B' for the light-adapted system. A plot of response vs. log (intensity), for both the dark-adapted and light-adapted cases, is also shown.

- f) Undershoot of the off-response for the light adapted case.
- g) Higher response gain for the dark adapted system than the light adapted one (due to the logarithmic transformation).
- h) Saturation effect for high response levels.
- i) The on-slope tends to be constant and independent of the levels of stimulus and response.

The photoreceptor responses predicted by the model cannot be checked because of lack of any intracellular photoreceptor data from the catfish. When such data become available the model equations can be changed so that these responses will also be fitted. For the time being the photoreceptor output of the structural model is simply an hypothesis. Some comparison can be made with the results of Chapter V.

Figure 6.17 shows the model sinusoidal responses for the system frequency bandwidth range. Trace L is the input light, trace S is the output S-potential and trace P is the photoreceptor response. The photoreceptor response is speculative, as explained, and can be ignored (nevertheless, compare with results of Chapter V). The model responses clearly mimic well the experimental responses to the same stimuli. In particular, we note:

- a) The slow-on, fast-off effect for frequencies higher than 4Hz present even for "small signals."
- b) The d.c. response shift as the frequency changes.
- c) The correct gain and phase characteristics.

Figure 6.18 shows the model response (trace C) to a white noise input (trace A) and the experimental response (trace B) to this same input. Trace D is the photoreceptor response and can be ignored.

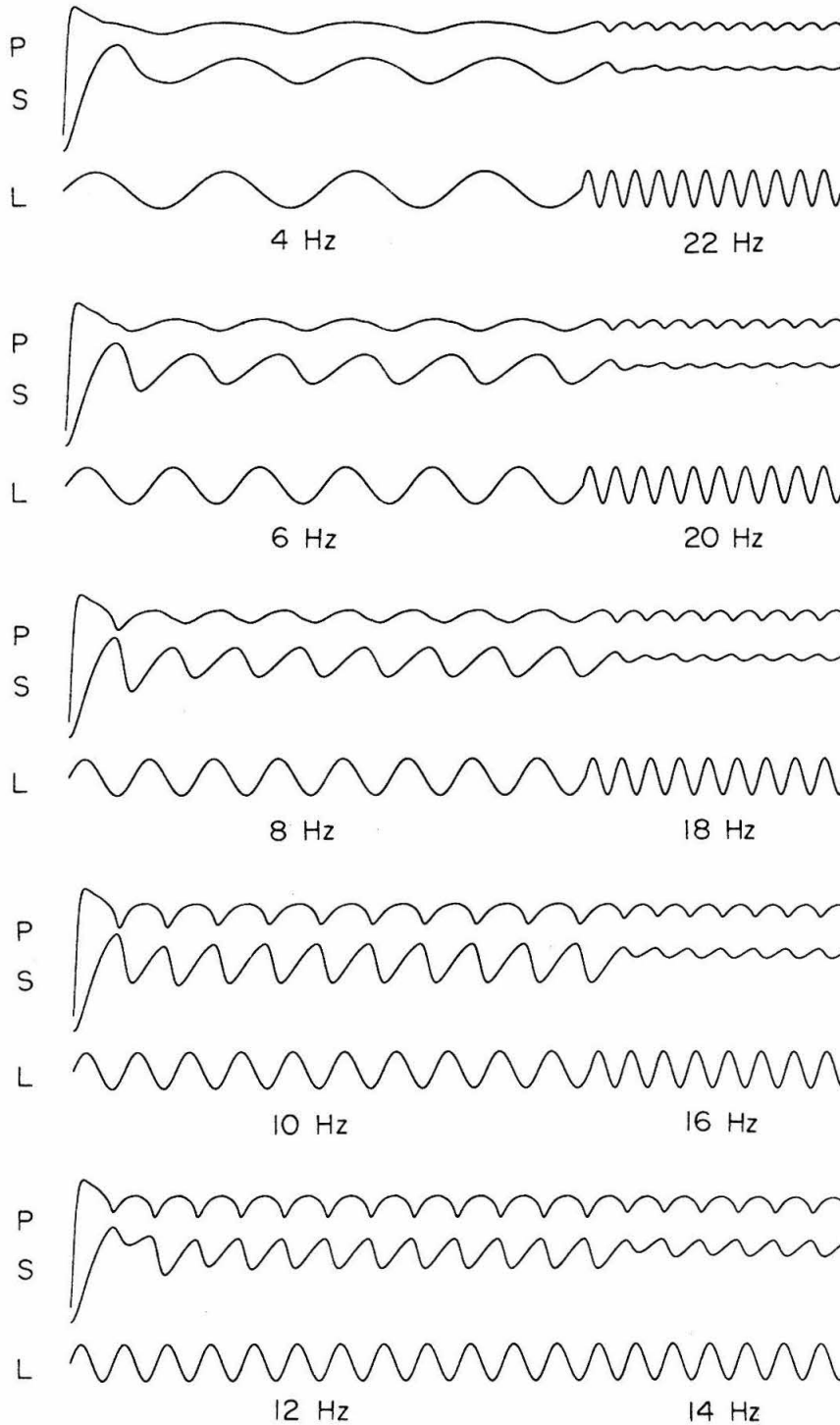


Fig. 6.17. Structural model sinusoidal responses (photoreceptor and H-cell). L: light stimulus, S: H-cell response, P: photoreceptor response.

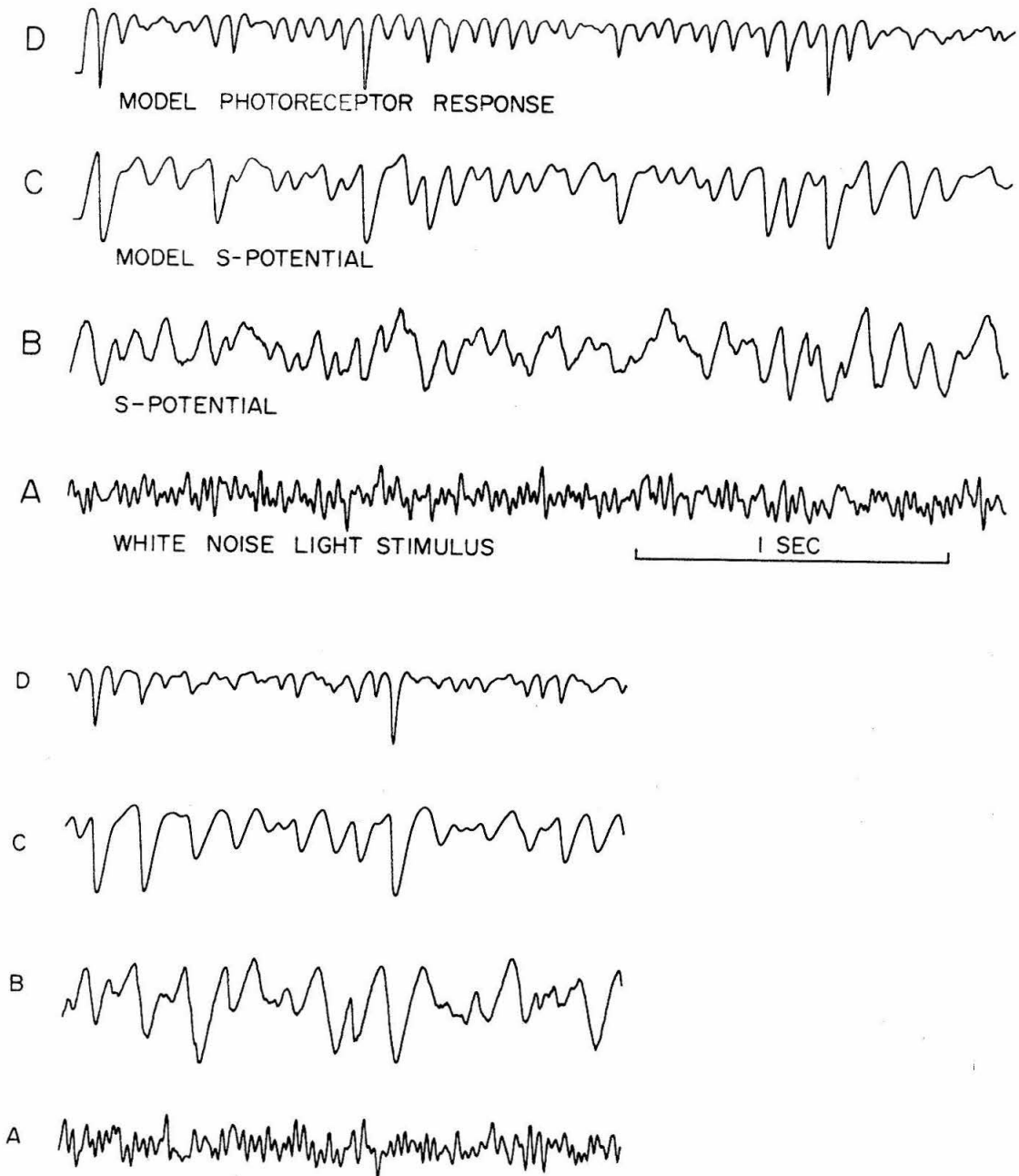


Fig. 6.18. Structural model and experimental responses to white-noise (photoreceptor and H-cell). A: light stimulus, B: H-cell response (experimental), C: H-cell response (structural model), D: photoreceptor response (structural model).

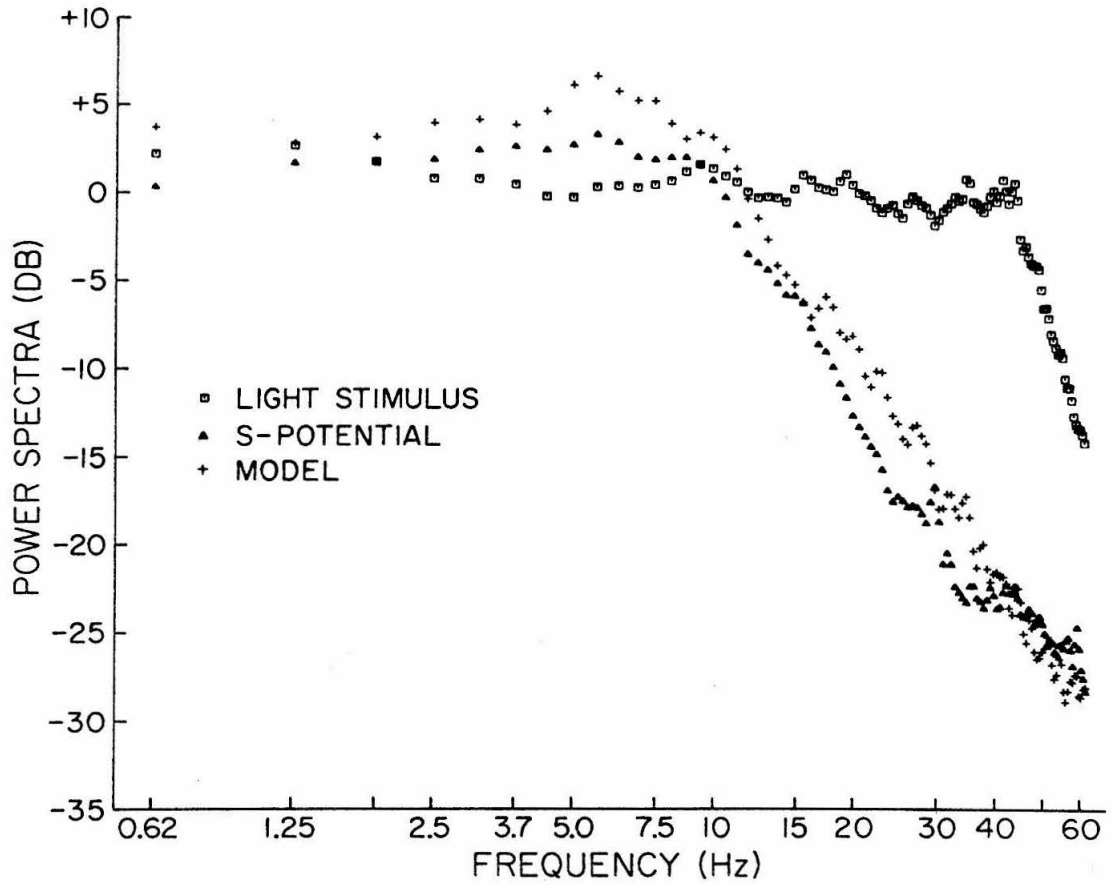


Fig. 6.19. Power spectra for experimental and structural model white-noise responses.

Obviously the model response for a white noise input is not satisfactory. One reason is that for the particular run shown in Fig. 6.18 the model is more light adapted (hence an obvious saturation effect for the positive peaks in the model response) than the physical system itself. This unsatisfactory model response to white-noise is not unexpected since this structural model was designed to fit step and sine responses. This must be contrasted with the white-noise derived model which produced excellent results for white-noise stimuli and less satisfactory results for the step stimuli (the sinusoidal responses of the white-noise derived model were excellent).

Figure 6.19 shows the power spectrum densities of the white-noise stimulus, the experimental response and the model response for the structural model. The agreement between model and experimental spectra is good. This indicates that the model has the correct frequency response.

5. Discussion of the Two Models

Figure 6.20 shows gain and phase characteristics of the sinusoidal responses for the physical system, the white-noise-derived model (Wiener model) and the structural model. The phase characteristic of the structural model is different (approaches asymptotically -2π at high frequencies, indicating a fourth-order system) because we have not incorporated the system latency (delay) in this model. If this delay (about 15 msec.) is added to the structural model the phase characteristic agrees well with the experimental one.

From the high frequency asymptotic slope of the phase characteristic of the experimental (or Wiener model) curve we can calculate the system latency. The phase shift ϕ due to a latency τ , as a function of

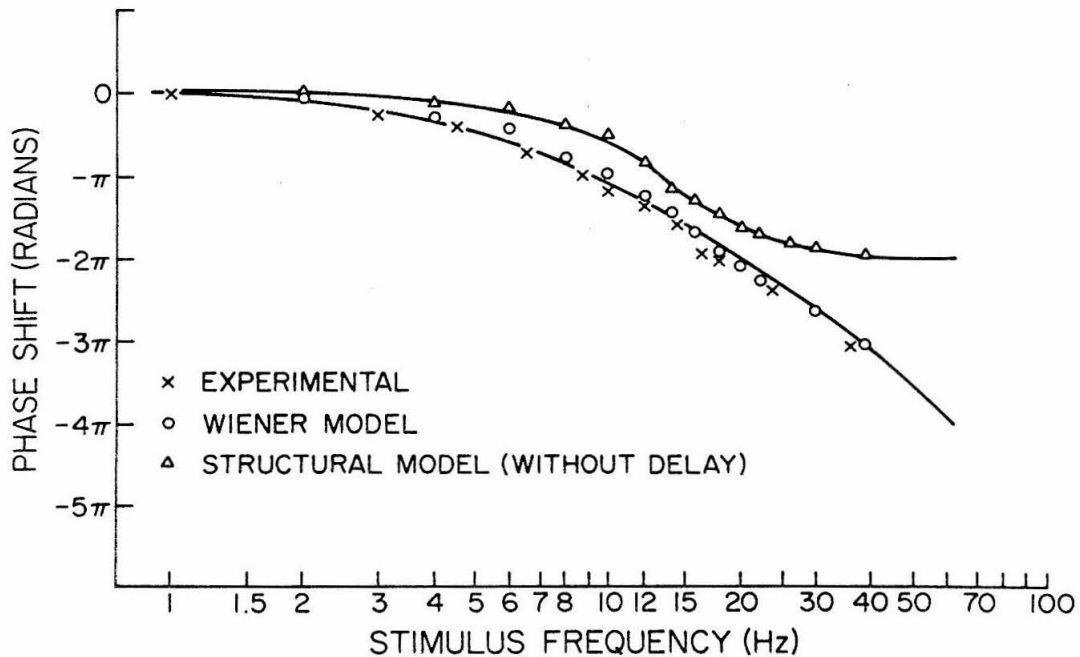
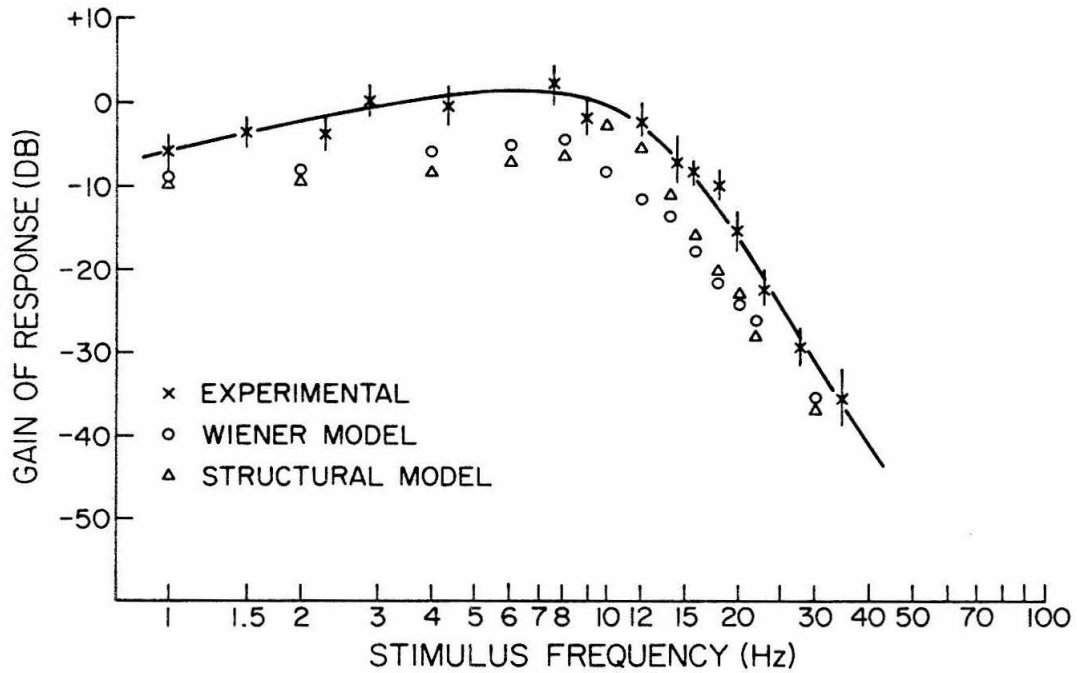


Fig. 6.20. Gain and phase plots of Light \rightarrow Horizontal system obtained from experiments and from the two types of model; the white-noise-derived (Wiener) model and the structural model. There is no transit delay incorporated in the structural model (phase plot).

frequency f , is

$$\phi = 2\pi f\tau \quad \text{and} \quad \tau = \frac{\Delta\phi}{\Delta f} \cdot \frac{1}{2\pi}$$

We obtain $\Delta\phi = \pi$ for $\Delta f \approx 30\text{Hz}$ and therefore

$$\tau = \frac{\pi}{30} \cdot \frac{1}{2\pi} = 0.016 \text{ sec}$$

which is in agreement with the latency measured from the first order kernel in a previous section (15 msec.).

Gain and phase measurements on a nonlinear system such as this do not have a clear meaning since superposition does not apply and the harmonic content at any frequency is high. The measurement of phase, especially, is a matter of the individual's choice and should be interpreted very carefully and with reservation.

It is obvious from the description presented so far that the white-noise derived model is superior from the functional point of view. That is, assuming that we are interested only in the input-output relationship, this model is a much more accurate descriptor of the system behavior. Its drawbacks are that it is valid only for a limited operational range and it does not account for the internal structure of the system. These two disadvantages are not present in the structural model which in turn is simply not a very good model for any other input besides pulses and sines. Moreover, the structural model is extremely time consuming in its design and it may have to be completely torn down in the light of new experimental information about the system.

In the rest of this work we utilize the white noise theory exclusively and derive very satisfactory models for several neuronal systems that contribute to the functional organization of the catfish retinal stages.

6. Conclusions

In this chapter we have derived nonlinear dynamic transfer functions for system LIGHT \rightarrow HORIZONTAL. Two models were derived; one, using the white-noise approach and the other using the conventional method of fitting a set of equations to a set of data (step and sine responses). The "goodness" of each model was tested with a variety of tests including steps, sine waves, white-noise, power spectra, gain and phase characteristics. Within its range of validity the white-noise-derived model produced much more satisfactory results overall than the "structural" model. The structural model has a good performance for the set of data for which it was designed (steps and sines) but poor performance for other stimuli (white-noise). The main additional conclusions about the LIGHT \rightarrow HORIZONTAL system are:

- (1) The system within a limited range (1.8 log units) is nearly linear (with some "small" nonlinearities).
- (2) There are several nonlinearities persistent even under small signal conditions, which include:
 - (a) Slow-on and fast-off response slopes for high frequencies and high mean intensity levels.
 - (b) An upward d.c. shift of the response with an increase in frequency. This nonlinearity also is more prominent at high mean intensity levels.

In addition, there are several "large signal" nonlinearities such as saturation, cutoff and others (see previous sections).

- (3) The system becomes considerably faster-responding as the mean light level is increased (cutoff frequency of about 8Hz at low levels and about 12Hz at high levels). Also the system becomes more underdamped as the mean intensity level is increased.
- (4) The high frequency asymptote has a slope of about 24 db/octave indicating (to the extent that the system is considered linear) a fourth order system.
- (5) The system has a latency that decreases from about 20 msec at low intensity levels to about 15 msec at high levels. Since we have found the same change in latency with mean light level for the LIGHT → RECEPTOR system, it is suggested that the RECEPTOR → HORIZONTAL latency does not change with mean light level. It is further suggested that the RECEPTOR → HORIZONTAL system has a latency of about 5 msec.

CHAPTER VII

SPATIAL DISTRIBUTION OF HORIZONTAL CELL POTENTIAL

1. Introduction

It was noticed by early investigators that the amplitude of the horizontal cell response (a potential usually referred to as S-potential) to a fixed intensity flash increased as the illuminated area of the retina was expanded [26, 68]. This phenomenon was referred to as the 'area effect' and it served to distinguish the receptor response from the horizontal cell response. Although the waveform of the receptor response is very similar to that of the horizontal cell response [3, 91] the amplitude of the receptor response is practically independent of the size of area illuminated [cf. Baylor, et al., 4].

Naka and Rushton [58] have described in detail the lateral spread of the horizontal cell response in a fish, the tench. They arrived at two conclusions; first, the spread of the potential was not due to scatter of stimulus light but was due to spread of potential inside the retina and, second, the structure responsible for the lateral spread of the potential could be approximated by a laminar structure which they referred to as the S-space (as it gives rise to the S-potential). Later, it was confirmed by dye injection experiments that the S-space corresponds to a layer of horizontal cells [Werblin and Dowling, 91; Kaneko, 34-35].

In the analysis of the horizontal cell response in the tench, it was assumed, based on experimental facts, that the decay of the potential inside the S-space could be approximated by a single exponen-

tial function. However, during the last few years, working with the catfish horizontal cells, we have noticed that the decay of potential in the S-space cannot be fitted by a simple exponential function. Published records by Negishi and Sutija [66] have also shown considerable deviation from this simple function.

Furthermore, the diameter of the receptive field of a teleost retinal ganglion cell extends up to 5 mm [cf. 33a] and Naka and Nye [61] have concluded that the signal was transmitted laterally by the S-space. However, if the potential decays exponentially from the site of excitation (as it was assumed for the tench S-space), a signal produced at large distances (such as 2.5 mm away) can hardly show its effect at the receptive field center (assuming that the decay constant is similar to that observed in the tench).

Therefore, the question arises whether such a geometry as that of the horizontal cell layer (as modeled by the S-space) and the physiological passive electrical properties of the membrane and intracellular media could indeed account for such a large spread of the S-potential. Although the electrical properties of a cable or axon have been a subject of extensive theoretical treatment, a similar study of the electrical properties of a flat cell has not been done except in two papers [21, 53].

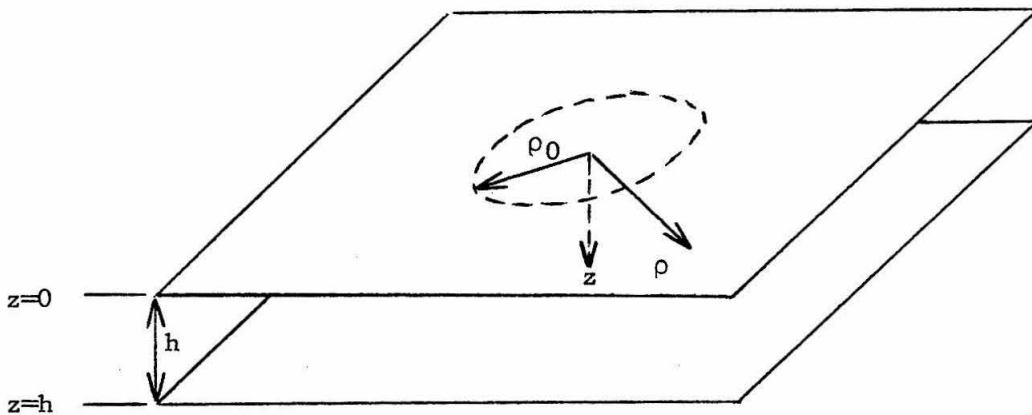
In this chapter, the electrical field problem posed by this geometry and these conditions is solved and the solution is compared with experimental results obtained from the catfish horizontal cells. We will conclude that the decay is not a simple exponential and that due to the geometry of a large flat cell like the S-space, signals can

be integrated over a far larger area than the area over which integration could take place if signals decayed exponentially in the S-space. Thus, the particular geometry of the S-space is exactly the feature which allows it to exhibit its functional characteristics.

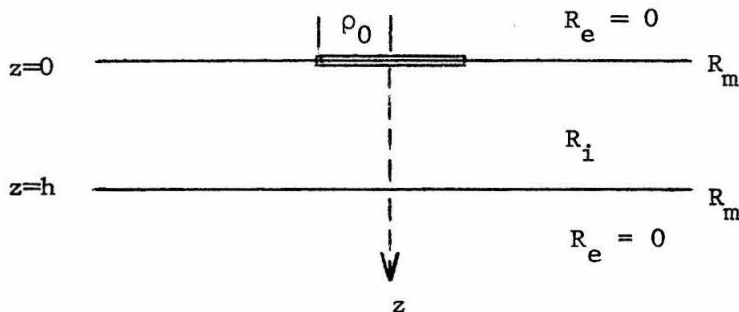
The effect of the membrane capacitance on the S-potential spread is briefly examined.

2. Problem Definition and Boundary Conditions

The layer of horizontal cells is modeled by a flat cell of finite width and extending infinitely in the other two dimensions.



The cell is bounded by two infinite plane parallel membranes of high resistivity R_m ($\Omega\text{-mm}^2$) and between them there is a medium of low resistivity R_i ($\Omega\text{-mm}$).



The resistivity of the external medium is taken to be zero since it is usually much smaller than the internal medium resistivity and membrane resistivity. This simplifies the mathematical formulation and solution of the problem.

The excitation of an H-cell site by the receptors is modeled in terms of an ideal conducting flat disc injecting constant current J in the intracellular space. The disc is placed against the inside surface of the top membrane.

We seek the potential distribution in the intracellular space. A cylindrical system of coordinates is introduced in a way such that the center of the disc is at point $(\rho = 0, z = 0)$ and the z -axis is perpendicular to the membrane surfaces.

The potential, $V(\rho, z, \theta)$, is found as the solution of Laplace's equation in cylindrical coordinates in the intracellular space. Because of the symmetry in the geometry of the problem the potential is not a function of θ and the equation reduces to

$$(1) \quad \left(\frac{\partial^2}{\partial \rho^2} + \frac{1}{\rho} \frac{\partial}{\partial \rho} + \frac{\partial^2}{\partial z^2} \right) V(\rho, z) = 0 .$$

It can easily be checked that the solution of equation (1) is of the form

$$(2) \quad V(\rho, z) = \int_0^{\infty} [\phi(v)e^{vz} + \psi(v)e^{-vz}] J_0(v\rho) dv ,$$

where $J_0(v\rho)$ is the Bessel function of zero order and $\phi(v)$, $\psi(v)$ are functions which will be determined by the boundary conditions.

The first boundary condition expresses the continuity of current flow from the intracellular medium through the membrane and perpendicular to the plane $z = h$. We ignore any current flowing

through the membrane at other than a right angle to it. This boundary condition is expressed by

$$(B. C. I.) \quad \frac{1}{R_i} \frac{\partial V(\rho, z)}{\partial z} \Big|_{z=h} = - \frac{V(\rho, z)}{R_m} \Big|_{z=h}$$

The boundary condition at the plane $z = 0$ is a mixed one. For the portion outside the charged disc it expresses the continuity of current flow through the membrane,

$$(B. C. IIa) \quad \frac{1}{R_i} \frac{\partial V}{\partial z} \Big|_{z=0} = - \frac{V}{R_m} \Big|_{z=0}, \quad \rho_0 \leq \rho < \infty.$$

It can be shown [cf. Sneddon, 77] that, in the case of a charged conducting disc immersed in a homogeneous medium of resistivity R_i , the current density on the surface of the disc is given by

$$\frac{\partial V}{\partial z} \Big|_{\text{disc surface}} = \frac{JR_i}{4\pi\rho_0} \frac{1}{\sqrt{\rho_0^2 - \rho^2}}, \quad 0 \leq \rho < \rho_0$$

where J is the current flowing from the disc and ρ_0 is the disc radius.

In the case of the disc of our problem, we approximate the current density by a similar dependence on ρ ,

$$(B. C. IIb) \quad \frac{\partial V}{\partial z} \Big|_{z=0} = -KJ \frac{1}{\sqrt{\rho_0^2 - \rho^2}}, \quad 0 \leq \rho < \rho_0$$

where the constant K (where units are ohms) is introduced to account for the approximation made. In general, K is a function of h , ρ_0 , R_i , R_m and can be picked after we have solved for $V(\rho, z)$ in order to make the total current flowing through the membrane into the external medium equal to J .

Thus, in conclusion, the potential should satisfy the following two boundary conditions:

$$(I) \quad \frac{1}{R_i} \frac{\partial V}{\partial z} \Big|_{z=h} = - \frac{V}{R_m} \Big|_{z=h}$$

$$(II) \quad \frac{\partial V}{\partial z} \Big|_{z=0} = \begin{cases} -KJ \frac{1}{\sqrt{\rho_o^2 - \rho^2}} & , \quad 0 \leq \rho < \rho_o \\ -R_i \frac{V}{R_m} & , \quad \rho_o \leq \rho < \infty \end{cases}$$

3. Solution of the Problem

We seek the solution of Laplace's equation in the intracellular space in the form

$$(1) \quad V(\rho, z) = \int_0^{\infty} [\phi(v)e^{vz} + \psi(v)e^{-vz}] J_0(v\rho) dv .$$

From the boundary condition (I) we have

$$\frac{1}{R_i} \int_0^{\infty} v[\phi(v)e^{vh} - \psi(v)e^{-vh}] J_0(v\rho) dv = - \frac{1}{R_m} \int_0^{\infty} [\phi(v)e^{vh} + \psi(v)e^{-vh}] J_0(v\rho) dv$$

Letting $R_i/R_m = \beta$ we have

$$(2) \quad \int_0^{\infty} [(v+\beta)\phi(v)e^{vh} - (v-\beta)\psi(v)e^{-vh}] J_0(v\rho) dv = 0 .$$

Since (2) must hold for all ρ , we must have

$$(3) \quad \phi(v) = \frac{v-\beta}{v+\beta} e^{-2vh} \psi(v) .$$

Substituting in (1) we get,

$$(4) \quad V(\rho, z) = \int_0^{\infty} \left[\frac{v-\beta}{v+\beta} e^{-2vh} e^{vh} + e^{-vh} \right] \psi(v) J_0(v\rho) dv .$$

Boundary condition II, in principle, determines $\psi(v)$. Trying to determine $\psi(v)$ from boundary condition (II) results in the following dual integral equations:

$$(5a) \quad \int_0^{\infty} v \left[\frac{v-\beta}{v+\beta} e^{-2vh} - 1 \right] \psi(v) J_0(v\rho) dv = -K \cdot J \cdot \frac{1}{\sqrt{\rho_0^2 - \rho^2}},$$

$$0 \leq \rho < \rho_0$$

$$(5b) \quad \int_0^{\infty} (v+\beta)(e^{-2vh} - 1) \psi(v) J_0(v\rho) dv = 0, \quad \rho_0 \leq \rho < \infty.$$

In general, the solution of such dual equations is difficult and involved.

We solve the pair (5a) and (5b) by making some approximations. First, we make the following normalizations and changes of variables:

$$\mu = v\rho_0, \quad r = \frac{\rho}{\rho_0}, \quad \bar{z} = \frac{z}{\rho_0}, \quad \delta = \frac{h}{\rho_0}, \quad \gamma = \beta\rho_0.$$

Then, equations (4), (5a), and (5b) become

$$(6) \quad V(r, \bar{z}) = \frac{1}{\rho_0} \int_0^{\infty} \left[\frac{\mu-\gamma}{\mu+\gamma} e^{-2\mu\delta} e^{\mu\bar{z}} + e^{-\mu\bar{z}} \right] \psi_1(\mu) J_0(\mu r) d\mu$$

$$(7a) \quad \int_0^{\infty} \mu \left[1 - \frac{\mu-\gamma}{\mu+\gamma} e^{-2\mu\delta} \right] \psi_1(\mu) J_0(\mu r) d\mu = K \cdot J \cdot \rho_0 \cdot \frac{1}{\sqrt{1-r^2}}, \quad 0 \leq r < 1$$

$$(7b) \quad \int_0^{\infty} (\mu+\gamma)(1 - e^{-2\mu\delta}) \psi_1(\mu) J_0(\mu r) d\mu = 0, \quad 1 \leq r < \infty$$

where

$$\psi_1(\mu) = \psi(\mu/\rho_0).$$

To solve the dual integral equations (7a) and (7b) we make some approximations in order to simplify them.

Consider, $\mu_0 \gg \gamma$, say, $\mu_0 = 10\gamma$. Then (7a) can be written

$$\int_0^{\mu_0} \mu \left[1 - \frac{\mu - \gamma}{\mu + \gamma} e^{-2\mu\delta} \right] \psi_1(\mu) J_0(\mu r) d\mu + \int_{\mu_0}^{\infty} \mu [1 - e^{-2\mu\delta}] \psi_1(\mu) d\mu =$$

$$K \cdot J \cdot \rho_0 \cdot \frac{1}{\sqrt{1-r^2}}, \quad 0 \leq r < 1.$$

On the left hand side, we add and subtract the term

$$\int_0^{\mu_0} \mu (1 - e^{-2\mu\delta}) \psi_1(\mu) J_0(\mu r) d\mu$$

and then collect terms to get

$$\int_0^{\mu_0} \frac{2\gamma\mu}{\mu + \gamma} e^{-2\mu\delta} \cdot \psi_1(\mu) J_0(\mu r) d\mu + \int_0^{\infty} \mu (1 - e^{-2\mu\delta}) \psi_1(\mu) J_0(\mu r) d\mu =$$

$$K \cdot J \cdot \rho_0 \cdot \frac{1}{\sqrt{1-r^2}}, \quad 0 \leq r < 1.$$

Now we add and subtract (on the left hand side) the term

$$\int_0^{\infty} \gamma (1 - e^{-2\mu\delta}) \psi_1(\mu) J_0(\mu r) d\mu$$

to obtain

$$(7a') \quad \int_0^{\mu_0} \frac{2\gamma\mu}{\mu + \gamma} e^{-2\mu\delta} \psi_1(\mu) J_0(\mu r) d\mu - \int_0^{\infty} \gamma (1 - e^{-2\mu\delta}) \psi_1(\mu) J_0(\mu r) d\mu$$

$$+ \int_0^{\infty} (\mu + \gamma) (1 - e^{-2\mu\delta}) \psi_1(\mu) J_0(\mu r) d\mu = K J \rho_0 \frac{1}{\sqrt{1-r^2}}, \quad 0 \leq r < 1.$$

We assume that the sum of the first two terms is small compared

to the third term (or the total on the right hand side, which is $1/\sqrt{1-r^2}$). We will justify this assumption shortly.

Neglecting the first two terms of (7a') and recalling the equation,

$$\int_0^{\infty} \sin \xi \cdot J_0(\rho \xi) d\xi = \begin{cases} \frac{1}{\sqrt{1-\rho^2}} & , \quad 0 \leq \rho < 1 \\ 0 & , \quad 1 \leq \rho < \infty \end{cases}$$

we find that the resulting dual integral equations (7a') and (7b) have the solution,

$$\psi_1(\mu) = K J \rho_0 \frac{\sin \mu}{(\mu + \gamma)(1 - e^{-2\mu\delta})} ,$$

and the expression for the potential becomes

$$(*) \quad V(r, \bar{z}) = K J \int_0^{\infty} \frac{(\mu - \gamma)e^{-\mu(2\delta - \bar{z})} + (\mu + \gamma)e^{-\mu\bar{z}}}{(\mu + \gamma)^2(1 - e^{-2\mu\delta})} \cdot \sin \mu \cdot J_0(\mu r) d\mu$$

where (as stated before) the arbitrary constant K can be fixed from the additional condition that the total current flowing through the membrane into the external medium should be equal to J.

Now, let us justify the assumption made above about the smallness of the sum of the first two terms of (7a'). The values of the parameters γ and δ are of the order

$$\gamma \sim 10^{-1} \quad , \quad \delta \sim 1 .$$

The first integral (let us call it I_1) is

$$I_1 = \int_0^{\mu_0} \frac{2\gamma\mu}{(\mu + \gamma)} e^{-2\mu\delta} \frac{\sin \mu}{(\mu + \gamma)(1 - e^{-2\mu\delta})} J_0(\mu r) d\mu \quad , \quad 0 \leq r < 1 \quad ,$$

and, considering that $\mu_0 = k \cdot \gamma$ ($k \sim 20$) and $0 \leq r < 1$, we can get an estimate of integral I_1 from integral

$$\frac{1}{2} \int_0^{\mu_0} \frac{\gamma \mu}{\mu + \gamma} \frac{\sin \mu}{(\mu + \gamma)(2\mu\delta)} d\mu$$

and considering $\sin \mu / \mu$ for $0 < \mu < \mu_0$, we finally get a rough estimate of I_1 as

$$I_1 \sim \frac{\gamma}{4\delta} .$$

The second integral (let us call it I_2) is

$$I_2 = \int_0^{\infty} \gamma \frac{\sin \mu}{\mu + \gamma} J_0(\mu r) d\mu , \quad 0 \leq r < 1$$

which we can write as

$$I_2 = \gamma \int_0^{\mu_0} \frac{\sin \mu}{\mu + \gamma} J_0(\mu r) d\mu + \gamma \int_{\mu_0}^{\infty} \frac{\sin \mu}{\mu} J_0(\mu r) d\mu , \quad 0 \leq r < 1$$

or

$$I_2 = \gamma \int_0^{\mu_0} \left[\frac{1}{\mu + \gamma} - \frac{1}{\mu} \right] \sin \mu J_0(\mu r) d\mu + \gamma \int_0^{\infty} \frac{\sin \mu}{\mu} J_0(\mu r) d\mu , \quad 0 \leq r < 1 .$$

The second term of this expression is equal to $\gamma \cdot \frac{\pi}{2}$ (see [27], p. 744).

The first term can be roughly approximated by

$$\frac{1}{2} \int_0^{\mu_0} \frac{-\gamma}{\mu + \gamma} \cdot \frac{\sin \mu}{\mu} d\mu \simeq -\frac{3\gamma}{4} .$$

Then I_2 is approximately

$$I_2 \sim \frac{3\gamma}{4} ,$$

and the sum of the neglected terms is roughly approximated (within the parameter range considered) by

$$\epsilon = I_1 - I_2 = \frac{\gamma}{4} \left(\frac{1}{\delta} - 3 \right) ,$$

which is of the order of 10^{-1} , and this is, indeed, small compared with $1/\sqrt{1-r^2}$ ($0 \leq r < 1$).

The error is of the same order (10^{-1}) for δ somewhat larger than 1. If δ is much larger than 1, the approximations used in evaluating integral I_1 are not quite valid, but the error is still of the same order (~ 0.1). This can be deduced by roughly approximating I_1 for large δ . It will be noted that I_1 has a smaller value.

In the case of the catfish horizontal cell, the maximum spot diameter of interest (where saturation occurs) is about 3 mm, and h is about 0.05 mm.

Clearly, for large δ , that is, small spot radii, the error is of the order of γ , and therefore very small. For very small δ , however, the error can become large. This corresponds to the case of very large diameter spots. However, in this case the approximations used to estimate integrals I_1 and I_2 are not valid, and therefore (*) cannot be used to estimate the error. Numerical approximations done by computer have shown that quantity $(I_1 - I_2)$ is small compared to $\{ 1/\sqrt{1-r^2}, 0 < r < 1 \}$ for the horizontal cell parameter values up to diameters of 5 mm. For larger (than 5 mm) diameters, the solution will have some error which may be significant.

Therefore, we conclude that within a large range of parameter values the posed problem of the potential distribution within a flat cell has the solution

$$(*) \quad V(r, \bar{z}) = K \cdot J \cdot \int_0^{\infty} \frac{(\mu - \gamma)e^{-\mu(2\delta - \bar{z})} + (\mu + \gamma)e^{-\mu\bar{z}}}{(\mu + \gamma)^2 (1 - e^{-2\mu\delta})} \sin\mu \cdot J_0(\mu r) d\mu$$

where, as defined previously, $r = \rho/\rho_0$, $\bar{z} = z/\rho_0$, and K is a constant.

4. Experimental Method

The eyecup preparation of the channel catfish, Ictarulus punctatus , was used for the experiment. Details of preparation and experimental procedure have already been described in a previous chapter. The horizontal cells from which responses were obtained were identified by injecting a Procion dye. Responses were registered on a penwriter and measured by a pencil and ruler.

5. Results and Discussion

An experiment was performed in which the spatial summation of the horizontal cell response was examined under a condition such that it does not involve the effect of spatial decay. The stimulus used was a segment of an annulus which was expanded in steps to form a complete annulus. As the recording electrode was placed at the center of the expanding annular segment, the attenuation function is just a proportional constant and the amplitude of the response depends only on the stimulus area. It was found that the amplitude of the response is a linear function of the illuminated area (as the annular segment is expanded), and that this relationship holds for three widely different intensity levels. This demonstrates the integrating (over an area) function that the S-space performs.

We proceed next to an experiment in which a small spot of light is moved away from the tip of the recording electrode to examine the decay of potential in the layer of horizontal cells. It should be mentioned that both the shape and dimensions of the horizontal cells are such that the lateral spread of potential, as described here,

spans many individual cells (cf. Matsumoto, Admorian and Naka, in preparation).

The results of these experiments fall into two distinct groups which are shown in Fig. 7.1. One set of data points, exhibiting a faster potential decay with distance was found (by dye injection) to originate from the external horizontal cells; while the other set of points, exhibiting a slower decay, was recorded from the internal horizontal cells. The initial parts of both potential decay curves can be approximated by an exponential decay (down to about 40 per cent of the maximum), but the decay for larger distances showed considerable deviation from the exponential decay. This is shown in Fig. 7.1. Figure 7.1A shows the potential decay inside a flat cell, calculated from equation (*) (solid curve) and also an exponential decay curve (dashed line with circles) picked with a space constant such that it would fit the initial decay portion. It is seen that the exponential decays much faster for large distances. We recall that the potential decays exponentially in the case of a cable structure.

The solid curve of Fig. 7.1, A is the same curve (i. e., same h , $\alpha = R_m/R_i$ parameter values) as the curve in Fig. 7.1, B which fits the data for the external horizontal cell. Thus, if one attempts to fit the data with a simple exponential function he will be making a considerable error for large distances even though he accurately fits the initial decay portion of the curve. It is exactly this slow decay for large distances (characteristic of a flat cell structure) that allows the S-space to perform its integrating function over large receptive fields.

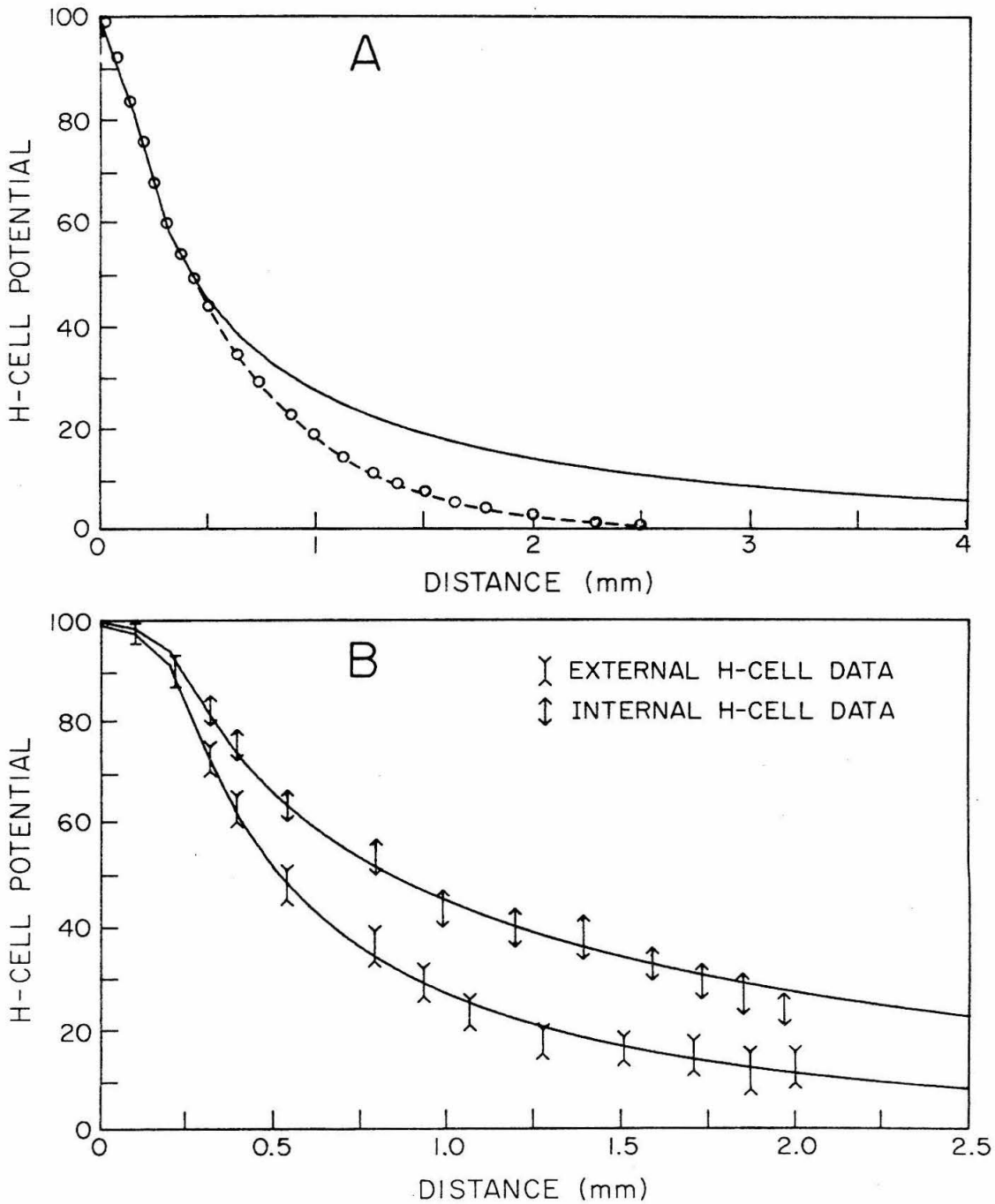


Fig. 7.1. A: Potential decay curves computed from equation (*) (solid line, $h=0.005$ mm, $\alpha=2$ mm, $\rho_0=0.025$ mm) and from an exponential, $e^{-x/\lambda}$, (circles, $\alpha=0.6$ mm). B: Data of potential decay from external and internal horizontal cells fitted by equation (*).

Figure 7. 1, B shows potential decay data recorded from the external and internal horizontal cells and the theoretical decay functions (for a flat cell) calculated from equation (*) and used to fit these data. The fit is indeed very good. The data were obtained using light spots of 0.5 mm in diameter, and this is exactly the disc diameter used in the calculations of equation (*). The parameter values for which these fits were obtained are:

$$h = 0.05 \text{ mm}, \quad \alpha = 6.2 \text{ mm} \quad (\text{internal H-cell}) ,$$

and

$$h = 0.05 \text{ mm}, \quad \alpha = 1.7 \text{ mm} \quad (\text{external H-cell}) .$$

For small distances we note a potential plateau which is a consequence of the disc dimensions. This plateau also exists in the experimental data (see Fig. 7. 1, B).

All curves, shown here and computed from equation (*), were for $x = \frac{h}{2}$, (i. e., the potential is calculated at the mid-plane between the two membranes). Preliminary calculations have shown that, for the range of h's (about 0.05 mm) and α 's in which we are interested, the potential variation in the z-direction is very small (at most about 5 per cent) for distances less than the disc radius and almost zero for distances greater than the disc radius.

Figure 7. 2, B shows the extent of the potential variation in the z-direction for two extreme cases; one for α equal to 1 mm, and the other for α equal to 8 mm. For the higher α , the decay in the z-direction is larger, but still only about 5 per cent, considering the potential at the top and bottom membranes. The potential variation in the z-direction becomes negligible for distances larger than the

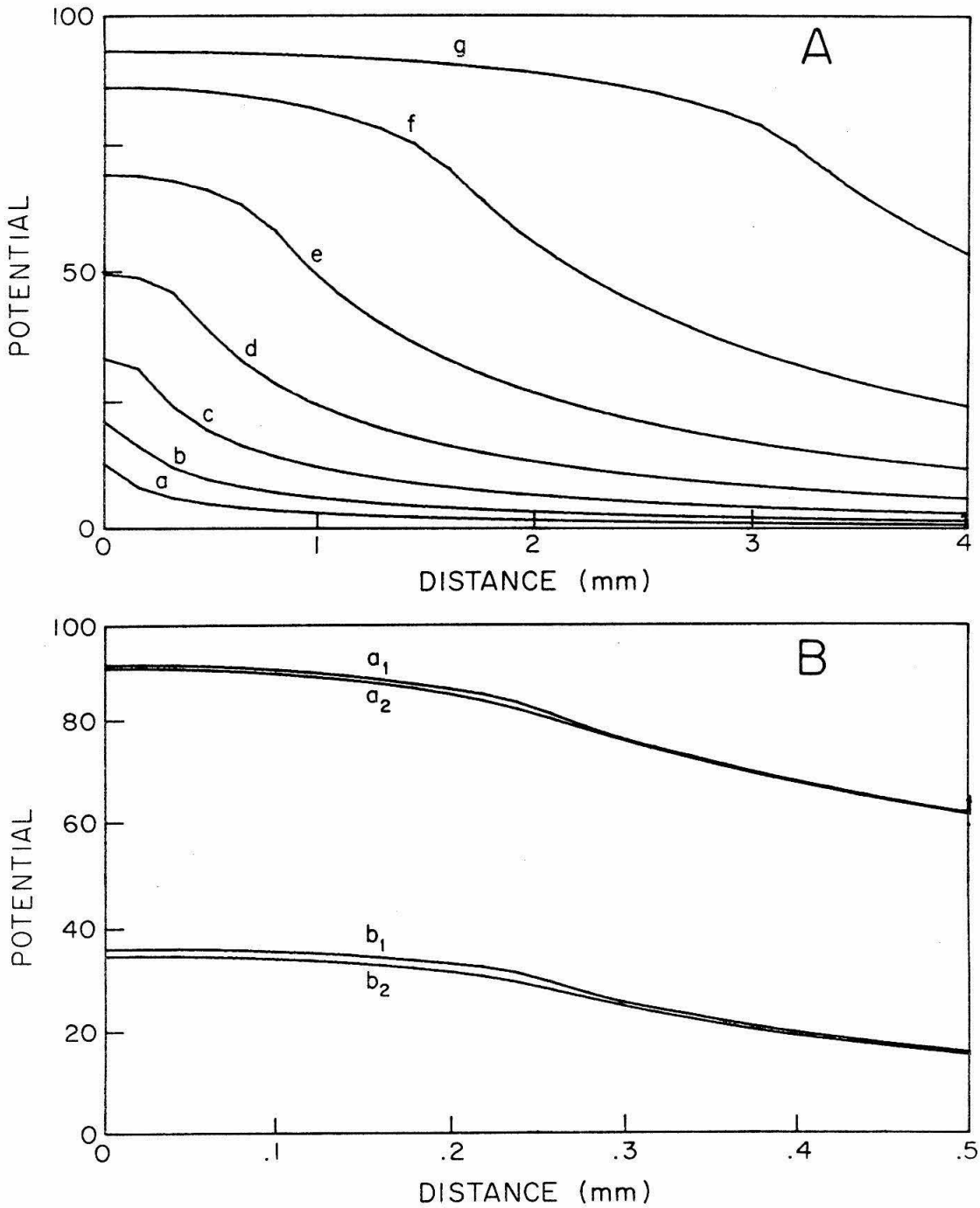


Fig. 7.2. A: Potential decay curves for different radii as computed from equation (*). Smallest radius, (a), is 0.05 mm and each succeeding radius is twice the previous one. ($L=0.05$ mm, $\alpha=4$ mm). B: Maximum potential variation in z-direction for $r=1$ mm (a_1, a_2) and for $r=8$ mm (b_1, b_2), as computed from equation (*).

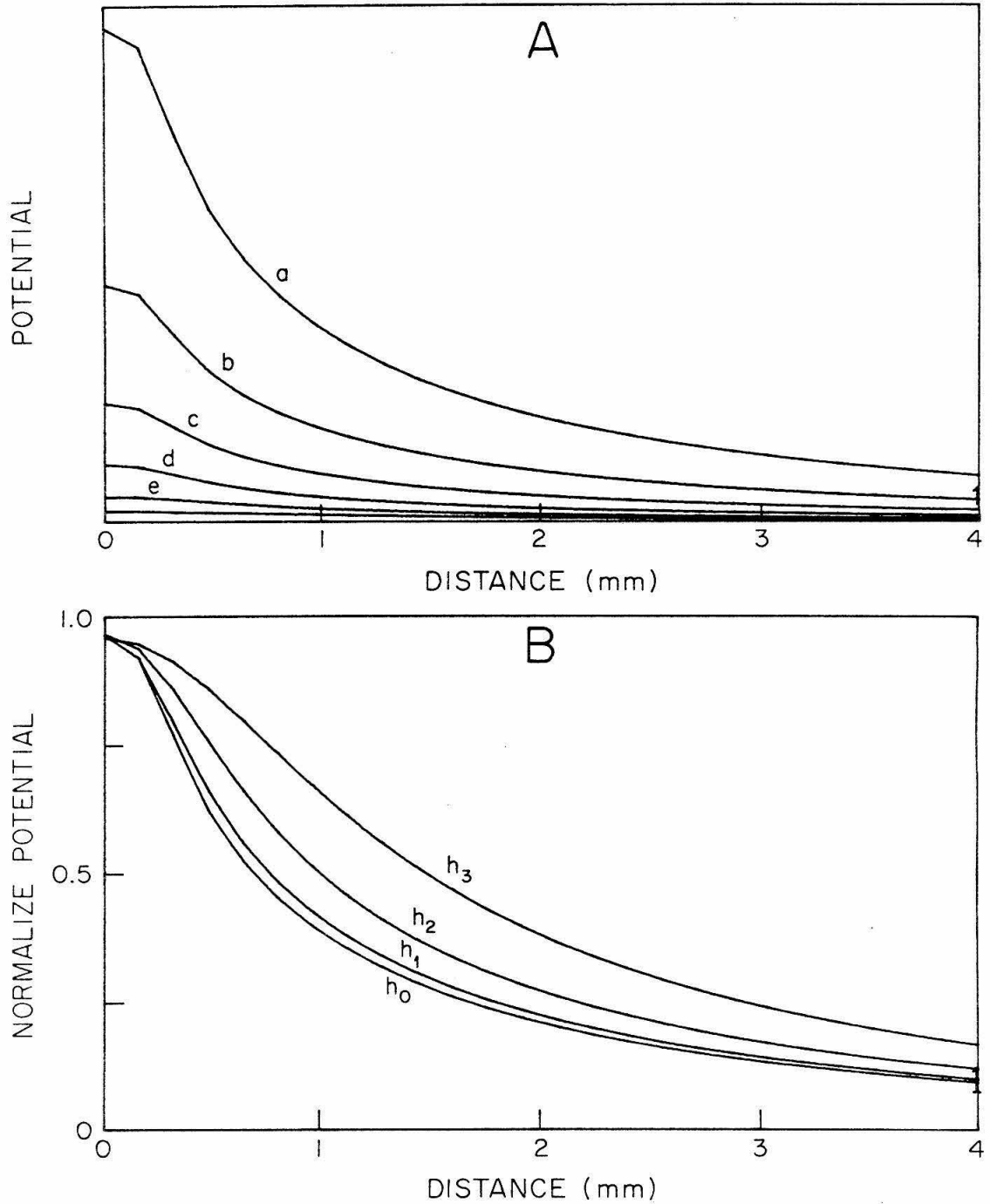


Fig. 7.3. A: Potential decay curves for various thicknesses, h , as computed from equation (*). Smallest h , (a), is 0.075 mm and each subsequent thickness is twice the previous one. B: The decay curves of (a) normalized. h_3 is 2 mm and h_0 is 0.25 mm. For $h \leq h_0$ the curves are almost identical to the one for $h = h_0$.

disc radius.

Figure 7.2, A shows the potential decay curves for different disc radii. Each successive curve is calculated for a disc whose radius is twice the previous one.

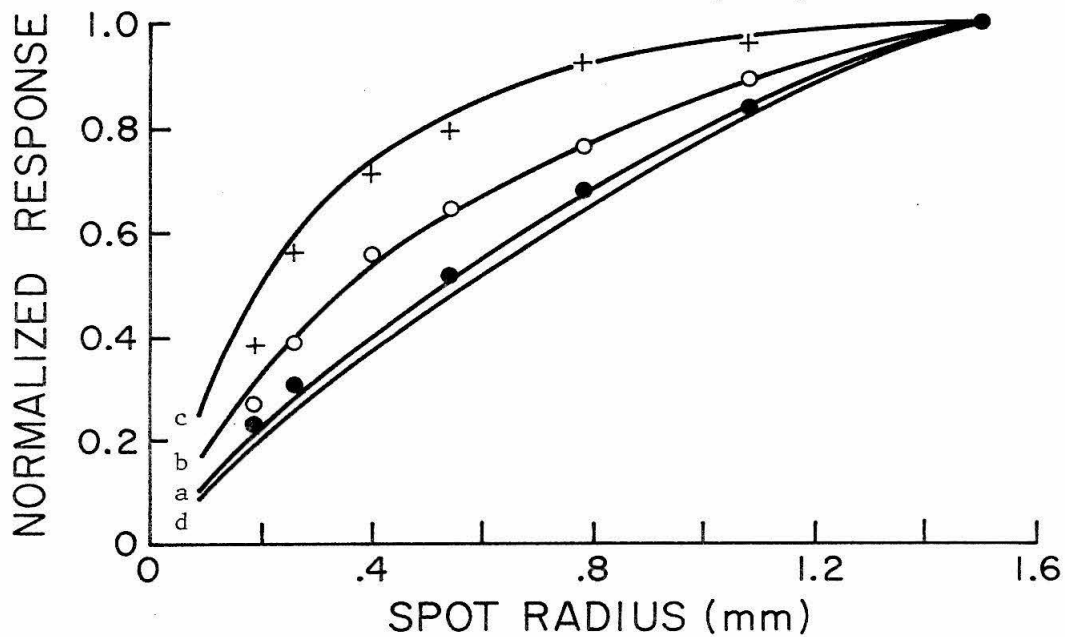
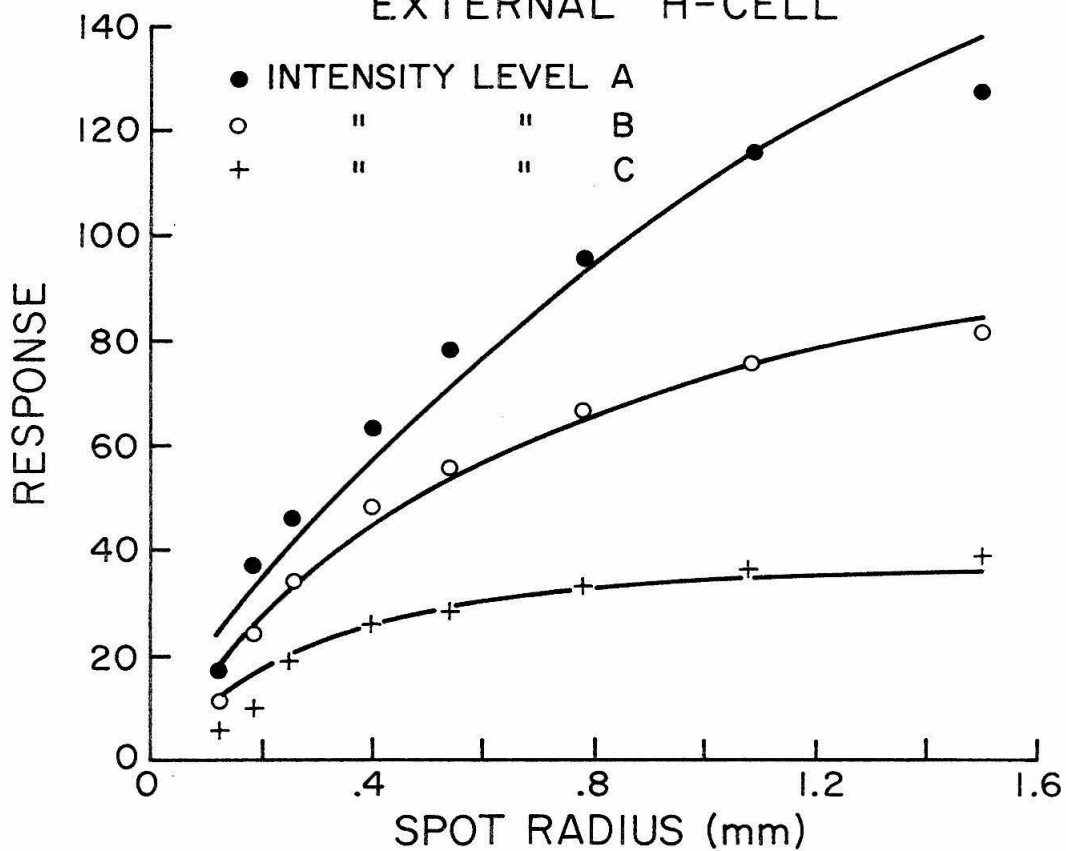
Figure 7.3A shows potential decay curves for flat cells of different thickness, h . We note that the potential increases for decreasing thickness h . Figure 7.3, B is a plot of such curves with the maximum potential value normalized. We conclude that, for the range of h 's that the horizontal cells exhibit ($\sim 30\mu$) and the range of α in which we are interested, the spatial decay is fairly independent of thickness h . Only for very large h 's does the spatial decay slow down, as shown in Fig. 7.3, B. Therefore, we conclude that the difference in spatial decay (found experimentally) between the internal and external horizontal cells is not due to a different cell thickness, but is solely due to different values for (R_m/R_i) [i. e., α].

Figure 7.4, A shows the results of experiments in which the potential was recorded at the center of a light spot for several spot radii and at several intensity levels. The recordings were from the external horizontal cell. The solid curves are calculated using equation (*) for the same range of spot radii. It is found that the data are well fitted by curves obtained for different values of α . In fact, increasing α , which corresponds to an increase in the membrane resistance, suffices to fit the data for increasing intensity levels. For small values of α , saturation occurs at small distances; while for larger values of α saturation occurs at larger distances, as would be expected from a mechanism that integrates signals over a large area.

Fig. 7.4

External horizontal cell. Data points (circles and crosses) and predictions (solid lines) of equation (*) for different intensity levels (A,B,C). Both unnormalized and normalized curves are shown. The response is computed for $\rho = 0$, $z = h/2$.

EXTERNAL H-CELL



In Fig. 7.4, B the data and model curves of Fig. 7.4, A are normalized so that the amplitude of the response caused by the largest light spot is set to unity for all the different intensity levels. This shows more clearly the extent of area integration performed by the external horizontal cell for the different intensity levels.

Curves a , b , c , and d correspond to the following values of (R_m/R_i) :

- c : 1.0 mm,
- b : 3.0 mm,
- a : 7.0 mm,
- d : 10.0 mm.

Since curves C' and D' are nearly identical, we conclude that increasing α beyond the value of about 7 mm does not change the integrating characteristic of a flat cell for spots of radius within a certain fixed range. This is, again, a natural consequence of a mechanism that integrates signals over a large area.

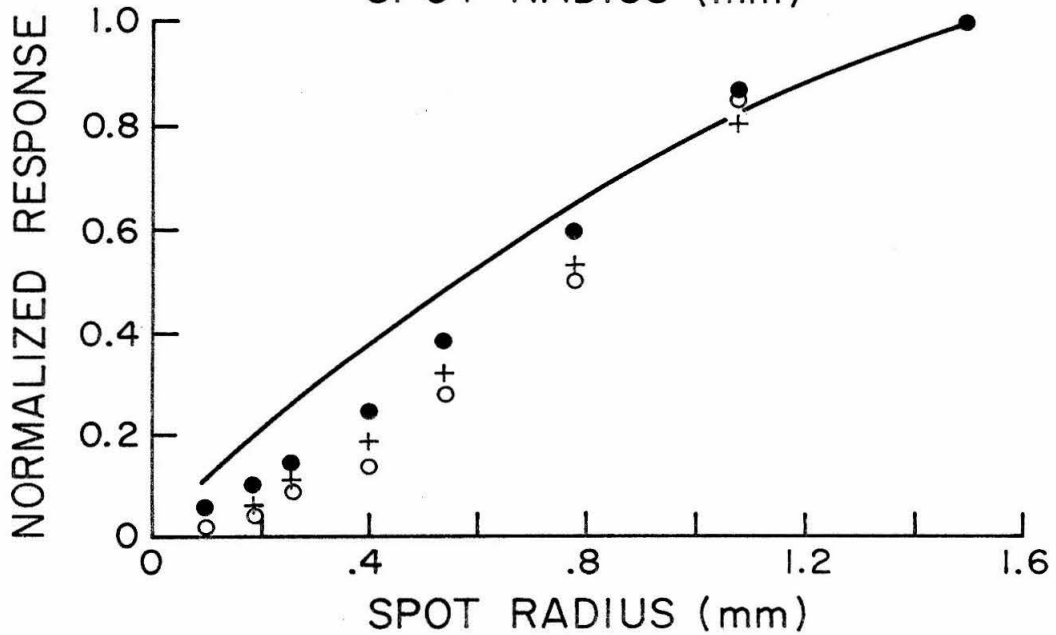
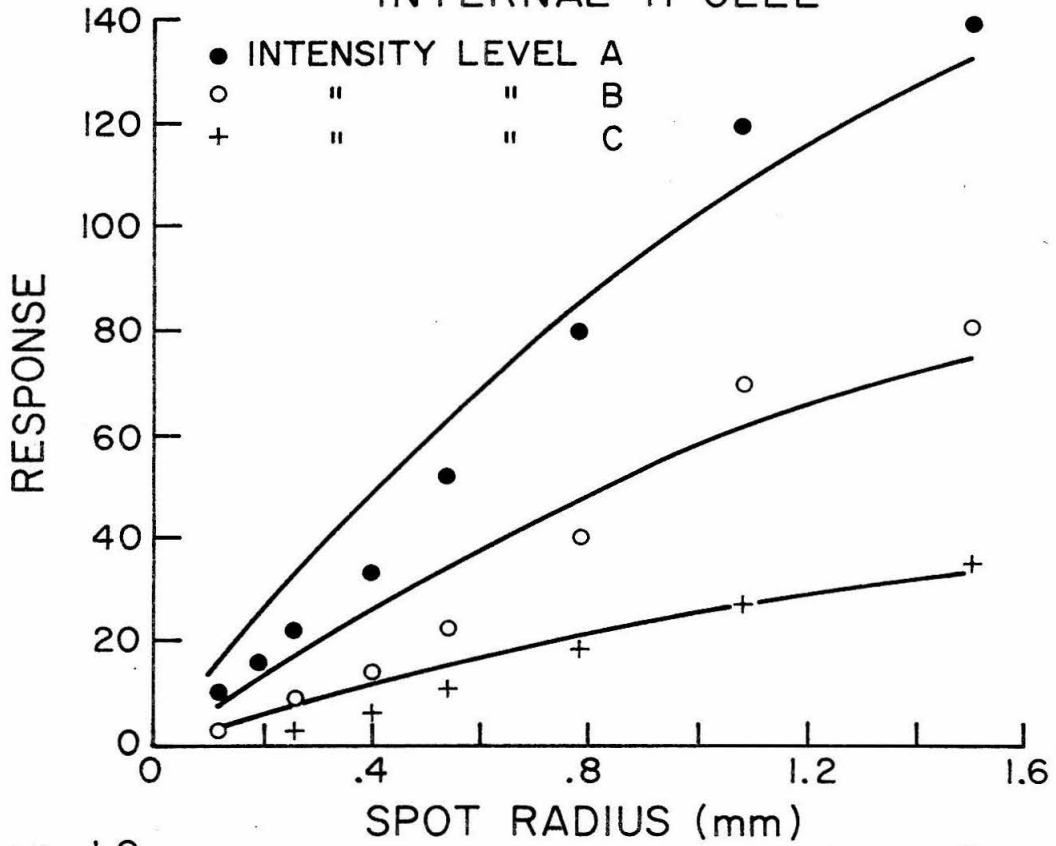
We have found, by fitting the potential decay data from the internal H-cell, that α in this case is about 6.2 mm. Therefore, we expect (because of the argument just made) that the normalized decay data (and calculated model curves) will show no difference for different intensity levels by further increasing α . In fact, they would exhibit the same characteristics as curves C' and D' of Fig. 7.4, B. This is indeed the case, as shown in Fig. 7.5, B.

In the case of the internal H-cell, the model fit for small spot radii is not as good as for the external H-cell. There may be many reasons for this, which will not be discussed here. Figure 7.5, A

Fig. 7.5

Internal horizontal cell. Data points (circles and crosses) and predictions (solid lines) of equation (*) for different intensity levels (A,B,C). Both unnormalized and normalized curves are shown. The response is computed for $\rho = 0$, $z = h/2$.

INTERNAL H-CELL



shows the unnormalized data for the internal H-cell. Since, in this case, a variation in α will not fit the data for the different intensity levels, we assume that by varying the intensity the (synaptic) current J [see equation (*)] varies. In fact, the effect of the different intensity level seems to introduce just a multiplicative constant in the data. From equation (*) we see that J is also just a multiplicative constant for the potential. The solid curves of Fig. 7.5, A are obtained for different values of J , corresponding to different intensity levels.

Although the spread of potential along a cable structure has been a subject of extensive study in neurophysiology, spread of potential inside a large flat cell or a laminar structure has been given little attention. Exceptions can be found in two recent theoretical treatments by Minor and Maksimov [53] and Eisenberg and Johnson [21]. In the first, a point current source is placed at the midplane between the two parallel membranes as the source of excitation. Such a formulation allows a simplification of the boundary conditions because of symmetry. Our model assumes a disc on one side of the two parallel membranes. This is a more realistic assumption as, whatever the generating mechanism may be, it is reasonable to postulate that the dendritic portion of the H-cell receives the signal from the photo-receptors and is the site of current generation. In [21], the problem is solved for point sources of current, and the derived formulas are harder to compute than the one derived by our formulation of the problem. The model proposed here makes no a priori assumptions, such as the exponential decay in the Naka-Rushton model, and is

based solely on the geometry of a flat cell (or a layer of horizontal cells) and the electrical properties of the membrane and intracellular media.

Spatial spread of the horizontal cell response has been a subject of several papers. Norton, et al. [67] and Dowling and Ripps [20] have treated the subject trying to establish physiological mechanisms for Ricco's law, which states that: $\text{Area} \times \text{Intensity} = \text{constant}$. Naka and Rushton [58] and Negishi and Sutija [66] have placed their emphasis on the decay of laterally spreading potential. The aim of the latter approach was to establish a model to account for the spread of potential. Negishi and Sutija stipulated the existence of chemical reactions to account for the large spread, while Naka and Rushton proposed a simple laminar conducting medium. There are, however, two independent observations which favor the view held by Naka and Rushton: first, morphologically the horizontal cells are coupled by 'gap' junctions, implying a low resistance electrical passage between cells [Yamada and Ishikawa, 96; Witkovsky and Dowling, 94]; and second, it was shown functionally that the dogfish horizontal cells are coupled electrically [Kaneko, 35].

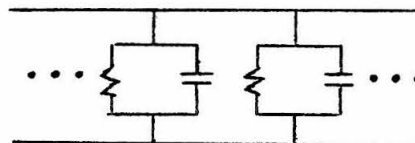
Thus, our assumed model of two parallel plane membranes separated by a medium of lower resistivity seems justified (as it is essentially the Naka-Rushton concept of the S-space). Our mathematical formulation has advantages over the one presented for the tench data in that it can fit better the results obtained in the catfish as well as results obtained by Negishi and Sutija. Moreover, our analysis has shown the differences in signal integration between the in-

ternal and external H-cells and it has suggested a difference in the synaptic forms of excitation for these two kinds of H-cell.

6. Effect of Membrane Capacitance on Potential Spread

In calculating the potential spread, so far, we have obtained the steady-state solution for an applied disc current of constant magnitude. This allowed us to neglect the capacitance of the membrane and to simplify the posed problem. If the applied excitation is time-varying, the membrane capacity comes into play and affects the potential spread. We assume the membrane model to be a resistance in parallel with a capacitance, thus presenting a membrane impedance

MEMBRANE MODEL



quite different from the purely resistive one. In fact, we expect the potential to attenuate faster with increasing frequency of excitation, because the capacitive impedance decreases, thus effectively shorting the membrane.

We have shown that the extent of potential spread increases with both the ratio (R_m/R_i) and cell thickness h . Thus, we define the quantity λ ,

$$\lambda = \sqrt{h \frac{R_m}{R_i}}$$

to indicate in a sense, the "space constant" with which the potential decays. This definition of a "space constant" is also made in analogy with the space constant in the case of a cable (see also [53]).

Let λ_D be the space constant in the dynamic case. Then λ_D is, in general, a function of frequency. Making an analogy with transmission line theory [38], it can be shown that $\lambda_D = 1/\alpha$ where $\gamma = \alpha + j\beta$ and γ is the propagation constant. The propagation constant, γ , can be found from the d. c., steady-state space constant by substituting the d. c. membrane impedance, R_m , by the dynamic impedance of the membrane, Z_m . Thus,

$$Z_m = R_m \parallel C_m = \frac{R_m}{1 + j\omega R_m C_m}$$

where ω is the frequency in radians, and

$$\gamma = \frac{1}{\lambda^*} = \frac{1}{\sqrt{h \frac{Z_m}{R_i}}}$$

from which, after some complex number algebra, we obtain (let $\theta = R_m/R_i$)

$$\alpha = \frac{1}{\sqrt{2}} \left[\frac{1}{h\theta} + \sqrt{\left(\frac{1}{h\theta}\right)^2 + \left(\frac{\omega R_i C_m}{h}\right)^2} \right]^{\frac{1}{2}},$$

$$\beta = \frac{1}{\sqrt{2}} \left[\sqrt{\left(\frac{1}{h\theta}\right)^2 + \left(\frac{\omega R_i C_m}{h}\right)^2} - \frac{1}{h\theta} \right]^{\frac{1}{2}}.$$

In transmission line theory it is shown [38] that α is the attenuation constant with distance and β gives information about how the phase varies with distance. Both quantities are a function of frequency. Thus, we obtain the dynamic space constant, λ_D ,

$$\lambda_D = \left[\frac{2}{\frac{1}{h\theta} + \sqrt{\left(\frac{1}{h\theta}\right)^2 + \left(\frac{\omega R_i C_m}{h}\right)^2}} \right]^{\frac{1}{2}}.$$

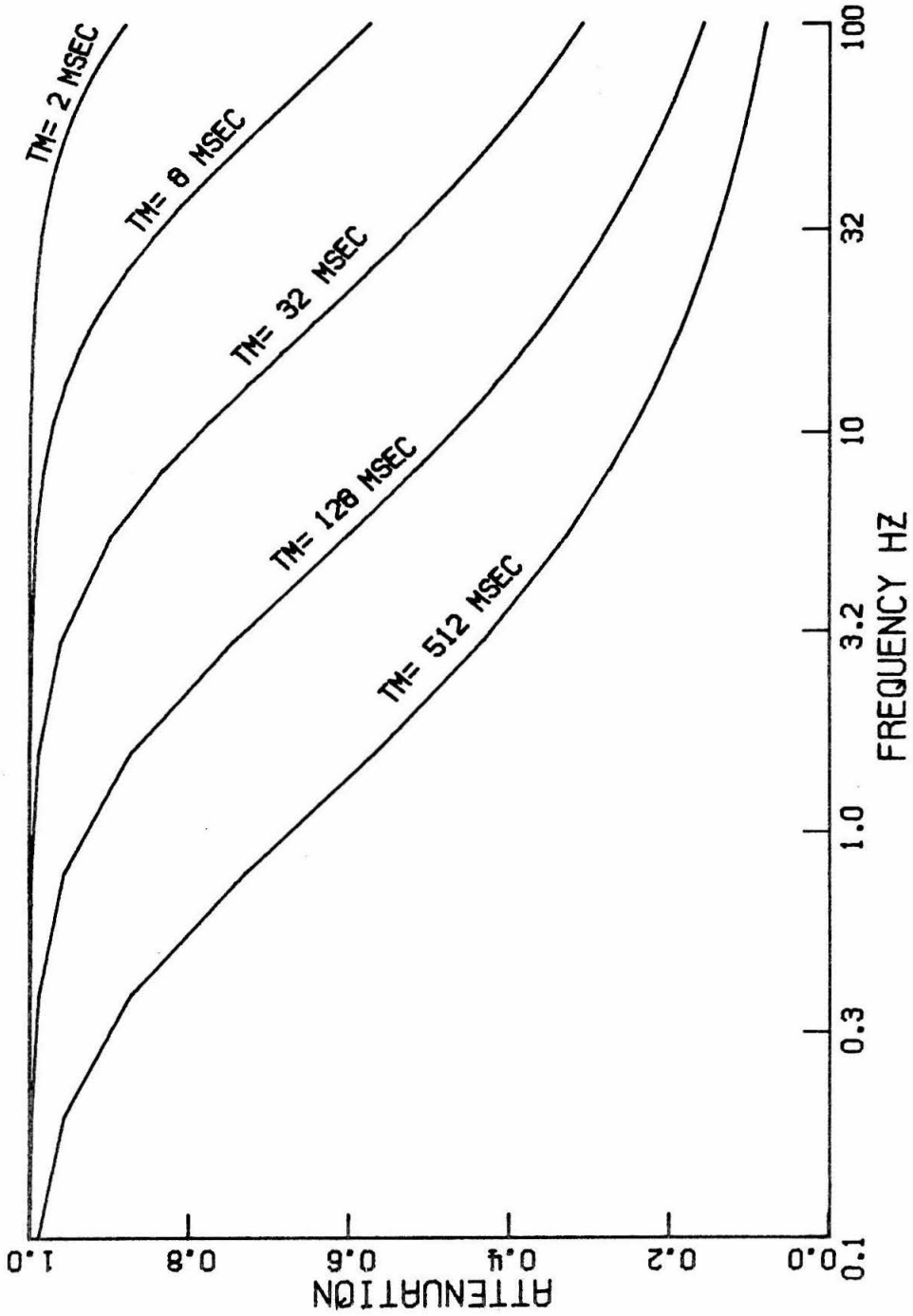


Fig. 7.6. Normalized reduction of the decay space constant as a function of frequency for different values of $\tau_m = R_m C_m$.

We normalized the dynamic space constant by the d. c. steady-state space constant,

$$(6) \quad \frac{\lambda_D}{\lambda} = \left[\frac{2}{1 + \sqrt{1 + (\omega R_m C_m)^2}} \right]^{\frac{1}{2}}$$

to obtain the per unit change in space constant as a function of frequency. Figure 7.6 shows a plot of equation (6) for several values of the parameter $\tau_m = R_m C_m$. By performing the appropriate experiment such a curve could be obtained and fitted by equation (6). This would measure, indirectly, the value of the membrane capacitance, C_m . This frequency dependence of the space constant also indicates the limit of spatial integration in the dynamic (time-varying) case.

7. Physiological Inferences

In the channel catfish there are three classes of horizontal cells; the external, intermediate, and internal horizontal cells [Matsumoto, Adomian and Naka, unpublished results]. The external horizontal cells send very short processes to the receptor terminals (presumably the cone pedicles) to receive inputs whereas the thinner, more proximally located intermediate horizontal cells send numerous processes (5 to 15 microns) toward the receptor terminals (presumably to make contact with the rode spherules [cf. Stell, 84, 85]. Stell [85] has classified them as the true horizontal cells. The internal horizontal cells have no apparent distal processes and their tubular structure (10 to 20 microns in the channel catfish) runs over a distance of nearly 500 microns. So far, studies made in the catfish and in other teleost fish failed to locate any synaptic contact made by

this cell.

In goldfish, the S-potentials arise from two classes of horizontal cells; one from the internal and the other from the external horizontal cells [Kaneko, 34], both of which possess structure very similar to those observed in the catfish. It was further noted that the internal horizontal cells integrate potentials from a larger area than the external horizontal cells, an observation confirmed in the present study.

The analysis made so far allows us to make several inferences on the physiology of the receptor-horizontal cell synapses in the catfish. (1) The decay of the potential induced by a small spot of light can be equally well predicated whether, in the S-space membrane model, we adapt a voltage source or a current source, as the synaptic form of excitation. However, the voltage source model fails to predict the results of the experiment in which the diameter of the spot was increased, while the model based on a current source (for a given intensity) fits well the experimental results. (2) In the external horizontal cells, an increase in the membrane resistance could account for the increase in the integration area with a brighter light. This agrees well with the observation that the resistance increases in proportion to the amplitude of the horizontal cell response. (3) In the internal horizontal cells, a simple increase in the resistance could not account for the data in which the spot diameter was increased. However, a reasonable fit could be obtained by assuming an increase in the magnitude of the synaptic current with increasing intensity.

The last point is very significant because so far we have failed to detect any functional difference between the external and internal horizontal cells, although morphologically they markedly differ from each other. The external horizontal cell has a clear synaptic input, while the internal horizontal cell does not seem to receive any input.

It is worth noting here that a formal analysis such as that performed in this chapter could make several qualifications on the receptor-horizontal cell synapses on the nature of which no concrete evidence has been obtained through a 'direct analysis.'

8. Conclusions

In this chapter we examined the potential distribution inside a flat cell, such as the horizontal cell, as a function of its geometry and electrical properties. We found that, within a very large range of parameter values, the potential is given by

$$(*) \quad V(r, \bar{z}) = K \cdot J \int_0^{\infty} \frac{(\mu - \gamma)e^{-\mu(2\delta - \bar{z})} + (\mu + \gamma)e^{-\mu\bar{z}}}{(\mu + \gamma)^2 (1 - e^{-2\mu\delta})} \sin\mu J_0(\mu r) d\mu$$

where

$$r = \rho/\rho_0, \quad \bar{z} = z/\rho_0, \quad \gamma = \frac{R_i}{R_m} \cdot \rho_0, \quad \delta = h/\rho_0;$$

K, J are constants; ρ, z are cylindrical coordinates; ρ_0 is the radius of the spot that excites the flat cell; h is the cell thickness; and R_i, R_m are the intracellular and membrane resistivities respectively.

Formula (*) closely fitted the spatial decay of potential data obtained from the internal and external horizontal cells. Equation (*)

predicts a decay which is exponential down to about 40 per cent of the maximum potential but is much slower than exponential below that level. Such a feature in the decay mode allows signal integration over the large retinal areas which have been observed experimentally. This slowing up of the decay for large distances is also exhibited by the data.

For the range of cell thicknesses of the horizontal cells (about 50μ) it was found that the decay rate does not change appreciably as a function of cell thickness. Cell thickness h does have an effect on decay rate for very large thicknesses. However, for H-cell thicknesses the decay rate was found to depend solely on the ratio (R_m/R_i) .

Data obtained from both types of horizontal cells by varying the diameter of the stimulating spot and for three widely different intensity levels were closely fitted by equation (*). The fit was better for the external horizontal cell data than for the internal horizontal cell data. In the first case (external H-cell) the fit for different intensities was obtained by varying the ratio (R_m/R_i) ; while in the second case it was found necessary in order to fit the different intensity data to vary the "synaptic" current J , which in (*) is just a multiplicative constant. This suggests two different membrane mechanisms of excitation for the two types of H-cells; an increase in membrane resistance with increase of intensity for the external H-cell, and an increase of the synaptic current with increase in intensity for the internal H-cell.

CHAPTER VIII

GANGLION TRANSFER FUNCTIONS

1. Introduction

In 1940, Hartline [30] showed that a single retinal ganglion cell received signals from a large retinal area corresponding to thousands of receptors. This (geometrical) sensitive area has been known as the "receptive field" and has been the focal point of the physiological study of the vertebrate retina.

Later, Kuffler [40] showed that the typical receptive field is organized in concentric rings, in which the central disc is called the receptive field center and the outer ring or annular area is called the surround of the field. In this concentric field organization the center and the surround act antagonistically to a light stimulus; namely, if the center gives rise to an 'on' response the surround responds by an 'off' discharge and vice versa. Although this type of receptive field was originally found in the cat retina, the concentric field organization has been observed in every vertebrate retina studied thus far. The induced ganglion responses are reproduced at the level of the lateral geniculate body and, furthermore, the concentric field is thought to be the building block of the more complex field organization found in the visual cortex [33a].

Although the receptive field organization has been a subject of extensive studies [14a, 33a, 46, 70a, 70b, 90], the dynamics of the ganglion cell discharge caused by the different components of the field are not known. An exception can be found in a recent study by Spekrijse [78].

In this chapter the white-noise nonlinear analysis technique is applied to the different catfish retinal neuronal systems that contribute to the ganglion response and nonlinear dynamic transfer functions are derived.

Two distinct advantages could be cited for choosing the catfish retina for this study of the dynamic characteristics of the ganglion systems: 1) the catfish ganglion cell has the simplest type of receptive field so far studied and 2) the ganglion cell discharge can be elicited by extrinsic polarization of the horizontal cell. The later provision is very important as it enables us to exclude the processes that starting from the absorption photons result in the generation of the horizontal cell potential. This allows us to break up the system into two sub-systems connection in tandem and thus establish a sequence in the processing of the input light signal.

Any formal analysis has to rely on a receptive field model. There are two principle receptive field models; one proposed by Rodieck and Stone [70a] and the other by Naka and Nye [61] for the catfish. In this chapter our analysis is based on the receptive field model proposed for the catfish retina.

2. Catfish Receptive Field

The receptive field organization of the catfish ganglion cell and the cellular mechanisms that subserve the field have been reported in a series of papers [Naka and Nye, 61, 62, 63]. Two types of fields (type A and type B) can be found which are exactly complementary to each other in their organization.

In the type A field, stimulation by a small spot of light produced a sustained ganglion discharge while a stimulating annulus gave rise to a transient ganglion response. In the type B field a transient ganglion discharge was obtained whenever the receptive field was stimulated by a spot of light while a sustained discharge resulted if the stimulus were an annulus.

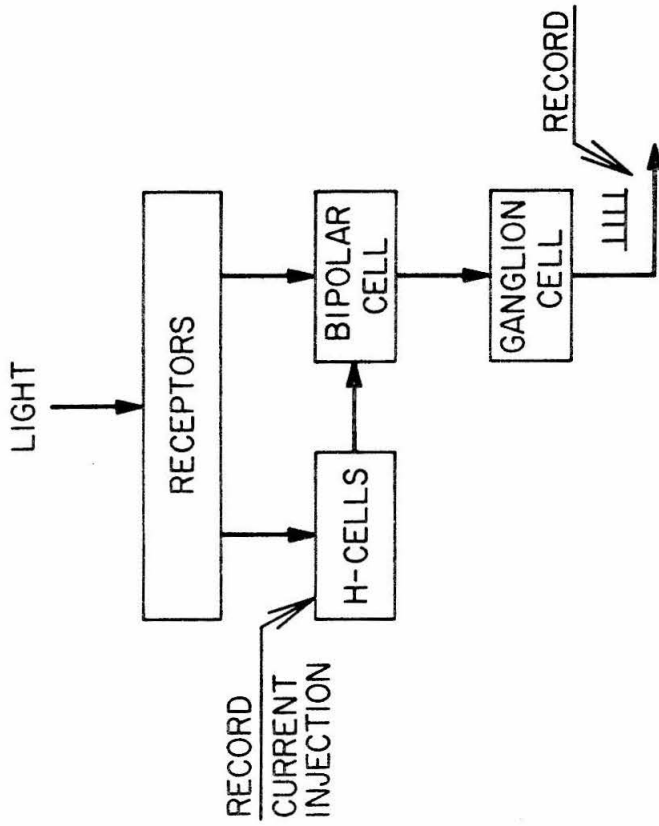
It was also shown [Naka, Naka and Nye] that current injected into the horizontal cell induced spike discharge patterns (of the ganglion cell) very similar to those elicited by spot or annulus stimulation (also [47]). Depolarization of the horizontal cell resulted in the same discharge pattern as stimulation by a spot of light while hyperpolarization of the horizontal cell produced the same discharge pattern as that elicited by a stimulating annulus. This was the case for both types of receptive field.

In view of these findings it was suggested [64] that two mechanisms are responsible for the receptive field organization. One is an "integrating" mechanism and the other a "local" mechanism. The "integrating" mechanism depends on the S-space to propagate and integrate stimuli over a large area (about 5 mm in

diameter) of the ganglion receptive field. This mechanism can be interpreted as measuring the average light present in the receptive field. The "local" mechanism responds to the peak local luminance. It was shown that in both types of field (A and B) the stimulus which gives rise to a transient discharge can suppress the sustained discharge. It was observed that decentered spots can also inhibit the sustained discharge thus implying the existence of a second lateral transmission system, besides the S-space, since a spot of light cannot sufficiently activate the S-space.

In this chapter we determine quantitative dynamic transfer functions for the two mechanisms activated by a spot and an annulus and resulting in the ganglion discharge. In view of all the findings described in the previous paragraphs it is suggested that a light spot activates the neural pathway formed by the chain Receptors→Bipolar→Ganglion while an annulus of light activates the chain Receptors→Horizontal→Bipolar→Ganglion, as depicted in Fig. 8.1. Whether this is an accurate account on the cellular level of the two mechanisms or not, the derivation of the dynamic transfer functions by use of the white-noise method is valid since it only describes the input-output behavior of these retinal systems.

The neural chain Horizontal→Bipolar→Ganglion is also studied as to its dynamic characteristics by injecting white-noise current into the S-space and recording ganglion cell discharges.



LIGHT : RECEPTOR → H-CELL
CURRENT INJECTION : H-CELL → BIPOLAR CELL → GANGLION CELL
LIGHT SPOT : RECEPTOR → BIPOLAR CELL → GANGLION CELL
LIGHT ANNULUS : RECEPTOR → H-CELL → BIPOLAR CELL → GANGLION CELL

Fig. 8.1

A simple schematic configuration of the different subsystems of the retina. Shown also is the description of several stimulus response systems and the corresponding activated neuronal chain.

3. The Horizontal Cell→Ganglion Cell System

The white-noise method will first be applied to the horizontal cell→ganglion cell neuronal chain to obtain its nonlinear dynamic transfer function. This neuron chain is part of the neuronal mechanisms which gives rise to the ganglion cell discharge upon absorption of photons by the receptors. In this analysis the horizontal cell potential was modulated by injecting extrinsic current in S-space. In turn, this H-cell potential modulation evoked the ganglion cell discharge. As the bipolar cell is the only neuronal element to connect the external plexiform layer to the internal plexiform layer, it was argued that the extrinsic polarization of the horizontal cell caused a change in the bipolar cell potential which, in turn, evoked the ganglion cell discharges. In essence, the system to be studied has an input which is extrinsic current injected into a horizontal cell and a output which is the ganglion cell discharge.

From preliminary harmonic analysis the system was found to have a cut-off frequency around 12 Hz. Accordingly, the white-noise input had a flat power spectrum from essentially d. c. up to 25 Hz. The input current produced a modulation of the horizontal cell potential whose average was the resting potential of the cell. Thus the system was tested for both the depolarized and hyperpolarized horizontal cell conditions.

A white-noise signal, 35 seconds long, was used as the input and an electrical circuit was designed so that the magnitude of the injected current was proportional to the input signal (i. e. original white-noise signal). The stimulus record was formed by

concatenating on magnetic tape this same 35 sec long white-noise signal with itself, ten times, to form a stimulus of 350 sec duration. The ganglion responses to these ten runs of identical white-noise were then superimposed and histogrammed in time to form effectively a post-stimulus-time histogram of the ganglion discharge in response to this white-noise input. Thus the spike discharge is transformed into a continuous function of time that can be interpreted to signify the instantaneous spike discharge frequency. Thus, we avoid the difficulty of dealing with the discrete (spike) events.

Fig. 8.2 shows a short portion of the same white-noise current for four different runs along with the corresponding evoked ganglion responses. These records show that: 1) the white-noise current inputs reproduced were identical and 2) the ganglion cell responses from four different runs are almost identical, implying that the system is time-invariant under the conditions employed in this experiment.

The ganglion cell discharge frequency becomes a smoother function of time as the number of (identical) runs is increased. However, as the life of the preparation is limited, the number of (identical) runs is also limited. In these experiments, 8 to 12 runs were repeated for each case and the smoothness of the resulting frequency function was satisfactory (varying a little with the mean spike discharge frequency of each case).

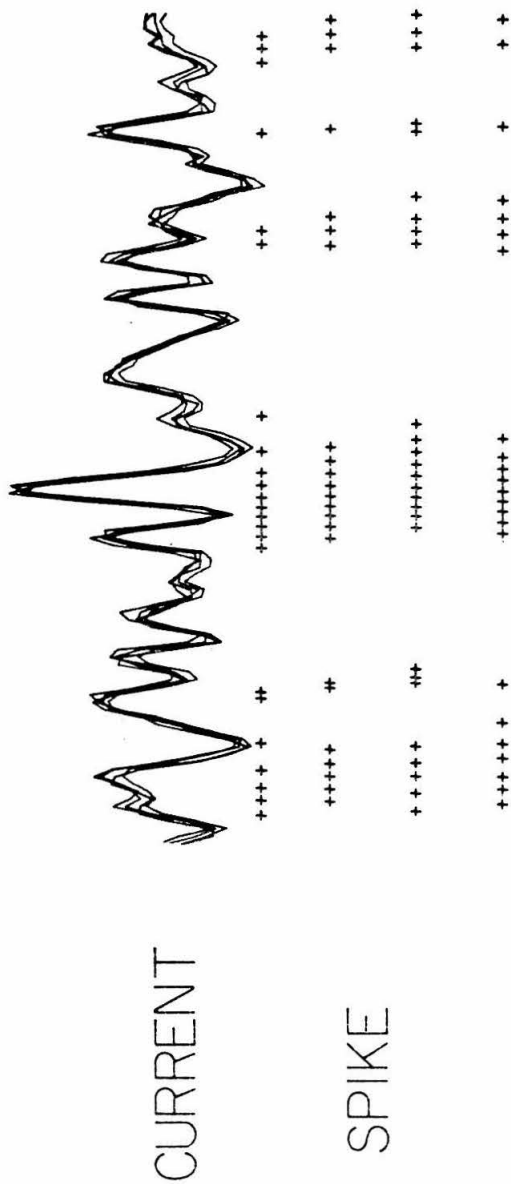
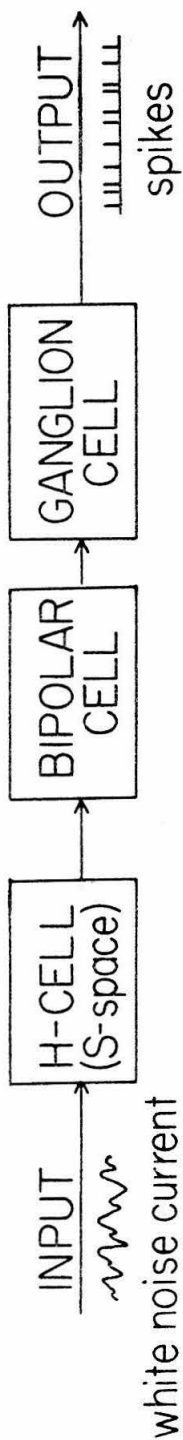


Fig. 8.2

White-noise current injected into H-cell and corresponding ganglion responses for four different runs of the same white-noise input. Each cross represents a ganglion spike (in time). The input waveforms for the four runs are superimposed (in time).

These input-output data were then treated for reduction of long term drifts (as described in Chapter IV) and subsequently the first and second order kernels were computed.

Figure 8.3 shows a plot of $h_1(\tau)$ which can be considered to be the impulse response of the "best" linear model of the system. We mean "best" in the sense that, for the white-noise record with which the system is tested, $h_1(\tau)$ is the linear system that minimizes the mean square error over the entire length of the record. In general, if the Wiener series is truncated after the n^{th} order term the resulting approximation to the system transfer function is the "best" among models of the n^{th} order, as it was discussed in Chapter II. From $h_1(\tau)$ we can get an idea of the latency (about 10 msec) as well as how fast (response rise time, frequency response) and how damped (underdamped) is the system. In the same figure (Fig. 8.3), superimposed on the same axes, is also shown an experimental response of the neuron chain to an impulse input. We note the agreement between h_1 and the neuron chain response in latency, response rise time, waveform and the complete absence of firing for the negative portion of h_1 .

The second order kernel $h_2(\tau_1, \tau_2)$ has been interpreted as indicating the nonlinear interaction between portions of the input signal τ_1 and τ_2 seconds in the past in affecting the response of the system at the present (deviation from time superposition).

Fig. 8.4, A,B show three-dimensional plots of $h_2(\tau_1, \tau_2)$. In plot A

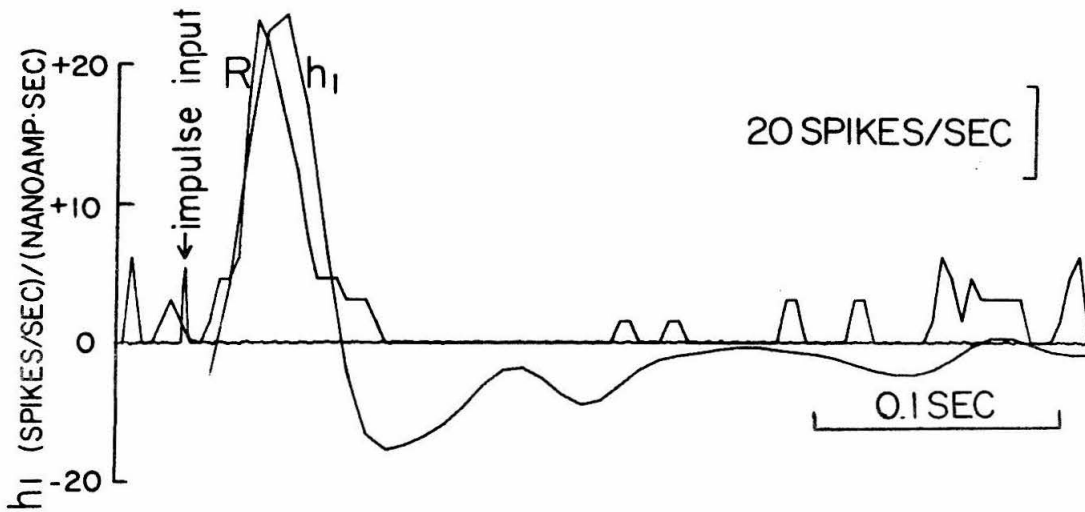


Fig. 8.3

First order kernel (h_1) of Horizontal \rightarrow Ganglion system and experimentally obtained response (R) of this system to an impulse (current) input. The ordinate for the h_1 plot is (spikes/sec)/(nanoamp sec) and for R it is (spikes/sec).

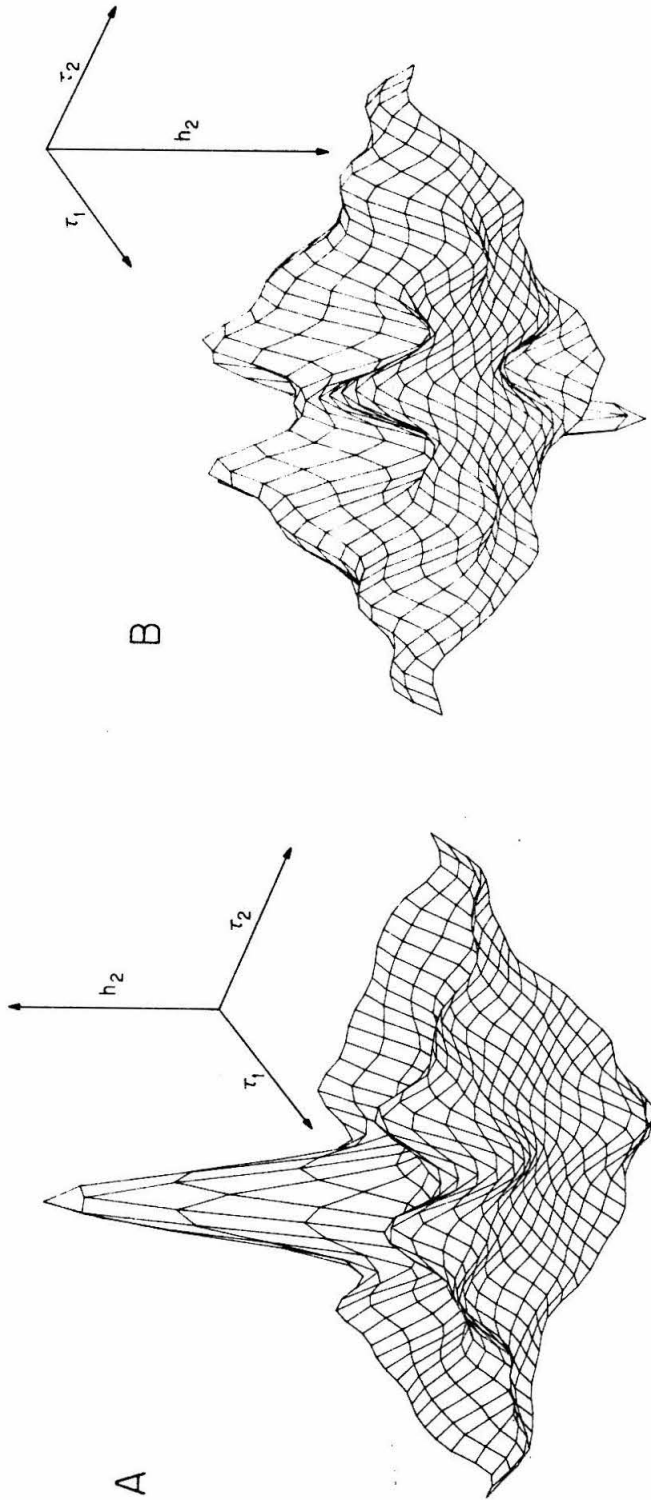


Fig. 8.4

Three-dimensional plots of the second order kernel $h_2(\tau_1, \tau_2)$ for system Horizontal \rightarrow Ganglion. For a clear view of h_2 the amplitude axis is reversed in polarity in plot B. View A shows well the peaks while view B permits a good view of the valleys (appearing as peaks) in $h_2(\tau_1, \tau_2)$. The grid lines are spaced 8 msec apart. The units for h_2 are (spikes/sec)/(nanoamp sec)².

SECOND ORDER KERNEL

0	8	16	24	32	40	48	56	64	72	80	88	96	104	112	120	128	136	144	152	160	
0	9	8																			
8	9	19																			
16	5	22	37																		
24	-2	17	40	53																	
32	-8	6	29	47	48																
40	-9	-4	11	27	32	24															
48	-6	-8	-5	4	10	8	1														
56	-1	-7	-12	-12	-8	-6	-7	-8													
64	2	-3	-11	-17	-16	-12	-8	-7	-8												
72	2	-2	-8	-14	-16	-11	-5	-3	-6	-8											
80	0	-3	-8	-12	-12	-7	-1	3	0	-6	-8										
88	0	-4	-9	-11	-10	-5	3	7	6	0	-6	-8									
96	1	-4	-9	-11	-10	-5	2	8	9	5	-2	-7	-9								
104	1	-2	-7	-10	-9	-5	0	4	7	6	2	-4	-7	-8							
112	1	-1	-5	-8	-8	-4	-1	1	3	3	2	-1	-4	-6	-6						
120	1	0	-3	-6	-6	-3	0	1	1	0	1	1	-1	-3	-4	-4					
128	1	0	-2	-5	-5	-3	1	2	2	1	0	1	1	0	-1	-2	-2				
136	2	1	-2	-5	-6	-3	1	4	3	2	2	2	1	1	0	-1	-2				
144	2	1	-3	-7	-7	-5	0	4	6	5	3	2	2	1	1	0	-1	-2			
152	2	0	-4	-8	-9	-6	-2	5	6	6	4	2	2	1	2	1	0	-2	-3		
160	1	0	-4	-7	-8	-6	-2	4	4	4	4	2	2	1	2	2	2	0	-3	-6	

Table 8.1

Values of $h_2(\tau_1, \tau_2)$. Horizontal (current injection) \rightarrow Ganglion. Axes in msec.

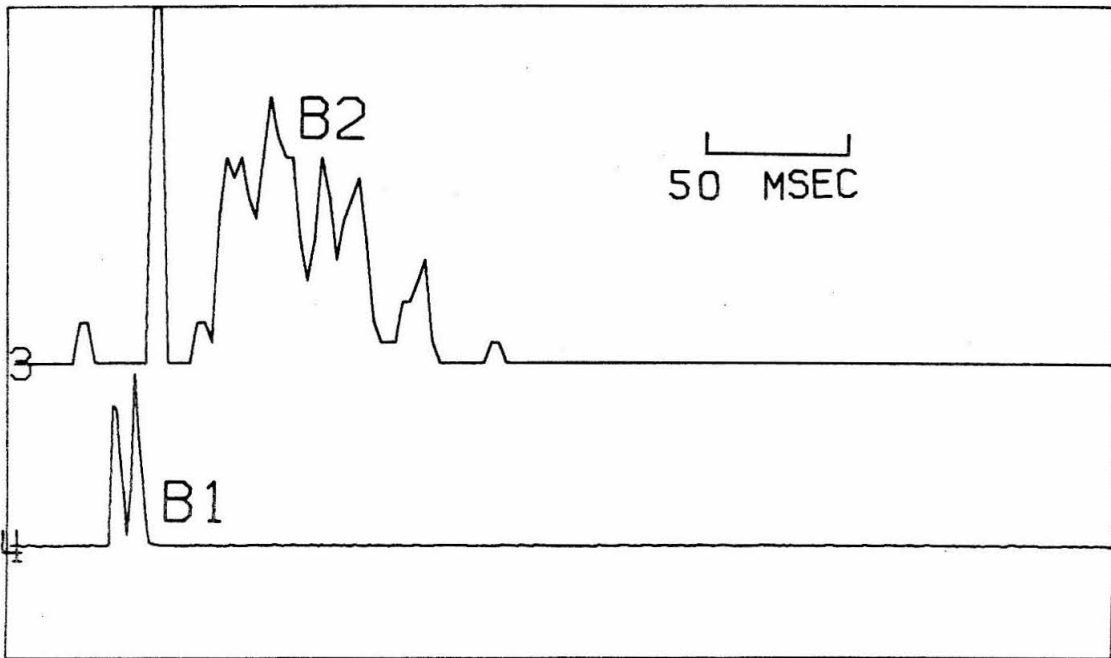
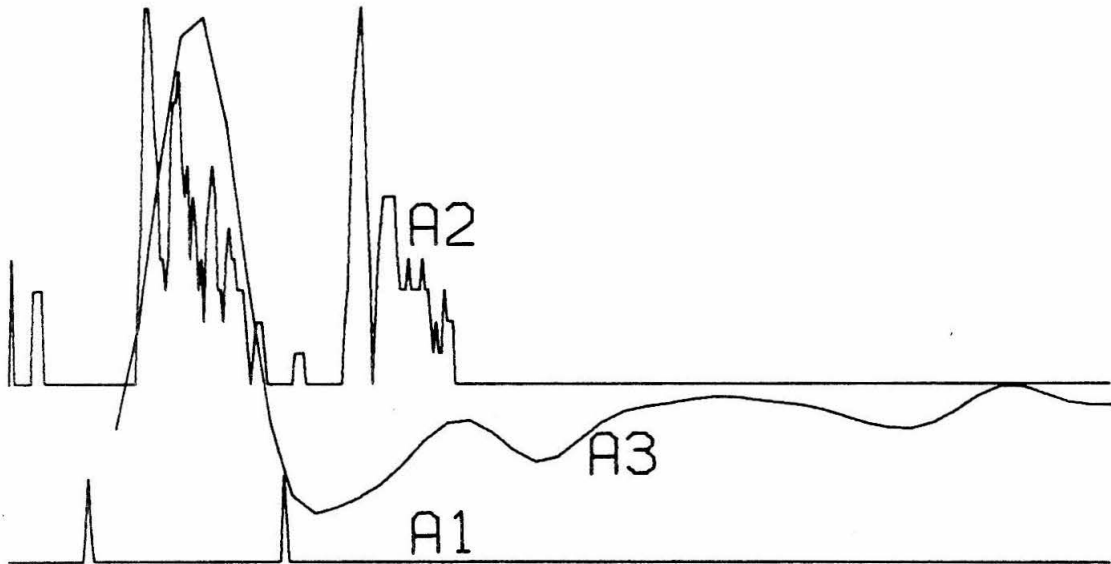


Fig. 8.5

Two two-pulse experiments for system Horizontal Ganglion that show the nonlinear interaction predicted by $h_2(\tau_1, \tau_2)$.

mountains represent nonlinear facilitation while valleys represent nonlinear inhibition between different portions of the input signal. Plot B is plot A inverted and here the roles of mountains and valleys are reversed. Plot B allows a better view of the inhibitory portions which now appear as mountains. Table 8.1 gives numerical values for $h_2(\tau_1, \tau_2)$. These plots of $h_2(\tau_1, \tau_2)$ suggest that pulses close together, about 10 msec, would produce a nonlinear interaction which initially (3-4 msec after the occurrence of the second input pulse) would tend to facilitate the ganglion response while pulses separated by about 40 msec would always tend to inhibit the ganglion response.

Two-pulse experiments were performed with various spacings between the pulses. The results confirmed the predictions of the model. When two short electrical pulses of current were injected into the horizontal cell an initial facilitation of the resulting ganglion discharge was observed when the first pulse preceded the second by 5 to 10 msec while a depression of the discharge resulting from the second pulse could be seen when the first pulse preceded the second by more than 40 msec. Fig. 8.5 shows two such experiments.

Fig. 8.6 shows the response of the system to a white-noise input and the corresponding model responses (first and second order) to this same input. White-noise current (trace A) was injected into the horizontal cell and caused the response of the ganglion cell shown in trace 'B' (this response being in terms of

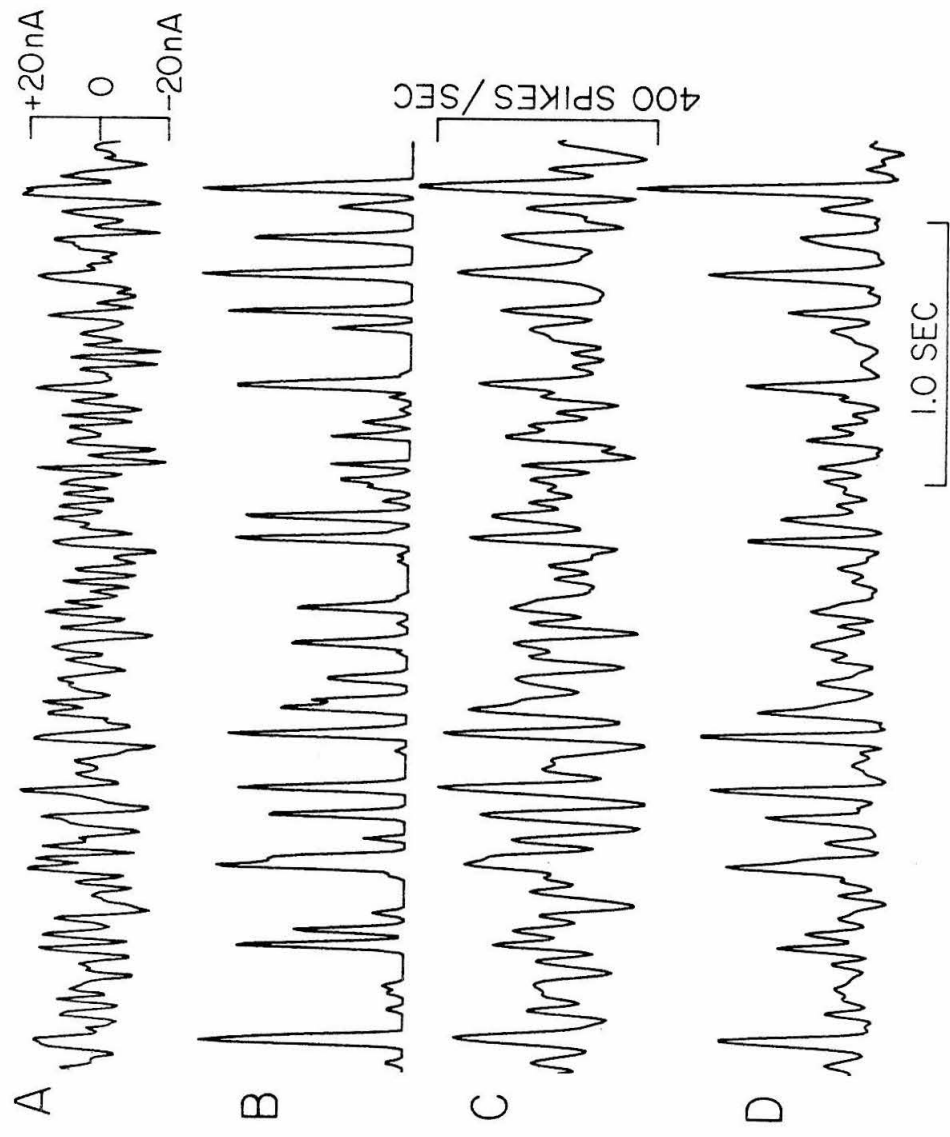


Fig. 8.6

Experimental and model responses to white-noise for system Horizontal \rightarrow Ganglion. A: input white-noise (current) stimulus, B: ganglion response (in spikes/sec) obtained experimentally, C: linear model response, D: nonlinear model response.

spike frequency). Trace 'C' is the first-order model (linear) response to this same white-noise input and trace 'D' is the second-order model (nonlinear) response. It is obvious that the model response improves markedly with the addition of the second order nonlinearities as it is demonstrated in this figure. The mean square error for the sequence of Wiener models, where the error for the (constant) h_0 model (zeroth order kernel, which is just the average value of the output), is normalized to 100 (arbitrary) units, is as follows:

<u>Model</u>		<u>Error</u>
constant	$\{h_0\}$	100
linear	$\{h_0, h_1\}$	43
nonlinear	$\{h_0, h_1, h_2\}$	20

Figure 8.7 shows the power spectra for the four signal records from which a time-portion is shown in Fig. 8.6. We note that the system has a cutoff around 12 Hz and that the nonlinear model spectrum improves significantly over the linear one especially in the high frequency region. The agreement between experimental response spectrum and nonlinear model spectrum is extremely good.

As discussed in Chapter III, examination of $h_2(\tau_1, \tau_2)$ suggests that the system can be represented by a linear system followed by a nonlinear one. The physiological interpretation of this implication is that the process taking place between the

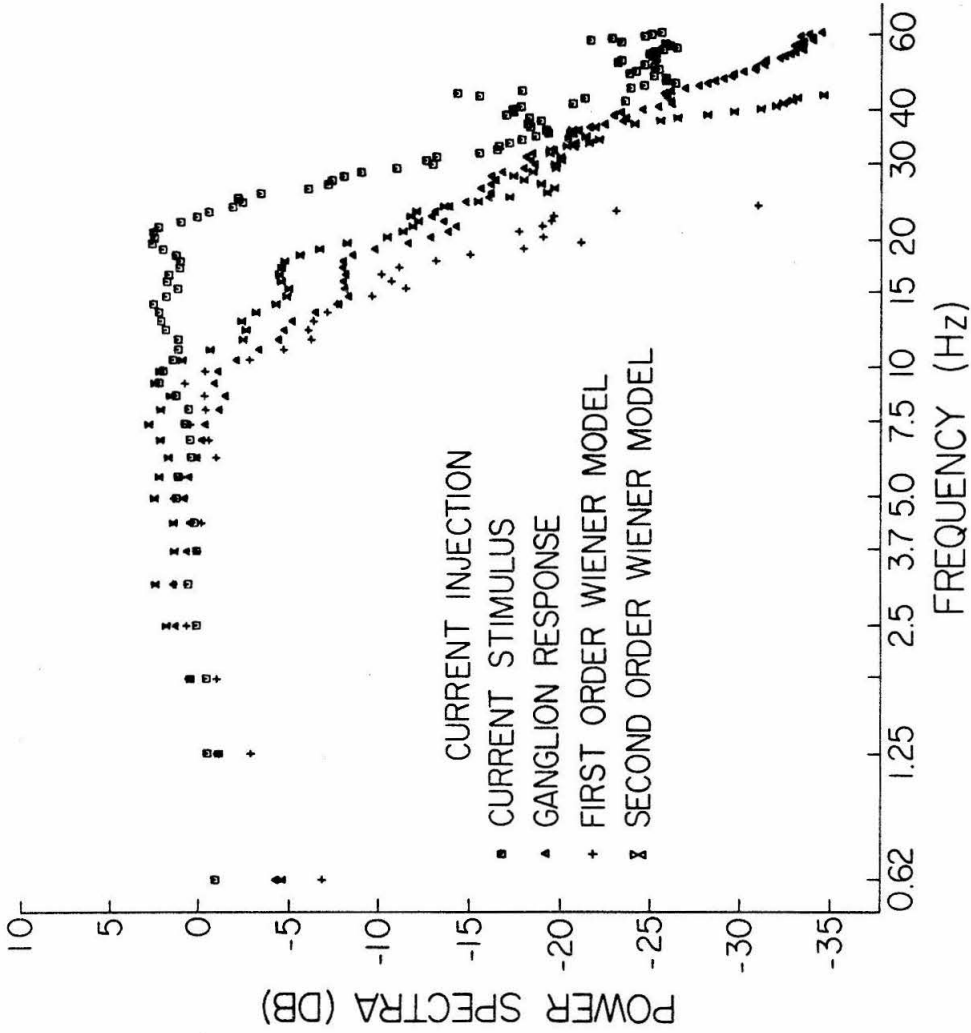


Fig. 8.7

Power spectra of experimental and model (both linear and nonlinear) responses to white-noise for system Horizontal → Ganglion.

horizontal and bipolar cells is essentially linear while the non-linearity occurs when the bipolar cell output triggers the ganglion cell spikes. The facts that the bipolar cell produces a slow continuous voltage while spike activity results from a threshold mechanism support this inference. We will examine the nature of this nonlinearity further.

Fig. 8.8, A1, A2 shows the model system responses to two pulses of different magnitudes (the stronger one is 2.5 times bigger in amplitude). Fig. 8.8, A1 shows the linear model response while Fig. 8.8, A2 shows the nonlinear model response. Fig. 8.8, A3, A4 show the model responses to negative-going pulses. Fig. 8.8, B1, B2, B3, B4 show again model step responses for the complementary ganglion (Type B). These model predictions (for positive-going pulses) agree extremely well with the experimental step responses reported by (Naka and Nye 1971).

Examining the model step responses we may conclude that the system responds mainly to the positive derivative of the input. Equivalently, we may say that the system could be represented by a low pass filter which responds to changes in the input followed by a half-wave rectifier. Examination of Fig. 8.6 (traces B, C and D) reveals exactly these same characteristics. The system function of responding mainly to positive changes of the input is also exhibited by the sine responses shown in Fig. 8.9. The question arises whether the system kernels indicate these functional traits. Assuming that the rectifying nonlinearity is almost a no-memory non-linearity we can easily show that the system second order

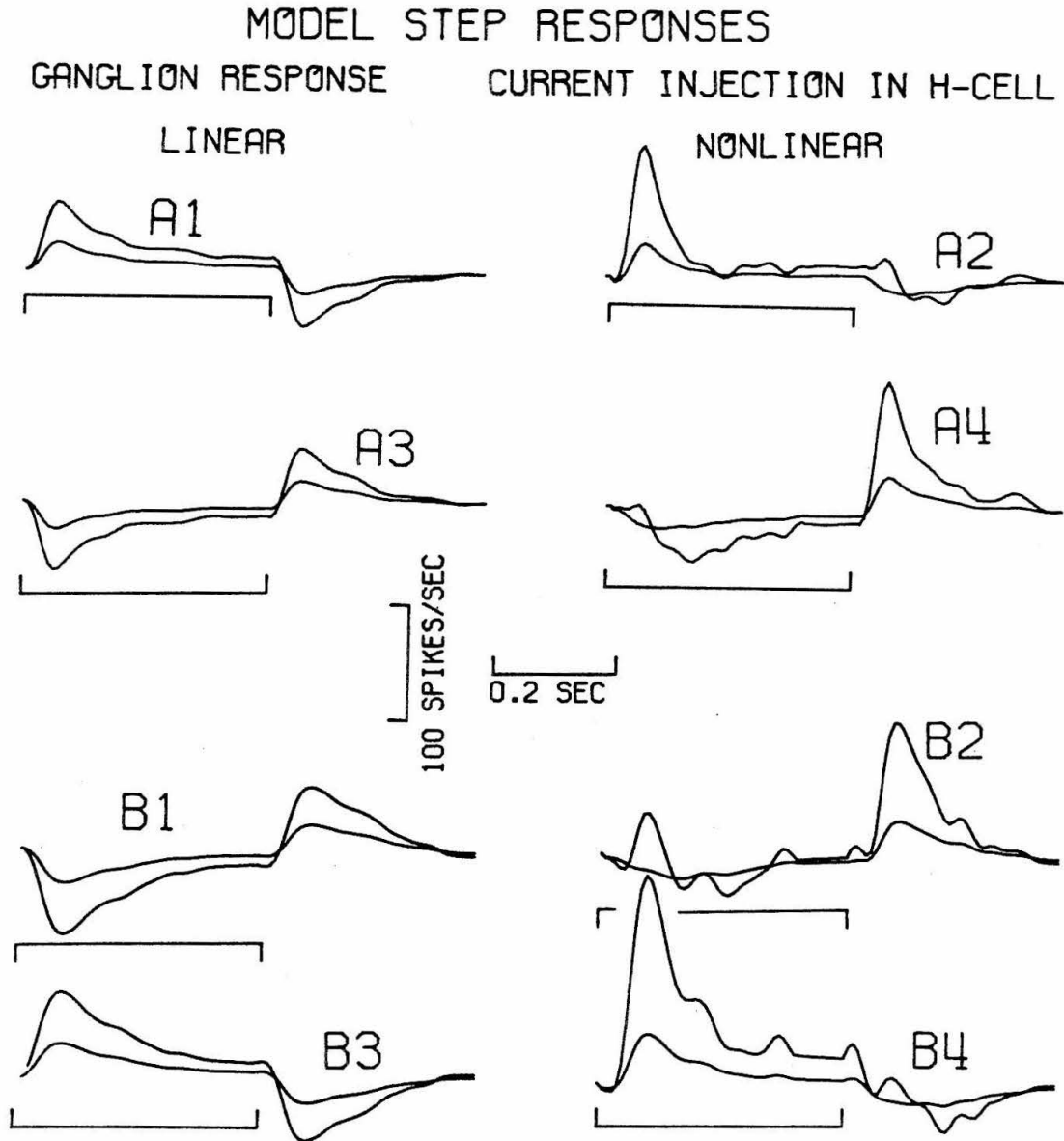


Fig. 8.8

Model-derived step responses for system Horizontal \rightarrow Ganglion. In each case, two input step levels are applied which are 0.4 log-units apart in magnitude. Responses are shown for both positive and negative pulses. A1, A3 are linear-model responses while A2, A4 are nonlinear-model responses for the type A ganglion. B1, B2, B3, B4 are similarly for the type B ganglion.

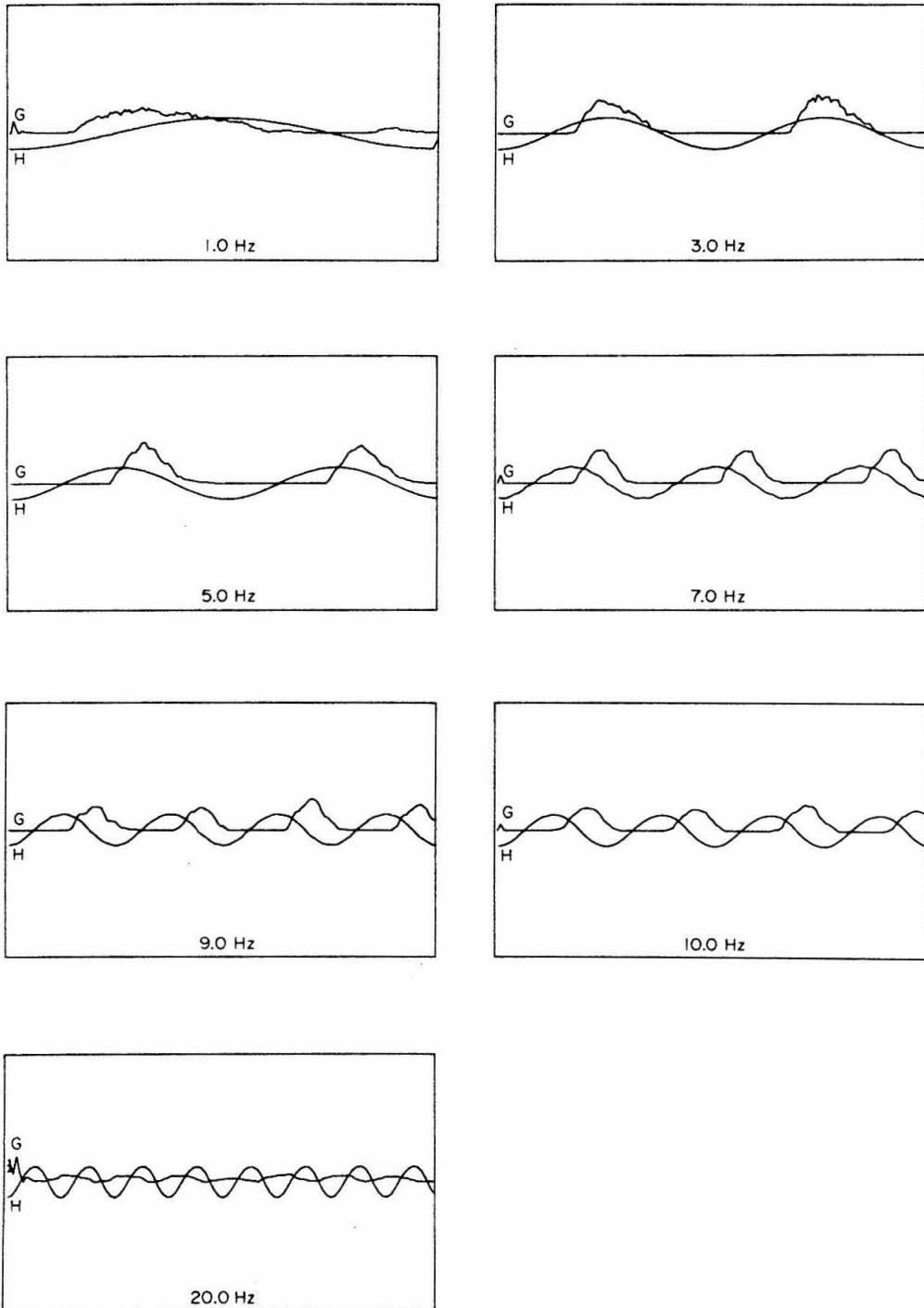


Fig. 8.9

Experimental sinusoidal responses for system Horizontal \rightarrow Ganglion.
H: input current, G: ganglion response (spikes/sec).

kernel should have, approximately, the form:

$$h_2(\tau_1, \tau_2) = \alpha \cdot h_1(\tau_1) \cdot h_1(\tau_2).$$

where α is a constant. Examination of h_1 and h_2 indicates that this is, indeed, the case.

In view of all these comparisons between model and experiment, we conclude that the white-noise-derived model, in this case, is very satisfactory.

4. Nonlinear, Dynamic Transfer Functions for Light→Ganglion Systems

In this section we derive transfer functions for the following neuronal chains that contribute to the ganglion receptive field organization:

(a) Receptor→Bipolar→Ganglion (System S)

(b) Receptor→Horizontal→Bipolar→Ganglion (System A)

as well as the transfer function between light intensity and ganglion response (System U) which results when both chains (a) and (b) are activated simultaneously by the same signal. From earlier arguments we have concluded that chain (a) is tested by a small spot of light at the center of the receptive field while chain (b) is activated by an annulus of light. The third transfer function (light intensity to ganglion response) is obtained through stimulation with uniform light over the entire receptive field. These three systems are characterized by their response to a white-noise input and the resulting kernels for each case.

In each case, light (spot or annulus or uniform) was modulated in white-noise fashion and used as the input. Its power spectrum was flat from essentially d. c. up to 25 Hz. This was judged to be adequate because these systems have cutoffs around 7 Hz. The identification procedure (data treatment and computations) is essentially the same as described in the previous section for the H-cell→Ganglion system and in Chapter IV. Therefore, it will not be repeated here.

Fig. 8.10 shows the first order kernels for all these systems. In addition, the kernels for the H-cell→Ganglion and Light→H-cell systems are shown. All kernels shown in Fig. 8.10 were computed from white-noise experimental data that were obtained from the same unit in a single preparation! (Thanks to the skill of Dr. Ken Naka).

There are several interesting functional features revealed in Fig. 8.10. The latency for system S (i. e. , chain: Receptor→Bipolar→Ganglion which is activated by spot stimulation) is considerably larger than that of system A (i. e. , chain: Receptor→Horizontal→Bipolar→Ganglion activated by annulus stimulation) or system U (uniform Light→Ganglion system).

The latencies are:

System S : ~ 55 msec.
System A : ~ 30 msec.
System U : ~ 30 msec.

This rather surprising result implies that the receptor-to-bipolar synapse introduces a large delay.

Considering the response rise time for these three systems we note that system S is much slower and more damped (less overshoot) than systems A and U which appear quite underdamped. System A and (even more so) system U exhibit the characteristics of a differentiator impulse response; a large positive impulse followed by a large negative impulse. Therefore, systems A and U act as differentiators, that is, they respond mainly to changes in the input rather than the input level. Since, for system A, the

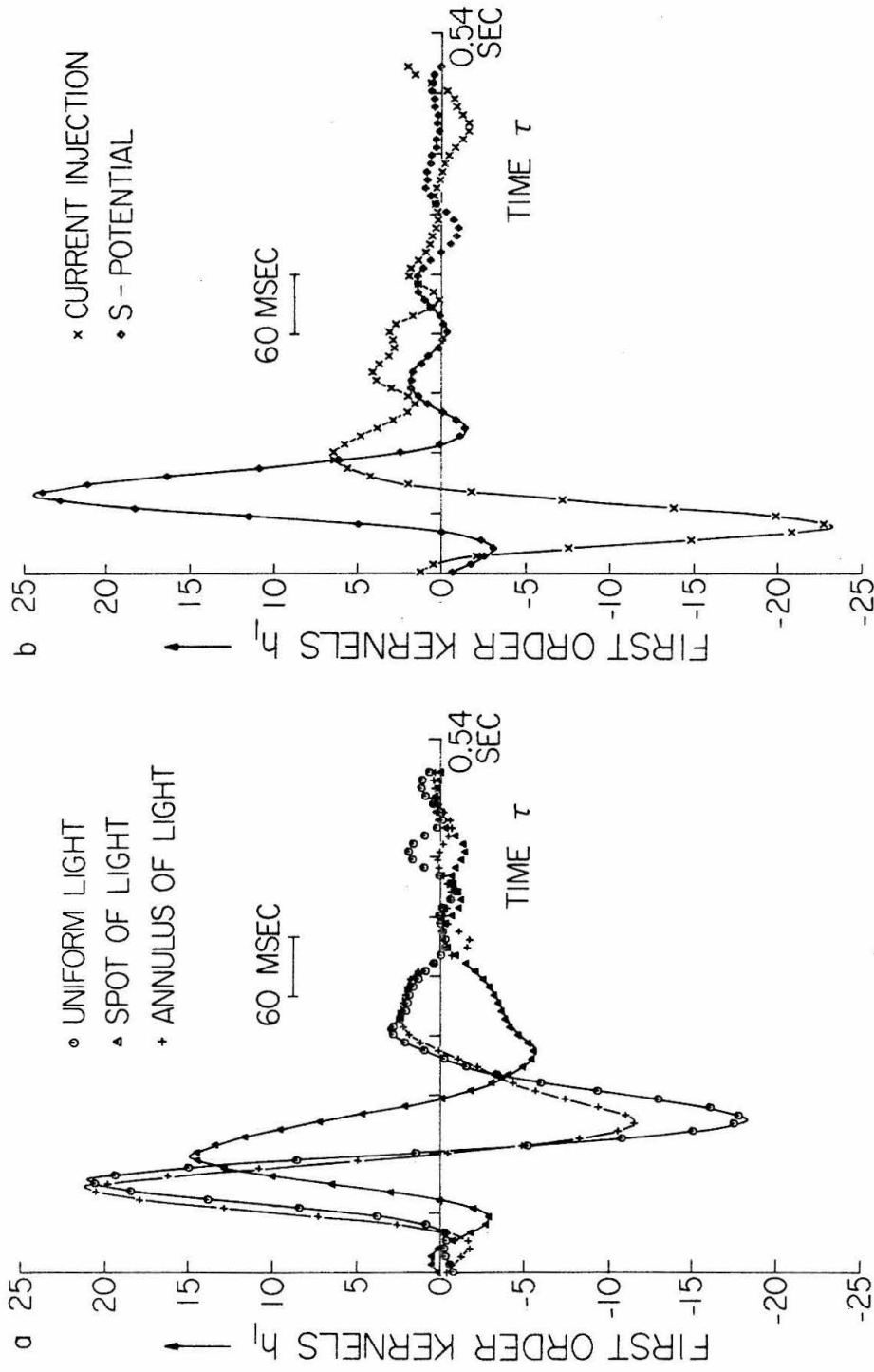


Fig. 8.10

First order kernels for systems Uniform \rightarrow Ganglion, Spot \rightarrow Ganglion, Annulus \rightarrow Ganglion, Horizontal \rightarrow Ganglion and Uniform \rightarrow Horizontal obtained from the same preparation and units. The ordinate is, in each case, (output units)/(input units sec).

negative portion is somewhat smaller than the positive one, this system also detects the magnitude of input level. However, system U acts as a good differentiator (positive and negative portions are of the same magnitude).

Since, as shown on the same figure (and in Chapter VI) the Light→H-cell system responds mainly to the magnitude of input level (notice h_1 for this system in Fig. 8.6) we may conclude that the differentiating process takes place in the chain Horizontal→Bipolar→Ganglion. This is in agreement with the results of the previous section where we found the system (chain: Horizontal→Bipolar→Ganglion) acting as a differentiator followed by a half-wave rectifier. Later, when examining the nonlinearities (second order kernels h_2) of these systems, we will also discover the rectification process. Thus, it is well established that differentiation and rectification, as evidenced in the ganglion response, take place in the neuronal chain Horizontal→Bipolar→Ganglion.

Another important implication of Fig. 1 is the following: If $(h_1)_{\text{spot}}$ is slightly delayed by a simple filter (i. e., physical mechanism) then the following relation is true:

$$(h_1)_{\text{uniform}} \simeq (h_1)_{\text{annulus}} - (h_1)_{\text{spot}}$$

This indicates the kind of interaction between the two mechanisms of the receptive field. This interaction, following previous arguments and morphological observations, takes place at the bipolar cell level. That is, the bipolar output is an almost-linear

function of the difference between the two inputs it receives from the receptors (as manifested by spot stimulation) and the horizontal cell (as manifested by annulus stimulation).

The first order kernels for the other two systems, which have already been described in other sections, are also shown in Fig. 8.10. We note the latencies:

System C : \sim 12 msec

System H : \sim 20 msec

which checks the latency for system U (\sim 30 msec) which is a concatenation of system H and system C.

Tables 8.2 through 8.5 describe the second order kernels of all these systems as computed from data obtained from the same unit and preparation. Following the same arguments as in the previous section we conclude that these nonlinear kernels describe a rectification process.

The set of kernels $\{h_1, h_2\}$, for each of the five systems, is the nonlinear, dynamic transfer function between the input and output of this neuronal chain.

Figures 8.11, 8.12, 8.14 show white-noise responses both experimental and for the linear and nonlinear models for all systems under study, as well as the corresponding power spectra for all signals in each case. We note that the rectification phenomenon is clearly exhibited in the nonlinear model response. The agreement between experimental response and nonlinear model response is extremely good, as can be seen in these figures.

SECOND ORDER KERNEL

	0	8	16	24	32	40	48	56	64	72	80	88	96	104	112	120	128	136	144	152	160	
0	0	-2	-2	-4	-5	-5	-3	0	7	18	25	25	19	6	-7	-15	-17	-18	-13	-7	-2	-1
8	-1	-1	-2	-3	-4	-4	1	5	14	15	22	25	14	7	-8	-12	-15	-18	-16	-7	-2	2
16	0	0	-1	-1	-1	0	7	14	22	25	29	25	5	3	-6	-11	-15	-18	-17	-7	3	4
24	-1	-1	-1	-1	-1	2	8	15	22	29	27	22	14	7	-1	-8	-12	-15	-14	-9	5	2
32	-3	-2	-1	-1	-1	3	15	22	29	27	22	14	7	3	-2	-8	-12	-15	-14	-9	3	2
40	-4	-5	-3	-1	0	7	14	22	29	27	22	14	7	3	-2	-8	-12	-15	-14	-9	5	2
48	-4	-6	-5	-1	2	7	14	22	29	27	22	14	7	3	-2	-8	-12	-15	-14	-9	5	2
56	-4	-6	-7	-4	3	7	14	22	29	27	22	14	7	3	-2	-8	-12	-15	-14	-9	5	2
64	-2	-3	-8	-7	-1	8	15	22	29	27	22	14	7	3	-2	-8	-12	-15	-14	-9	5	2
72	2	1	-5	-9	-6	8	15	22	29	27	22	14	7	3	-2	-8	-12	-15	-14	-9	5	2
80	4	4	-1	-6	-8	3	15	22	29	27	22	14	7	3	-2	-8	-12	-15	-14	-9	5	2
88	3	4	-1	-6	-8	3	15	22	29	27	22	14	7	3	-2	-8	-12	-15	-14	-9	5	2
96	1	3	3	-1	-5	-1	2	14	23	27	22	14	7	3	-2	-8	-12	-15	-14	-9	5	2
104	1	2	4	3	-1	-4	-2	5	13	16	14	7	3	-2	-8	-12	-15	-14	-9	5	2	2
112	4	4	4	3	0	-2	-2	1	4	5	3	3	3	-2	-8	-12	-15	-14	-9	5	2	2
120	6	6	5	3	0	-2	-2	0	1	-1	-6	-11	-15	-17	-18	-17	-18	-16	-13	5	2	2
128	4	6	5	2	0	-3	-3	-1	-1	-4	-9	-15	-18	-19	-18	-16	-13	-13	-7	5	2	2
136	1	4	4	2	0	-2	-4	-5	-6	-8	-12	-15	-17	-17	-14	-11	-9	-9	-7	5	2	2
144	-1	2	3	2	0	-2	-5	-9	-13	-15	-16	-15	-14	-11	-7	-4	-2	-2	-1	5	2	2
152	-1	1	3	2	0	-2	-6	-12	-17	-20	-20	-17	-12	-6	0	4	6	5	3	5	2	2
160	-1	0	2	2	0	-2	-6	-12	-17	-21	-21	-18	-12	-5	3	8	11	11	8	8	4	2

Table 8.2

Values of $h_2(\tau_1, \tau_2)$. Annulus \rightarrow Ganglion. Axes in msec.

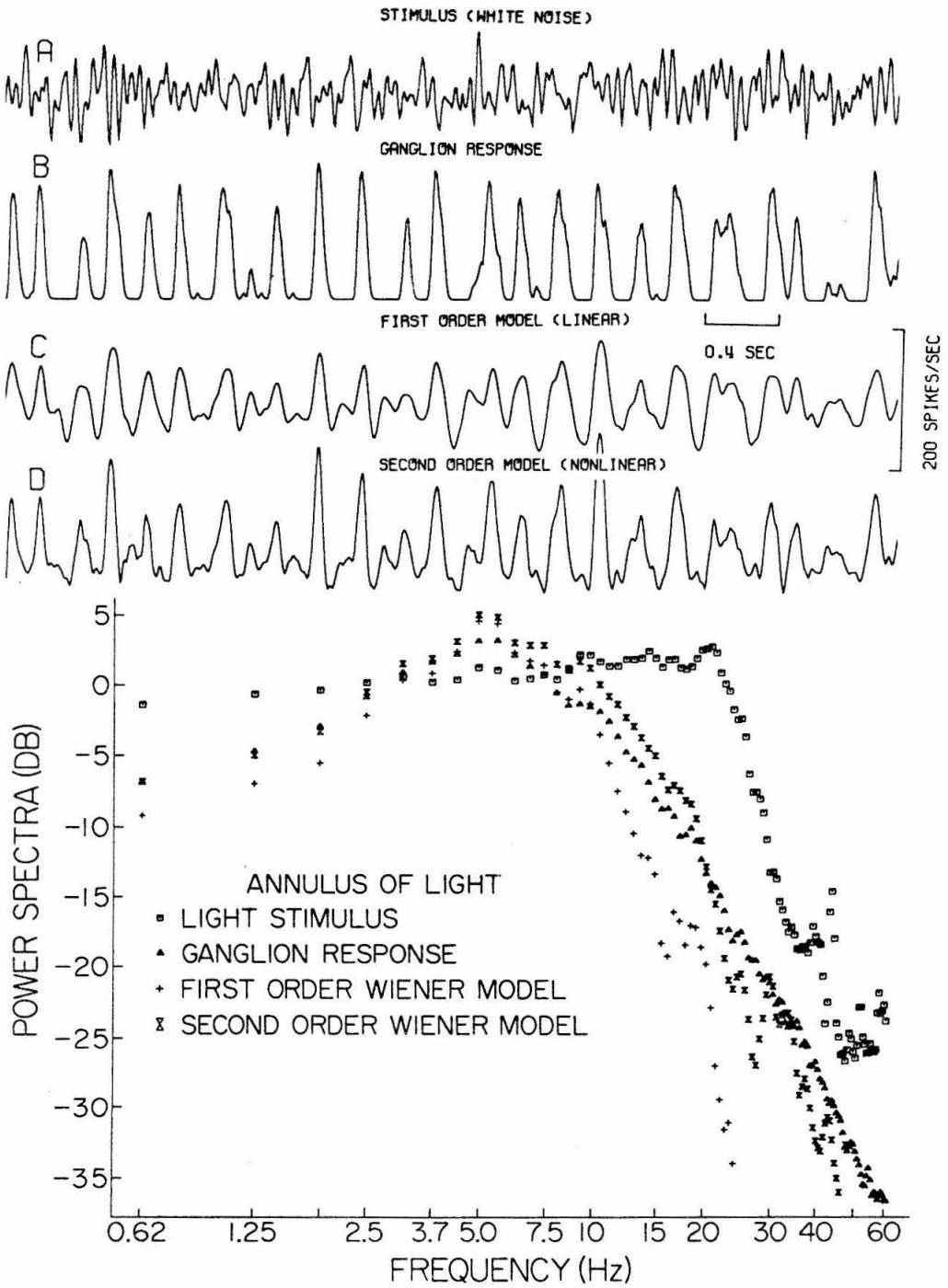


Fig. 8.11

Experimental and model responses to white-noise and corresponding power spectra for system Annulus → Ganglion.

SECCND ORDER KERNEL

0	0	8	16	24	32	40	48	56	64	72	80	88	96	104	112	120	128	136	144	152	160
0	0	-1	1	0	-1	-1	0	3	10	20	28	37	45	49	48	43	36	30	23	14	6
8	-1	0	-1	0	-1	-1	2	6	13	21	28	35	41	41	41	38	32	26	22	15	8
16	-4	-1	-1	-1	-1	-1	3	7	13	21	28	35	41	41	41	38	32	26	22	15	8
24	-6	-3	-3	-3	-3	-3	4	8	13	21	28	35	41	41	41	38	32	26	22	15	8
32	-5	-4	-4	-4	-4	-4	5	9	13	21	28	35	41	41	41	38	32	26	22	15	8
40	-3	-4	-4	-4	-4	-4	5	9	13	21	28	35	41	41	41	38	32	26	22	15	8
48	-2	-3	-3	-3	-3	-3	5	9	13	21	28	35	41	41	41	38	32	26	22	15	8
56	-1	-2	-3	-3	-3	-3	5	9	13	21	28	35	41	41	41	38	32	26	22	15	8
64	-1	-2	-3	-3	-3	-3	5	9	13	21	28	35	41	41	41	38	32	26	22	15	8
72	-2	-3	-3	-3	-3	-3	5	9	13	21	28	35	41	41	41	38	32	26	22	15	8
80	-2	-3	-3	-3	-3	-3	5	9	13	21	28	35	41	41	41	38	32	26	22	15	8
88	-1	-1	-2	-2	-2	-2	5	9	13	21	28	35	41	41	41	38	32	26	22	15	8
96	0	2	1	0	0	2	5	6	6	9	20	35	45	49	48	43	36	30	23	14	6
104	-2	1	4	3	1	1	4	6	5	5	10	24	41	41	48	43	36	30	23	14	6
112	-5	-2	2	5	4	2	2	5	7	5	4	10	24	41	48	43	36	30	23	14	6
120	-5	-6	-3	2	4	3	2	3	7	8	5	2	7	21	38	43	36	30	23	14	6
128	-2	-6	-7	-3	2	4	2	2	5	9	8	2	-3	2	17	32	36	30	23	14	6
136	1	-2	-6	-7	-3	2	3	1	2	6	9	7	-2	-8	-3	12	26	30	23	14	6
144	1	1	-2	-6	-7	-3	1	1	1	3	7	9	4	-6	-11	-5	9	22	23	14	6
152	-1	1	1	-2	-6	-6	-3	0	0	0	3	6	6	0	-8	-11	-4	8	15	14	6
160	-3	-2	1	1	-3	-5	-4	-1	0	0	-1	1	4	3	-2	-7	-8	-2	5	8	6

Table 8.3

Values of $h_2(\tau_1, \tau_2)$. Spot \rightarrow Ganglion. Axes in msec.

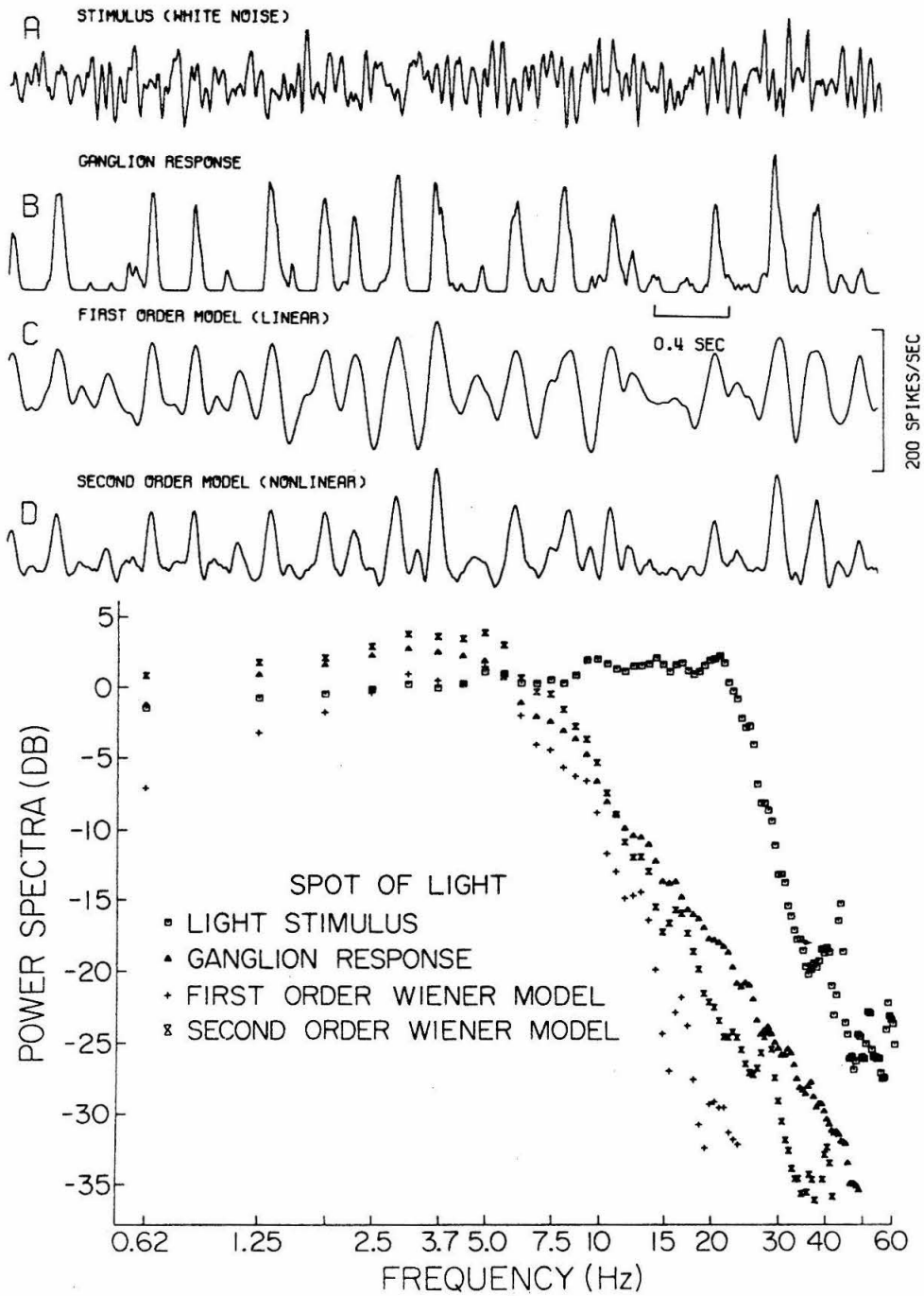


Fig. 8.12

Experimental and model responses to white-noise and corresponding power spectra for system Spot → Ganglion.

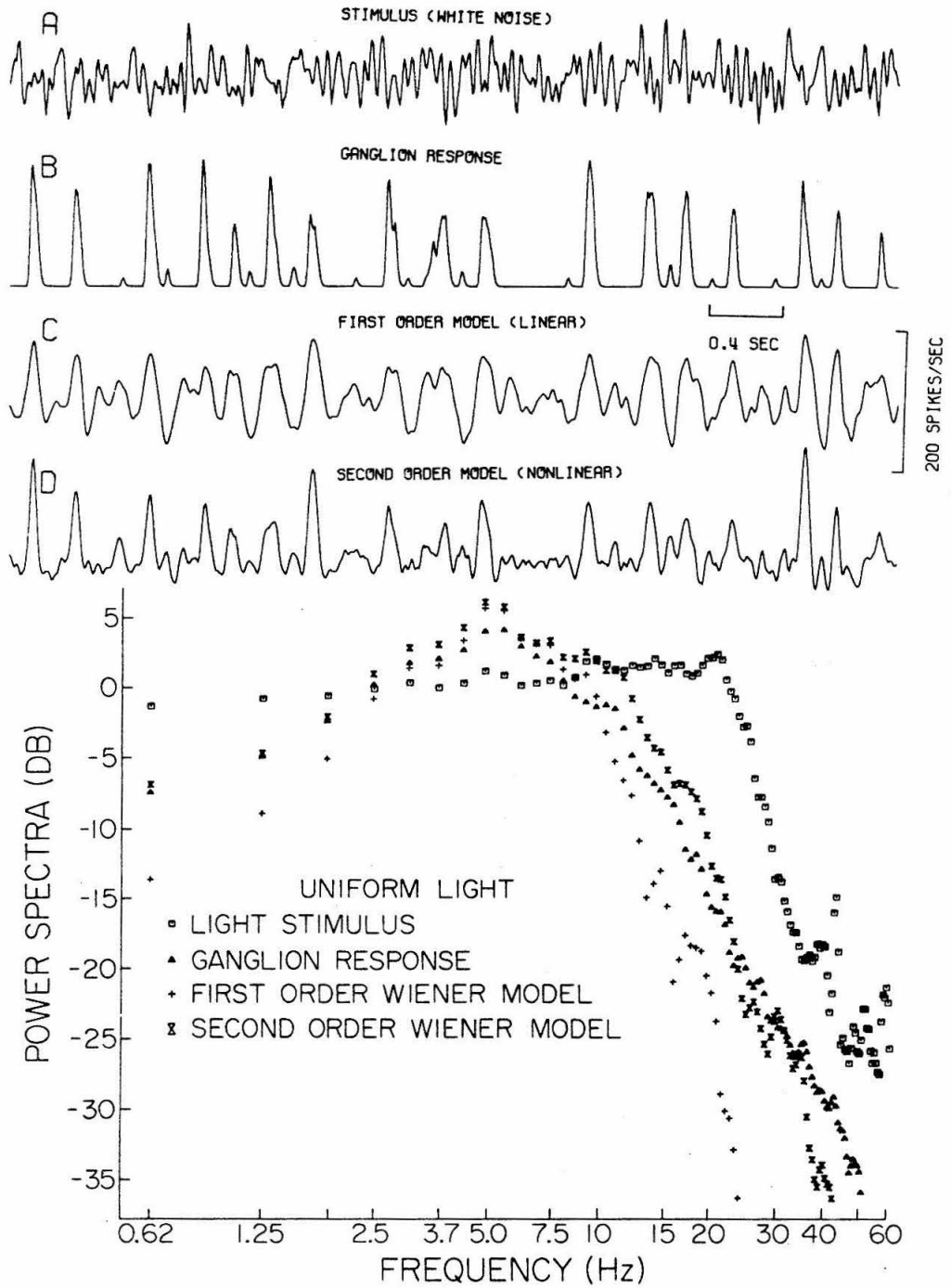


Fig. 8.14

Experimental and model responses to white-noise and corresponding power spectra for system Uniform → Ganglion.

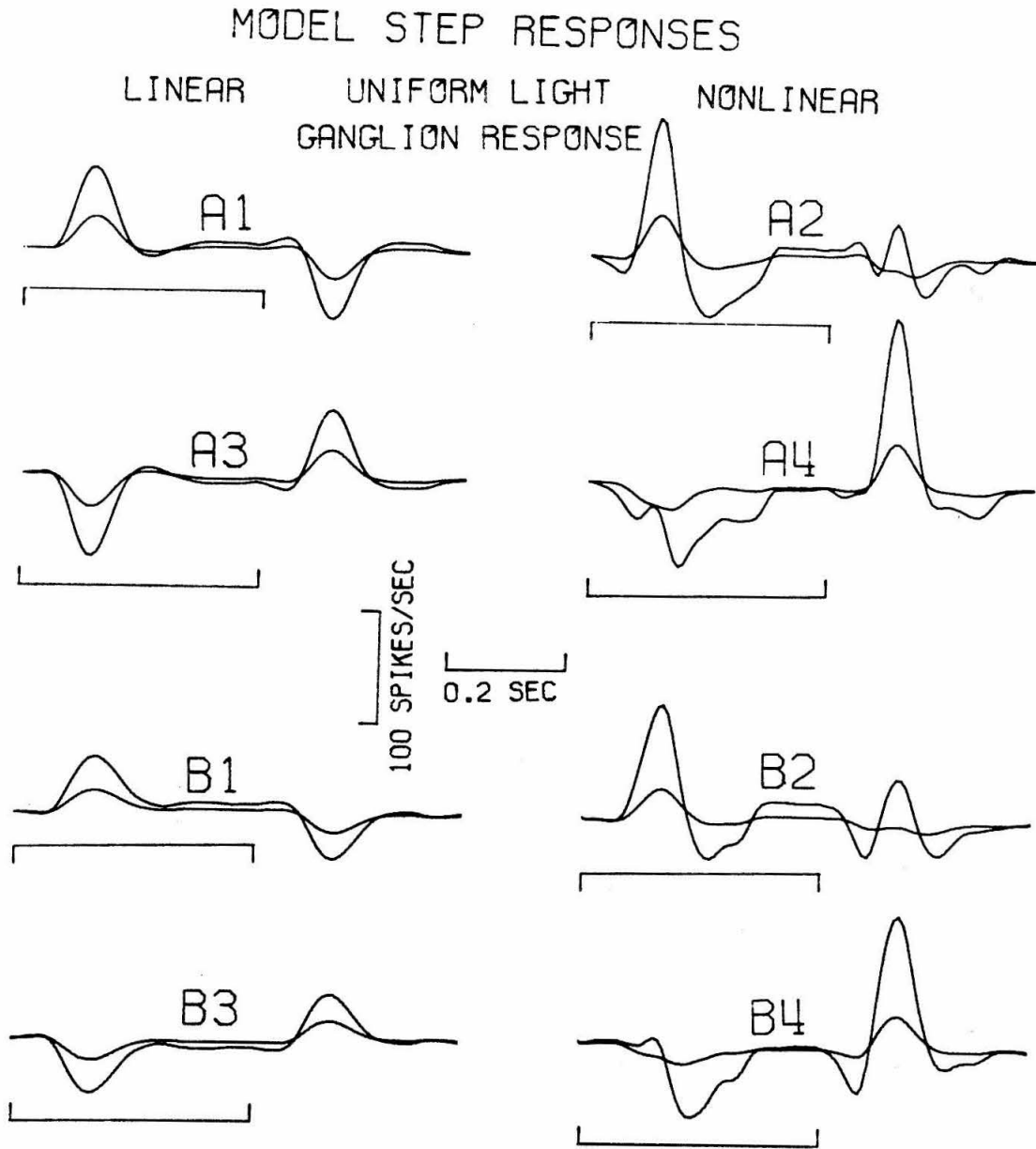


Fig. 8.15

Model step responses for system Uniform \rightarrow Ganglion. Both positive (A1, A2) and negative (A3, A4) steps are considered. Both linear-model (A1, A3) and nonlinear-model (A2, A4) responses are shown. B1, B2, B3, B4 are similarly for a different preparation.

The mean square error, normalized so that for the model of zeroth order (just h_0 , which is a constant equal to the average of the output) is 100 arbitrary units, is reduced as follows:

Mean Square Error			
System A	System S	System V	Model
100	100	100	a constant $\{h_0\}$
41	45	38	linear $\{h_0, h_1\}$
21	24	19	nonlinear $\{h_0, h_1, h_2\}$

The power spectra show the close agreement between experimental and model frequency response. We note again that the nonlinear system improves the model performance, especially for high frequencies. In addition, these spectra reveal a cutoff frequency of about 5 Hz for system S and a cutoff of about 9 Hz for system A and system U. Also, system S is very slightly underdamped while system A and system U are quite underdamped.

Fig. 8.13 shows model step responses for systems A and S. We note that (for positive steps) spot stimulation gives rise to a "sustained" response (subfigure A2) while annulus stimulation gives rise to a transient "ON-OFF" response (subfigure B2). These model predictions are well in agreement with experimental data for step responses [Naka, 62]. There are no available data for negative step responses. The model predictions for negative steps show "ON-OFF" behavior for system A and "sustained + OFF" response for system S. Thus, we again observe the phenomenon of

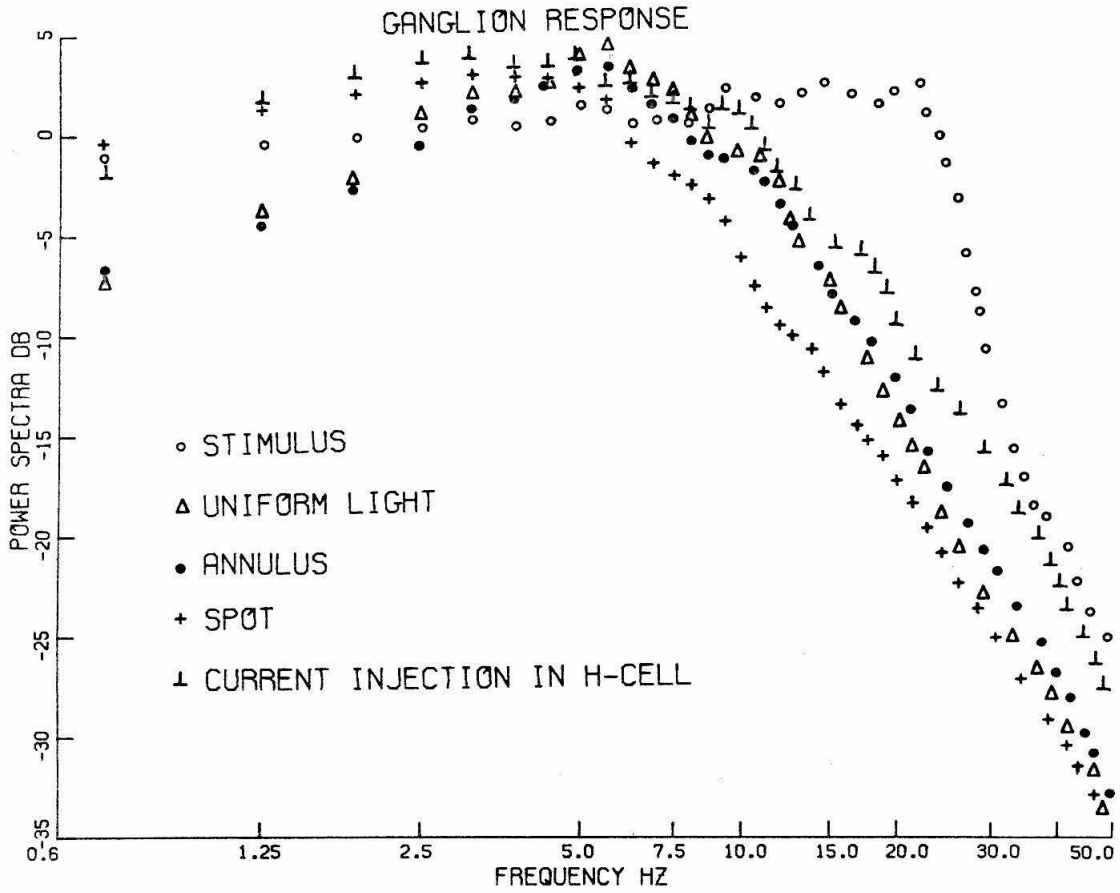


Fig. 8.16. Power spectra of experimental responses to white-noise for certain ganglion systems.

differentiation and rectification. Moreover, we note that for this ganglion type (Type A) system A responds only to changes in the input while system S responds to both the input level and positive changes of it.

Fig. 8.15 shows model step responses for system U. We note that this system responds mainly to positive changes of its input.

Fig. 8.16 shows power spectra (of the same unit and preparation) for systems A, S, U and C for the same white-noise input stimulus. As expected, system C is the fastest one and system S is considerably slower than systems A and U. For high frequencies the gain of system S, A and U attenuates at about the same rate.

Thus far we have examined the behavior of the ganglion response for spot (annulus) stimulation while the annulus (spot) was kept at darkness. Also, in all cases so far studied, the stimulus was concentric with the ganglion receptive field. Now, we examine some additional cases:

- a) eccentric spot stimulation (system SE)
- b) concentric spot + steady annulus stimulation (system SAC)
- c) eccentric spot + steady annulus stimulation (system SAE)

Fig. 8.17 shows a schematic description of the experiment for each case as well as the resulting first order kernel h_1 . There are several interesting implications. Considering subfigures A and B (Fig. 8.17) we see that an eccentric spot produced a ganglion response of the opposite sign from a concentric spot. Noting also

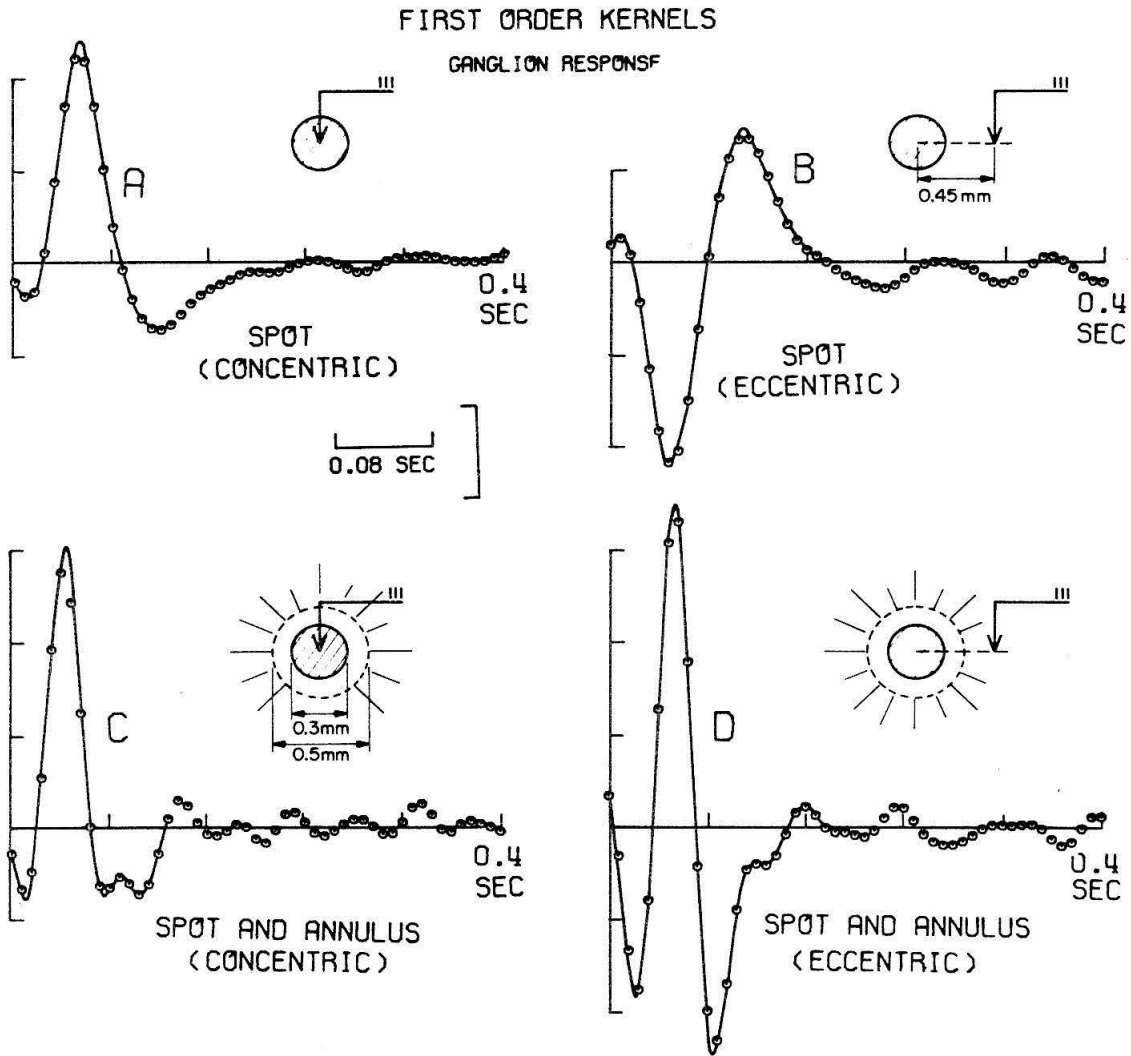


Fig. 8.17

First order kernels. A: Spot (concentric) Ganglion, B: Spot (eccentric) Ganglion, C: Spot & Steady Annulus (concentric) → Ganglion, D: Spot & Steady Annulus (eccentric) → Ganglion. The ordinate units are (output units)/(input units sec).

that the latency is the same in both cases, we conclude the existence of a lateral pathway that is capable of affecting the ganglion response by quickly transmitting signals from the periphery to the center of the receptive field. This function could conceivably be performed by the S-space, since, as we have shown in Chapter VII, a spot of 0.3 mm diameter produces considerable excitation at a distance of 0.45 mm away from its center. Therefore, it is suggested that for case A (Fig. 8.17) the neuronal path utilized to excite the ganglion is mainly Receptor→Bipolar→Ganglion while for case B (Fig. 8.17) it is Receptor→Horizontal→Bipolar→Ganglion. Earlier we stipulated that a spot stimulation and an annulus stimulus interact at the bipolar with the following functional relationship:

(*) (bipolar output) = (center excitation) - (periphery excitation)
or equivalently,

$$\begin{aligned} \text{(bipolar output)} &= \text{(input received from receptors)} - \\ &\quad - \text{(input received from horizontal cell)} \end{aligned}$$

for a Type A ganglion field. The results for cases A and B (Fig. 8.17) verify relation (*) since for case A we would have

$$\text{(bipolar output)} = \text{(center excitation)}$$

while for case B we have

$$\text{(bipolar output)} = - \text{(periphery excitation)}.$$

Considering cases C and D (Fig. 8.17) we note that the inhibitory influence of the annulus is greater in case D (as would be expected) as evidenced by the large negative undershoots of the kernel of case D and the fact that the positive peak occurs at the

same time as in case C. This is, again, in support of relation (*).

Considering cases B and D we note that the addition of the steady annulus illumination (corresponding to a change of "bias point") changes drastically the dynamic characteristics of the system. In case D, the system is very underdamped and it exhibits (considering case B) an additional excitatory (positive peak) component.

Tables 8.6 through 8.9 describe the second order (non-linear) kernels for all systems under consideration here.

Figures 8.18, 8.19, 8.21, 8.22, show responses (both experimental and model-derived) to a portion of the white-noise input used to stimulate these systems. The nonlinear model responses, indeed, agree very well with the experimental ones. These same figures also show the power spectra for the stimulus, experimental response, linear model response and nonlinear model response.

The mean square error (normalized to 100 arbitrary units for the model which is just h_0) is as follows:

Mean Square Error				Model
System S	System SE	System SAC	System SAE	
100	100	100	100	a constant $\{h_0\}$
49	41	38	45	linear $\{h_0, h_1\}$
26	20	17	22	nonlinear $\{h_0, h_1, h_2\}$

Fig. 8.20 shows model step responses (for both positive and negative steps) for systems S and SAC. The change of "bias point", caused by the addition of a steady annulus, has the following effect; it raises the sustained firing level while the system still exhibits the same transient behavior of responding mainly to a positive change of the input.

Fig. 8.23 shows model step responses for systems SE and SAE. In this case, the change of "bias" has the effect of changing the system from one which responds only to positive input changes (half-wave rectification) to one which responds to both positive and negative changes in the input (full-wave rectification).

Fig. 8.24 shows power spectra of white-noise responses for systems S, SE, SAC SAE. We note that,

- a) The frequency characteristics of systems S and SC are the same,
- b) System SAC is faster than system S, (a change brought by the "bias" change of steady annulus illumination),
- c) System SAE is faster than system SE (again due to "bias" change by the steady annulus),
- d) System SAC and SAE have approximately the same frequency characteristics.

These findings suggest that the "lateral mechanism" involved in systems SE and SAE is extremely fast (from both the frequency response and latency points of view). Moreover, in all cases the addition of a steady annulus makes the system much faster-responding.

SECOND ORDER KERNEL

0	4	8	16	24	32	40	48	56	64	72	80	88	96	104	112	120	128	136	144	152	160
4	4	2	-1	-1	1	8	14	22	27	33	41	50	60	71	83	96	110	125	141	158	176
8	4	2	-1	-1	0	5	9	16	22	28	35	44	54	65	77	90	104	120	137	155	174
16	3	2	-1	1	1	8	14	22	27	33	41	50	60	71	83	96	110	125	141	158	176
24	1	2	-1	1	0	5	9	16	22	28	35	44	54	65	77	90	104	120	137	155	174
32	-3	1	1	1	1	8	14	22	27	33	41	50	60	71	83	96	110	125	141	158	176
40	-7	-3	2	2	5	9	16	22	27	33	41	50	60	71	83	96	110	125	141	158	176
48	-9	-8	-1	-5	6	19	26	33	41	50	60	71	83	96	110	125	141	158	176	195	216
56	-8	-11	-5	6	19	26	33	41	50	60	71	83	96	110	125	141	158	176	195	216	238
64	-6	-10	-9	1	13	22	23	18	11	3	-1	-5	-6	-7	-8	-9	-10	-11	-12	-13	-14
72	-2	-6	-8	-4	4	11	13	8	3	-1	-5	-6	-7	-8	-9	-10	-11	-12	-13	-14	-15
80	2	0	-3	-5	-3	0	1	-1	-5	-6	-7	-8	-9	-10	-11	-12	-13	-14	-15	-16	-17
88	6	6	3	-1	-5	-7	-7	-8	-10	-10	-10	-10	-10	-10	-10	-10	-10	-10	-10	-10	-10
96	5	8	7	2	-5	-9	-12	-12	-12	-12	-12	-12	-12	-12	-12	-12	-12	-12	-12	-12	-12
104	4	7	7	2	-5	-11	-14	-14	-14	-14	-14	-14	-14	-14	-14	-14	-14	-14	-14	-14	-14
112	4	5	4	0	-7	-13	-16	-15	-11	-7	-5	-3	-2	-1	-1	-1	-1	-1	-1	-1	-1
120	5	3	2	-1	-8	-14	-16	-14	-10	-5	-2	0	0	0	0	0	0	0	0	0	0
128	7	4	1	-3	-8	-14	-15	-12	-9	-3	0	3	4	3	1	-2	-3	-3	-3	-3	-3
136	6	6	3	-2	-8	-13	-14	-10	-5	-1	2	5	6	6	4	1	-3	-5	-5	-5	-5
144	4	6	4	0	-5	-11	-13	-9	-3	2	5	6	6	6	6	4	1	-4	-5	-5	-5
152	2	4	4	2	-2	-7	-11	-9	-3	3	6	7	7	6	6	6	4	1	-4	-5	-5
160	0	2	3	2	0	-3	-7	-8	-4	2	6	8	8	7	7	6	3	-2	-7	-7	-7

Table 8.5

Values of $h_2(\tau_1, \tau_2)$. Spot (concentric) \rightarrow Ganglion. Axes in msec.

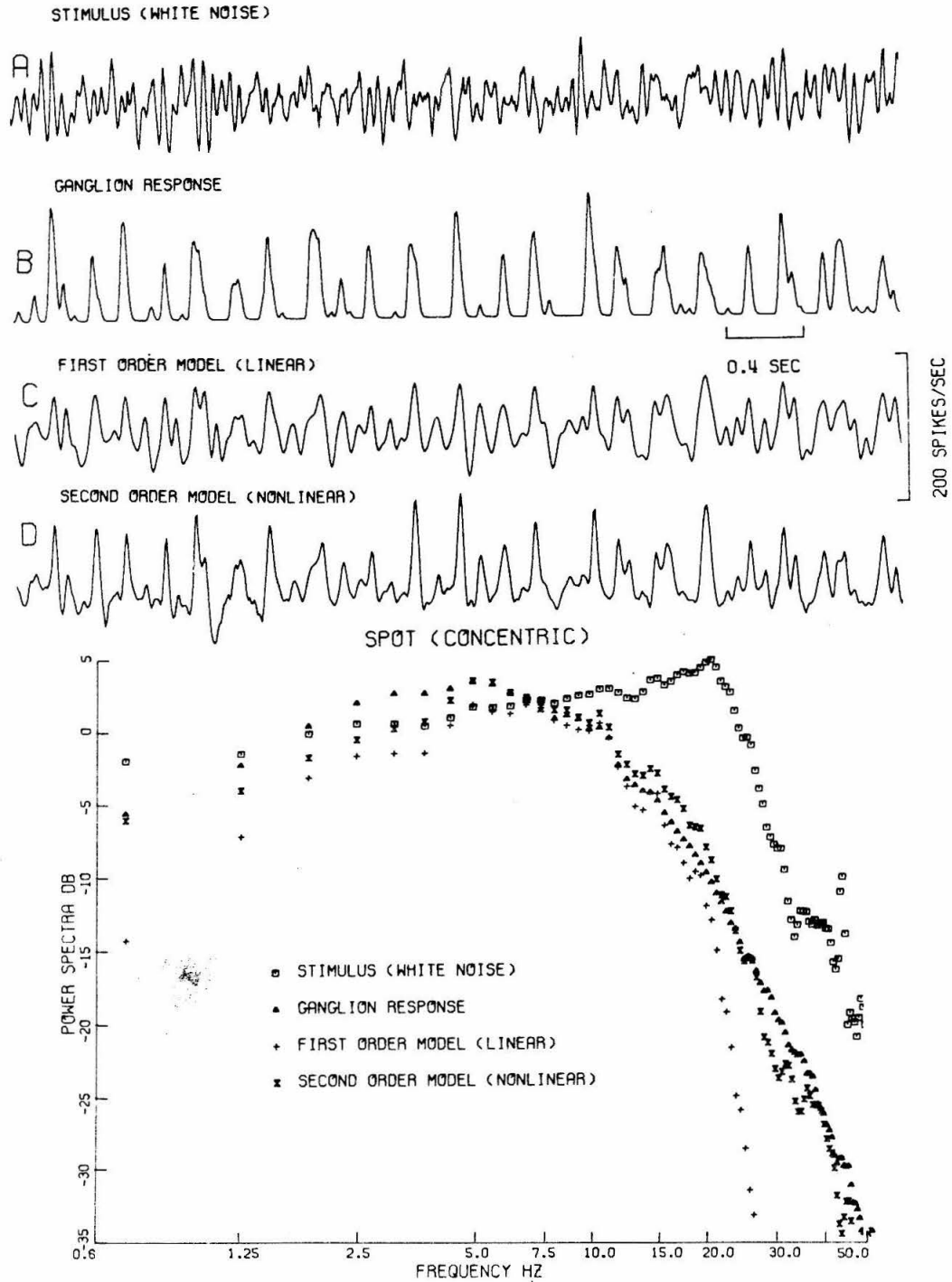


Fig. 8.18

Experimental and model responses to white-noise and corresponding power spectra for system Spot (concentric) → Ganglion.

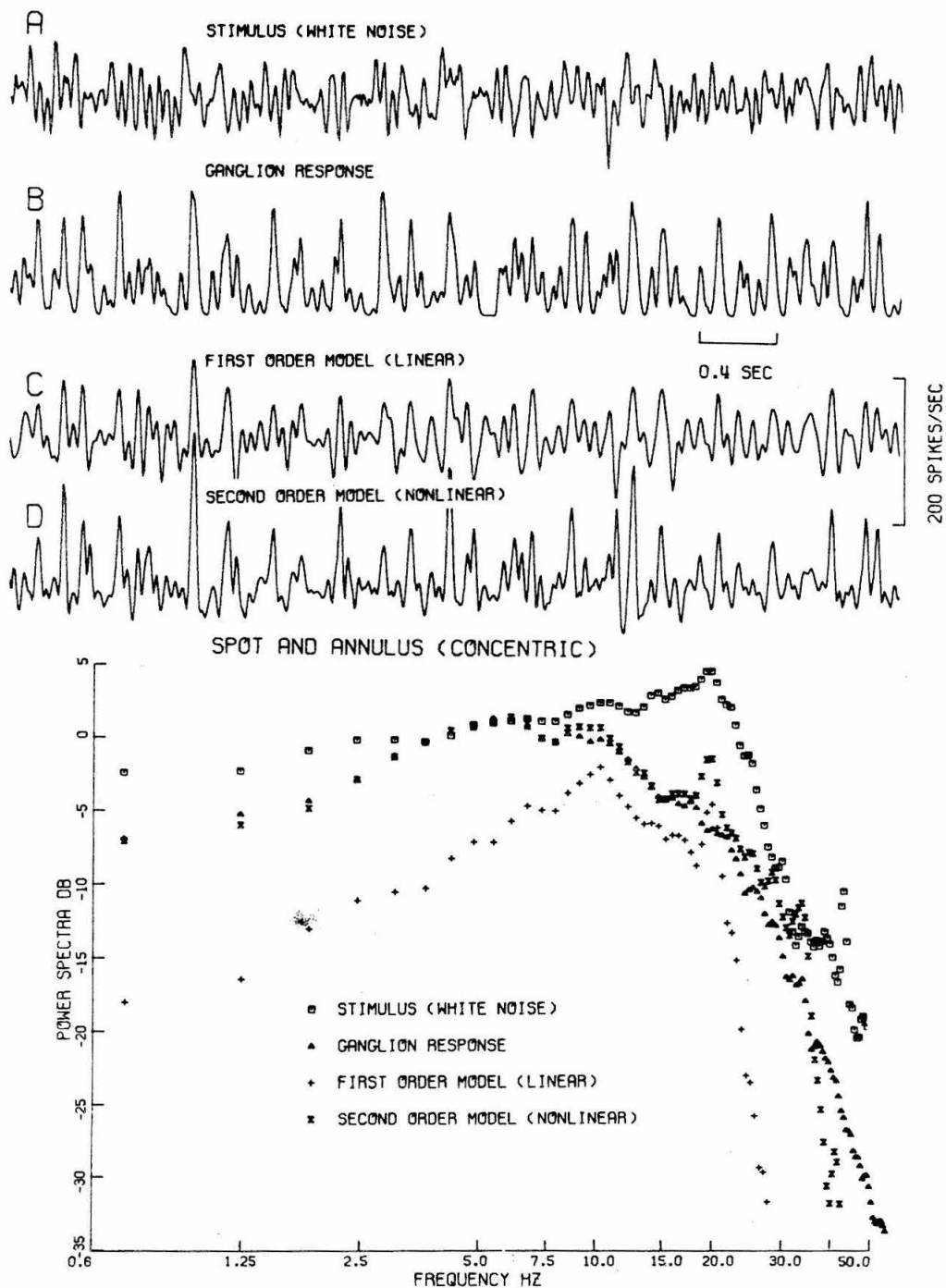


Fig. 8.19

Experimental and model responses to white-noise and corresponding power spectra for system Spot & Steady Annulus (concentric) -> Ganglion.

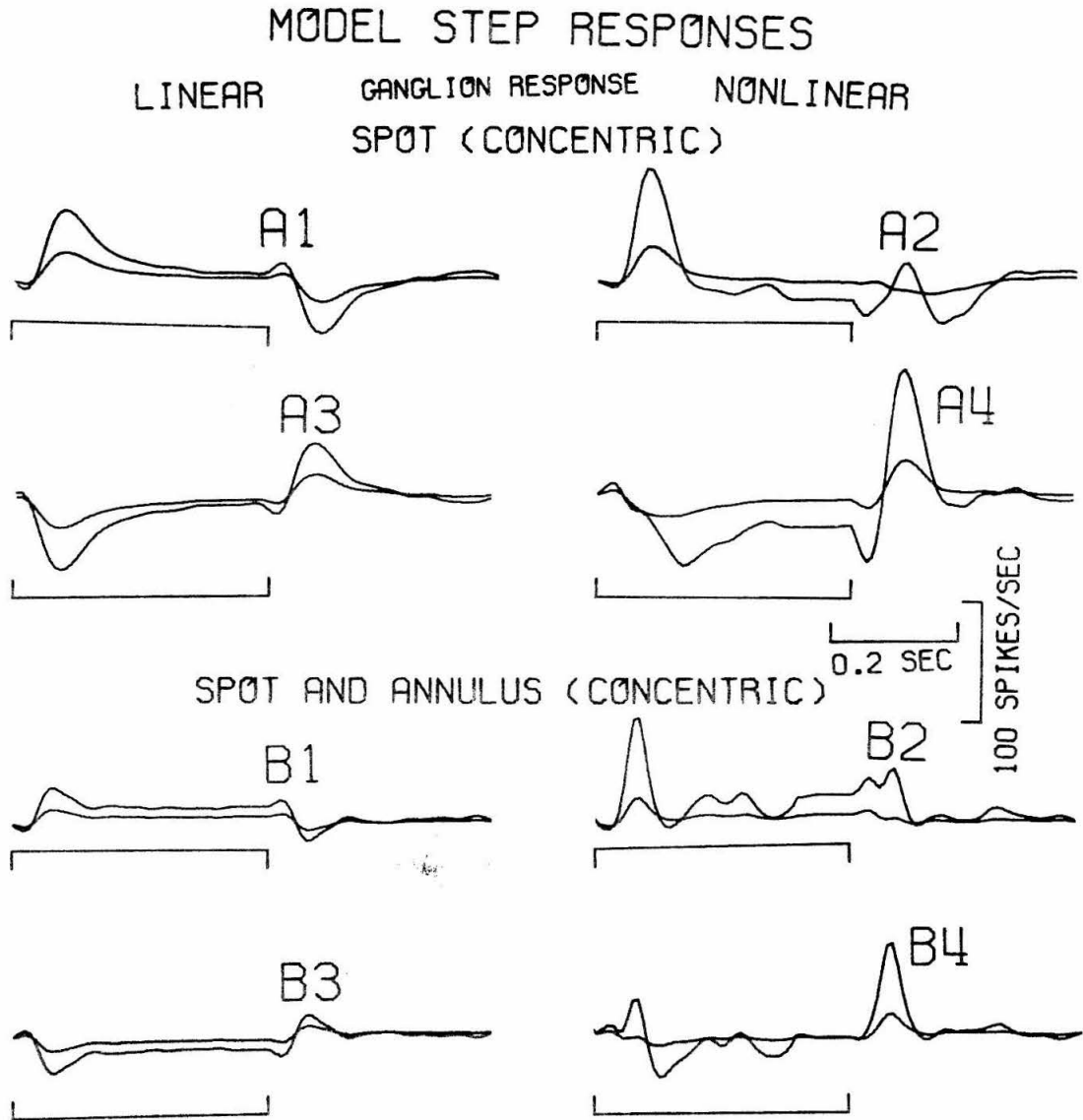


Fig. 8.20

Systems Spot (concentric) → Ganglion and Spot & Steady Annulus (concentric) → Ganglion. Both positive and negative steps are considered. Both linear-model and nonlinear-model responses are shown.

SECOND ORDER KERNEL

0	8	16	24	32	40	48	56	64	72	80	88	96	104	112	120	128	136	144	152	160	
-8	-7	-12																			
-1	-9	-13																			
3	-2	-9																			
3	3	0	-2																		
0	3	5	7	10	16																
-2	1	6	11	17	21	24															
-2	-2	3	10	18	23	23	20														
0	-2	-1	5	12	17	17	13	7													
3	0	-2	0	4	7	6	3	-1	-4												
5	3	0	-3	-4	-4	-5	-8	-9	-8	-8											
6	7	3	-4	-9	-12	-13	-15	-15	-13	-9	-5										
6	7	4	-3	-11	-16	-17	-17	-16	-14	-9	-4										
5	5	3	-2	-9	-16	-17	-16	-14	-11	-8	-3										
4	4	1	-3	-8	-13	-15	-14	-10	-7	-4	-1	4									
3	5	2	-3	-8	-12	-13	-11	-6	-1	2	2	1	4								
0	5	5	-1	-8	-12	-12	-9	-3	3	6	6	3	1	1	3	5					
-3	3	5	1	-6	-11	-11	-6	-1	5	8	8	6	3	1	1	4	6				
-4	0	4	3	-3	-8	-8	-3	2	5	7	7	8	5	2	0	2	4	4			
-3	-1	2	4	0	-4	-5	0	4	5	5	5	7	7	5	0	0	1	1	0		
-1	-1	1	4	3	0	-2	0	5	6	5	3	4	6	2	-2	-2	-3	-3	-3	-3	-3

Table 8.7

Values of $h_2(\tau_1, \tau_2)$. Spot (eccentric) \rightarrow Ganglion. Axes in msec.

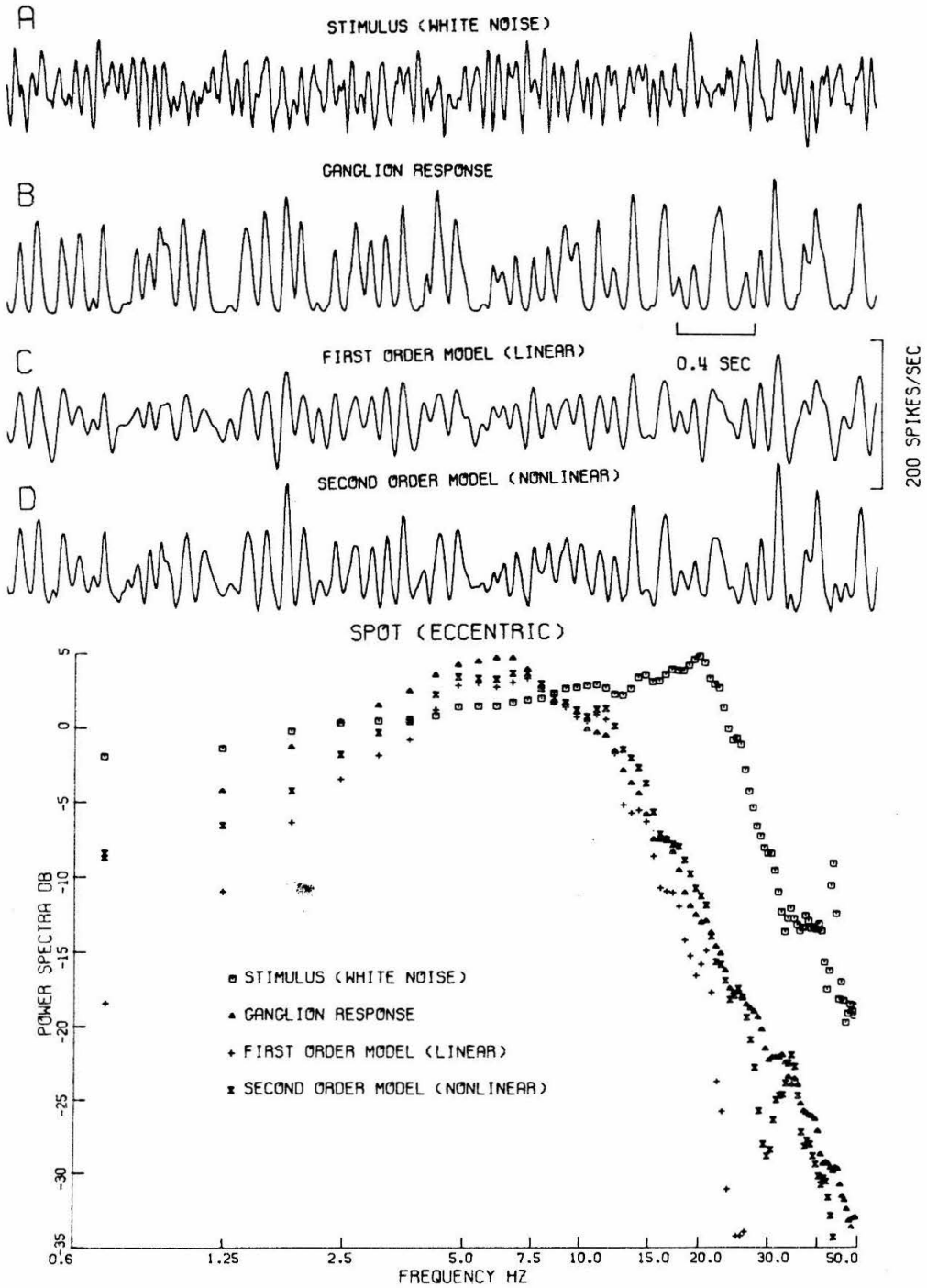


Fig. 8.21

Experimental and model responses to white-noise and corresponding power spectra for system Spot (eccentric) → Ganglion.

SECOND ORDER KERNEL

	0	8	16	24	32	40	48	56	64	72	80	88	96	104	112	120	128	136	144	152	160	
0	-1																					
8	0	3																				
16	-2	5	13																			
24	-5	4	16	22																		
32	-3	1	10	14	9																	
40	2	0	-2	-2	-2	1																
48	6	0	-11	-18	-13	5	25															
56	7	0	-15	-24	-16	8	32	38														
64	3	-1	-11	-19	-13	4	20	22	12													
72	-3	-1	-3	-7	-10	-9	-6	-4	-2	3												
80	-5	0	7	5	-7	-23	-31	-25	-9	10	20											
88	-5	3	13	12	-5	-27	-39	-29	-5	15	21	14										
96	-4	3	12	12	-2	-21	-30	-21	1	17	17	5	-6									
104	-3	1	6	8	1	-9	-13	-7	4	13	12	2	-6	-8								
112	0	1	2	3	1	-2	-2	1	4	8	9	7	1	-4	-8							
120	3	2	2	1	0	-2	-3	0	3	7	10	11	7	-2	-10	-14						
128	3	2	2	2	1	-3	-7	-6	0	7	13	13	8	-1	-9	-12	-9					
136	1	0	0	1	1	-2	-5	-6	-1	5	10	11	6	0	-4	-5	-4	-2				
144	0	-2	-3	-1	0	1	0	0	0	2	3	3	3	2	2	2	1	-1	-3			
152	0	0	-2	-2	0	2	5	5	2	-1	-3	-3	-1	3	5	6	4	1	-3	-6		
160	0	1	1	0	0	2	5	5	2	-2	-5	-4	-1	2	3	4	4	3	-1	-5	-6	

Table 8.8

Values of $h_2(\tau_1, \tau_2)$. Spot & Steady Annulus (eccentric) → Ganglion. Axes in msec.

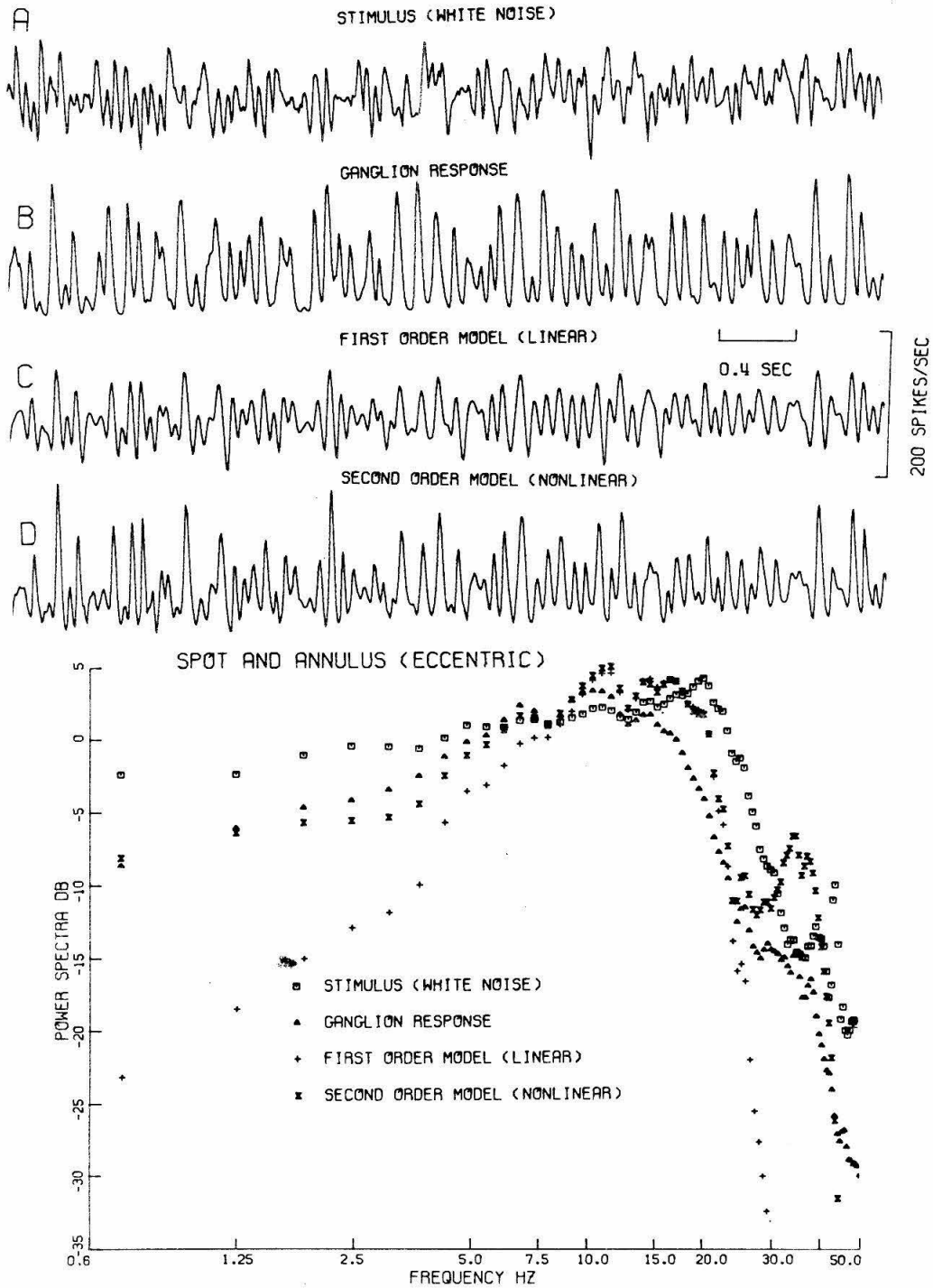


Fig. 8.22. Experimental and model responses to white-noise and corresponding power spectra for system Spot & Steady Annulus (eccentric) → Ganglion.

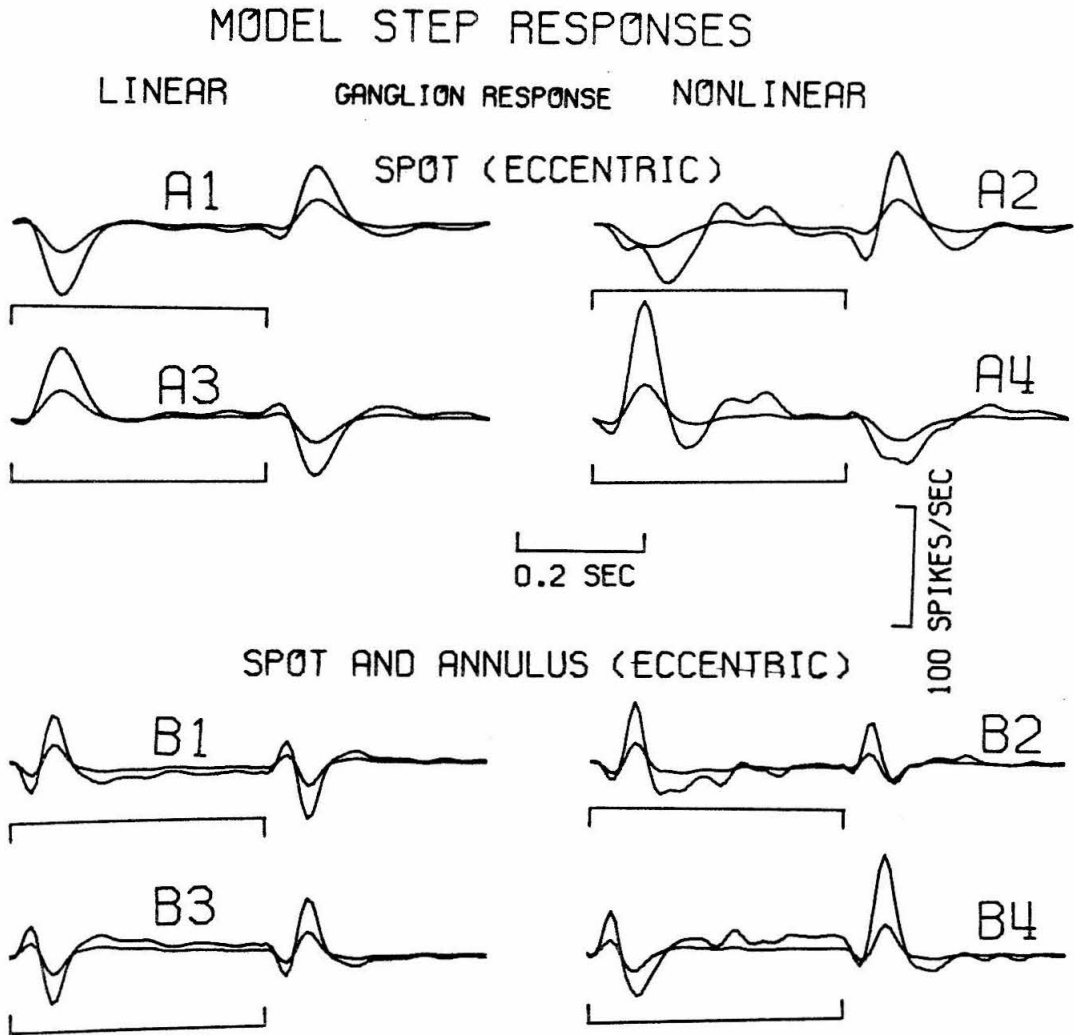


Fig. 8.23

Systems Spot (eccentric) → Ganglion and Spot & Steady Annulus (eccentric) → Ganglion. Both positive and negative steps are considered. Both linear-model and nonlinear-model responses are shown.

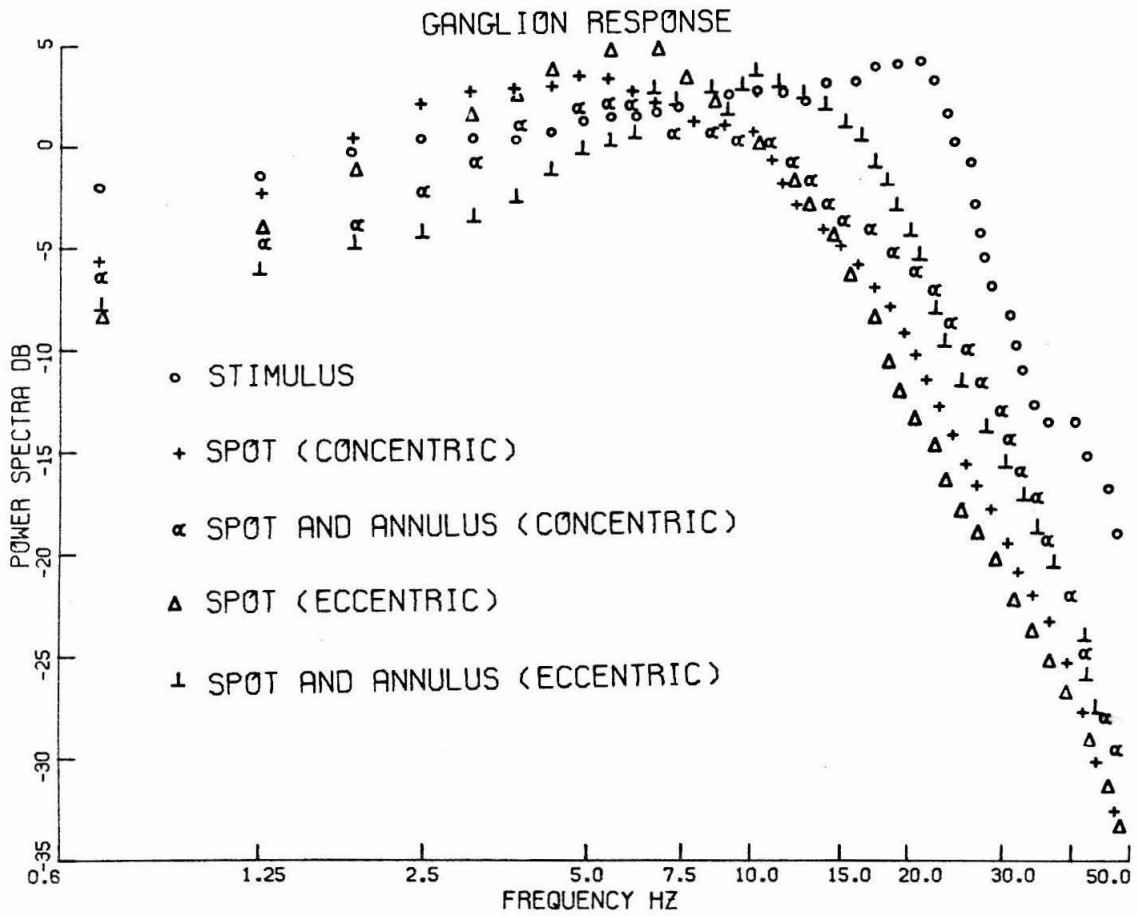


Fig. 8.24. Power spectra of experimental responses to white-noise for certain ganglion systems.

5. Conclusions

In this chapter we have derived transfer functions for the following system:

Horizontal → Ganglion (system C)

Light spot → Ganglion (system S)

Light annulus → Ganglion (system A)

Light uniform → Ganglion (system U)

Eccentric light spot → Ganglion (system SE)

(Light spot) + (steady annulus) → Ganglion (system SAC)

Eccentric (Light spot) + (steady annulus) → Ganglion (system SAE)

These nonlinear, dynamic models can predict the system behavior with small error for a great number of tests, the most stringent of which is the test with the same white-noise with which the physical system was tested. Other tests include step responses and power spectra.

The main additional results of this chapter are the following:

(a) System Horizontal → Ganglion has the following characteristics:

(1) It is nonlinear, exhibiting strong half-wave rectification.

(2) Functionally, it acts as a low-pass differentiator followed by a rectifier.

(3) It is suggested (by the derived kernels and morphology) that the bipolar cell processes the signal

linearly while the nonlinearity occurs at the ganglion stage.

(4) It has a cutoff frequency of about 12 Hz. and a high frequency attenuation of about 12 db/octave.

(5) It has a latency of about 10 msec.

(6) It is underdamped.

(b) Systems A, S, U have the following characteristics:

(1) They are nonlinear (half-wave rectification).

(2) They act like differentiators followed by rectifiers.

System S also responds to the level of input stimulus while systems A, U respond mainly to (positive) changes in the input magnitude.

(c) System S is much slower (latency-wise) than systems A and U. The latencies are:

system S : ~ 55 msec

system A : ~ 30 msec

system U : ~ 30 msec

(d) System S is much slower-responding (frequency response) than systems A and U. The cutoff frequencies are:

system S : ~ 6 Hz

system A : ~ 10 Hz

system U : ~ 10 Hz

(e) Examination of the kernels suggests [cf. 19] that
(bipolar output) \simeq (spot excitation) - (annulus excitation)

or

(bipolar output) \simeq (input from receptors) - (input from H-cell)

(f) Examining systems SE and S we concluded that the periphery of the receptive field exerts an antagonistic influence to that of the receptive field center (as to the ganglion response).

(g) Examining the frequency response of systems S, SE, SAC and SAE we conclude:

(1) The eccentric system has the same frequency response as the concentric one.

(2) The addition of a steady annulus to the stimulus increases considerably the system response figure making it faster-responding (frequency response).

(h) Examining the latency of systems S, SE and SAC, SAE we conclude that the eccentric system is just as fast (latency-wise) as the concentric one.

(i) Conclusions (g) and (h) suggest the existence of a lateral mechanism (to communicate the influence of the periphery on the center of the receptive field) which is extremely fast both latency-wise and frequency-response-wise. This mechanism is likely the layer of horizontal cells.

CHAPTER IX

TRANSFER FUNCTIONS OF LIGHT → ERG SYSTEM

1. Introduction

The ERG is a continuous potential recorded extracellularly in the retina and indicating a mass neural activity response. It is thought to derive from the electrical activity of several neuronal structures; one, from the receptors, is known as the late receptor potential (LRP) and the other, from the pigment epithelium, is known as the L-wave. The rest of the ERG is thought to originate somewhere in the inner plexiform layer and inner nuclear layer [88].

As it is a continuous function of time, and as it is easy to record, the ERG has been a subject of extensive (linear) analysis studies. In these studies, the system was tested either by a step function or by sine waves of various modulations and frequencies. Conclusions drawn are presented in several recent papers. A brief review follows.

Rodieck and Ford [70b] recorded the cat local electroretinogram (LERG) and concluded that the component of the LERG arising from the LRP is linear and the nonlinearity is due to the L-wave arising from the pigment epithelium. Therefore, their conclusion agrees well with our conclusions about the receptor potential in the catfish in being a nearly linear system (see Chapter V).

Similarly, Poppele and Maffei [46b], working on the cat, did not differentiate the different ERG components but concluded that the system was linear when the modulation was less than 50 per cent. They also noted that the system is essentially a low pass filter with a

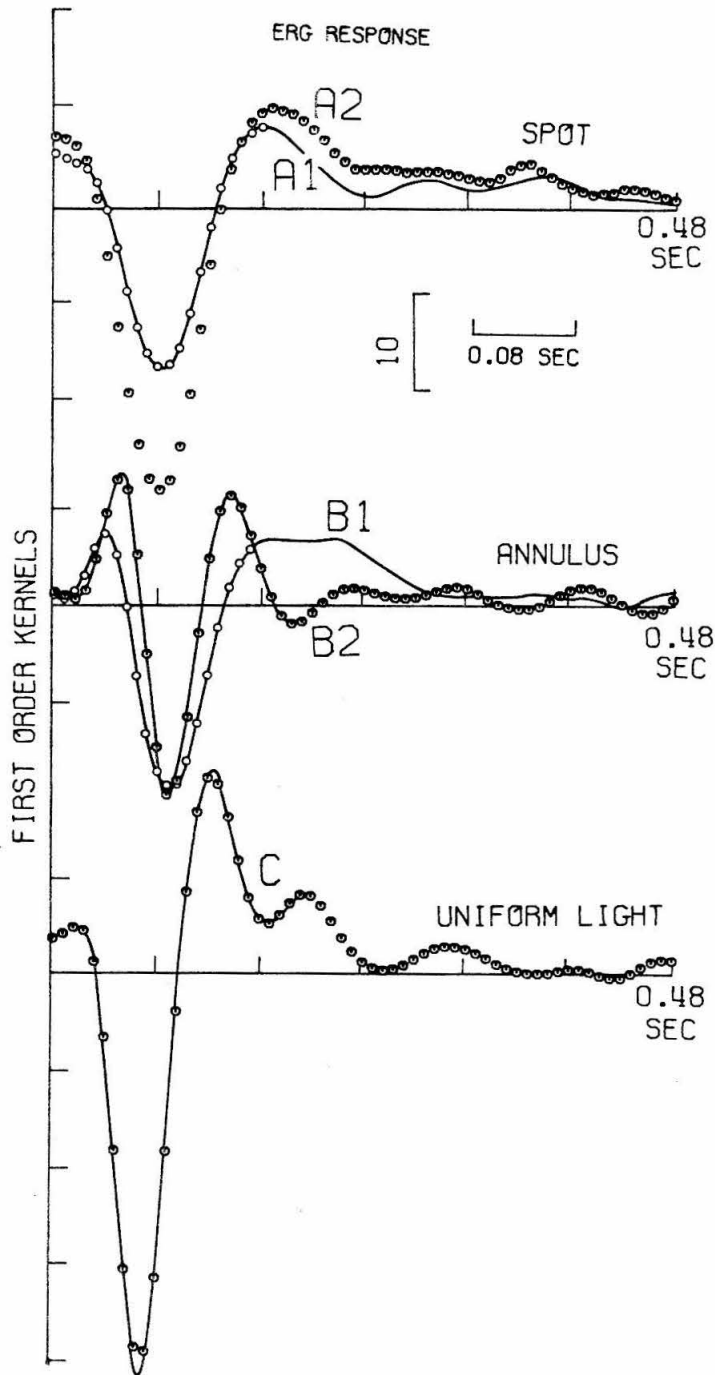


Fig. 9.1. First order kernels for several Light \rightarrow ERG systems. A1: high mean intensity, A2: low mean intensity, B1: low mean intensity, B2: high mean intensity, C: low mean intensity. Low mean intensity is 2.5×10^{10} photons/mm² sec and high mean intensity is 1.5×10^{11} photons/mm².sec.

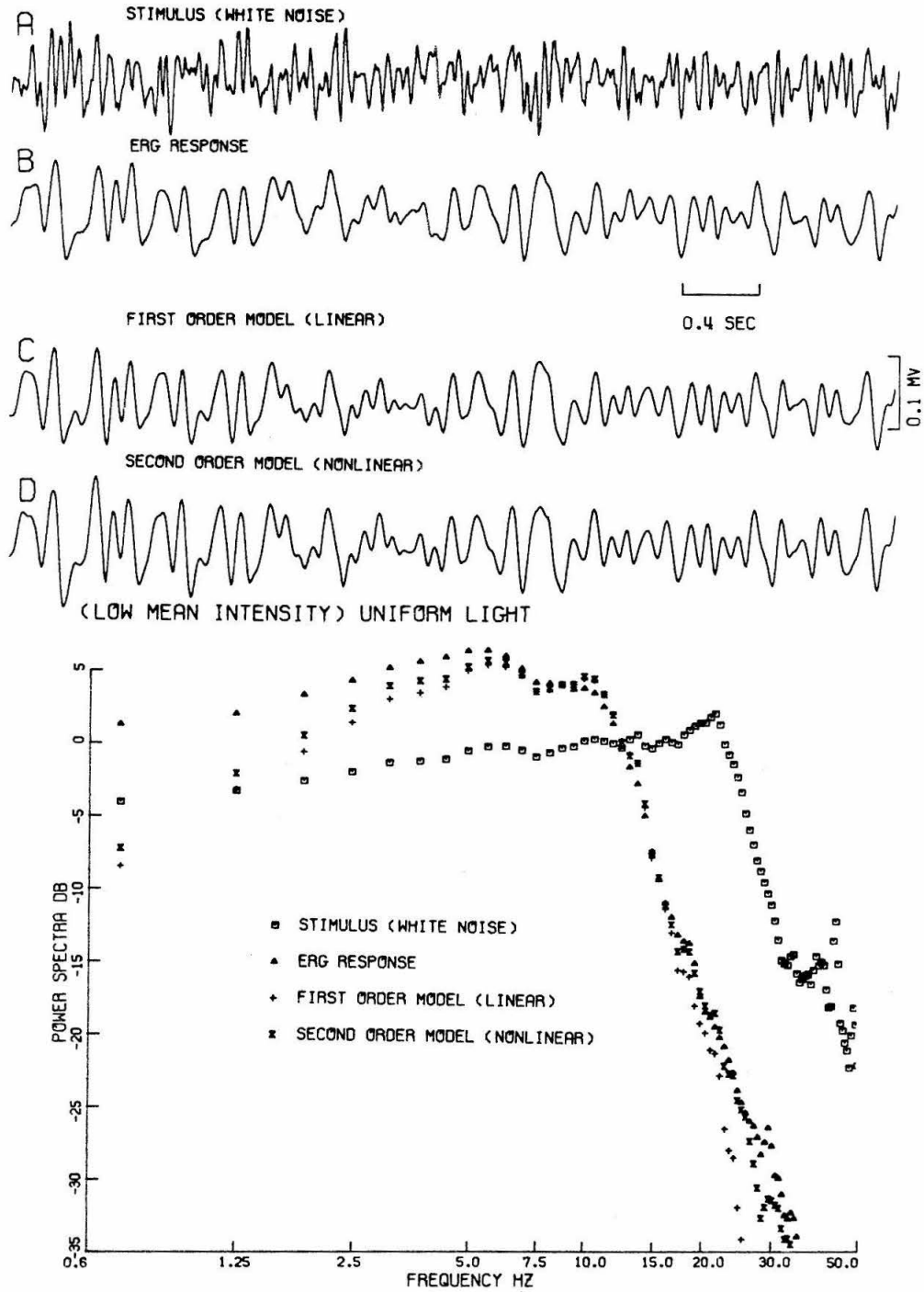


Fig. 9.2. Experimental and model responses to white-noise and corresponding power spectra for system Uniform \rightarrow ERG (mean intensity, 2.5×10^{10} photons/mm²·sec).

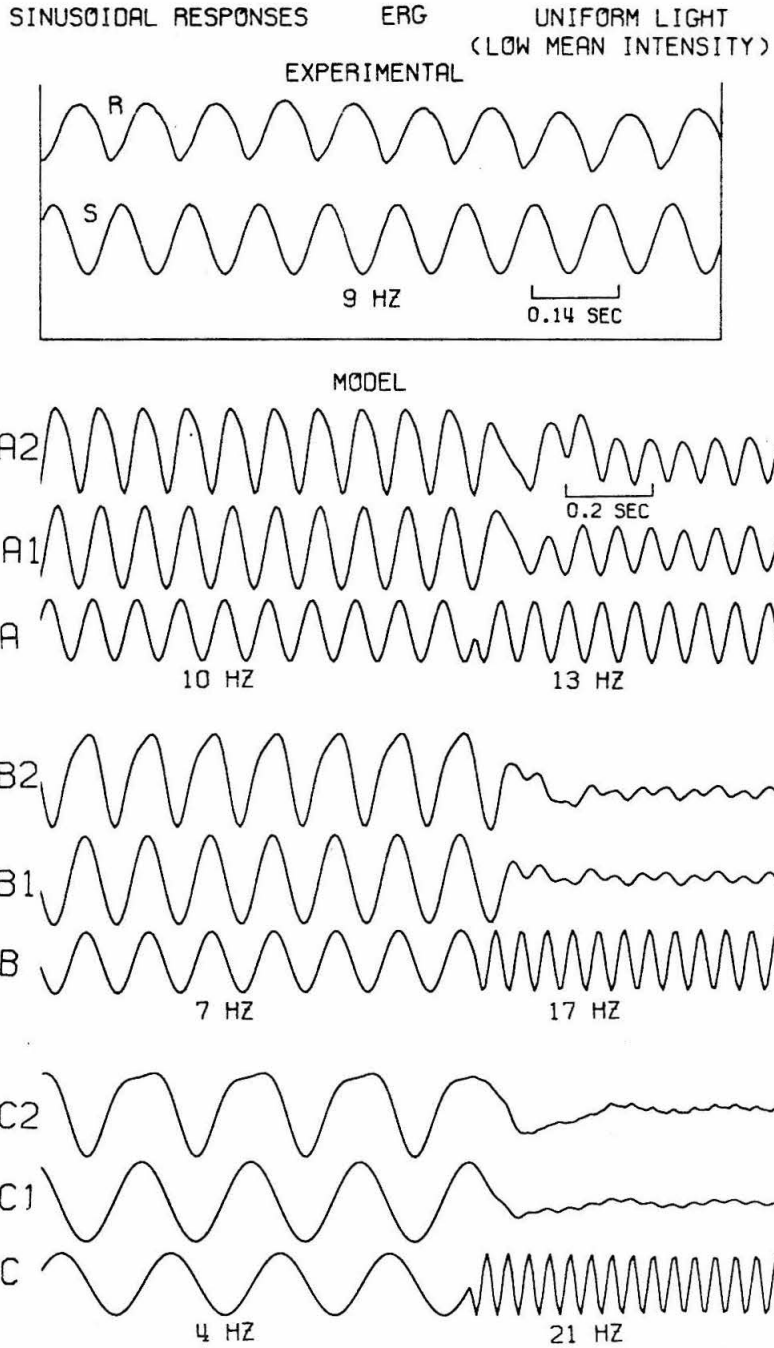


Fig. 9.3. Experimental and model sinusoidal responses for system Uniform \rightarrow ERG (mean intensity 2.5×10^{10} photons/mm²·sec). For model responses, A: stimulus, A1: linear-model response, A2: nonlinear-model response, etc.

SECOND ORDER KERNEL

0	8	16	24	32	40	48	56	64	72	80	88	96	104	112	120	128	136	144	152	160	
-1	0	-2	-1	-3	2	4	2	-1	-4	3	4	2	-1	-3	2	4	2	-1	-4	3	4
8	0	-1	-2	-1	-3	2	4	2	-1	-4	3	4	2	-1	-3	2	4	2	-1	-4	3
16	2	-1	-3	2	4	2	-1	-4	3	4	2	-1	-3	2	4	2	-1	-4	3	4	2
24	4	2	-1	-3	2	4	2	-1	-4	3	4	2	-1	-3	2	4	2	-1	-4	3	4
32	3	4	2	-1	-3	2	4	2	-1	-4	3	4	2	-1	-3	2	4	2	-1	-4	3
40	1	4	5	1	-5	-9	-8	-12	1	1	1	1	1	1	1	1	1	1	1	1	1
48	0	2	4	3	-1	-8	-12	-16	-11	-4	3	4	2	-1	-3	2	4	2	-1	-4	3
56	6	1	2	3	1	-5	-10	-11	-4	3	4	2	-1	-3	2	4	2	-1	-4	3	4
64	0	-1	0	1	1	-1	-5	-6	-4	3	4	2	-1	-3	2	4	2	-1	-4	3	4
72	-1	-1	-2	-2	-1	0	1	2	3	6	10	10	9	6	4	3	4	2	-1	-3	4
80	0	-1	-2	-3	-3	-1	3	8	10	10	9	6	4	3	0	0	3	2	0	-2	3
88	1	0	-1	-3	-3	-2	3	8	12	12	9	6	4	3	0	0	3	2	0	-2	3
96	1	1	1	0	-1	-1	1	5	9	11	8	4	1	0	-1	0	4	3	-1	-5	3
104	0	1	1	2	2	2	1	2	4	5	3	0	-1	0	-1	0	4	3	-1	-5	3
112	-1	-1	1	2	4	4	3	0	-2	-2	0	3	2	0	-2	0	4	3	-1	-5	3
120	-2	-2	-1	1	3	5	5	0	-5	-8	-5	0	4	3	-1	-5	4	3	-1	-5	3
128	-1	-2	-2	-1	1	4	5	1	-5	-9	-9	-3	4	7	3	-3	4	7	3	-3	3
136	-1	-1	-2	-2	-1	1	2	2	-3	-7	-9	-5	2	7	7	1	4	7	1	-6	-9
144	-1	0	0	-1	-1	0	0	0	-3	-5	-4	1	5	7	4	-2	4	0	-5	-8	-9
152	-1	0	1	0	-1	-2	-1	1	1	1	-2	0	3	5	4	0	4	0	-5	-8	-8
160	-2	-1	1	1	0	-1	-2	-1	1	3	3	1	0	1	3	3	1	-3	-6	-7	-6

Table 9.2

Values of $h_2(\tau_1, \tau_2)$. Annulus \rightarrow ERG. Mean intensity, 2.5×10^{10} photons/mm²·sec. Axes in msec.

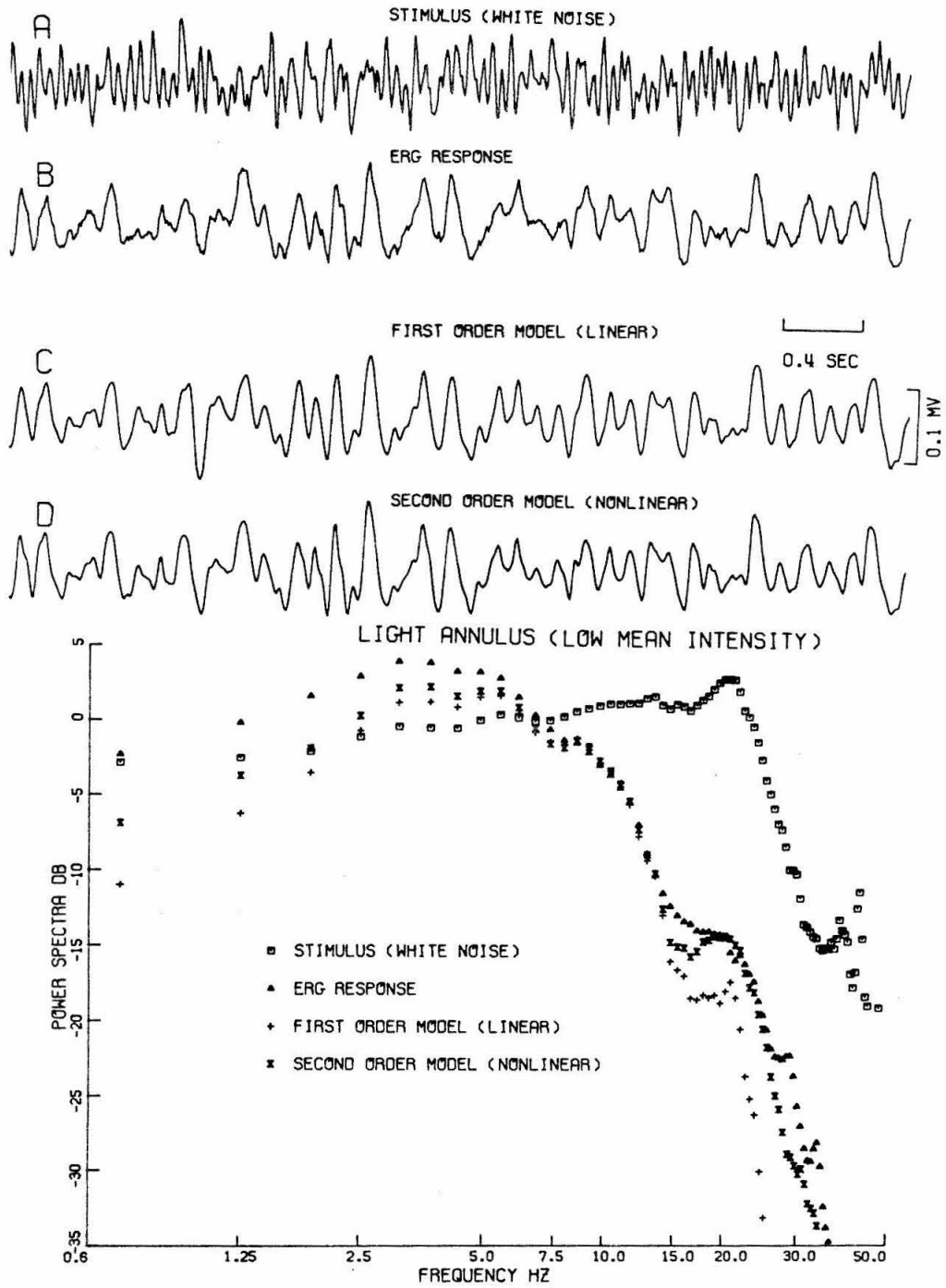


Fig. 9.4. Experimental and model responses to white-noise and corresponding power spectra for system Annulus to ERG (mean intensity, 2.5×10^{10} photons/mm²·sec).

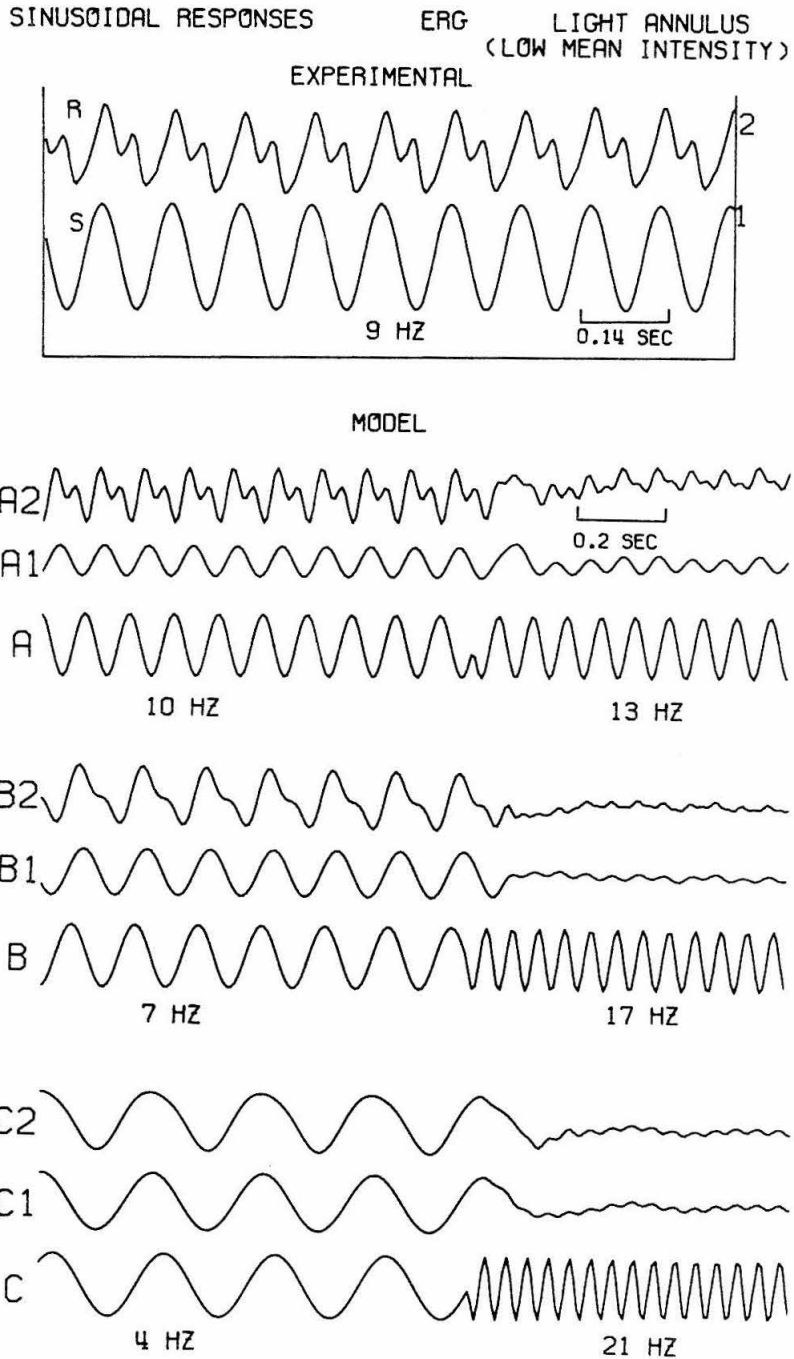


Fig. 9.5. Experimental and model sinusoidal responses for system Annulus \rightarrow ERG (mean intensity, 2.5×10^{10} photons/mm²·sec). For model responses, A: stimulus, A1: linear-model response, A2: nonlinear-model response, etc.

SECOND ORDER KERNEL

	0	8	16	24	32	40	48	56	64	72	80	88	96	104	112	120	128	136	144	152	160
0	3																				
8	1	1																			
16	-1	-1	-1																		
24	0	-1	-2	-2																	
32	3	1	0	-2	-3																
40	4	4	3	0	-4	-8															
48	3	5	6	3	-2	-9	-14														
56	2	3	5	4	0	-6	-12	-12													
64	2	2	2	2	1	-2	-5	-6	-3												
72	1	1	1	0	0	0	0	1	3	6											
80	0	1	1	1	0	0	2	4	7	8	9										
88	-3	-1	2	3	3	1	0	1	4	8	9	9									
96	-4	-4	0	4	7	5	-1	-5	-4	2	8	10	11								
104	-3	-5	-3	1	7	7	0	-9	-13	-8	3	11	13	14							
112	1	-3	-4	-2	3	6	2	-8	-16	-16	-5	9	15	15	14						
120	3	0	-3	-4	-1	3	3	-4	-14	-19	-13	1	13	16	14	11					
128	2	2	-1	-3	-3	-1	2	-1	-9	-16	-17	-8	5	13	13	10	8				
136	-1	0	0	-1	-2	-1	1	1	-3	-10	-14	-12	-4	5	9	8	7	6			
144	-1	-2	-1	-1	0	0	1	2	0	-5	-9	-11	-8	-2	3	4	3	4	5		
152	0	-3	-3	-2	0	2	3	4	3	-1	-6	-7	-7	-4	-2	-1	-2	0	3	4	
160	1	-2	-3	-3	-1	2	5	5	4	1	-3	-5	-4	-3	-2	-3	-4	-5	-2	2	4

Table 9.3

Values of $h_2(\tau_1, \tau_2)$. Annulus \rightarrow ERG. Mean intensity, 1.5×10^{11} photons/mm²·sec. Axes in msec.

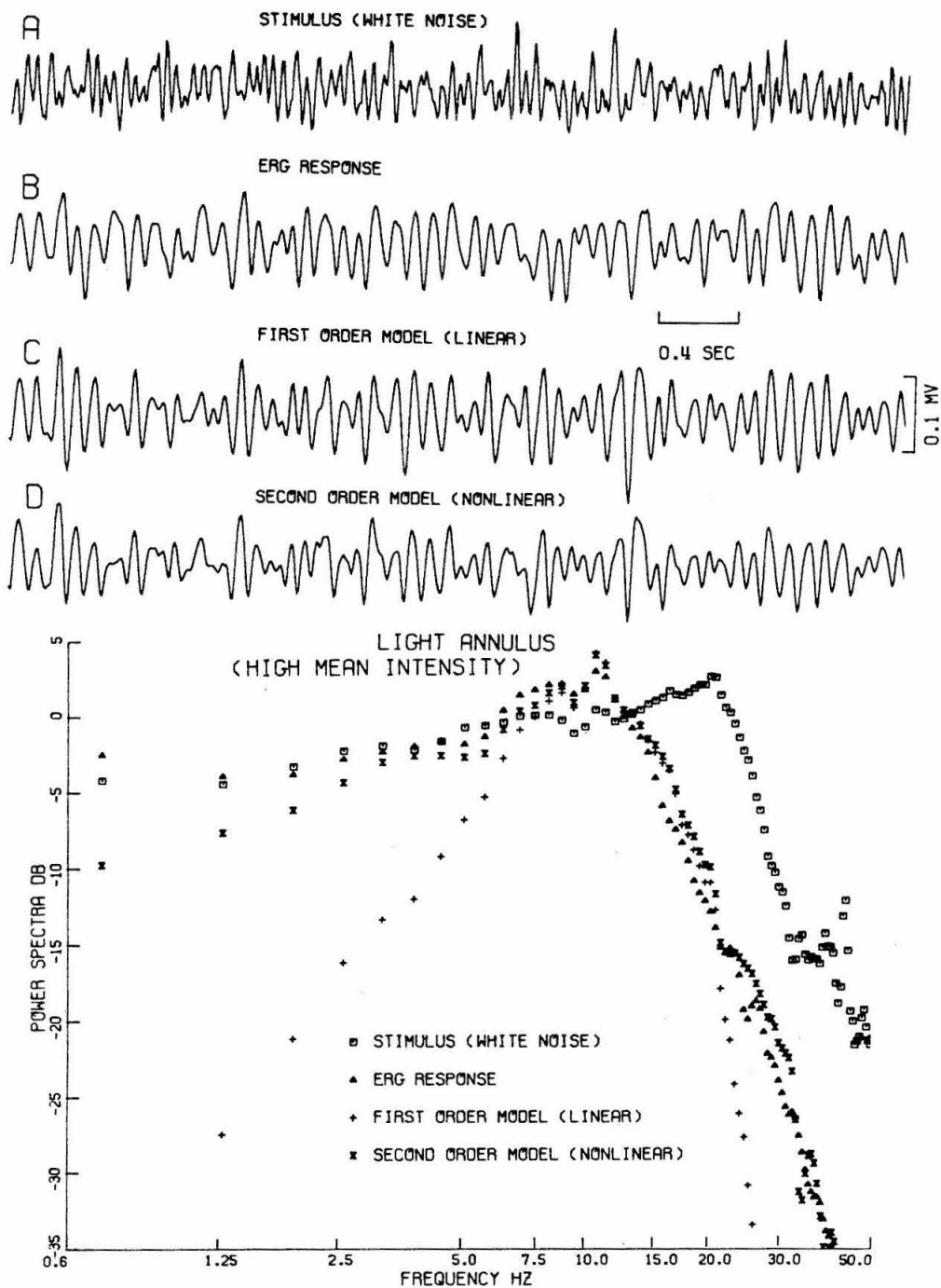


Fig. 9.6. Experimental and model responses to white-noise and corresponding power spectra for system Annulus → ERG (mean intensity, 1.5×10^{11} photons/mm²·sec).

SINUSOIDAL RESPONSES ERG LIGHT ANNULUS
(HIGH MEAN INTENSITY)

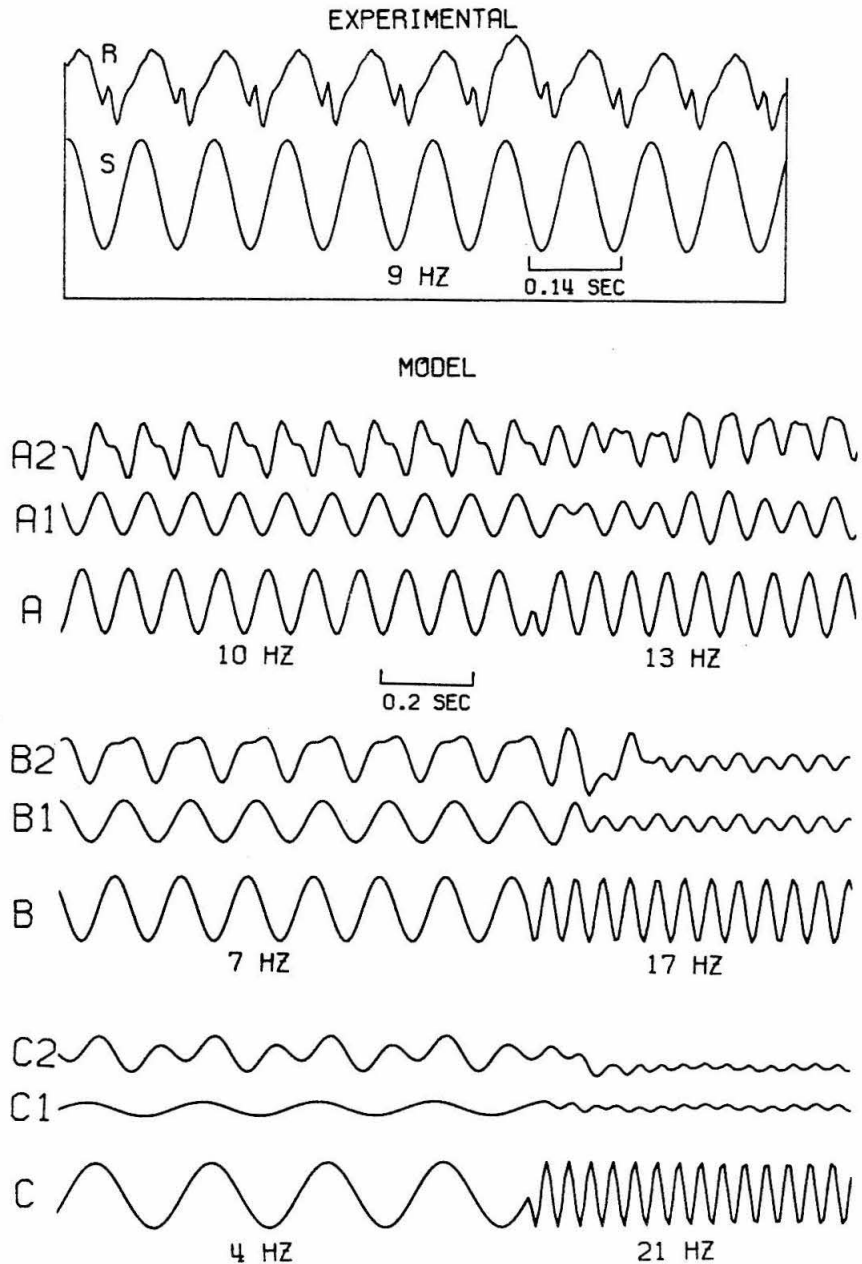


Fig. 9.7. Experimental and model sinusoidal responses for system Annulus → ERG (mean intensity, 1.5×10^{11} photons/mm²·sec). For model responses, A: stimulus, A1: linear-model response, A2: nonlinear-model response, etc.

SECOND ORDER KERNEL

0	8	16	24	32	40	48	56	64	72	80	88	96	104	112	120	128	136	144	152	160	
-4	-3	-5																			
16	1	-4	-5																		
24	4	0	-3	-3																	
32	4	3	0	-1	0																
40	1	2	2	1	0	0															
48	-2	-1	0	1	2	2	3														
56	-3	-4	-3	0	3	5	6	7													
64	-2	-4	-5	-3	2	8	11	11	10												
72	-3	-3	-4	-5	-1	7	16	18	15	13											
80	-6	-3	-4	-4	-2	4	15	23	24	17	13										
88	-9	-6	-4	-4	-3	2	10	21	29	26	17	11									
96	-9	-8	-4	-4	-2	1	6	15	26	31	26	14	7								
104	-5	-7	-6	-7	-3	1	4	9	17	25	29	22	9	2							
112	-1	-4	-6	-7	-5	0	4	6	9	15	22	23	15	4	2						
120	3	1	-2	-6	-6	-3	1	5	5	6	10	16	16	9	9	-5					
128	4	5	3	-1	-5	-6	-3	2	4	4	3	5	10	10	4	-3	-7				
136	2	5	6	4	0	-5	-6	-3	2	4	2	0	1	4	5	1	-4	-6			
144	-2	2	7	7	5	-1	-5	-7	-3	1	4	1	-2	-2	0	2	0	-4	-4		
152	-4	-2	3	7	7	4	-2	-7	-8	-4	2	4	1	-3	-4	-2	0	-1	-3	-3	
160	-2	-4	-2	3	6	6	2	-5	-9	-9	-4	2	4	2	-3	-5	-3	0	0	-2	-3

Table 9.4

Values of $h_2(\tau_1, \tau_2)$. Spot \rightarrow ERG. Mean intensity, 2.5×10^{10} photons/mm²·sec. Axes in msec.

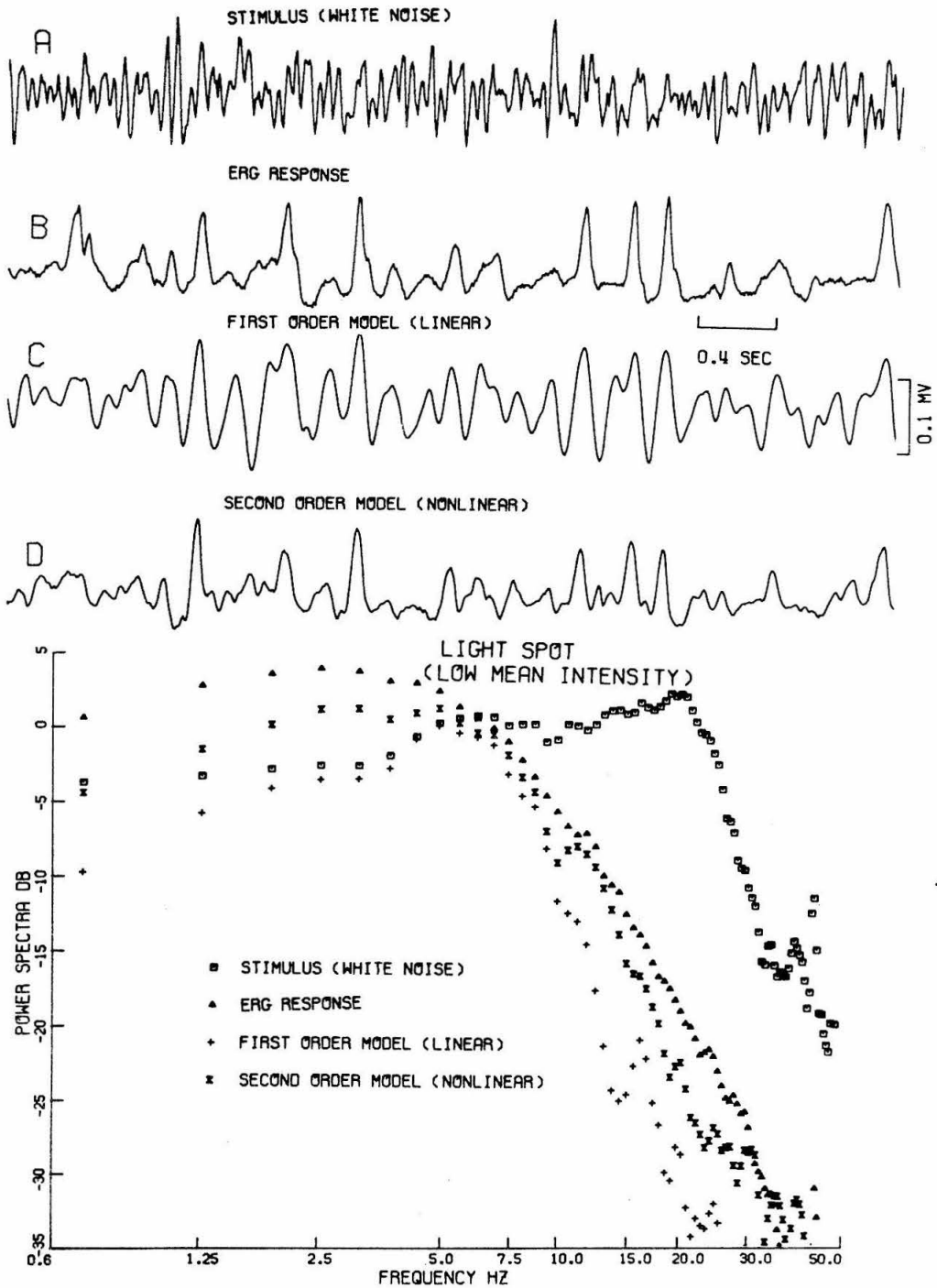


Fig. 9.8. Experimental and model responses to white-noise and corresponding power spectra for system Spot \rightarrow ERG (mean intensity, 2.5×10^{10} photons/mm²·sec).

SECOND ORDER KERNEL

0 8 16 24 32 40 48 56 64 72 80 88 96 104 112 120 128 136 144 152 160

0	-1																			
8	-1	-1																		
16	1	-1	-1																	
24	2	1	-1	-1																
32	2	2	1	-1	-1															
40	1	2	2	1	-1	-1														
48	-1	-1	1	2	1	0	-1													
56	-2	-2	-2	1	2	1	0	0												
64	-1	-2	-3	-2	1	4	5	3	2											
72	-1	-1	-2	-4	-2	3	8	8	6	5										
80	-3	-1	-1	-3	-4	0	7	12	12	9	6									
88	-5	-2	0	-1	-3	-2	3	11	16	15	10	6								
96	-6	-5	-2	0	-1	-2	0	6	14	18	15	9	5							
104	-4	-5	-4	-2	0	-1	-1	2	8	15	17	13	6	2						
112	-1	-3	-4	-3	-1	0	0	0	2	7	13	14	9	3	-1					
120	1	0	-2	-3	-3	-1	0	0	0	1	5	9	10	6	0	-2				
128	2	2	0	-1	-3	-3	-1	0	0	-1	0	2	5	6	3	-1	-3			
136	1	2	2	1	-1	-3	-3	-2	0	0	-1	0	3	3	1	-2	-3			
144	0	1	3	3	1	-1	-3	-4	-3	-1	0	-1	-2	-1	1	1	0	-2	-2	
152	-1	-1	1	3	3	2	-1	-4	-5	-3	-1	0	0	-2	-2	-1	0	-1	-1	-1
160	0	-1	0	2	3	3	1	-3	-6	-6	-3	0	1	1	-1	-2	-2	-1	-1	-1

Table 9.5

Values of $h_2(\tau_1, \tau_2)$. Spot \rightarrow ERG. Mean intensity, 1.5×10^{11} photons/mm².sec. Axes in msec.

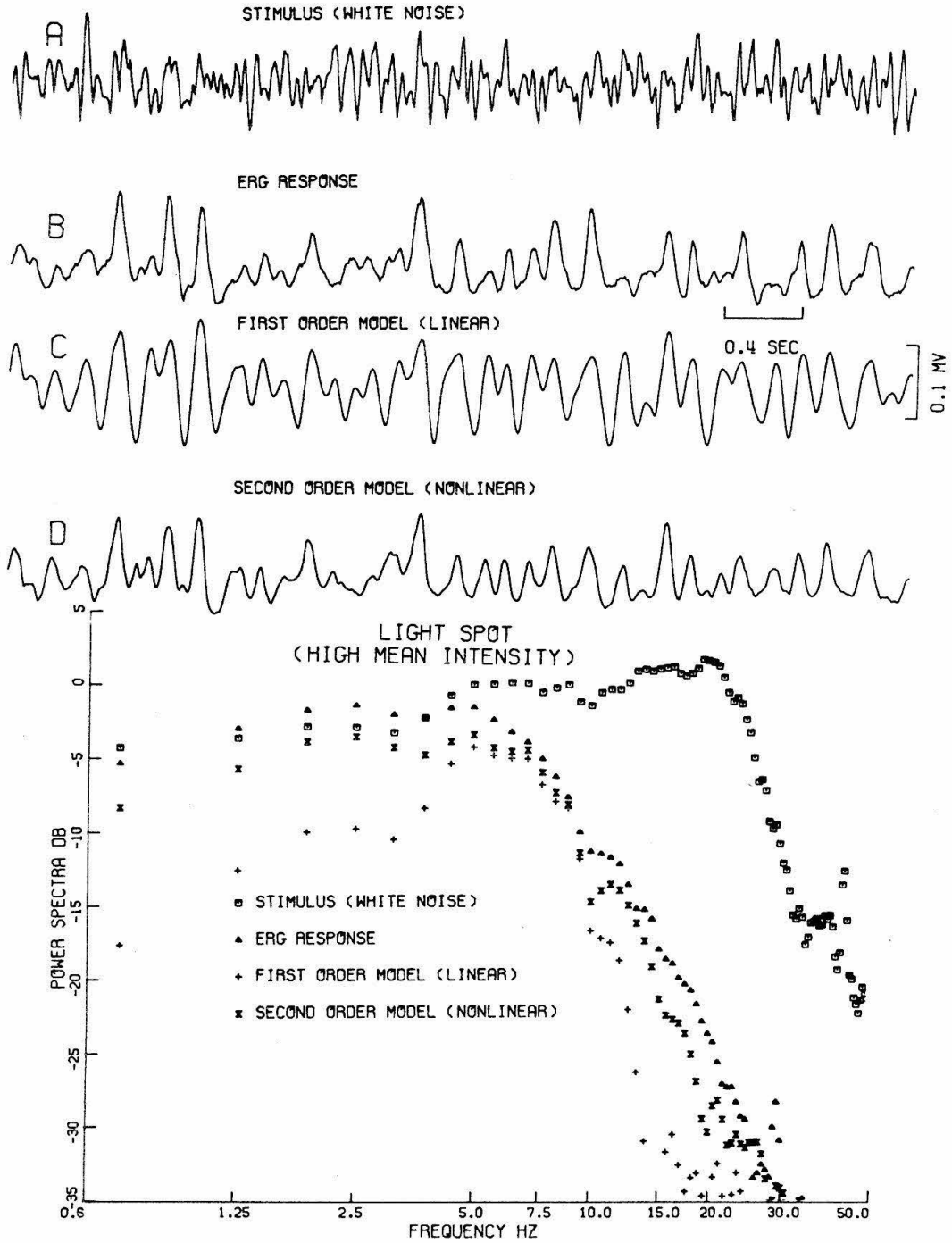


Fig. 9.9. Experimental and model responses to white-noise and corresponding power spectra for system Spot \rightarrow ERG (mean intensity, 1.5×10^{11} photons/mm²·sec).

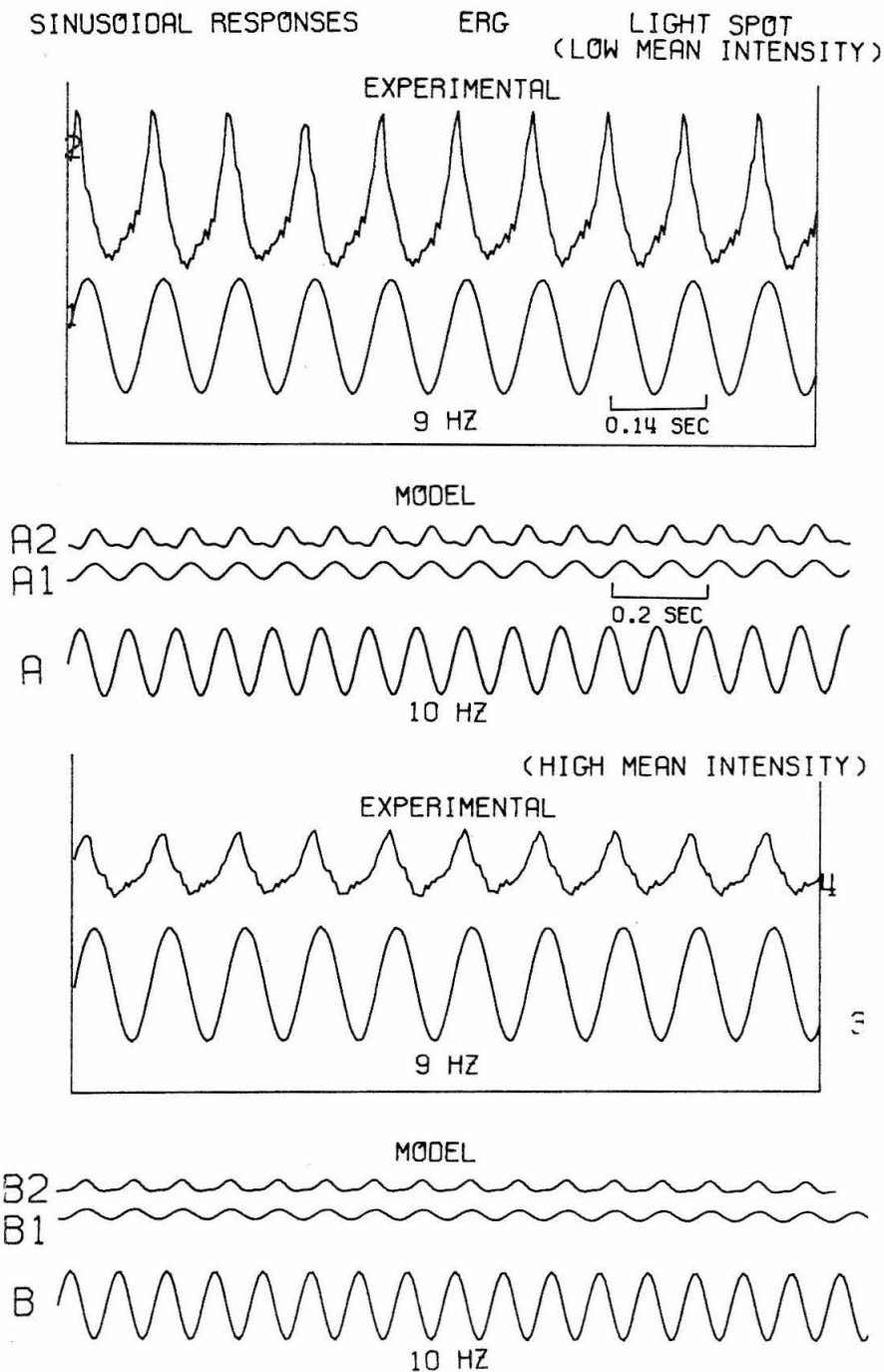


Fig. 9.10. Experimental and model sinusoidal responses for system Spot → ERG (low mean intensity, $2.5 \cdot 10^{10}$ photons/mm²·sec). A: stimulus, A1: linear model, A2: nonlinear model, etc.

8 Hz cutoff. Brindley and Westheimer [8] implied that the baboon ERG is linear when the intensity of a step input is less than 1/3 of the background illumination. On the other hand, Levett [42] reported that the frog intra-retinal electroretinogram is nonlinear at low frequencies, whatever the modulation depth, but it becomes linear for high frequency sine waves.

2. Light \rightarrow ERG Transfer Functions

In this section we derive nonlinear, dynamic transfer functions for systems whose input is light (spot, annulus, and uniform) and whose output is the evoked ERG potential. Two widely different average intensity levels are used. The procedure used to perform the experiment, analyze the data, and compute the transfer functions has already been described in detail in the previous chapters. In this chapter we will limit ourselves to presenting the results for the ERG systems considered.

Figure 9.1 shows the first order kernels for systems spot light \rightarrow ERG, annulus light \rightarrow ERG, and uniform light \rightarrow ERG, for both low and high average intensity levels (in the first two cases). Tables 9.1 through 9.5 describe the second order kernels for each case. The set $\{h_1, h_2\}$ for each system is effectively a description of its transfer function.

Figures 9.2, 9.4, 9.6, 9.8, 9.9 show white-noise responses both experimental and model-predicted for a portion of the white-noise input used in the characterization process. The agreement between experimental response and model response is obviously ex-

tremely good, as can be seen from these figures. The mean square error reduction is as follows:

<u>SYSTEM</u>	<u>MODEL</u>		
	constant { h_o }	linear { h_o, h_r }	nonlinear { h_o, h_r, h_z }
<hr/>			
SPOT → ERG			
low level	100	43	19
high level	100	40	16
ANNULUS → ERG			
low level	100	25	19
high level	100	21	18
UNIFORM → ERG			
low level	100	22	15
<hr/>			

Noting the white-noise responses of these systems and the corresponding linear and nonlinear model white-noise responses, it is suggested that systems annulus light → ERG and uniform light → ERG are almost linear, while system spot light → ERG is very nonlinear, exhibiting a rectification phenomenon reminiscent of the ganglion response. In view of this observation, we propose that the ERG induced by annulus and uniform light stimulation is mainly due to receptor (and possibly horizontal cell) excitation, while the ERG induced by spot stimulation is mainly due to the neural activity in the inner plexiform and inner nuclear layers. This inference derives from the fact that we established (in previous chapters) the near linearity of systems light → horizontal cell and light → receptor and the rectifying nonlinearity of system bipolar-ganglion. We have also found that a spot stimulus can hardly excite the horizontal cell.

Moreover, the first-order kernel of spot \rightarrow ERG system is very similar to the first-order kernel of spot \rightarrow ganglion system, and the second order kernels in the two cases are very similar (thus describing the same type of nonlinearity).

Figures 9.3, 9.5, 9.7, 9.10 show sinusoidal responses both for the model and (a few) experimental ones. We note that our previous assumption of linearity for system annulus light \rightarrow ERG is not quite valid and the system becomes nonlinear (with a strong second harmonic) for frequencies around 10 Hz. This nonlinearity is more prominent at low mean intensity levels. We note the remarkable (!) agreement between model prediction and experimental response for sine waves. This is due to the fact that the system under study appears to be a second-order nonlinear system, and therefore it allows an accurate description in terms of the first two kernels of the Wiener series (i. e., h_1 and h_2 only). Sinusoidal responses of system uniform light \rightarrow ERG uphold our previous assumption of linearity for this system, while system spot light \rightarrow ERG exhibits the predicted nonlinearity of rectification.

The power spectra of experimental and model (linear and nonlinear) white-noise responses show very good agreement. The nonlinear model improves the linear model performance (from the frequency response point of view) considerably.

Figure 9.11 shows power spectra for the white-noise stimulus and the system response for all ERG systems considered. We note the following:

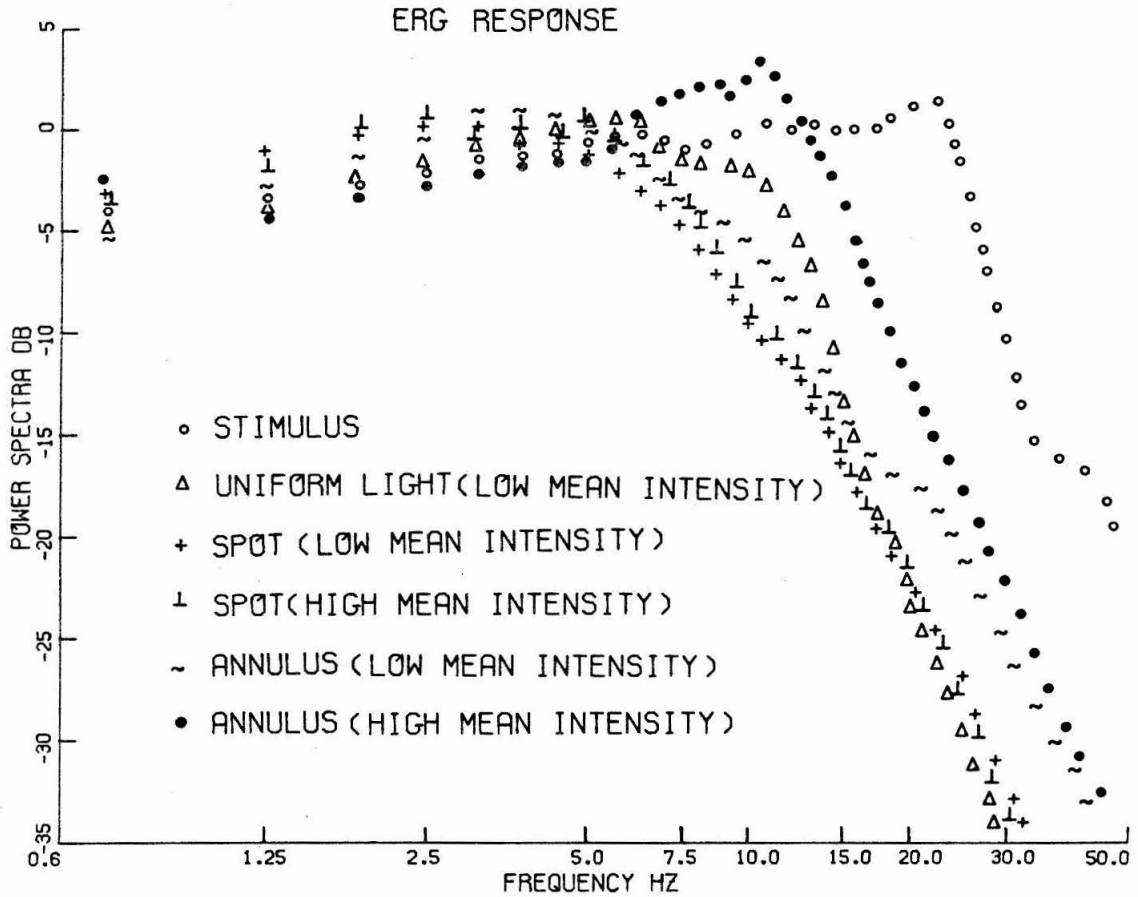


Fig. 9.11. Power spectra of experimental responses to white-noise for several Light \rightarrow ERG systems. Low mean intensity is 2.5×10^{10} photons/mm²·sec and high mean intensity is 1.5×10^{11} photons/mm²·sec.

- 1) System spot light \rightarrow ERG is the slowest one and its frequency response does not change with mean intensity level.
- 2) The cutoff frequency for spot \rightarrow ERG system is about 7 Hz.
- 3) System annulus light \rightarrow ERG has a cutoff of about 7 Hz at low mean intensity levels and 12 Hz at high mean intensity levels.
- 4) The spectrum of annulus \rightarrow ERG system reveals the existence of a strong 20 Hz frequency contribution (compare with sinusoidal response at 10 Hz) which decreases as the mean intensity level increases.
- 5) System uniform light \rightarrow ERG has a cutoff at about 10 Hz.

For the spot \rightarrow ERG system, the high-frequency asymptotic slope is about 18 db/octave, indicating that the system is of third order. Systems annulus \rightarrow ERG and uniform \rightarrow ERG have a high-frequency asymptote of less steep slope (about 12 db/octave). This difference supports our claim that the spot-induced ERG comes from the inner plexiform and inner nuclear layers, while the annulus or uniform light-evoked ERG originates in the receptors (and perhaps horizontal cells). Such a claim, of course, can be made only if the systems can be considered nearly linear (which is not the case for system spot \rightarrow ERG).

3. Conclusions

In this chapter we derived nonlinear dynamic transfer functions for several light \rightarrow ERG systems. The derived models were

very satisfactory in that they accurately predicted the experimental response for a number of strict tests. These tests were white-noise responses, sinusoidal responses, and power spectra.

The additional main conclusions are:

- (a) System uniform light \rightarrow ERG is nearly linear.
- (b) System annulus light \rightarrow ERG is nonlinear around 10 Hz, exhibiting a strong second harmonic (20 Hz).
- (c) System spot light \rightarrow ERG is very nonlinear, exhibiting the same type of nonlinear response as system spot light \rightarrow ganglion discharge (rectification).
- (d) It is proposed that in systems annulus \rightarrow ERG and uniform \rightarrow ERG the ERG is mainly due to receptor (and possibly horizontal cell) activity, while in system spot \rightarrow ERG the ERG is mainly due to activity in the inner plexiform and inner nuclear layers.
- (e) System spot \rightarrow ERG has a cutoff around 7 Hz and the frequency response does not change with intensity level. System annulus \rightarrow ERG has a cutoff of about 7 Hz at low levels and about 12 Hz at high average intensity levels. System uniform light \rightarrow ERG has a cutoff frequency of about 10 Hz.
- (f) The high-frequency attenuation asymptote is steeper (~ 18 db/octave) in the spot \rightarrow ERG case than in the annulus \rightarrow ERG and uniform \rightarrow ERG cases (~ 12 db/octave), thus supporting our proposition made in conclusion (d).
- (g) All systems have a latency of about 25 msec.

CHAPTER X

SUMMARY AND DISCUSSION OF RESULTS

1. Applicability of the White-Noise Method

Wiener showed that a nonlinear system can be identified by its response to white noise, since, in this way, the system is tested uniformly over its entire input function space. Wiener's formulation (of the white noise theory), in terms of Laguerre and Hermite expansions, is impractical and difficult to apply to a physical system for the following reasons:

- (a) The number of characterizing coefficients $\{\alpha_{i\dots k}\}$ is extremely large (of the order of 10^{10}).
- (b) The computation time is very long.
- (c) It is very difficult to interpret the derived model $\{\alpha_{ij\dots k}\}$ in terms of the physical characteristics of the system.
- (d) The method is essentially a curve-fitting procedure and not a descriptive algebra of systems.
- (e) A linear system is very cumbersome identified by this method.
- (f) A priori information about the system cannot be utilized to reduce the complexity of the identification procedure.
- (g) The derived model is too cumbersome to use for prediction.

The Lee-Schetzen formulation of the Wiener theory removes almost all of these difficulties and makes the application possible (with few restrictions). This method, based on cross-correlation techniques, has the following advantages over Wiener's formulation

- (a) The derived model can be interpreted easily to reveal gross system features.
- (b) It is much simpler computationally.
- (c) A linear system is easily recognized, and a priori information is easily utilized to reduce the identification effort.
- (d) The derived model is easily used to predict the system response.
- (e) Alternative "structural" models are easily constructed from the initial model.
- (f) The approximation error is smaller.

Alternative formulations of the white-noise theory can easily be developed to account for peculiarities of a class of systems in a way that could drastically reduce the computational effort.

In applying the white-noise theory (cross-correlation formulation), several considerations have to be taken into account.

- (a) The time-invariancy of the system must be secured.
- (b) The bandwidth of the white-noise input should be chosen large enough to cover completely the system bandwidth but small enough in order to result in a small statistical variance of the cross-correlation estimates. The error introduced by too small or too large a bandwidth was analyzed.
- (c) The number of kernels to be computed can be decided by preliminary harmonic analysis.
- (d) The memory of the system must be found in order to deter-

mine the extent to which the kernels should be computed.

- (e) The temporal length of the white-noise experiment is determined by the acceptable variance in the estimates of the cross-correlations and it depends on the white-noise bandwidth and the system memory.

The total computing time for the calculation of the n^{th} degree kernel is approximately

$$T_n = \alpha_n \cdot N \cdot n \cdot \frac{(m+n-1)(m+n-2)\dots(m)}{n!}$$

where α_n is a constant, N is the total number of samples in the record, and $m = (\text{system memory})/(\text{sampling interval})$. Thus, computing time increases almost exponentially with the order of the kernel. Error analysis of the kernel estimates has shown the following:

- (a) The statistical error increases with increasing bandwidth of the white noise.
- (b) The statistical error increases by increasing the system memory for a record of constant length.
- (c) Noise present at the output introduces error terms which do not increase with increasing the order of system nonlinearity or the order of the computed kernel.
- (d) Noise present at the input is more serious than noise at the output. In this case, the error terms increase as the order of system nonlinearity or the order of computer kernel is increased. In particular, it was shown that the error introduced

by the truncation of the gaussian signal is negligible if the truncation level is higher than 2.5 standard deviations.

2. Neuronal Systems

The white-noise method was used to obtain nonlinear, dynamic transfer functions for several neuronal systems of the catfish retina. These nonlinear models can predict, with reasonable accuracy, the response of the neuron systems to any input. Comparison of model responses with experimental responses for a great number of inputs showed close agreement. The most stringent of these tests was the comparison of model and experimental responses to the same white-noise input.

Transfer functions were obtained, for different average intensity levels, for the following light \rightarrow receptor systems:

(SPOT) \rightarrow RECEPTORS

(ANNULUS) \rightarrow RECEPTORS

(UNIFORM) \rightarrow RECEPTORS

Each transfer function is in the form of a set of kernels $\{h_1(\tau), h_2(\tau_1, \tau_2)\}$. Some of the system characteristics revealed by these models are:

- (a) The systems are nearly linear (within a range of 1.8 log-units) with small nonlinearities which are persistent even for "small signals."
- (b) Latency decreases with increasing average intensity (from about 15 to 10 msec).
- (c) The systems become faster-responding (frequency response)

with increasing average intensity. Cutoff frequency is 6 Hz at low levels and 11 Hz at high levels.

- (d) For high frequencies the response attenuates at 12 db/octave.

Dynamic transfer functions were obtained, for different average intensity levels, for the system light → horizontal by two different methods; (1) the white-noise method and (2) by fitting a set of equations to step and sine response data. Considering overall performance, the white-noise-derived model is much more satisfactory. Some system characteristics are the following:

- (a) The system is nearly linear (within a range of 1.8 log-units), with small nonlinearities which are persistent even for "small signals." These nonlinearities are very similar to those exhibited by the receptor systems.
- (b) Latency decreases with increasing average intensity from about 20 to 15 msec. In view of the results for the light → receptor systems it was concluded that the receptor → horizontal system has a latency of about 5 msec which is independent of the mean input level.
- (c) The system becomes faster-responding at higher mean light levels. Cutoff frequency is about 7 Hz at low levels and about 12 Hz at high levels. In view of the results for the light → receptor system it is suggested that the receptor → horizontal system has a cutoff frequency higher than 12 Hz and therefore does not introduce response time limitations on system light → horizontal.

- (d) For very high frequencies the response attenuates at 24 db/octave.

The spatial distribution of potential within a flat cell (horizontal cell layer) was determined as a solution of Laplace's equation with appropriate boundary conditions. The membrane potential V , as a function of cylindrical coordinates (ρ, z) , is given by

$$(*) \quad V(r, \bar{z}) = K \cdot J \cdot \int_0^{\infty} \frac{(\mu - \gamma)e^{-\mu(2\delta - \bar{z})} + (\mu + \gamma)e^{-\mu\bar{z}}}{(\mu + \gamma)^2(1 - e^{-2\mu\delta})} \cdot \sin\mu \cdot J_0(\mu r) d\mu$$

where

$$r = \rho/\rho_0, \quad \bar{z} = z/\rho_0 = \gamma = \frac{R_i}{R_m} \rho_0, \quad \delta = h/\rho_0;$$

K is a constant, J is the exciting current, ρ_0 is the radius of the disc of excitation, h is the cell thickness, and R_i, R_m are the intracellular, membrane resistivities, respectively. Potential decay data from both external and internal horizontal cells were closely predicted by equation (*). The decay rate predicted by equation (*) is exponential for small distances but becomes much slower for larger distances, thus allowing the experimentally-observed spatial integration over large areas. The equation shows that the decay space constant depends only on (R_m/R_i) and not on thickness. Data obtained from both types of H-cell by varying the diameter of the stimulating spot and for different intensity levels were well fitted by equation (*). For the external H-cell data the fit was obtained by varying parameter (R_m/R_i) for the different intensity levels, while for the data obtained from the internal H-cell it was necessary to vary synaptic current J

to obtain a fit. This suggests two different synaptic mechanisms for the two types of horizontal cell; an increase of membrane resistance for the external H-cell and an increase of the synaptic current for the internal H-cell, with increase in stimulus intensity.

Nonlinear dynamic ^{transfer} functions have been obtained in terms of kernel sets $\{h_1, h_2\}$ for the following systems:

Horizontal	→ Ganglion	(system C)
(Spot)	→ Ganglion	(system S)
(Annulus)	→ Ganglion	(system A)
(Uniform)	→ Ganglion	(system U)
(Eccentric Spot)	→ Ganglion	(system SE)
(Spot + Steady Annulus)	→ Ganglion	(system SAC)
(Eccentric Spot + Steady Annulus)	→ Ganglion	(system SAE)

Some system characteristics revealed by these models are:

- (a) System C is strongly nonlinear, acting as a low-pass differentiator followed by a half-wave rectifier.
- (b) It is suggested that the bipolar processes the signal linearly, while the nonlinearity occurs at the ganglion stage.
- (c) System C is underdamped, has a latency of 10 msec, a cutoff frequency of 12 Hz, and a high frequency attenuation of 12 db/octave.
- (d) Systems A, S, U are strongly nonlinear, acting as low-pass differentiator followed by rectifier (system S, in addition, responds to input level magnitude).
- (e) Latency-wise, system S is much slower (~ 55 msec) than systems A and U (~ 30 msec).

- (f) Frequency response-wise, system S is slower (cutoff frequency is 6 Hz) than systems A and U (cutoff frequency is 10 Hz).
- (g) It is suggested that
(bipolar output) \simeq (spot excitation) - (annulus excitation)
or
(bipolar output) \simeq (input from receptors) - (input from horizontal cell).
- (h) As to the ganglion response, the receptive field surround is antagonistic to the receptive field center.
- (i) The eccentric system has the same latency and frequency response as the concentric system, thus implying that the lateral mechanism of the receptive field is extremely fast (both latency-wise and frequency response-wise). It is suggested that this function could be performed by the later of horizontal cells (S-space).
- (j) The addition of a steady annulus to the stimulus increases considerably the frequency response (bandwidth) of the system.

Nonlinear, dynamic transfer functions have been obtained for several Light \rightarrow ERG systems. These models are given in terms of kernel sets $\{h_1, h_2\}$. The following systems were studied:

(Spot)	\rightarrow ERG	(system ERS)
(Annulus)	\rightarrow ERG	(system ERA)
(Uniform)	\rightarrow ERG	(system ERU)

Some system characteristics, revealed by these models, are:

- (a) System ERU is nearly linear. System ERA is nonlinear for a frequencies around 10 Hz, exhibiting a strong second harmonic. System ERS is very nonlinear, exhibiting the same kind of nonlinearity (rectification) as system (Spot)→Ganglion.
- (b) It is suggested that for systems ERA and ERU the ERG response is mainly due to receptor (and possibly horizontal cell) activity, while for system ERS it is mainly due to neural activity in the inner plexiform and inner nuclear layers.
- (c) System ERS has a cutoff frequency of 7 Hz, which does not change with average intensity level. System ERA has a cutoff of 7 Hz at low levels and 12 Hz at high levels. System ERU has a cutoff frequency of 10 Hz at high levels and 7 Hz at low levels. High frequency attenuation is 18 db/octave for system ERS and 12 db/octave for systems ERA and ERU.
- (d) All systems have a latency of 25 msec.

The following table summarizes some of the results about latencies, cutoff frequencies, high frequency asymptotes and nonlinearities for the different systems.

We conclude that the photo-receptor stages are the limiting subsystems as to the frequency response of the overall retinal processing of the visual signal. Moreover, these stages (and the horizontal and bipolar cells) process the signal almost linearly, while major nonlinearities occur only at the ganglion cell stage.

Finally, it should be stressed that the derived models in terms of the set of kernels $\{h_1, h_2\}$ are global models that can an-

System	Latency (msec)		Cutoff Freq. (Hz)		High Freq. Asymptote db/octave	(Non)linearity
	Low level	High level	Low level	High level		
Light → Receptor	15	10	6	11	12	linear
Light → Horizontal	20	15	7	12	24	linear
Horizontal → Ganglion	10	10	12	12	12	nonlinear
Light Spot → Ganglion	60	55	6	6	36	nonlinear
Light → Ganglion (annulus or uniform)	30	25	7	11	36	nonlinear
Light Spot → ERG	25	25	7	7	18	nonlinear
Light Annulus → ERG	25	25	7	12	12	nonlinear
Uniform Light → ERG	25	25	7	10	12	linear

swer any question about the system input - output behavior, with reasonable accuracy. Therefore, the above-mentioned results are only a part of the information contained in the set $\{h_1, h_2\}$ and have been stated here to show that results obtainable by classical methods are already included in the white-noise-derived models. An analogy can be made with the task of describing a man's appearance: it can be said that he is tall, thin, bow-legged, blond, etc. (corresponding to saying a system is underdamped, has τ sec latency, 6 db/octave high-frequency attenuation, etc.). On the other hand, providing a photograph of the man can reveal all this information plus a lot more (corresponding to providing the kernel set $\{h_1, h_2\}$ for the system).

REFERENCES

- 1a. Arnett, D.W., "Information processing by the first optic ganglion in Dipterans", Ph.D. thesis, California Institute of Technology, Pasadena, California, 1971.
- 1b. Balakrishnan, A.V., "Prediction and filtering", IRE Trans. Inform. Theory, 9, pp. 237-240, 1963.
2. Barrett, J.F., "The use of functionals in the analysis of non-linear physical systems", J. Electron Control, 15, pp. 567-615, 1963.
3. Baylor, D.A. and M.G.F. Fuortes, "Electrical responses of single cones in the retina of the turtle", J. Physiol., 207, pp. 77-92, 1970.
4. Baylor, D., M. Fuortes and P. O'Bryan, "Receptive fields of cones in the retina of the turtle", J. Physiol., 214, pp. 265-294, 1971.
5. Blackman, R.B. and J.W. Tukey, The Measurement of Power Spectra, Dover, N.Y., 1958.
6. Bose, A.G., "A theory of nonlinear systems", Tech. Rept. 309, Research Lab. of Electronics, M.I.T., 1956.
7. Brilliant, M.B., "Theory of the analysis of nonlinear systems", Tech. Rept. 345, Research Lab. of Electronics, M.I.T., 1958.
8. Brindley, G.S. and G. Westheimer, "How deeply nonlinear is the electroretinogram?", J. Physiol., 196, pp. 78-79, 1968.
9. Byzov, A.L., "Horizontal cells of the retina as regulators of synaptic transmission", Fiziologicheskii Zhurnal SSSR imeni J.M. Sechenova, 53, pp. 1115-1124, 1967. Neuroscience translations 3,

- pp. 268-276, 1967-8.
10. Byzov, A.L., "Role of horizontal cells in the mechanism of retinal adaptation", Neurofiziologiya, 1, pp. 210-217, 1969. Neuroscience translation 14, pp. 63-70, 1970-71.
 11. Cameron, R.H. and W.T. Martin, "The orthogonal development of non-linear functionals in series of Fourier-Hermite functionals", Annals of Math., 48, No. 2, pp. 385-392, 1947.
 12. Clynes, M. and J.H. Milsum, Biomedical Engineering Systems, McGraw-Hill, New York, 1970.
 13. Cosgriff, R.L., Nonlinear Control Systems, McGraw-Hill, New York, 1958.
 - 14a. Creutzfeldt, O., B. Sakmann, H. Scheich and A. Korn, "Sensitivity distribution and spatial summation within receptive-field center of retinal on-center ganglion cells and transfer function of the retina", J. Neurophys., 33, pp. 654-671, 1970.
 - 14b. Detwiler, S.R., Vertebrate Photoreceptors, MacMillan, New York, 1943.
 - 14c. DeVoe, R.D., "Linear relations between stimulus amplitudes and amplitudes of retinal action potentials from the eye of the wolf spider", J. Gen. Physiol., 47, pp. 13-32, 1963.
 15. Deutsch, R., "On a method of Wiener for noise through nonlinear devices", IRE Convention Record, Part 4, pp. 186-192, 1955.
 16. Deutsch, R., "Piecewise quadratic detector", IRE Convention Record, Part 4, p. 15, 1956.
 17. Deutsch, R., Nonlinear Transformations of Random Processes, Prentice-Hall, New Jersey, 1962.

18. Dill, J.C., "A computer-aided investigation of motion detection units in the fly", Ph.D. Thesis, California Institute of Technology, Pasadena, California, 1970.
19. Dowling, J.E., J.E. Brown and D. Major, "Synapses of horizontal cells in rabbit and cat retina", Nature, 153, pp. 1639-1641, 1966.
20. Dowling, J.E. and H. Ripps, "S-potentials in the skate retina. Intracellular recordings during light and dark adaptation", J. Gen. Physiol. 58, pp. 163-189, 1971.
21. Eisenberg, R.S. and E.A. Johnson, "Three-dimensional electrical field problems in physiology", Prog. Biophys. Molec. Biol., 20, 1-65, 1970.
22. Fender, D.H., "Techniques of systems-analysis applied to feedback pathways in the control of eye movements", Symp. Soc. Exp. Biol., 18, pp. 401-419, 1964.
23. Fender, D.H., "The eye-movement control system; evolution of a model", in R.F. Reiss (Ed.), Neural Theory and Modeling, pp. 306-324, Stanford University Press, Stanford, California, 1964.
24. Fender, D.H., "Applications of a computing facility in experiments on human visual perception", Proc. of the IBM Scientific Computing Symp. on Man-Machine Communication, pp. 129-147, 1966.
25. George, D.A., "Continuous nonlinear systems", Tech. Rept. 355, Research Lab. of Electronics, M.I.T., 1958.
26. Gouras, P., "Graded potentials of bream retina", J. Physiol., 152, pp. 487-505, 1960.
27. Gradshteyn, I.S. and I.M. Ryzhik, Table of Integrals, Series and Products, Academic Press, New York, 1965.

28. Graham, D. and D. McRuer, Analysis of Nonlinear Control Systems, John Wiley, New York, 1961.
29. Harmon, L.D. and E.R. Lewis, "Neural modeling", Physiol. Reviews, 46, pp. 513-591, 1966.
30. Hartline, H.K., "The receptive field of the optic nerve fibers", Amer. J. Physiol., 130, pp. 690-699, 1940.
31. Harris, G.H., "The identification of nonlinear systems with two-level inputs", Ph.D. thesis, Princeton University, Princeton, New Jersey, 1965.
- 32a. Hecht, S., S. Shlaer and M.H. Pirenn, "Energy, quanta, and vision", J. Gen. Physiol., 25, pp. 819-840, 1942.
- 32b. Ho, Y.C. and R.C.K. Lee, "Identification of linear dynamic systems", Inform. Control, 8, pp. 93-110, 1965.
- 33a. Jacobs, G., "Receptive fields in visual systems", Brain Research 14, pp. 553-573, 1969.
- 33b. Kalman, R.E. and R.S. Bucy, "New results in linear filtering and prediction theory", J. Basic Engin. (ASME Trans.), 83, pp. 95-108, 1961.
34. Kaneko, A., "Physiological and morphological identification of horizontal, bipolar and amacrine cells in goldfish retina", J. Physiol., 207, pp. 623-633, 1970.
35. Kaneko, A., "Electrical connexions between horizontal cells in the dogfish retina", J. Physiol., 213, pp. 95-105, 1971.
36. Katzenelson, J. and L.A. Gould, "The design of nonlinear filters and control systems, part I", Inform. & Control, 5, pp. 108-143, 1962.

37. Katzenelson, J. and L.A. Gould, "The design of nonlinear filters and control systems, part II", Inform. & Control, 7, pp. 117-145, 1964.
38. King, R.W.P., Transmission-line Theory, McGraw-Hill, New York, 1955.
39. Kolb, H., "Organization of the outer plexiform layer of the primate retina: electron microscopy of GOLGI-impregnated cells", Proc. Roy. Soc. Lond. B, 258, pp. 261-283, 1970.
40. Kuffler, S.W., "Neurons in the retina: organization, inhibition and excitation problems", Cold Spr.Harb. Symp. Quant. Biol., 17, pp. 281-292, 1952.
41. Lee, Y.W. and M. Schetzen, "Measurement of the kernels of a non-linear system by crosscorrelation", Quarterly Progress Rept. No. 60, Research Lab. of Electronics, M.I.T., 1961.
- 42a. Leondes, C.T., Ed., Modern Control Systems Theory, Ch. 6, McGraw-Hill, New York, 1966.
- 42b. Levett, J., "Nonlinear-linear transition in the frog intraretinal electroretinogram", Vision Res., 10, pp. 1347-1353, 1970.
43. Lipetz, L.E., "The transfer functions of sensory intensity in the nervous system", Vision Res. 9, pp. 1205-1234, 1969.
44. Lockeman, P.C. and D.W.Knutsen, "A multiprogramming environment for on-line data acquisition and analysis", Comm. ACM, 10, p. 758, 1967.
45. MacNichoal, E.F. and G. Svaetichin, "Electric responses from the isolated retinas of fishes", Amer. J. Ophthalm., 46 (3, Part II), pp. 26-46, 1958.

- 46a. Maffei, L., A. Fiorentini and L. Cervetto, "Homeostasis in retinal receptive fields", J. Neurophysiol., 34, pp. 579-587, 1971.
- 46b. Maffei, L. and R.E. Poppele, "Frequency analysis of the late receptor potential", J. Neurophysiol., 30, pp. 993-999, 1967.
47. Maksimov, J.M., "Effects of intracellular polarization of horizontal cells on the activity of the ganglionic cells of the retina of the fish", Biophysics, 14, pp. 570-577, 1969.
48. McCann, G.D. and D.H. Fender, "Computer data processing and systems analysis applied to research on visual perception", in R.F. Reiss (Ed.), Neural Theory and Modeling, pp. 232-252, Stanford University Press, Stanford, California, 1964.
49. McCann, G.D., "Toward a true understanding of the nervous system", Annals of Internal Medicine, 62, pp. 823-837, 1965.
50. McCann, G.D., "New research techniques for the life sciences", IBM J. Research and Development, 13, p. 28, 1969.
51. McCann, G.D., "Information science and the living nervous system; new concepts for insect nervous system research", Rept., California Institute of Technology, Pasadena, California.
52. McFee, R., "Determining the response of nonlinear systems to arbitrary inputs", Trans. AIEE, Part II, 80, p. 189, 1961.
53. Minor, A.V. and V.V. Maksimov, "Passive electrical properties of the model of a flat cell", Biophysics, 14 (2), pp. 349-357, 1969.
- 54a. Mishkin, E., and L. Braun, Eds., Adaptive Control Systems, McGraw-Hill, New York, 1961.

- 54b. Mowery, V.O., "Least squares recursive differential-correction estimation in nonlinear problems", IEEE Trans. Auto. Control, 10, pp. 399-407, 1965.
55. Naka, K.I. and W.A.H. Rushton, "S-potentials from colour units in the retina of fish (Cyprinidae)", J. Physiol., 185, pp. 536-555, 1966.
56. Naka, K.I. and W.A.H. Rushton, "An attempt to analyze colour receptor by electrophysiology", J. Physiol., 185, pp. 556-586, 1966.
57. Naka, K.I. and W.A.H. Rushton, "S-potentials from luminosity units in the retina of fish (Cyprinidae)", J. Physiol., 185, pp. 587-599, 1966.
58. Naka, K.I. and W.A.H. Rushton, "The generation and spread of S-potentials in fish (Cyprinidae)", J. Physiol., 192, pp. 437-461, 1967.
59. Naka, K.I., "Factors influencing the time course of S-potentials resulting from brief flashes", J. Physiol., 200, pp. 373-385, 1969.
60. Naka, K.I., "Computer assisted analysis of S-potentials", Biophys. Journal, 9, No. 6, pp. 845-859, 1969.
61. Naka, K.I. and P.W. Nye, "Receptive-field organization of the catfish retina: are at least two lateral mechanisms involved?", J. Neurophysiol., 33, pp. 625-642, 1970.
62. Naka, K.I., "Receptive field mechanism in the vertebrate retina", Science, 171, pp. 691-693, 1971.
63. Naka, K.I. and P.W. Nye, "Function of horizontal cells", J. Neurophysiol., 34, pp. 785-801, 1971.
64. Naka, K.I., "The horizontal cell", Vision Res., in press.

65. Negishi, K., M. Laufer and G. Svaetichin, "Excitation spread along horizontal and amacrine cell layers in the teleost retina", Nature, 218, pp. 39-40, 1968.
66. Negishi, K. and V. Sutija, "Lateral spread of light-induced potentials along different cell layers in the teleost retina", Vision Research, 9, pp. 881-893, 1969.
67. Norton, A.L., H. Spekrijse, M.L. Wolbarsht and H.G. Wagner, "Receptive field organization of the S-potential", Science, 160, pp. 1021-1022, 1968.
68. Oikawa, K., T. Ogawa and K. Motokawa, "Origin of so-called cone action potential", J. Neurophysiol., 22, pp. 102-111, 1959.
69. Richards, P.I., "Computing reliable power spectra", IEEE Spectrum, 4, p. 83, 1967.
- 70a. Rodieck, R.W. and J. Stone, "Analysis of receptive fields of cat retina ganglion cells", J. Neurophysiol., 28, pp. 832-849, 1965.
- 70b. Rodieck, R.W. and R.W. Ford, "The cat local electroretinogram in incremental stimuli", Vision Res., 9, pp. 1-24, 1969.
71. Rushton, W.A.H., "Vision as a photic process", Photophysiology, 2, pp. 123-162, 1964.
72. Schetzen, M., "Measurement of the kernels of a non-linear system of finite order", Quarterly Progress Rept. No. 71, Research Lab. of Electronics, M.I.T., 1963.
73. Schetzen, M., "Synthesis of a class of nonlinear systems", Quarterly Progress Report No. 68, Research Lab. of Electronics, M.I.T., pp. 122-130, 1964.

74. Sillman, A.J., H. Ito, and T. Tomita, "Studies on the mass receptor potential of the isolated frog retina", Vision Res., 9, pp. 1435-1442, 1969.
75. Sillman, A.J., H. Ito, and T. Tomita, "Studies on the mass receptor potential of the isolated frog retina", Vision Res., 9, pp. 1443-1451, 1969.
76. Singleton, H.E., "Theory of nonlinear transducers", Tech. Rept. 160, Research Lab. of Electronics, M.I.T., 1950.
77. Sneddon, I.N., Mixed Boundary Value Problems in Potential Theory, John Wiley and Sons, Inc., New York, 1966.
78. Spekrijse, H., "Rectification in the goldfish retina: analysis by sinusoidal and auxiliary stimulation", Vision Res., 9, p. 1461, 1969.
79. Spekrijse, H. and A.L. Norton, "The dynamic characteristics of color-coded S-potentials", J. Gen. Physiol.,
80. Stark, L., F.W. Campbell and J. Atwood, "Pupil unrest: an example of noise in a biological servomechanism", Nature, 182, pp. 857-858, 1958.
81. Stark, L., Neurological Control Systems, Studies in Bioengineering, Ch. 4, Plenum Press, New York, 1968.
82. Steinberg, R.H., "Rod and cone contributions to S-potentials from the cat retina", Vision Res., 9, pp. 1319-1329, 1969.
83. Steinberg, R.H. and R. Schmidt, "Identification of horizontal cells as S-potential generators in the cat retina by intracellular dye injection", Vision Res., 10, pp. 817-820, 1970.

84. Stell, W.K., "The structure and relationship of horizontal cells and photoreceptor-bipolar synaptic complexes in goldfish retina", Am. J. Anat., 121, pp. 401-424, 1967.
85. Stell, W.K., "The morphological organization of the vertebrate retina", in M.G.F. Fuortes (Ed.), Handbook of Sensory Physiology, 7/1B, Springer-Verlag, Berlin, 1971.
86. Svaetichin, G., "The cone action potential", Acta. Physiol. Scand., 29, Suppl. 106, pp. 565-600, 1953.
87. Thaler, G.J. and M.P. Pastel, Analysis and Design of Nonlinear Feedback Control Systems, McGraw-Hill, New York, 1962.
88. Tomita, T., "Electrophysiological study of the mechanisms subserving color coding in the fish retina", Cold Spring Harbor Symp. Quant. Biol. XXX, pp. 559-566, 1965.
89. Volterra, V., Theory of Functionals and of Integral and Integro-Differential Equations, Dover Publications, New York, 1959.
90. Wagner, H.G., E.F. MacNichol and M.L. Wolbarsht, "The response properties of single ganglion cells in the goldfish retina", J. Gen. Physiol., Suppl. 43, pp. 45-62, 1960.
91. Werblin, F.S. and J.E. Dowling, "Organization of the retina of the mudpuppy, Nocturus maculosus II intracellular recording", J. Neurophysiol., 32, pp. 339-355, 1969.
92. Wiener, N., "Response of a nonlinear device to noise", Rept. 129, Radiation Lab., M.I.T., 1942.
93. Wiener, N., Nonlinear Problems in Random Theory, Wiley, New York, 1958.

94. Witkovsky, P. and J.E. Dowling, "Synaptic relationships in the plexiform layers of carp retina", Z. Zellforsch., 100, pp. 60-82, 1969.
95. Wolf, A.A., "Some recent advances in the analysis and synthesis of nonlinear systems", Trans. AIEE, Part II, 80, pp. 289-300, 1961.
96. Yamada, E. and T. Ishikawa, "The fine structure of the horizontal cells in some vertebrate retinae", Cold Spr. Harb. Symp. Quant. Biol., 30, pp. 383-392, 1965.
97. Zadeh, L.A., "A contribution to the theory of nonlinear systems", J. Franklin Inst., 255, pp. 387-408, 1953.
98. Zadeh, L.A., "On the identification problem", IRE Trans. Circuit Theory, 3, pp. 277-281, 1956.
99. Zadeh, L.A., "On the representation of nonlinear operators", IRE Wescon Conv. Rec., Pt. 2, pp. 105-113, 1957.
100. Zadeh, L.A., "Part 5: prediction and filtering", IRE Trans. Inform. Theory, 7, pp. 139-144, 1961.